Objective and quantitative methods in the study of dinosaur tracks

Dissertation
zur
Erlangung des Doktorgrades (Dr. rer. nat.)
der
Mathematisch-Naturwissenschaftlichen Fakultät
der
Rheinischen Friedrich-Wilhelms-Universität Bonn

vorgelegt von

Jens Nikolaus Lallensack

aus

Höxter

Bonn 2018

Angefertigt mit Genehmigung der Mathematisch-Naturwissenschaftlichen Fakultät der
Rheinischen Friedrich-Wilhelms-Universität Bonn

1. Gutachter	Prof. Dr. P. Martin Sander
2. Gutachter	Prof. Dr. Thomas Martin
Tag der Promotion	05.10.2018
Erscheinungsjahr	2019

Acknowledgements

First of all, I would like to thank my supervisor P. Martin Sander for all his support, input, encouragement, and flexibility regarding topic choices. I also thank Thomas Martin for kindly agreeing to be second reviewer, and Nikolaus Froitzheim and Herbert Koch for being part of the dissertation committee. I am grateful to all current and former members of the AG Sander for allowing me to be part of this supportive and productive community.

Most chapters of the present dissertation are joint efforts, and would not have been possible without the input of many. My special thanks is dedicated to Oliver Wings, who provided valuable data and encouraged me to work on additional projects, three of which became key chapters. My gratitude is furthermore owed to Michael Buchwitz for his advice and fruitful discussions, especially concerning statistical methods and photogrammetry. I furthermore thank Sashima Läbe for many discussions on tracks and photogrammetry; Anthony Romilio for contributing data and ideas concerning the objective definition of footprint outlines; Karl Bernhardi for discussions on numerical data analysis and programming; and Anneke van Heteren for her advice and input on statistical data analysis. To my fiends and colleagues Tzu-Ruei Yang, Jonas Barthel, and Thomas Engler, I thank you for your friendship and support during my entire dissertation. I furthermore express my deepest gratitude to all yet unmentioned co-authors of the chapters presented in this thesis—Shinobu Ishigaki, Abdelouahed Lagnaoui, Hendrik Klein, Jesper Milàn, Octávio Mateus, and Lars B. Clemmensen—for the very successful cooperations. It was a pleasure working with you.

My deepest thanks are dedicated to my parents, Eva and Nikolaus Lallensack, my brother, Marius Lallensack, and my girlfriend Yan-An Juo, for their understanding, support, and encouragement.

Summary

This dissertation develops and employs objective and quantitative methods for the analysis of dinosaur tracks. Tracks are—besides the familiar bones and teeth—a crucial data source for inferences on dinosaur biology and evolution. Tracks allow for insights that cannot be directly obtained from bones and teeth. Most obviously, their nature as life traces allows for inferences on behavior, posture, gait, and speed. Track data, however, are often more ambiguous than data derived from bones. Footprint margins, for example, are difficult to define objectively, and footprint shape is the result of a combination of many factors including anatomy, substrate, and behavior, complicating their interpretation. Although quantitative methods are needed to constrain this ambiguity and to effectively analyze the often non-discrete characters of footprint shape, the study of dinosaur tracks is still a largely subjective endeavor. This dissertation aims to demonstrate the utility of these methods for studying dinosaur tracks, not only to improve on objectivity and reproducibility of results, but also to gain novel insights into dinosaur biology and evolution.

In a case study of Lower Cretaceous theropod and ornithopod trackways from Münchehagen, Germany, geometric morphometric analysis is employed to quantify footprint shape variation within trackways, revealing that many shape features may not reflect foot anatomy. Furthermore, inferences on the discrimination between the footprints of theropod and ornithopod trackmakers and between footprints of the left and right foot are made (**chapter 2**). A larger (n=303) sample of tridactyl footprints from all over the world was analyzed using an approach combining geometric morphometrics and linear and angular measurements, revealing that footprint shape carries a strong functional signal. Cursorial, graviportal, and stabilizing adaptations may be differentiated based on footprints. Furthermore, footprint size evolution is analyzed separately for theropods and ornithischians, revealing reverse trends (**chapter 3**). In an attempt to provide a solution for the vexing problem of defining objective footprint margins, a program was written that is, for the first time, able to compute outlines automatically from 3D-models of footprints, providing the basis for fully objective shape analyses **(chapter 4)**. An extensive sauropod tracksite from the Middle Jurassic of Morocco was analyzed in detail, revealing trackways with laterally orientated manual impressions, which is rare in sauropods. Statistical analysis of trackway parameters of these and other trackways from around the world (n=79) demonstrates that the manus orientation is determined by both relative locomotion speed (and thus, behavior) and the position of the center of mass (anatomy). Furthermore, the gleno-acetabular length is evaluated as an alternative size proxy for quadrupedal trackways, and attempts are made to quantify trackway asymmetries and to produce trackway mean configurations **(chapter 5)**. The synapomorphy-based approach, sometimes considered the most rigorous objective approach for trackmaker identification, is used to identify a sauropod trackway from the Late Triassic of Greenland, currently constituting the most unambiguous evidence for sauropods before the Jurassic **(chapter 6)**. Another trackway from the Late Triassic of Lesotho shows somewhat sprawling forelimbs, and thus may pertain to a recently identified group of large and quadrupedal non-sauropod sauropodomorphs, the Lessemsauridae **(chapter 7)**. The state of research is reviewed, identifying five principal challenges that add significant ambiguity to previous interpretations and can possibly be accounted for by the use of objective and quantitative methods. It is argued that currently employed ichnotaxonomy lacks an objective basis, but that other approaches to the study of tracks, in particular functional interpretations, may add more to our understanding of dinosaurs than previously recognized **(chapter 8)**.

Contents

Chapter 1 – Introduction and description of chapters

Non-avian dinosaurs existed during a time span of ca 175 million years, from the Middle Triassic (ca 240 mya, Brusatte et al., 2011) to the end of the Late Cretaceous (66 mya). They were the dominant vertebrates on land during most of this time, and thus played a hugely important role in vertebrate evolution. The study of dinosaurs is of high relevance for the understanding of important biological phenomena, including extinction, warm bloodedness, giant body sizes, and powered flight, and thus also adds to the understanding of modern ecosystems. The fossil record of dinosaurs, however, is limited—most information is deduced from body fossils (bones and teeth), with soft tissue only preserved in exceptional cases. The fossil record is furthermore patchy, both in time and space. Because of these limitations, a second category of fossils—trace fossils, most importantly tracks—is of high relevance as an additional and independent data source.

Tracks, given their nature as life traces, allow for very different insights into dinosaur biology than do bones, thus opening a window allowing for the study of dinosaurs from a different perspective. Tracks record the activities of an animal at a certain place during a brief time span of its life, thus giving clues about behavior and locomotion, including gregariousness, posture, gait, and speed. Tracks inform on pedal morphology, which is important given the scarcity of complete pedal skeletons in the fossil record. Tracks also have a different preservation potential than body fossils, and thus are frequently preserved in rock units devoid of bones (see chapter 8 for a review).

Interpretations of dinosaur tracks, however, are in many cases ambiguous, and often to a greater degree than are interpretations based on bones. This ambiguity is introduced at all levels: At the level of the individual footprint, the footprint margins are difficult to define objectively, leading to subjectivity in shape characterizations and measurements (chapter 4; Falkingham, 2016). The different factors resulting in the final shape of the footprint (including trackmaker anatomy and behavior as well as substrate properties) are difficult to tell apart (chapter 2; Falkingham, 2014). At the level of a trackway, identical footfall patterns may be produced by animals showing different combinations of gait, size, and built (Stevens et al., 2016). At the level of a tracksite, the time span and sequence at which animals traversed a surface is difficult to constrain, adding ambiguity to behavioral interpretations (Myers and Fiorillo, 2009).

These many sources of ambiguity also make the application of objective and quantitative methods challenging. In fact, such methods are still rarely used in the study of dinosaur tracks, although they are needed to account for this ambiguity. As a result, many inferences made based on tracks are difficult to reproduce, and consequently are often ignored by studies focusing on body fossils.

This dissertation is dedicated to developing and applying objective and quantitative methods to dinosaur tracks. Such methods are used both to constrain ambiguity and to arrive at novel conclu-

sions about dinosaur biology and evolution, and were conducted both in the limits of case studies and by analyzing larger data sets. While objective and quantitative methods are a central theme in this work, they are attempted to be used in combination with traditional methods and qualitative descriptions, always with the scope of gaining as much insights from the analyzed tracks as possible.

The first two chapters advance the understanding of the determinants of footprint shape variation. **Chapter 2** (Lallensack et al., 2016) is a case study of three exceptionally long tridactyl trackways from the Lower Cretaceous of Germany. Footprint shape variation along these trackways was analyzed using geometric morphometrics, allowing for assessing the influence of variations in substrate properties and behavior on separate footprint shape features. **Chapter 23** (Lallensack et al., unpubl.) analyzes shapes of tridactyl footprints based on a larger sample (n=303) using an approach that combines linear and angular measurements and geometric morphometrics. This research indicates that many aspects of the shapes can be explained by size and function, with phylogeny playing a less important role than previously thought. New inferences on functional anatomy of tridactyl dinosaur feet are provided. **Chapter 4** (Lallensack, unpubl.) offers a solution for a long-standing problem in track research: the definition of the footprint margins. Footprint margins are often highly ambiguous, and so far have mostly been determined subjectively, rendering any derived size and shape data equally subjective (Falkingham, 2016). In this chapter, fully objective footprint outlines were, for the first time, produced automatically using a computer script.

Chapter 5 (Lallensack et al., accepted) is focusing on the quantitative analysis not of individual footprints but whole trackways. A large sauropod tracksite from the Middle Jurassic of Morocco was documented using photogrammetry and analyzed in detail, revealing trackways with laterally directed manual impressions. Statistical analysis of these trackways and a larger statistical sample of sauropod trackways from around the world provide new insights into sauropod locomotion. **Chapters 6** (Lallensack et al., 2017) is concerned with another fundamental problem in track research: the identification of the trackmaker taxon. By applying the most rigorous objective approach for trackmaker identification—the synapomorphy-based approach—a trackway from the Late Triassic of Greenland was identified as belonging to a sauropod, and currently represents the least ambiguous fossil of this clade dating to the Triassic. **Chapter 7** (Sander and Lallensack, submitted), designed as a dispatch to accompany a research paper to be published in the journal Current Biology, picks up this research and provides additional interpretations in light of new evidence, reminding of the importance of track evidence for many questions regarding dinosaur biology and evolution.

Chapter 8 (Lallensack, unpubl.) provides a review on the significance tracks had and still have for the modern understanding of dinosaurs. It furthermore reviews the existing problems of the field, and reminds of the importance of objective and quantitative methods to account for them. In this context, the inferences made in this dissertation are emphasized and summarized.

REFERENCES

Brusatte, S.L., Niedźwiedzki, G., Butler, R.J., 2011. Footprints pull origin and diversification of dinosaur stem lineage deep into Early Triassic. Proceedings of the Royal Society of London B: Biological Sciences 278, 1107–1113.

Falkingham, P.L., 2016. Applying Objective Methods to Subjective Track Outlines, in: Falkingham, P.L., Marty, D., Richter, A. (Eds.), Dinosaur Tracks: The Next Steps. Indiana University Press, Bloomington, pp. 72–81.

Falkingham, P.L., 2014. Interpreting ecology and behaviour from the vertebrate fossil track record. Journal of Zoology 292, 222–228.

Lallensack, J.N., unpubl. Automatic generation of objective footprint outlines. Doctoral thesis 2018 (chapter 3). Bonn, Germany.

Lallensack, J.N., unpubl. Dinosaur tracks: state of research, challenges, and prospectus. Doctoral thesis 2018 (chapter 7). Bonn, Germany.

Lallensack, J.N., Engler, T., Barthel, H.J., unpubl. Shape variability in tridactyl dinosaur footprints: The significance of size and function. Doctoral thesis 2018 (chapter 2). Bonn, Germany.

Lallensack, J.N., Ishigaki, S., Lagnaoui, A., Buchwitz, M., Wings, O., accepted. Forelimb orientation and locomotion of sauropod dinosaurs: insights from the Middle Jurassic Tafaytour Tracksite (Argana Basin, Morocco). Journal of Vertebrate Paleontology.

Lallensack, J.N., Klein, H., Milàn, J., Wings, O., Mateus, O., Clemmensen, L.B., 2017. Sauropodomorph dinosaur trackways from the Fleming Fjord Formation of East Greenland: evidence for Late Triassic sauropods. Acta Palaeontologica Polonica 62, 833–843.

Lallensack, J.N., van Heteren, A.H., Wings, O., 2016. Geometric morphometric analysis of intratrackway variability: a case study on theropod and ornithopod dinosaur trackways from Münchehagen (Lower Cretaceous, Germany). PeerJ 4, e2059.

Myers, T.S., Fiorillo, A.R., 2009. Evidence for gregarious behavior and age segregation in sauropod dinosaurs. Palaeogeography, Palaeoclimatology, Palaeoecology 274, 96–104.

Sander, P.M., Lallensack, J.N., submitted. Dinosaurs: Four legs good, two legs bad. Doctoral thesis 2018 (chapter 6). Bonn, Germany.

Stevens, K.A., Ernst, S., Marty, D., 2016. Uncertainty and ambiguity in the interpretation of sauropod trackways, in: Falkingham, P.L., Marty, D., Richter, A. (Eds.), Dinosaur Tracks: The Next Steps. Indiana University Press, pp. 226–243.

Chapter 2

Published as:

Lallensack, J.N., van Heteren, A.H., Wings, O., 2016. Geometric morphometric analysis of intratrackway variability: a case study on theropod and ornithopod dinosaur trackways from Münchehagen (Lower Cretaceous, Germany). PeerJ 4, e2059. **p. 5–56.**

Author contributions:

- Jens N. Lallensack conceived and designed the experiments, performed the experiments, analyzed the data, contributed reagents/materials/analysis tools, wrote the paper, prepared figures and/or tables, reviewed drafts of the paper.
- Anneke H. van Heteren and Oliver Wings conceived and designed the experiments, analyzed the data, contributed reagents/materials/analysis tools, wrote the paper, reviewed drafts of the paper.

Supplementary Material:

- Supplemental figures S1 and S2: Principal component analysis results of steepest slope approach. **p. 57–58.**
- Supplemental table S1: Measurements of trackway parameters. **p. 59–60.**
- Photogrammetric 3D-data (available from DVD or Figshare, see Table 1 in main text).

PeerJ

Geometric morphometric analysis of intratrackway variability: a case study on theropod and ornithopod dinosaur trackways from Münchehagen (Lower Cretaceous, Germany)

Jens N. Lallensack[1], Anneke H. van Heteren[1,3] and Oliver Wings[2]

[1] Division of Paleontology, Steinmann Institute, University of Bonn, Bonn, Germany
[2] Niedersächsisches Landesmuseum, Hannover, Germany
[3] Current affiliation: Sektion Mammalogie, Zoologische Staatssammlung München, München, Germany

ABSTRACT

A profound understanding of the influence of trackmaker anatomy, foot movements and substrate properties is crucial for any interpretation of fossil tracks. In this case study we analyze variability of footprint shape within one large theropod (T3), one medium-sized theropod (T2) and one ornithopod (I1) trackway from the Lower Cretaceous of Münchehagen (Lower Saxony, Germany) in order to determine the informativeness of individual features and measurements for ichnotaxonomy, trackmaker identification, and the discrimination between left and right footprints. Landmark analysis is employed based on interpretative outline drawings derived from photogrammetric data, allowing for the location of variability within the footprint and the assessment of covariation of separate footprint parts. Objective methods to define the margins of a footprint are tested and shown to be sufficiently accurate to reproduce the most important results. The lateral hypex and the heel are the most variable regions in the two theropod trackways. As indicated by principal component analysis, a posterior shift of the lateral hypex is correlated with an anterior shift of the margin of the heel. This pattern is less pronounced in the ornithopod trackway, indicating that variation patterns can differ in separate trackways. In all trackways, hypices vary independently from each other, suggesting that their relative position a questionable feature for ichnotaxonomic purposes. Most criteria commonly employed to differentiate between left and right footprints assigned to theropods are found to be reasonably reliable. The described ornithopod footprints are asymmetrical, again allowing for a left–right differentiation. Strikingly, 12 out of 19 measured footprints of the T2 trackway are stepped over the trackway midline, rendering the trackway pattern a misleading left–right criterion for this trackway. Traditional measurements were unable to differentiate between the theropod and the ornithopod trackways. Geometric morphometric analysis reveals potential for improvement of existing discriminant methods.

Subjects Paleontology

Keywords Lower Cretaceous, Trackways, Germany, Dinosaur tracks, Geometric morphometrics, Theropods, Ornithopods, Fossil footprints, Photogrammetry

Submitted 4 March 2016
Accepted 29 April 2016
Published 8 June 2016

Corresponding author
Jens N. Lallensack,
jens.lallensack@uni-bonn.de

Academic editor
Herbert Maschner

Additional Information and Declarations can be found on page 43

DOI **10.7717/peerj.2059**

How to cite this article Lallensack et al. (2016), Geometric morphometric analysis of intratrackway variability: a case study on theropod and ornithopod dinosaur trackways from Münchehagen (Lower Cretaceous, Germany). **PeerJ 4:e2059; DOI 10.7717/peerj.2059**

INTRODUCTION

The shape of a footprint is determined by the anatomy and the behavior (foot movements) of the trackmaker as well as the substrate properties (*Falkingham, 2014*). For many applications, especially for ichnotaxonomy and trackmaker identification, foot anatomy is the component of interest, and alterations of the footprint shape from the foot shape introduced by substrate and behavior are regarded as "extramorphological" noise (*Peabody, 1948*). The influence of extramorphological variability on footprint shapes is difficult to assess. The presence of anatomical details, most importantly digital pads, is probably the best available criterion for the assessment of footprint quality (*Belvedere & Farlow, in press*). However, even high-quality footprints can be greatly influenced by extramorphological, often behavioral variability, and significant deformation can occur even when fine anatomical details such as skin impressions are preserved (e.g. *Currie, Nadon & Lockley, 1991*, Fig. 4). Furthermore, it is unclear if a lack of phalangeal pads is necessarily related to poor footprint quality, as it in some cases might reflect the soft part anatomy of the trackmaker's foot (*Lockley, 1998*; *Lockley, Meyer & Moratalla, 1998*). A thorough understanding of the influence of the anatomy, the behavior, and the substrate properties on footprint shape is therefore fundamental for any interpretation of fossil footprints, independent of their quality of preservation.

The influence of substrate and behavior becomes obvious within trackways. As foot anatomy can be considered constant within a trackway, at least amongst all footprints left by the same foot, in theory any variability can be attributed to behavior and substrate properties. In our case study, we analyze variability within three long and well preserved tridactyl trackways from the Lower Cretaceous Münchehagen locality in Germany, left by one ornithopod and two theropod trackmakers. We describe the morphology of the analyzed footprints, both qualitatively based on the best-defined footprint of the respective trackway, and quantitatively based on Procrustes mean-shapes. We then assess and review the variability, and thus informativeness, of track features commonly employed for ichnotaxonomy, trackmaker identification, and the discrimination between left and right footprints. Geometric morphometrics is utilized to measure variability and covariation of individual landmarks representing separate parts of the footprints. Principal component analysis reveals variation patterns that possibly are controlled by the trackmaker's behavior. Criteria for the discrimination of left and right footprints are evaluated for both the theropod and the ornithopod trackways. We furthermore assess and discuss the ability of both linear measurements and geometric morphometric methods to discriminate between the ornithopod and theropod footprints. Although our analyses are based on interpretative, and thus subjective, outline drawings, we were able to reproduce important results using a fully objective approach to define footprint extents.

HISTORY AND SEDIMENTOLOGY OF THE MÜNCHEHAGEN LOCALITY

The Wesling sandstone quarry in Münchehagen (municipality of Rehburg-Loccum, Lower Saxony, Germany) represents one of the most productive dinosaur track localities in

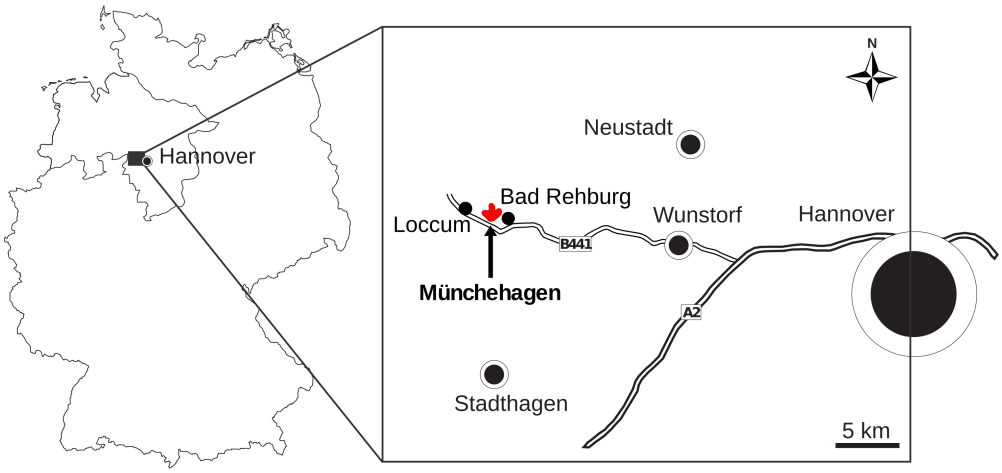

Figure 1 **Map showing the location of Münchehagen in Germany.**

Germany (*Wings et al., 2012*) (Fig. 1). The site belongs to the Obernkirchen Sandstone in the Lower Saxony Basin, which is Berriasian in age and traditionally attributed to the "German Wealden" (*Erbacher et al., 2014*; *Mutterlose, Bodin & Fähnrich, 2014*). According to the terminology recently introduced by *Erbacher et al. (2014)*, the Obernkirchen Sandstone is part of the Barsinghausen Subformation within the Deister Formation, which falls within the Bückeberg Group (formerly known as Bückeberg Formation). In the Obernkirchen Sandstone, dinosaur tracks have been discovered since the nineteenth century (*Grabbe, 1881*; *Hornung et al., 2012*). The first track-bearing layer in Münchehagen was discovered in 1980 in an abandoned part of the Wesling quarry. Containing multiple trackways of sauropod dinosaurs, this site was granted national monument status, sheltered by a protective building, and included in the exhibition of the newly built Dinosaurier-Freilichtmuseum Münchehagen soon after its discovery (*Hendricks, 1981*; *Fischer, 1998*; *Lockley, Wright & Thies, 2004*; *Wings et al., 2012*). Multiple isolated slabs containing ornithopod pes and manus tracks have been recovered and described from overlaying strata (*Lockley & Wright, 2001*; *Lockley, Wright & Thies, 2004*; *Gierlinski et al., 2008*). Large-scale excavations of footprints from these overlaying strata are carried out since 2004 in the nearby active part of the Wesling quarry (*Wings et al., 2012*; *Wings, Lallensack & Mallison, in press*). In contrast to the old Wesling quarry, the new Wesling quarry prevailingly comprised tridactyl footprints referable to both ornithopod and theropod dinosaurs (*Wings, Lallensack & Mallison, in press*), although discoveries of sauropod tracks in the new quarry have been made recently.

In this case study, we analyze three trackways from the lower level of the new Wesling quarry, which have been previously assigned to theropod (trackways T2 and T3) and ornithopod (trackway I1) trackmakers (*Wings et al., 2012*; *Wings, Lallensack & Mallison, in press*). These trackways are amongst the longest and best preserved dinosaur trackways from Germany (Fig. 2). The T3 trackway was composed of 47 consecutive footprints. With a continuously recorded length of more than 55 m, it can be regarded as one of the longest

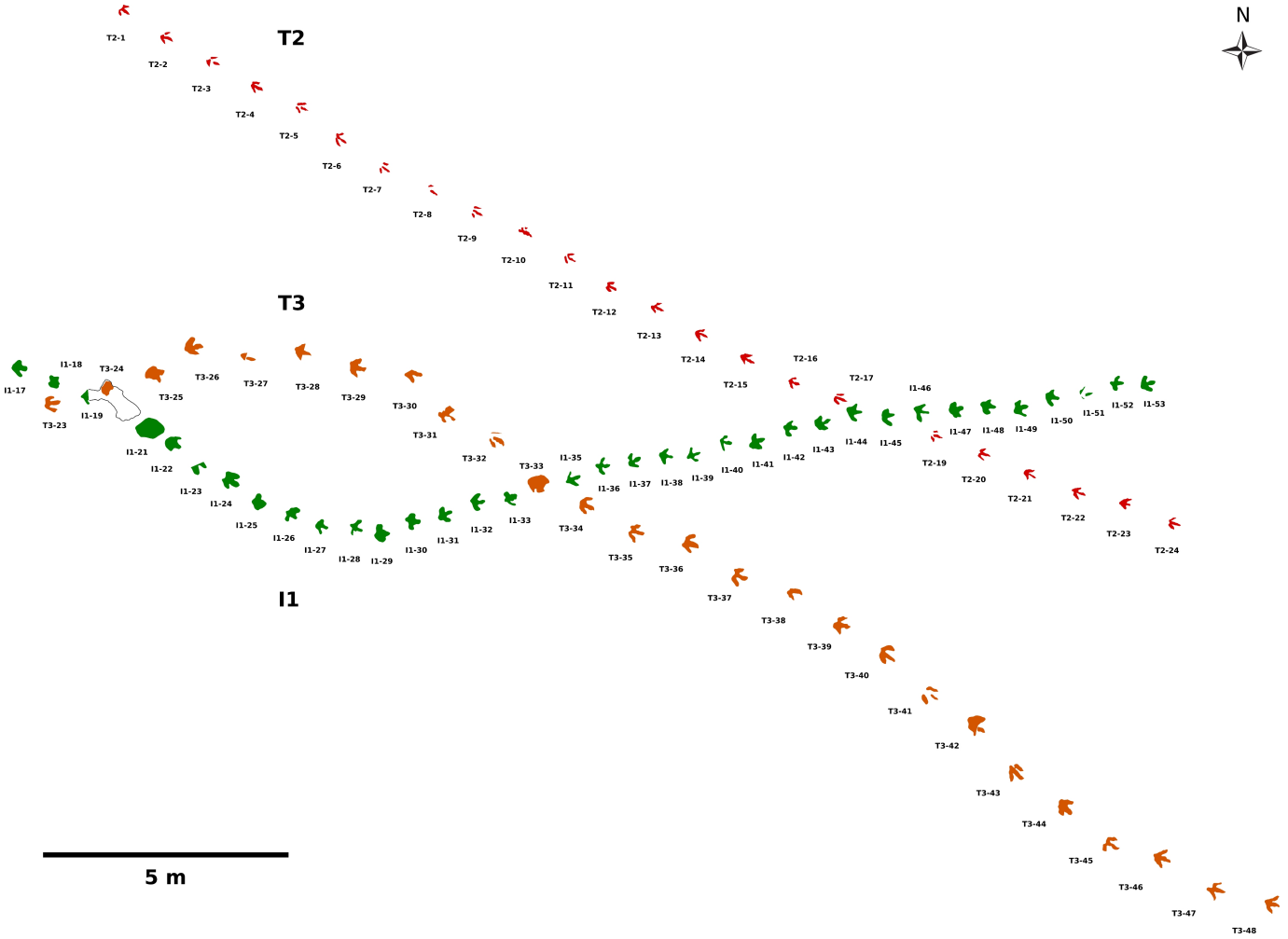

Figure 2 Sitemap based on photogrammetric data showing the three analyzed trackways (T3, T2, and I1), which represent some of the longest dinosaur trackways from Germany. The proximal sections of the T3 and I1 trackways, excavated before 2011, were not included because photogrammetric documentation is not available. Possible continuations of the T3 and T2 trackways discovered in 2015 are also not included.

dinosaur trackways in the world (cf. *Xing et al., 2015*). The I1 trackway, composed of 53 consecutive footprints, measured ca. 35 m in total length, while the 24 footprints of the T2 trackway account for a total length of 24.95 m. The trackways have been excavated between 2009 and 2011. Additional footprints of the T3 and possibly of the T2 trackway have been discovered in 2015, extending the length of these trackways even further. These new finds are not included in the present study.

The Münchehagen locality mainly exposes fine to medium quartz sandstones, which are brown to yellow-gray in color and strongly siliceously cemented. The dip of the beds is between 3° and 6° towards the west (*Wings et al., 2012*; *Wings, Lallensack & Mallison, in press*). Although laterally variable, the beds can be classified in 19 lithological units (LU) (*Wings et al., 2012*). Coaly layers covering parts of some of the bedding planes are

attributed to plant detritus. Symmetrical ripple marks, generally orientated in north-south direction and classified as small-scale wave ripples, are present on most bedding planes, indicating that flow and wave direction were constant during deposition of several beds (*Wings et al., 2012*; *Wings, Lallensack & Mallison, in press*). Drainage structures on few bedding planes indicate a paleoflow direction to the west (*Wings et al., 2012*; *Wings, Lallensack & Mallison, in press*). The paleoenvironment has been interpreted as brackish with both freshwater and marine influences (*Mutterlose, 1997*).

The three trackways analyzed herein stem from LU7, which measures ca. 8 cm in thickness and encompasses fine to medium, very well sorted quartz sandstones topped by a thinly layered stack of silty mudstones (*Wings et al., 2012*). The true tracks are found on top of the silty mudstones, with undertracks preserved in the sandstones of LU7, LU6, and LU5, and natural track casts preserved on the underside of LU8 (*Wings, Lallensack & Mallison, in press*). The silty mudstones are very variable in thickness laterally, but do not exceed 3 cm. Within the footprints, the thickness of the silty mudstones accounts for less than a centimeter. The silty mudstones were destroyed during excavation in approximately 40% of the footprints due to their fragility, exposing the undertracks within the sandstones. Evidence for aerial exposure is lacking, raising the possibility that the layer was constantly covered by water during track formation.

MATERIAL & METHODS

Data acquisition

The majority of the footprints analyzed herein was destroyed by weathering after their removal from the sediment layers, with only a section of the T2 trackway (T2/01–15) and several slabs with natural casts being preserved, including the excellently preserved casts of T2/4, T3/18 and T3/39–41 (Figs. 3 and 4). A section of the T2 trackway was re-assembled after excavation for display within the protective building of the Dinosaurier-Freilichtmuseum Münchehagen. The present study is mostly based on photogrammetric documentation carried out in 2011, which encompasses the analyzed sections of the T3 and I1 trackways, as well as part of the T2 trackway section. For the remainder of the T2 trackway, photogrammetric data collected in 2009 and a recent photogrammetry of the re-assembled and exhibited section of the trackway was used. Photogrammetric documentation was carried out by one of us (OW), using methods outlined in *Mallison & Wings (2014)*. No photogrammetric data is available of the first sections of the T3 (T3/1–T3/23) and I1 (I1/1–I1/17) trackways, except for few excavated slabs that have been brought into the protective building of the Dinosaurier-Freilichtmuseum and are still accessible (see *Wings et al., 2012*, Fig. 13 for a sketch of the complete presumed trackway course). Five photogrammetric models of the trackway sections were created (T3/23–47; T2/01–15; T2/11–16; T2/16–24; I1/17–53) using the software Agisoft PhotoScan Professional 1.0.4 (www.agisoft.com). The horizontal planes were defined by setting three marker points on the surfaces of the models, respectively. To reduce the influence of the unevenness of the surfaces, the distance between the marker points was maximized. Individual footprints were cropped out of the trackway models for further analysis. Orthophotos of each trackway

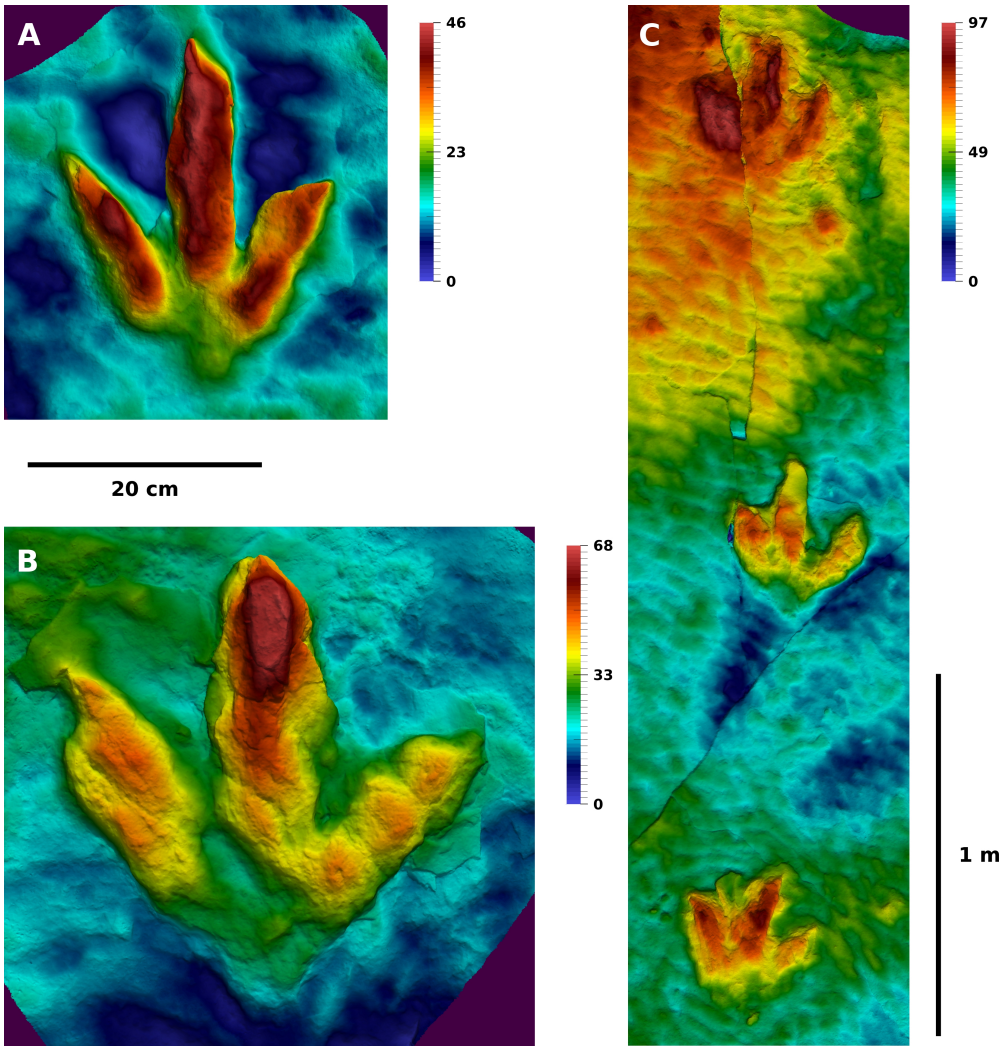

Figure 3 Depth-color images of well preserved footprint casts of the T2 and T3 trackways. (A) The cast of T2/4, which belongs to a left foot, is the best preserved cast of the T2 trackway. It shows an excellently preserved claw impression on digit III. (B) The cast of T3/18, belonging to a left foot, is the best preserved cast of the T3 trackway. It features well preserved claw impressions, phalangeal pads, and a complete heel region. (C) The casts of T3/39–T3/41. The respective moulds of T3/39 and T3/41 are illustrated in Fig. 5. (A) and (B) to scale. Color legend scales in mm.

section were generated with Agisoft Photoscan. All surface meshes are reposited at Figshare (Table 1). The original photographs are available from OW on request.

For the morphometric analysis, we selected 13 well preserved footprints of the T3 trackway (Fig. 5), 8 of the T2 trackway (Fig. 6), and 17 of the I1 trackway (Fig. 7). Criteria for the selection included the presence of a largely intact layer of silty mudstones, therefore excluding undertracks. Furthermore, only footprints were selected that could be fully defined by a single contour line; this excludes any shallow and incomplete footprints. Contoured depth-color images were created for each selected individual footprint with the open source software Paraview 4.1 (www.paraview.org). For each image, a fixed number of

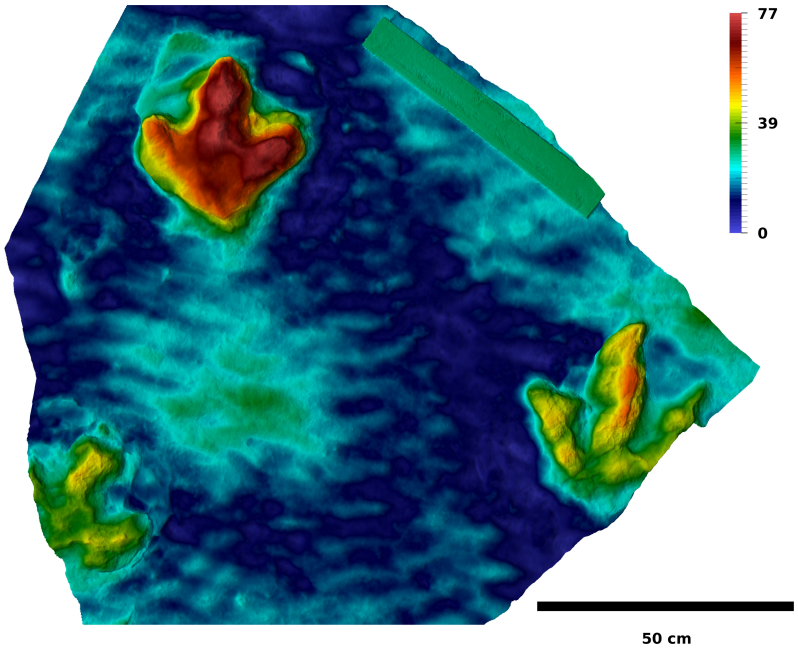

Figure 4 Depth-color image of a slab containing the natural casts of I1/16 (lower left), I1/17 (upper left), and T3/22 (right). The mould of I1/16 is illustrated in Fig. 7A. Color legend scale in mm.

Table 1 Photogrammetric surface models available via Figshare.

Footprints	Preservation	Status	URL
T3/25–T3/48	Moulds	*in situ*, 2011	http://dx.doi.org/10.6084/m9.figshare.3027211
I1/17–I1/53	Moulds	*in situ*, 2011	http://dx.doi.org/10.6084/m9.figshare.2972329
T2/1–T2/15	Moulds	Excavated and reassembled	http://dx.doi.org/10.6084/m9.figshare.3025144
T2/11–T2/16	Moulds	*in situ*, 2009	http://dx.doi.org/10.6084/m9.figshare.3026863
T2/16–T2/24	Moulds	*in situ*, 2011	http://dx.doi.org/10.6084/m9.figshare.3027067
T3/39–T3/41	Natural casts	Excavated and reassembled	http://dx.doi.org/10.6084/m9.figshare.3027949
T3/22; I1/16–I1/17	Natural casts	Excavated	http://dx.doi.org/10.6084/m9.figshare.3027553
T3/18	Natural cast	Excavated	http://dx.doi.org/10.6084/m9.figshare.3027385
T2/4	Natural cast	Excavated	http://dx.doi.org/10.6084/m9.figshare.3029698

30 contour lines are used, whose spacing is relative to the total height of the cropped-out footprint model along the z-axis. Therefore, the same contour lines will represent different total depths in separate images. This approach of relative contour lines allows for the direct comparison of individual contour lines in separate models, independent of the depth and size of the footprints. All left footprints were mirrored to fit the right ones. Outlines were traced on the contoured depth-color images using the open source software Inkscape (www.inkscape.org).

A site map (Fig. 2, Fig. S3) was drawn directly from the combined orthophotos and elevation models of all three trackways. A preliminary sitemap has already been published by Wings et al. (*2012*, *in press*, Fig. 13). This map appears to be deformed, and compared

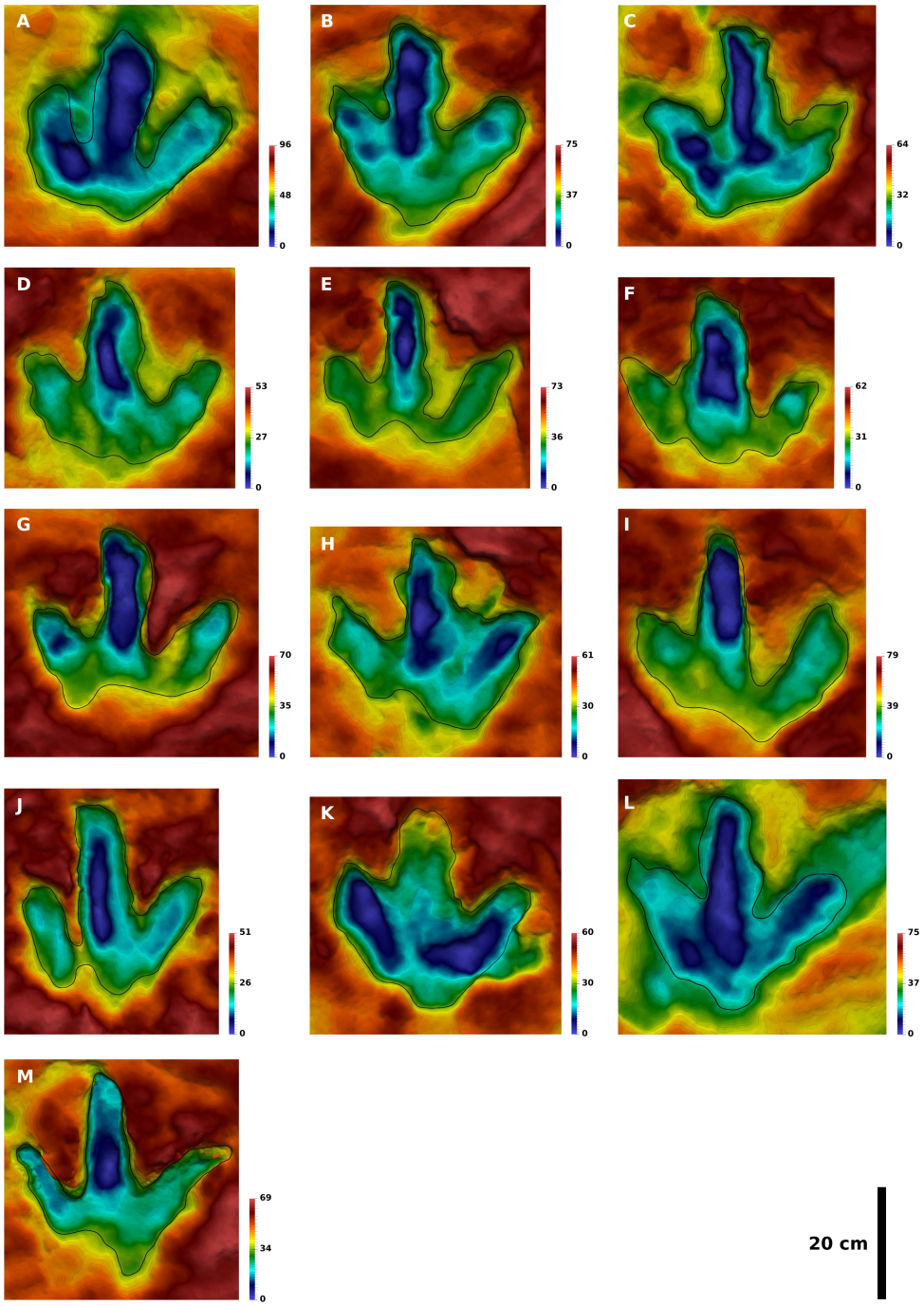

Figure 5 Contoured depth-color images with interpretative outlines of the 13 footprints of the T3 trackway analyzed herein. All footprints are to scale, and all left footprints were mirrored to fit the right ones. The color scale ranges from the lowest point (blue) to the highest point of the model (red); given the different depths in separate models, the depth of a specific color varies. (A) T3/23. (B) T3/26. (C) T3/29. (D) T3/34. (E) T3/35. (F) T3/36. (G) T3/37. (H) T3/39. (I) T3/40. (J) T3/43. (K) T3/44. (L) T3/46. (M) T3/47. Color legend scales in mm.

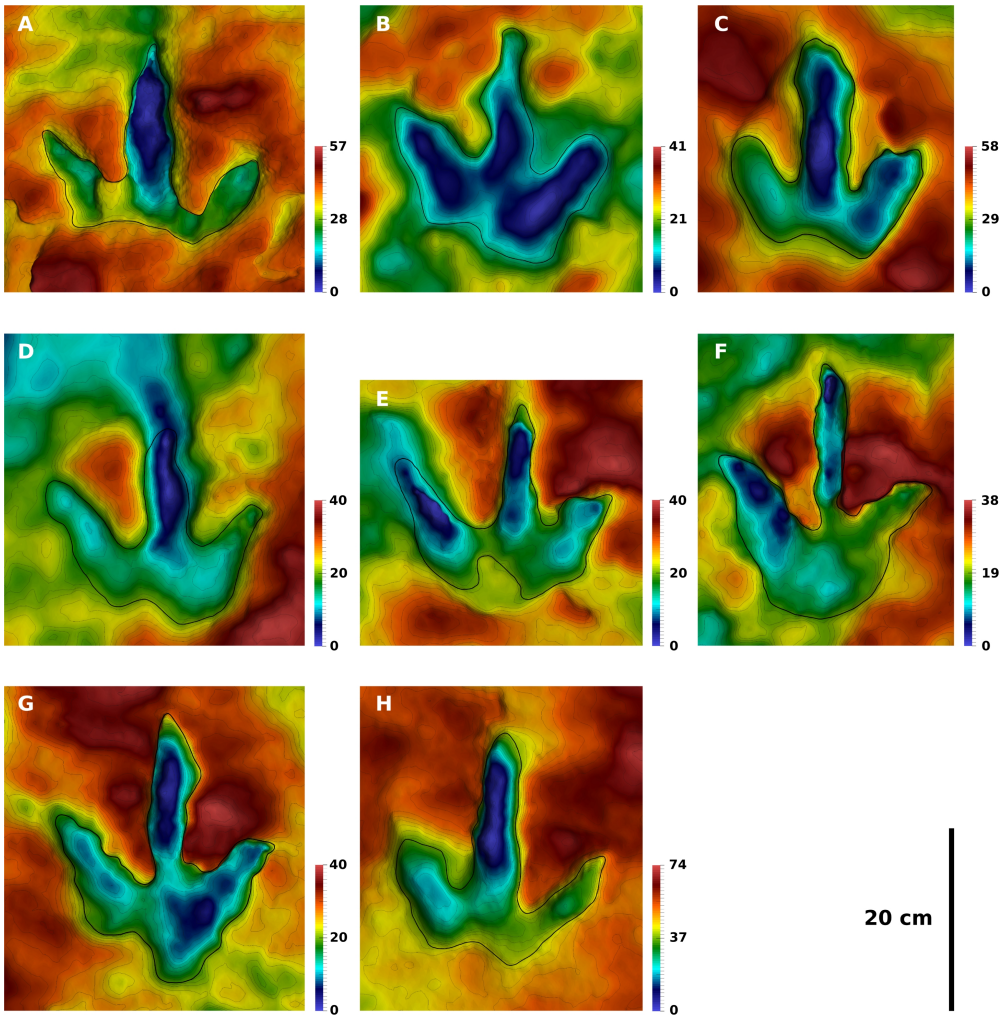

Figure 6 Contoured depth-color images with interpretative outlines of the eight footprints of the T2 trackway analyzed herein. All footprints are to scale, and all left footprints were mirrored to fit the right ones. The color scale ranges from the lowest point (blue) to the highest point of the model (red); given the different depths in separate models, the depth of a specific color varies. (A) T2/01. (B) T2/11. (C) T2/12. (D) T2/13. (E) T2/14. (F) T2/21. (G) T2/22. (H) T2/24. Color legend scales in mm.

to our map is stretched to a degree of ca. 12%. The original numbering scheme published in *Wings et al. (2012)* is inconsistent in the T3 and I1 trackways, a result of the complex excavation process between 2009 and 2011. We therefore felt the need to develop a new consistent numbering scheme, which is already employed in *Wings, Lallensack & Mallison (in press)* for the T3 trackway. The new numbers are always notated in the form trackway/number, to avoid any confusion with the old scheme.

Definition of footprint margins: Interpretative and objective methods

The determination of the margin of a footprint can involve a problematical degree of subjective interpretation, compromising any quantitative analysis of footprint

shape (*Falkingham, in press*). This problem most drastically affects footprints that lack well-defined phalangeal pads, fade gradually into the surrounding sediment and/or show multiple edges (*Sarjeant, 1975*; *Thulborn, 1990*; *Falkingham, 2010*), which is the case in many deeper dinosaur tracks. Subjectivity equally affects both measurements and outline drawings, and both the size and shape of a footprint can differ considerably when separate approaches are employed. Previously adopted approaches range from tracing along the margin between the flat floor and the sloping wall of the footprint (minimum outline approach, *Martin et al., 2012*) to tracing at the level of the surface of the surrounding sediment (*Falkingham, 2010*). Only few studies elaborate on the criteria used to define the outlines (for exceptions, see e.g., *Pittman & Gillette, 1989*; *Belvedere, 2008*; *Martin et al., 2012*), making comparisons of published outline drawings and measurements ambiguous. Although a number of objective approaches for the definition of footprint margins exist (*Falkingham, in press*), all have practical problems and so far are rarely employed in actual studies.

All interpretational outlines were performed by one of us (JNL) in order to avoid interobserver variability. In order to reduce subjectivity in our interpretational outlines, we followed three criteria, namely the steepest slope, a consistent elevation, and the maximization of digit length. To achieve the latter, the most proximal slope of the sediment bar separating the digit impressions is interpreted as the hypex point when multiple slopes are present. As all three criteria cannot be completely fulfilled at the same time, a "best guess" approach was adopted, attempting a best fit between all three criteria. Exceptions were made to exclude extramorphological features (T3/44; Fig. 5K) and to include partly filled digit impressions (I1/32; Fig. 7D). Despite these criteria, many decisions made in drawing the outlines were rather ambiguous. To check for an interpretational bias of our results, we defined two alternative, objective approaches to determine landmark positions, as described below.

Our first objective approach is based on the steepest slope (the turning point of the surface inclination according to *Ishigaki & Fujisaki (1989)*, equivalent to the inflection point) of the footprint wall, henceforth called the steepest slope approach. The steepest slope is probably the most frequently used criterion for the definition of the margin of a track, although its determination by the naked eye of the observer usually is subjective (*Ishigaki & Fujisaki, 1989*). Implementing this criterion, we consequently selected the middle one of the three most closely spaced contour lines along the digital and hypex axes, respectively. To avoid that ripple marks of the surrounding sediment are traced rather then the footprints, only the lower two thirds of the 30 contour lines were used. Our second objective approach employs a specific contour line, and henceforth is dubbed the contour line approach. Since various methods for the three-dimensional digitalization of footprints have become available to ichnologists, contour lines have been repeatedly used instead of traditional interpretational drawings in order to reduce subjectivity (e.g., *Petti et al., 2008*; *Falkingham, 2010*; *Romilio & Salisbury, 2014*). In our approach, we placed landmarks on the intersection of the contour line with the digital and hypex axes in all of the tracks. Only the 11th and 12th contour lines were able to capture the complete outline in all T3

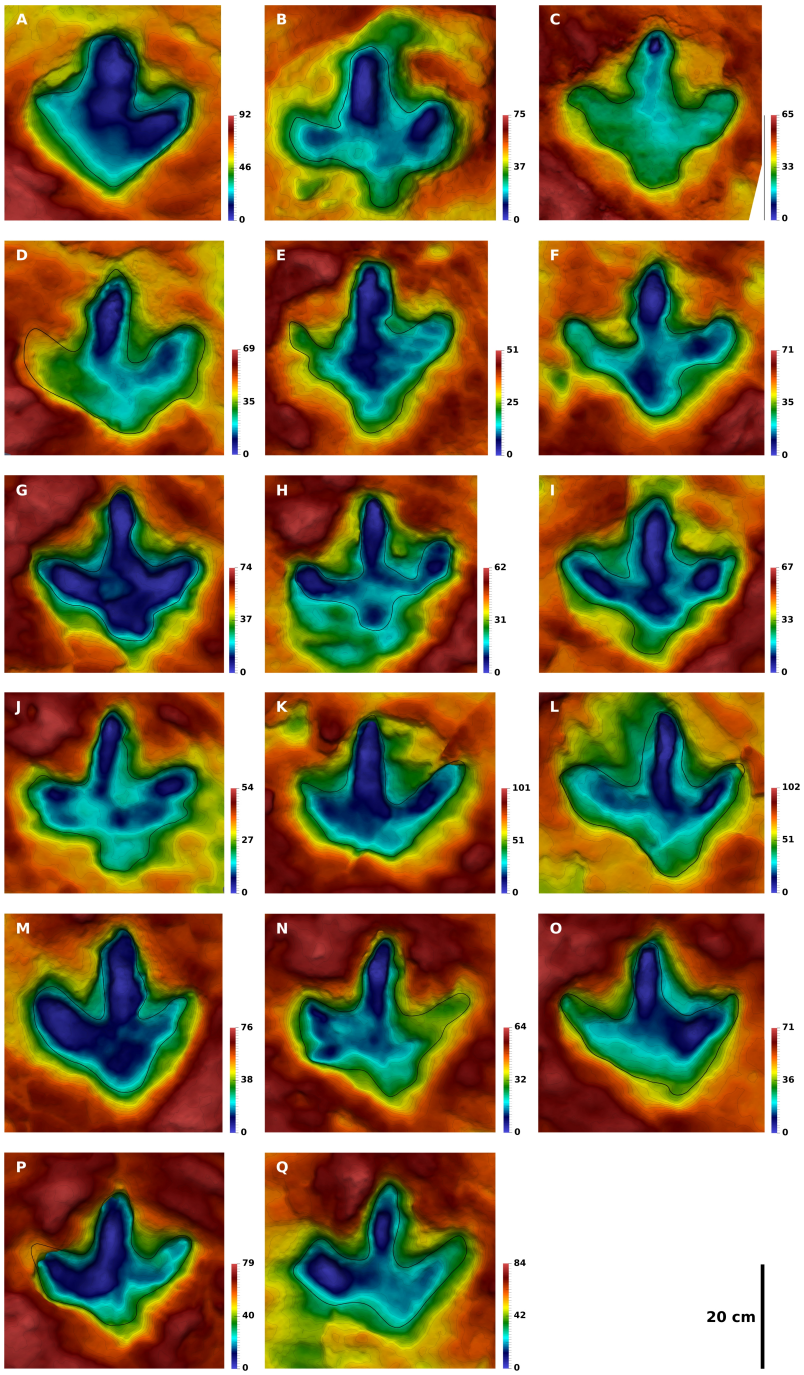

Figure 7 Contoured depth-color images with interpretative outlines of the 17 footprints of the I1 trackway analyzed herein. All footprints are to scale, and all left footprints were mirrored to fit the right ones. (A) I1/17. (B) I1/30. (C) I1/31. (D) I1/32. (E) I1/35. (F) I1/36. (G) I1/38. (H) I1/39. (I) I1/40. (J) I1/41. (K) I1/45. (L) I1/46. (M) I1/48. (N) I1/49. (O) I1/50. (P) I1/52. (Q) I1/53. Color legend scales in mm.

footprints selected for geometric morphometric analysis; the analysis was executed for both. Both objective approaches were performed on the T3 footprints.

An interpretational outline drawing usually aims to reproduce the anatomy of the trackmaker's foot as best as possible, while minimizing the influence of intratrackway variability. The objective approach showing the lower overall variability of the landmark positions is therefore less influenced by intratrackway variability. This more repeatable approach was then equally performed on the T2 and I1 trackways (Figs. S1 and S2), and the results compared with those based on the interpretational outlines.

Trackway parameters and traditional morphometrics

Trackway parameters (i.e., the pace and stride lengths, pace angulation, and footprint rotation) were calculated from xy-coordinates taken from photogrammetric data by employing trigonometric functions. The measurement of trackway parameters requires the selection of a homologous reference point on the footprints. To analyze the influence of reference point choice on the measured values, we measured all trackway parameters twice, once with the tip of digit impression III and once with the base of digit impression III as reference point. In practice, the reference point on the base of digit impression III is difficult to measure in the more poorly preserved footprints (*Thulborn, 1990*). To obviate this problem, we measured the free length of digit impression III in a well-preserved footprint of the given trackway. Then we determined the position of the reference point in all footprints of that trackway according to the distance measured in the well preserved footprint from the tip of digit impression III down the footprint long axis (Fig. 8). Unless noted otherwise, all trackway parameters and speed estimates given below are based on coordinates determined by this procedure.

Footprint mean shapes of all three trackways were measured according to *Moratalla, Sanz & Jimenez (1988)*, in order to determine the ability of traditional measurements to discriminate between theropod and ornithopod footprints (Fig. 8). Hip height of the trackmakers was assumed to equal 4 times footprint length, following *Alexander (1976)*. Despite its simplicity, this relationship was shown to be the most accurate of various approaches (*Henderson, 2003*). The approximate body length of the theropod trackmakers was calculated using the average ratio of hip height to body length proposed by *Xing et al. (2009)*, which is 1:2.63. For speed estimates, we employed the formula of *Alexander (1976)* for trackways with a S/h (relative stride length) of < 2.0:

$$v \approx 0.25 g^{0.5} S^{1.67} h^{-1.17}$$

where v = locomotion speed $[m/s]$, g = gravitational constant (9.81 m/s^2), S = stride length $[m]$, and h = hip height $[m]$.

Geometric morphometrics

For the geometric morphometric analysis, six landmarks were defined (Fig. 8A). Landmarks 1, 3, and 5 are located at the tips of the digit impressions (i.e., the ends of the digital axes of digits II, III and IV, respectively). Landmarks 2 and 4 represent the hypex positions (i.e., the midpoints between digit impressions II and III, and III and IV). Landmark 6 is located on the heel and defined as the intersection of the footprint long axis with the proximal heel

margin. The footprint long axis corresponds with the axis of digit impression III, following *Leonardi (1987)*. Given the straight morphology of digit III in the examined footprints, the mediolateral position of landmark 6 also roughly corresponds to the midpoint of the footprint when measured between digit impressions II and IV. All landmark placements were performed by one of us (JNL), in order to avoid interobserver variability.

The six landmarks were digitized for each outline using the freeware tpsDig 2.17 (*Rohlf, 2014*). In order to calculate detailed mean shapes, six curves of equally spaced semi-landmarks were placed along the outline using tpsDig, each connecting two adjacent landmarks. To allow for an equal distribution of the semi-landmarks across all six curves, the number of semi-landmarks was calculated for each curve by measuring the relative lengths of each curve for each outline. These measurements were done using the "Measure Path" function in Inkscape. In total, 114 semi-landmarks were used for the T2 and T3 and 101 for the I1 outlines. The curves were converted to regular landmarks using tpsUtil 1.85 (*Rohlf, 2014*) and subjected to Generalized Procrustes Analysis (GPA) in the open source software MorphoJ 1.06c (*Klingenberg, 2011*). The GPA is a statistical analysis that provides a best fit between the footprint shapes by translating, rotating and scaling, eliminating any information but the mere shape of the footprints. GPA was shown to be the most accurate of several approaches for the estimation of mean shapes (*Rohlf, 2003*). We did not slide the semi-landmarks as part of the GPA, as we regard the curve as the unit of homology, not the individual semi-landmark. Vector plots were created using tpsRelw 1.54 (*Rohlf, 2014*), in order to illustrate the variability along the outline of the Procrustes mean shape, the average shape of all analyzed footprints. The vector arrows originating from each landmark and semi-landmark of the mean shape illustrate the deviations of each of the individual outlines.

It can be argued that the scaling step of the GPA is undesirable when calculating footprint mean shapes for single trackways, as all footprints stem from the same individual. Testing the influence of scaling, the digitized landmarks and semi-landmarks of the T3 footprints were imported into the open source software PAST 3.01 (*Hammer, Harper & Ryan, 2001*), which provides an option for rescaling the individual outlines to their original sizes after performing the GPA. The coordinates of the resulting mean shape then were imported into MorphoJ and compared with the standard GPA mean shape. The Procrustes distance between both shapes is negligibly small, accounting for $3.62 \cdot 10^{-6}$. For comparison, the Procrustes distance between the T3 and I1 mean shape is as high as $6.1 \cdot 10^{-3}$. GPA, therefore, can be used instead of a partial Procrustes analysis (which retains the original size), even though the deviation can be expected to be greater in small sample sizes and with very large variability in footprint shapes.

Principal component analyses (PCA) were carried out using MorphoJ to assess co-variation of separate footprint regions. Only the six landmarks were used, not the semi-landmarks, in order to reduce noise. Separate analyses were performed for each trackway, revealing trackway-specific variation patterns and allowing for the quantification of the variability of individual landmarks. The calculated Procrustes mean shapes were imported into MorphoJ in order to make use of the warped outline drawing function, allowing for a better visualization of shape deformations. An additional PCA incorporates all three trackways in order to investigate whether PCA is capable of separating these trackways. For

all PCAs, only the first three principal components were taken into account as they describe the majority of the total variation. Furthermore, a canonical variate analysis (CVA) was carried out using MorphoJ, which again was restricted to the six true landmarks.

RESULTS

Objective methods for the definition of footprint margins

When based on interpretational outlines, the Procrustes-fitted landmarks of the selected T3 footprints show a variance of 0.027. Employing the objective contour line approach as described above, the total variance is markedly higher, accounting for 0.0453 for the 12th and 0.0457 for the 11th contour line. This higher variance suggests an increased influence of substrate properties and behavior on the individual outlines. The steepest slope approach resulted in a total variance of 0.0379, and therefore falls between the interpretational and the contour line approach. Of both objective approaches, the steepest slope approach is therefore least affected by intratrackway variability.

Results from the objective steepest slope approach for all three trackways were then compared with those of the interpretational approach. For the two theropod trackways, landmark positions of both approaches are reasonably close to each other in most cases, with few outliers. Consequently, the recorded shape changes are very similar, with notable differences occurring only in PC2. In PC1, both approaches show an anterior shift in the position of the heel together with a posterior shift in the position of the lateral hypex, while other landmarks are rather stationary (Fig. 12, Fig. S2). In the steepest slope approach, PC1 describes 53% in the T3 and 66% in the T2 trackway, which is higher than in the interpretative approach (46% and 55%, respectively; Fig. 11, Fig. S1).

For the I1 footprints, landmark positions of both approaches differ markedly in many examples (Fig. S2). Particularly large differences occur in the position of the hypices; in many I1 footprints, both a proximal and a distal slope, often separated by an extensive plateau, can qualify as a landmark position. Consequently, the resulting mean shape of the steepest slope approach is less well defined, with the hypex positions located more distally, significantly reducing the free length of the digit impressions. In two footprints (I1/49, I1/32), partially filled digit impressions caused the steepest slope approach to drastically underestimate digit lengths. Despite these differences in landmark placement, PC1 and PC2 of both the steepest slope and the interpretative approach concur that the lateral hypex and the heel do not show an increased variability, in contrast to the theropod footprints. However, PC1 of the steepest slope approach shows a pronounced proximal displacement of the position of the medial hypex, in contrast to the interpretative approach. Again, the eigenvalue of PC1 is higher in the steepest slope approach, amounting to 33%, compared to 28% in the interpretative approach. PC2 describes 30% of the total variability in the steepest slope approach; as in the interpretative approach, this value is only slightly smaller than that of PC1.

Qualitative and quantitative description of footprint shapes

Trackway T3. Traditionally, footprint morphology is often assessed by describing and illustrating the best preserved or most representative footprints of a sample (*Thulborn,*

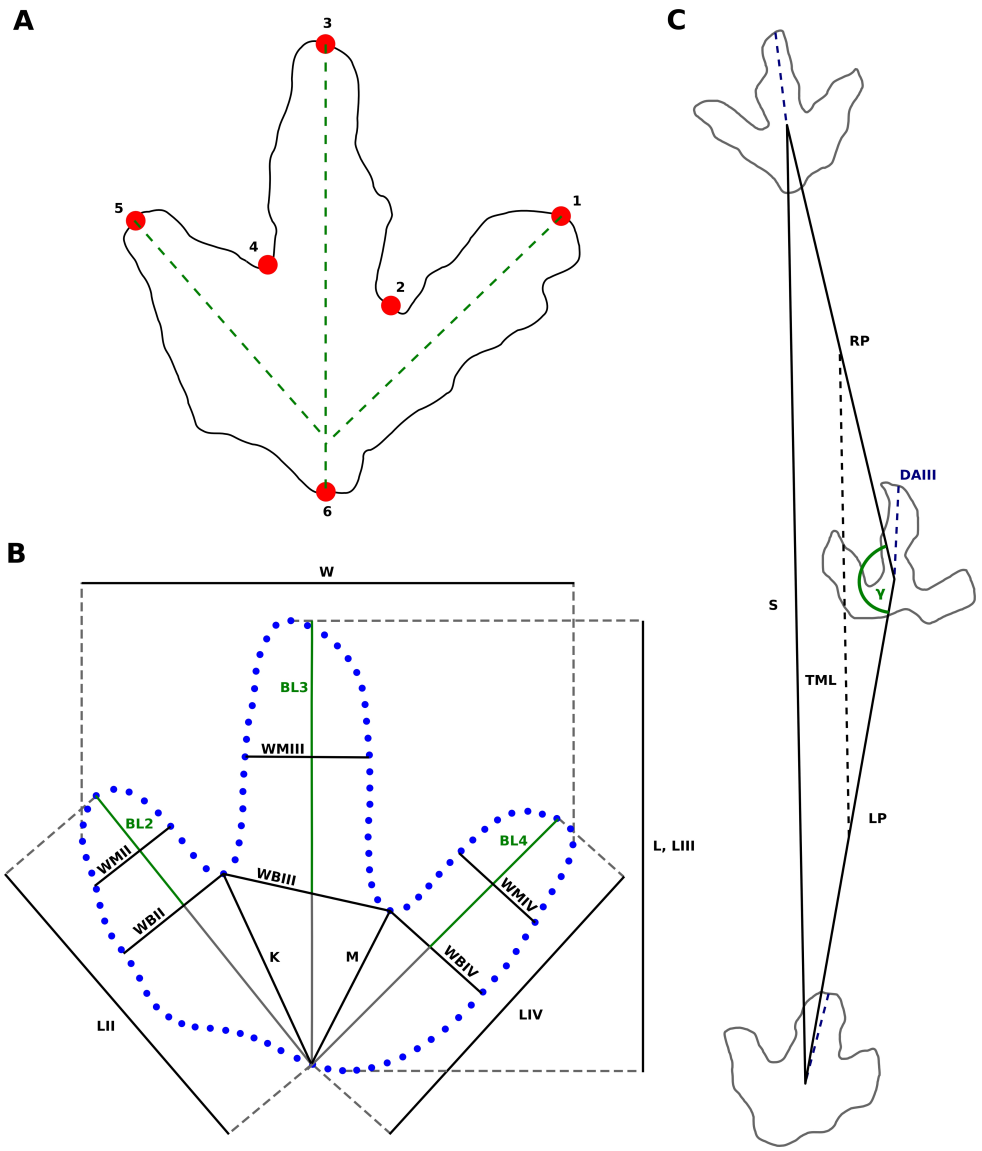

Figure 8 Landmarks and measurements of footprint shapes used in this study, exemplified on the T3 trackway. (A) Footprint sketch indicating landmark placement. Landmarks 1, 3, and 5 represent the tips of the digit impressions and are placed at the endpoints of the digital axes of digit impressions IV, III, and II, respectively. Landmarks 2 and 4 represent the hypex positions, and are placed at the midpoints between digit impressions III and IV and II and III, respectively. Landmark 6 captures the heel, and is defined as the intersection of an extension of the digital axes of digit impression III with the outline. (B) The measuring scheme proposed by *Moratalla, Sanz and Jimenez (1988)*, applied to the T3 mean shape, adapted from *Moratalla, Sanz and Jimenez (1988)* and *Romilio and Salisbury (2011)*. Measurements are done in order to determine the ability of traditional measurements to differentiate between the theropod and ornithopod footprints analyzed herein. Deviations from the original scheme are discussed in the text. Abbreviations: L, footprint length; W, footprint width; K, M, heel-interdigital distances; LII–IV, digit lengths; BL2–4, basal digit lengths (digit free lengths); WBII–IV, basal digit widths; WMIII-IV, middle digit widths. (C) Measured trackway parameters. Reference points (continued on next page…)

Figure 8 (…continued)
for the pace- (LP, RP) and stride (S) lengths are determined by measuring a fixed distance down the axis of digit impression III (DAIII), reducing the influence of variation in footprint rotation, as discussed in the text. The trackway midline (TML) is parallel to the opposing stride of the footprint in question. Pace angulation (γ) is the angle between the left and right paces, and footprint rotation is the angle between the axis of digit impression III and the opposing stride.

1990). In the T3 trackway, footprint morphology is best seen in the well preserved natural cast of T3/18 (Fig. 3). With a length-to-width ratio of 1.08, this footprint is only slightly longer than wide even when the weakly impressed metatarsophalangeal pad of digit IV is taken into account. The interdigital angle between digit impressions III and IV (43.5°) is larger than that between digit impressions II and III (33.7°). Digit IV is impressed along its whole length, although only the part proximal to the metatarsophalangeal pad is deeply impressed, with the metatarsophalangeal pad appearing very shallow. The deeply impressed part is similar in proximal extension to that of digit impression II; digit impression III is much shorter proximally. Three well defined phalangeal pads are present in digit impression IV. On digit II and III, the phalangeal pads are deformed obliquely, and are not readily distinguishable. Digit impression IV is more narrow than the other two digit impressions, which are similar in width. Digit impression III is the deepest, particularly in its distal part; digit impressions III and IV are connected with each other at their bases, while digit impression II appears isolated. Distinct claw marks are present in all three digit impressions, but vary greatly in size and position. The claw mark of digit impression II is the largest, being located lateral to the digital axis and slightly curved medially. In digit impression III, the claw mark appears much shorter, is located medial to the digital axis and curved towards the medial side. The claw mark of digit impression IV is less well pronounced, being located lateral to the digit axis. Claw marks of digits II and IV are thus strongly asymmetric in their position. The heel region is V-shaped, with a slight medial indentation below the base of digit impression II.

We subjected 13 selected natural molds to a geometric morphometric analysis. The resulting mean shape, although based on footprints of a generally lesser quality than the natural cast of T3/18, is a very informative quantification of footprint shape, as intratrackway variability is leveled out. In the molds, digital pad impressions are frequently preserved, but only in few footprints a nearly complete set is discernible (best seen in T3/26, Fig. 5B). In most footprints the pad impressions are interior topographical features that do not contribute to the traced outline, and thus do not contribute to the mean shape. This often leads to a steplike topography, where a maximization in the steepness of the slope delimits the footprint extents, and a second maximization in the steepness delimits the digital pads. The position and orientation of the deeply impressed bottom of the digit impressions does not always correspond to the traced footprint margins (Figs. 5A, 5C, 5D and 5I). In footprint T3/34 (Fig. 5D), the deeply impressed bottom of digit impression III even appears to follow an arc, while the traced outline of this digit is relatively straight. This might be attributed to foot movements, indicating that the latter have a great influence on the shape of the footprint.

The T3 mean shape is wider than long (length-width ratio: 0.92), a consequence of the incomplete or lacking impression of the metatarsophalangeal pad of digit impression IV in most of the footprints. In comparison with the natural cast of T3/18, the heel is much broader and more asymmetrically shaped, with the lateral bulge protruding beyond the medial bulge. The mean shape is dominated by the robust digit impression III, which is significantly longer and wider than the impressions of digits II and IV. The free length of digit impression III accounts for 61% of the total length of the shape. The digit impressions are straight, and indentations indicating phalangeal pads are not clearly visible. The apex of digit III, marking the position of the claw mark, is located medially to the digital axis, giving the digit impression an asymmetrical shape, with the lateral margin of the distal half forming a broad arc. The distal end of digit II appears to be symmetrical, while the distal end of digit IV shows an apex laterally to the digital axis, inverting the condition seen in digit III. The lateral hypex is located posteriorly relative to the medial hypex; accordingly, the free length of digit IV is greater than that of digit II. The depth of the selected footprints varies from 38 to 72 mm, with a mean of 51 mm and a coefficient of variation of 0.17. A significant correlation between maximum footprint depth and footprint shape could not be observed, which might be due to the limited sample size.

Trackway T2. The well preserved natural cast of T2/22 may be regarded as one of the best preserved ichnites known from the T2 trackway. This footprint shows a length-width ratio of 1.23. Digital pads are indistinct in most footprints, although T2/22 probably shows two pads in digit impression II and four pads in digit impression IV, including the metatarsophalangeal pad. Digit impression III of the mean shape shows a slight constriction at around half of its free length, possibly delimiting the two distalmost phalangeal pads of this digit. The T2 mean shape, which is based on eight selected footprints, is only slightly longer than wide (length-width ratio: 1.04), due to the incomplete impression of the heel in most footprints. It is more gracile in appearance compared to the T3 mean shape, mostly due to the slender and elongated digit impression III. Digit widths are similar in all three digits, unlike the T3 mean shape where digit III is wider. Digit III is substantially longer than digits II and IV; its free length accounts for 64% of the total footprint length, similar to the T3 mean shape. Digit II is longer than digit IV and shows a slight medial bend at midlength, while the distal end is symmetrical. Digit III is straight. Claw marks of digit III are either located centrally (e.g., T2/1) or medial with respect to the digital axis (e.g., T2/4, Fig. 3). In the mean shape, the medial tendency of the claw mark is recorded by the asymmetrical morphology of the tip of digit III, although this asymmetry is less pronounced than in the T3 mean shape. Digit IV is straight, with the apex of the distal end being located laterally to the digital axis, suggesting a lateral position of the claw mark. This lateral position is best seen in the well preserved cast of T2/4 (Fig. 3). The hypices do not show any offset, unlike the T3 mean shape. The maximum depth of the selected footprints varies between 29 and 59 mm, with a mean of 36 mm and a coefficient of variation of 0.27. Thus, the depth is more variable than in the T3 trackway. Digit III usually represents the most deeply impressed part of the footprints.

Trackway I1. While the overall footprint proportions remain similar within the I1 trackway, shape varies considerably. A representative footprint is difficult to designate, but I1/36 (Fig.

7F) might show the best approximation of the trackmaker's anatomy, given the degree of detail shown by this footprint. The following description is based on both this footprint and the mean shape. The length-width ratio of the mean shape is 0.91. The heel, rather than digit impression III, is the most prominent feature of the shape. Digit impression III is the longest digit, but the difference in length between digit III and digits II and IV is not as great as in the theropod footprints. Its free length accounts for only 48% of the total footprint length, less than in the theropod footprints. Digit impressions II and IV are both bended anteriorly, resulting in a crescent-like shape. At their bases, digit impressions II and IV protrude nearly horizontally from the heel region in the mean shape. Their posterior margin shows a pronounced kink at about midlength, resulting in a more anteriorly directed distal half of the digits. The bend in the anterior margin is less pronounced. The apex of digit impressions II and IV is located laterally and medially to the digital axis, respectively. Thus, the posterior margins of the distal thirds of both digit impressions are rounded, while the anterior margins are more straight. Digit impression III is straight and slightly tilted laterally; its apex tapers to a blunt ungual mark. The anteroposterior position of the lateral and medial hypex is equal. The heel shows a broad semicircular extension, which is separated from the bases of digits II and IV by an embayment on either side of the footprint. The semicircular extension is shifted laterally relative to the remainder of the shape. The footprints are similar in depth to the T3 footprints, varying from 41 to 77 mm in depth, with a mean depth of 55 mm and a coefficient of variation of 0.19.

Comparison of mean shapes. Two additional GPAs were performed to compare the T3 mean shape with the T2 and I1 mean shapes (Fig. 9C). The strongest shape difference between the T2 and the T3 mean shape occurs in digit impression III. In the T3 mean shape, this impression is both shorter and broader, with the main difference in width occurring on the medial margin. Thus, digit impression III is located more closely to digit impression II than to IV in the T3 shape, while the reverse is true for the T2 shape. This medial thickening of digit impression III in the T3 shape seems to be directly associated with a more anterior position of the medial hypex. The asymmetry of the termination of digit impression III is more pronounced in the T3 mean shape. Digit impression II is shorter in the T3 shape, while digit impression IV is laterally expanded on its distal end. The heel is best defined in the T2 shape and is more leveled in the T3 shape. The greatest difference between the T3 and I1 shapes (Fig. 9B) can be seen in the heel region. In the T3 shape, the heel shows two distal pads separated by a central embayment, with the lateralmost pad being located more proximally than the medial one. In the I1 shape, one single large heel pad is present, which on both sides is separated from the digit impressions by an embayment. Furthermore, the interdigital angle between digit impressions II and III is smaller in the T3 shape than in the I1 shape. The distal end of digit III is asymmetrical in the T3 shape, but symmetrical in the I1 shape, and the lateral hypex is placed more posteriorly in the T3 shape.

Variability of footprint shape

Variability in the heel. The heel region is highly variable in the T3 footprints in both extension and morphology. In the well preserved natural cast T3/18, the heel is fully

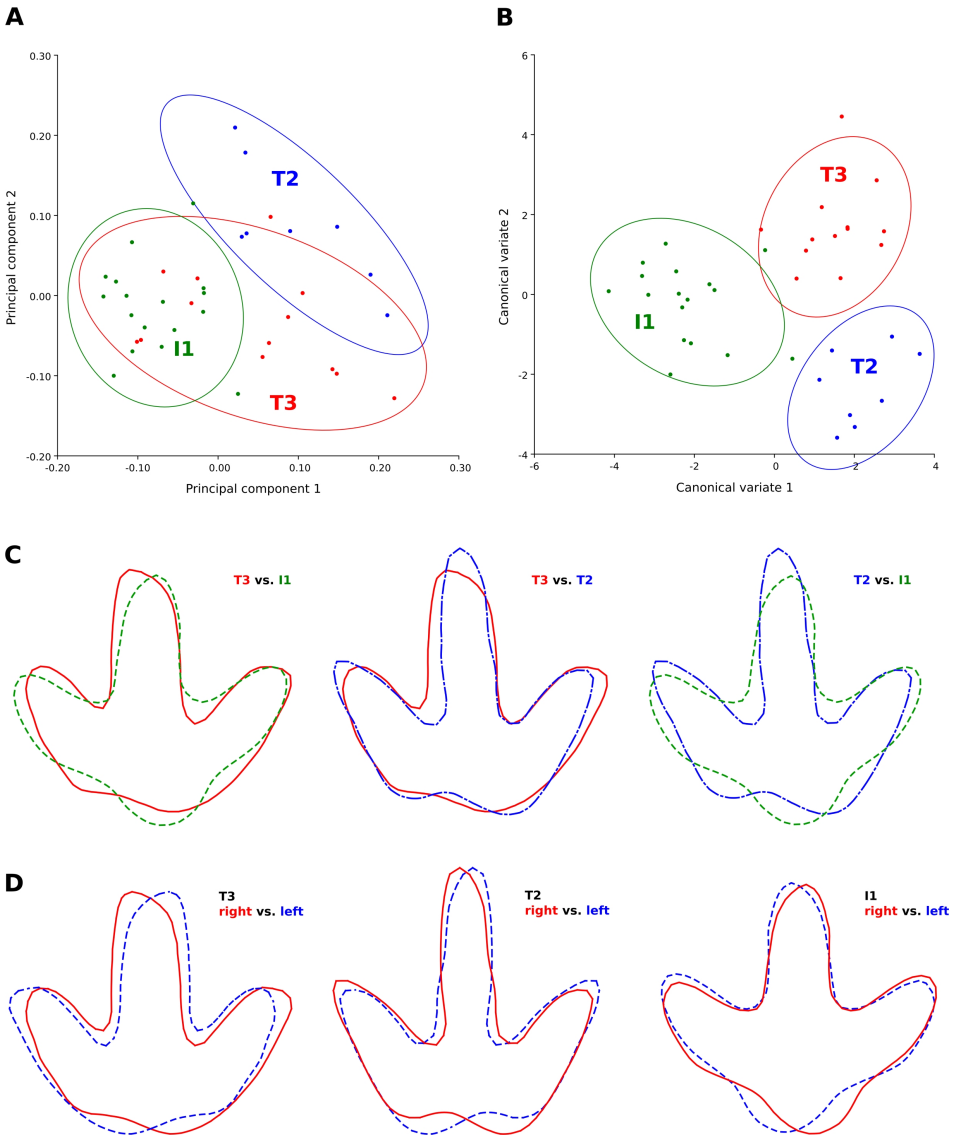

Figure 9 Discrimination between the footprint shapes of the T3, T2, and I1 trackway. (A) Principal component analysis (PC1 vs. PC2) of the T3 (red), T2 (blue) and I1 (green) shapes based on six landmarks. 90% confidence ellipses are shown for each point cloud. High loadings on the first principal component indicate a more posterior position of the lateral hypex and a more anterior position of the heel landmark, while high loadings on the second principal component indicate a more slender footprint and a more posteriorly located medial hypex. (B) Canonical variate analysis (CV1 vs. CV2) of the T3, T2, and I1 shapes based on six landmarks. The best separation between the ornithopod and the theropod trackways is reached by CV1, high values of which describe a more posterior placement of the hypices, a more anterior position in the heel, and an anteriorly extended digit impression III. Coloring and confidence ellipses as in (A). (C) Procrustes-fitted mean shapes, allowing for pairwise comparisons (T3 vs. I1, T3 vs. T2, and T2 vs. I1). The T3 shape is shown in a continuous red line, the T2 shape in a blue dashed line with alternating short and long segments, and the I1 trackway in a dashed green line. Note that the shapes, while visually distinct, are very similar in their proportions. (D) Procrustes fitted pairs of mean shapes (continuous red line) and their respective mirror images (dashed blue line), highlighting footprint asymmetry. Note the pronounced asymmetry in the I1 ornithopod mean shape.

impressed, showing a V-shaped morphology with an rounded proximal apex representing the metatarsophalangeal pad of digit IV (*Farlow et al., 2000*). This pad shows a slight lateral displacement relative to the axes of digit impression III; the medial side of this footprint features a weakly pronounced indentation directly below the proximalmost phalangeal pad of digit II. The impression of the metatarsophalangeal pad is significantly shallower than the phalangeal pads. Several of the natural molds show a similar morphology (T3/26, T3/40, T3/43–44, T3/46–48). In these footprints, the metatarsophalangeal pad can be located more centrally (T3/26, T3/43) or more laterally (T3/40; T3/47) with respect to digit impression III. In T3/47, the proximal part of digit II is not impressed, resulting in a very pronounced medial indentation. In the remaining footprints, the metatarsophalangeal pad of digit IV is not or only partly impressed, resulting in a foreshortened footprint with a broader rather than V-shaped heel. In some examples (T3/23, T3/39), both digits II and IV are shortened proximally to an equal degree, maintaining the asymmetry typical for theropod footprints. In other examples (T3/29, T3/36), digit II is fully impressed and more extensive than digit IV, which is shortened proximally, reversing the asymmetry seen in most of the other footprints. Finally, the shortest footprints result from incomplete impressions of both digits II and IV (T3/35, T3/37, T3/45). Most frequently, this results in a sub-symmetrical, bilobed morphology with a central indentation below digit impression III. These variations in the extent and shape of the heel strongly influence any associated measurements; for example, the coefficient of variation for footprint length is as high as 0.1 in the 13 analyzed T3 footprints, while it is only 0.04 for footprint width in the same footprints.

The heel is poorly impressed in most T2 footprints. In well preserved examples with pronounced phalangeal pads, the metatarsophalangeal pad is slightly displaced laterally relative to digit impression III, while digit impression II is distinctly shorter than digit impression IV, resulting in a very pronounced, step-like medial concavity. In the majority of footprints, the metatarsophalangeal pad is not or only partly impressed, shortening the impression of digit IV. When this pad is absent, proximal extension is similar in digit impressions II and IV; in this case, the medial concavity has transformed into a central concavity below digit III, giving the rear margin of the footprint a bilobed, subsymmetrical appearance. Few footprints show an extended, U-shaped heel impression, without any indication of a medial concavity.

Landmark analysis indicates that the extension of the heel is relatively stable in the I1 footprints. However, position and morphology can vary considerably. Typically, the heel pad forms a subcircular impression separated from the digital pads by a lateral and medial indentation, as shown by the I1 mean shape. In the individual footprints, the heel can appear V-shaped (I1/17, I1/53) or broadly rounded (I1/45, I1/50, I1/32, lacking the medial and lateral indentations. At the other extreme, the heel pad can be sub-rectangular in shape, with its lateral and medial sides forming angles of almost 90° to the impressions of digits IV and II, respectively (e.g., I1/28, I1/30). The position of the heel pad varies from being located centrally I1/31, I1/48) to strongly laterally (e.g., I1/30, I1/49, I1/53) with respect to digit impression III.

Variability in the digit impressions. In the T3 trackway, digit impressions are generally straight. An exception can be seen in T3/47 (Fig. 5M), where digit impression IV appears to be bowed laterally. Digit impression III is frequently widened; in T3/36, the absolute width of digit III exceeds that of the preceding footprint (T3/35) of more than 50% (Figs. 5E and 5F). Claw positions vary greatly. The well preserved natural cast of T3/18 shows a massive digit impression II with a subrectangular termination featuring a large claw mark located laterally with respect to the digital axis. This morphology is seen in several additional some footprints (best seen in T3/39). In other footprints (e.g., T3/39, T3/40, T3/26; Figs. 3 and 5), the claw mark can be located centrally, creating V-shaped digit terminations reminiscent of those recently described for the ichnogenus *Bellatoripes* (*McCrea et al., 2014*). In yet other footprints, the claw mark of digit II is located medially to the digital axis (best seen in T3/37, Fig. 5G). In digit impression III, the claw mark usually is located medial to the digital axis, but frequently is located centrally. In digit impression IV, the mean shape indicates a preferred claw mark location lateral to the digital axis.

In contrast to the T3 footprints, several of the digit impressions in the T2 trackway are very narrow and irregular slit-like, most strikingly digit III in T2/21 (Fig. 6F). Variability and position of the claw marks is similar to that observed in the T3 trackway. The T2 mean shape mirrors the condition seen in the T3 mean shape, with a medial tendency in the tip of digit impression III and a lateral tendency in the tip of digit impression IV, resulting either from the foot kinematics or preferred claw orientations. Exceptionally preserved claw impressions can be seen in digit impression III of the natural cast of T2/4 (Fig. 3A), where it is located medial to the digital axis, and T2/1 (Fig. 6A), where it is located centrally.

Variability in digit impression morphology and dimensions is particularly striking in the I1 trackway. The width of digit impression III at mid-length ranges from 14% (I1/38; Fig. 7G) up to 33% (I1/17; Fig. 7A) of footprint width. Digit impressions II and IV are generally rather narrow, with an abrupt bend at around midlength, as shown by the mean shape and the well preserved footprint I1/36 (Fig. 7F). In other footprints of this trackway, these digit impressions can be narrow and straight, lacking the bend (best seen in I1/45, Fig. 7K). These impressions can also appear short and thick, approaching a cloverleaf-shape (e.g., I1/17 and 30, Figs. 7A and 7B). The outer margin of digit impressions II and IV can display two pronounced steps, the first resulting from the subrectangular heel impression and the second from the bend at the midlength of the digit impression (e.g., I1/30, 31 and 36; Figs. 7B, 7C and 7F). In other footprints, the same margin can appear as a straight line (e.g., I1/17, 45 and 53; Figs. 7A, 7K and 7Q).

Quantification of footprint shape variability. Landmark analysis was carried out on the selected footprints of all three trackways. Vector plots are used to illustrate the deviations of the Procrustes-fitted landmark and semi-landmark coordinates of the individual footprints from the respective coordinates of the mean shape. For the T3 footprints, the vector plot indicates a high variability in the lateral hypex, in the entire posterior margin of the heel region, and in the medial hypex (Fig. 10A). Digit shape, on the other hand, appears to be comparatively stable. The vector plot of the T2 shape reveals a high variability in the lateral hypex and in the right half of the heel region (Fig. 10B). Digit width also appears to be very variable. The I1 vector plot, on the other hand, indicates that the variance is more equally

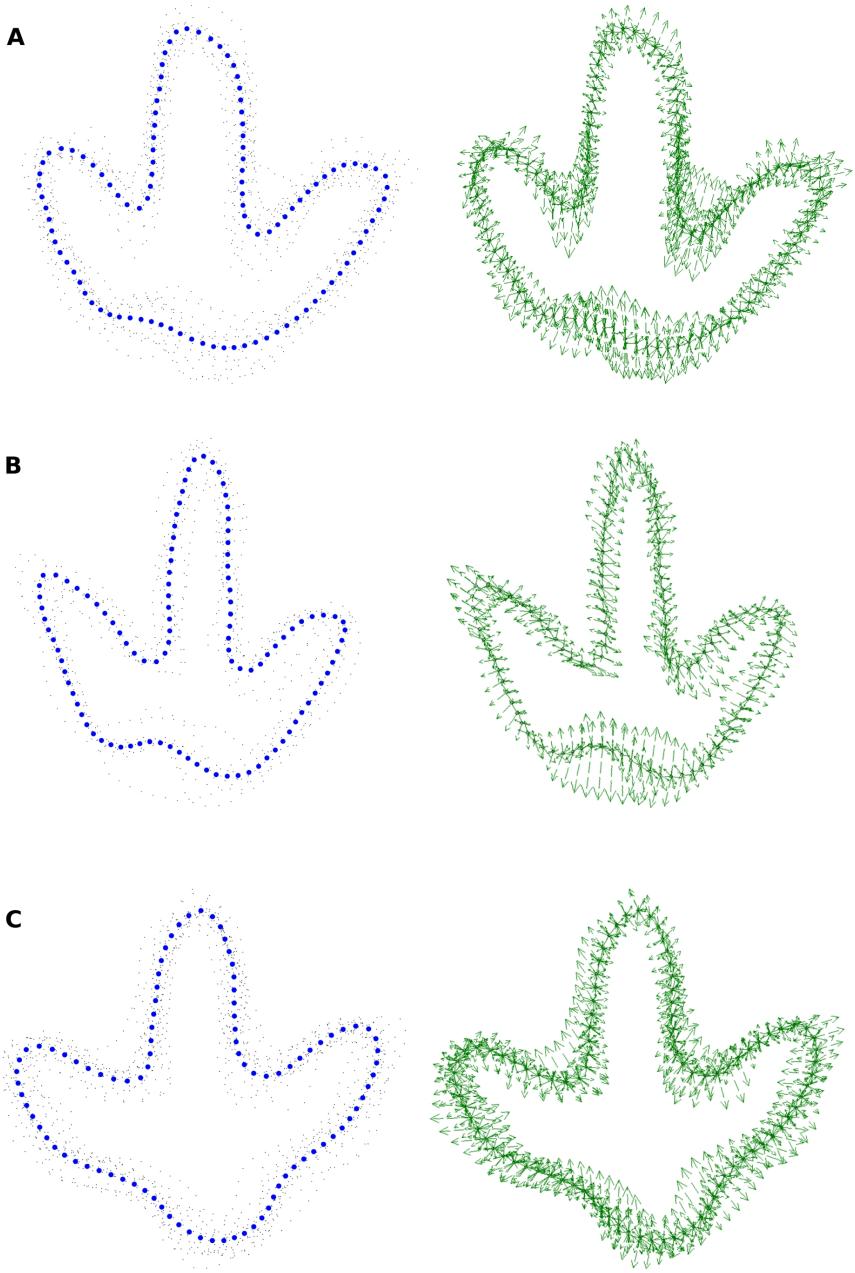

Figure 10 Procrustes-fitted coordinates of the analyzed trackways. On the left-hand side, the mean shape is indicated by thick blue dots and the individual outlines as small black dots. On the right hand side, the variability relative to the mean shape is indicated by vector arrows. (A) Trackway T3. (B) Trackway T2. (C) Trackway I1.

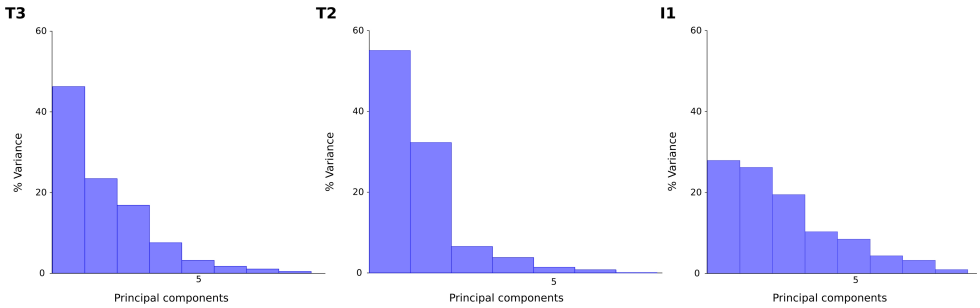

Figure 11 Loadings of the principal components of the T3, T2 and I1 trackways. For the two theropod (T3 and T2) trackways, most of the variation is explained by the first principal component. For the ornithopod (I1) trackway, on the other hand, variability is more equally dispersed amongst the principal components as no clear variation patterns are discernible.

distributed along the outline, lacking variation hotspots in the hypex and heel as seen in the theropod footprints (Fig. 10C).

Further statistical analyses are based only on the six landmark points, while semi-landmarks are not used. Direct comparison of landmark variances confirms observations made based on the vector plots (Fig. 13). In the T3 outlines, variance is most unevenly distributed among the landmarks, with major variation occurring in the lateral hypex, and, to a lesser degree, in the heel and in the medial hypex. In the T2 landmarks, variance is highest in the lateral hypex and the heel, while the variance in the medial hypex is on par with the variance of landmarks 3 and 5. Amongst the I1 landmarks, variance is more evenly distributed, with the greatest variance seen in the lateral hypex and the lowest variance seen in the middle digit. The variance in the heel is a bit below the average variance of all six landmarks.

The principal component analysis of the T3 outlines reveals a high loading on the first principal component, which describes 46% of the total variance (Fig. 11). The main shape change in PC1 occurs in the lateral hypex (landmark 2), which is shifted posteriorly relative to the mean shape, and in the heel point (landmark 6), which is shifted anteriorly (Fig. 12). PC2, accounting for 23% of the total variance, mainly describes the variation in the medial hypex, which is shifted anteriorly compared to the mean shape. PC3, describing 17% of the variance, describes a somewhat reduced digit divarication. For the T2 outlines, PC1 accounts for 55% and PC2 for 32% of the total variance. Thus, 87% of the total variance can be described by the first two PCs (Fig. 11). In PC1, the lateral hypex is shifted posteriorly while the heel point is shifted anteriorly, closely resembling PC1 of the T3 outlines (Fig. 12). PC2 shows shape changes in the tips of digits II and III. The remaining PCs were disregarded as they slowly level out, forming a plateau. The I1 outlines show low loadings on the first PCs, with 28% of the total variation described by PC1, 26% by PC2 and 19% by PC3 (Fig. 11). Variation patterns are less clear, with the main variation of the heel point being described by PC1, the main variation in the lateral hypex described by PC2 and the main variation of the medial hypex described by PC3 (Fig. 12).

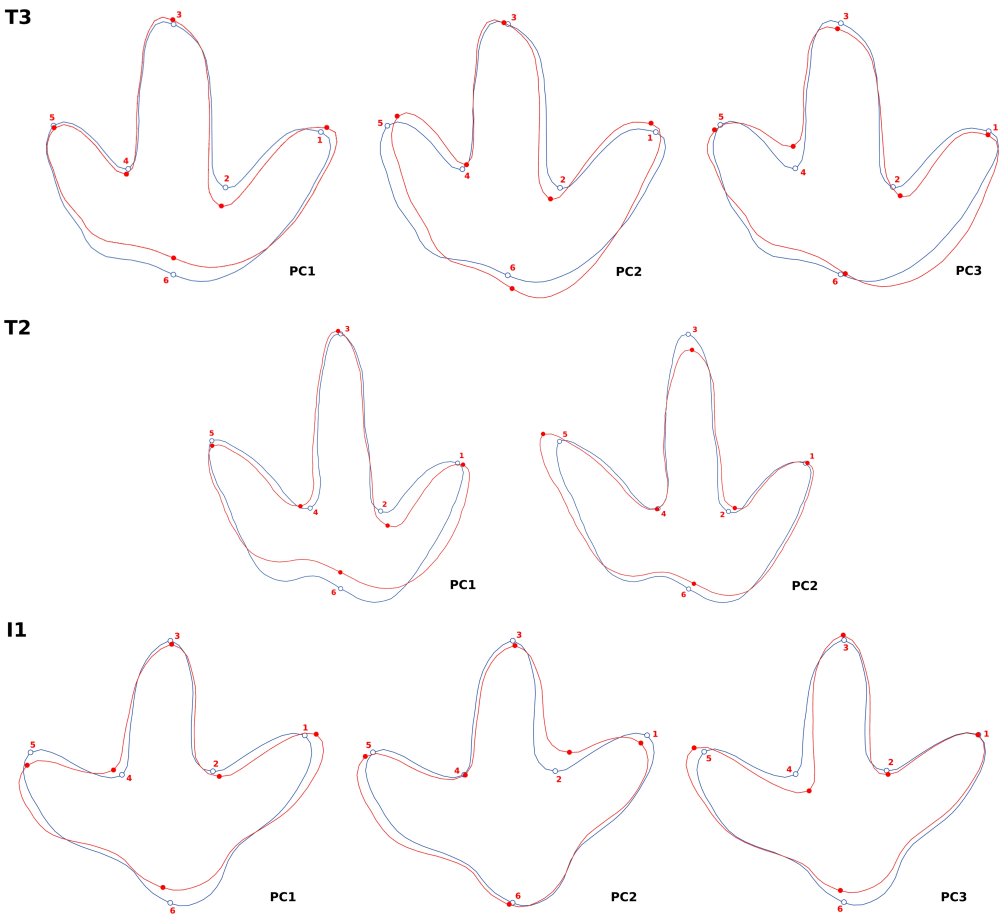

Figure 12 Warped outline drawings illustrating shape changes described by the principal components (red outlines, solid dots) relative to the mean shapes (blue outlines, hollow dots) in positive direction (scale factor: 0.1). Note that the principal component analysis was based only on the six landmarks (red and blue dots), and that the warped outline drawing connecting the dots is shown only for visualization purposes. For T2, only the first two principal components are taken into account as the third principal component only accounts for 7% of the total variation and forms a plateau with the remaining PCs, thus being uninformative.

Variability of trackway parameters

The analyzed section of the T3 trackway (T3/23–T3/48, Fig. 2) starts with a broad right turn, where it crosses the I1 trackway twice. After the second crossing, the direction of the trackway remains constant, although its course is sigmoidal. At the second crossing, footprint T3/33 appears to be stepped over I1/34, suggesting that the T3 trackway was made after the I1 trackway. The best preserved footprint (the cast of T3/18) measures 40.4 cm in length, including the metatarsophalangeal pad, translating into a hip height of 162 cm and a body length of 426 cm. The average pace length is 115 cm, and the average stride length 228 cm. Pace angulation amounts to 163° and footprint rotation to 1.7° on average. The average speed equals 1.77 m/s (6.36 km/h), with a maximum value of 1.93 m/s (6.96 km/h).

The T2 trackway (T2/1–T2/24, Fig. 2) is more straight than the T3 trackway, only showing a very slight tendency towards the left during its course. It runs sub-parallel to the

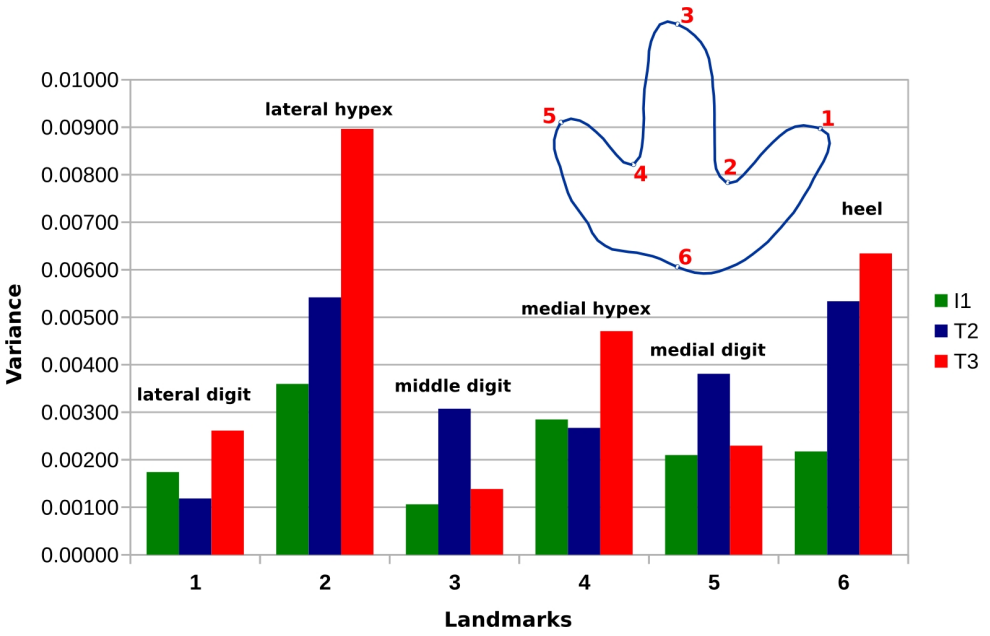

Figure 13 Bar chart showing the variance of the individual landmarks for the I1, T2, and T3 trackways. In contrast to the I1 trackway, the T2 and T3 trackways show a strikingly high variability in landmark 2 (lateral hypex) and 6 (heel).

distal two thirds of the T3 trackway. T2/18 is missing, being overstepped by the crossing I1 trackway, indicating that the T2 trackway already existed when the I1 trackmaker left its track. Thus, the T2 trackmaker probably was the first of the three animals to cross the surface. Pace lengths average at 104 cm and stride lengths at 208 cm. Footprint rotation is very weak and close to 0° on average. Foot placement in the T2 trackway is remarkable, as 12 of 19 footprints are located medial to the trackway midline, a condition henceforth called cross-over gait following *McClay & Cavanagh (1994)*. The pace angulation averages at 183°, with a maximum value as high as 193°. Most footprints lack a fully impressed heel. The completely preserved mold of T2/22 measures 29.5 cm in length, indicating a hip height of 118 cm and a body length of 311 cm. The calculated speed averages at 2.19 m/s (7.91 km/h), with a maximum value of 2.27 m/s (8.18 km/h).

The analyzed part of the I1 trackway (I1/17–I1/53) crosses the T3 trackway two times (at I1/19 and I1/34). Between the two crossings, it describes a turn to the left, after which it is continuing rather straight, crossing the T2 trackway at I1/45. As indicated by the oversteppings at the crossings, the I1 trackmaker probably crossed the surface after the T2 trackmaker, but before the T3 trackmaker. The mean footprint length of the selected footprints is 29.5 cm, suggesting a hip height of 118 cm. Pace length accounts for 66 cm and stride length for 131 cm on average. Pace angulation equals 167°, and footprint rotation −11.2°, indicating pronounced inward rotation. The speed averages at 1.02 m/s (3.66 km/h); thus, the ornithopod was progressing significantly slower than both theropods.

All three Münchehagen trackways show relatively constant locomotion speeds; the difference between maximum and minimum values accounts for 0.18 m/s in the T2, 0.31 m/s in the I1, and 0.44 m/s in the T3 trackway. Pace lengths are most variable in the I1 trackway, with a coefficient of variation (CV) of 5.70, followed by the T3 (4.13) and the T2 trackway (2.88). Likewise, stride lengths vary with a CV of 4.39 in the I1, 3.86 in the T3 and 1.76 in the T2 trackway. Variation of pace angulation is greatest in the T3 trackway, with a standard deviation (SD) of 10.78, followed by the I1 (8.00) and T2 (5.94) trackways. Footprint rotation is slightly more variable in the I1 (SD = 8.83) than in the T3 (SD = 8.70) trackways; in the T2 trackway, SD is only 5.95.

DISCUSSION

Objective definition of footprint margins: comparison of methods

The definition of the margin of a footprint constitutes a complex three-dimensional problem. Three-dimensional surfaces can be reduced to contour maps, transforming the three-dimensional problem into an easier-to-handle two-dimensional one, greatly facilitating the definition and application of specific criteria. Although the interpretational approach employed here captured the foot anatomy more faithfully than the tested objective approaches, it may involve a problematical degree of subjectivity. Thus, results of any subsequent quantitative analysis can not be fully objective (*Falkingham, in press*). The development of objective approaches for the definition of footprint extents is therefore of urgent importance for the quantitative study of fossil footprints.

Working with contour maps, the most straightforward approach is the selection of a single contour line, in order to define the footprint boundary on a constant height level (e.g., *Romilio & Salisbury, 2014*). Testing this approach on the Münchehagen footprints revealed important shortcomings. Since contour lines at different depths may differ considerably in shape within a single footprint, the necessary selection of a single contour line still introduces a significant amount of subjectivity (*Falkingham, in press*). Furthermore, a single contour line is strongly affected by noise and extramorphological influences, and often cannot depict a footprint in its full extents. While an interpretative outline aims to capture the important features of the footprint wall, a single contour line can only represent a much less informative, arbitrary representation of the footprint, as features outside of the height level of the contour line are ignored. These problems might be partly solved by calculating the mean shape of all contour lines describing the footprint wall using GPA. In practice, however, the height of the footprint wall varies within the footprint. The stack of contour lines that can be analyzed will therefore be restricted by the shallowest part of the footprint wall, so that deeper parts are only partly covered by the analyzed stack of contour lines.

A different approach, the consistent selection of the steepest slope, is associated with different practical problems. First, the steepest slope does not necessarily represent the margin of the actual footprint stamp. The steepest slope can occur both on the outer area of the footprint close to the border to the undeformed sediment, and inside the footprint, e.g., when the distal part of a digit impression is partly filled with sediment, forming a steep slope at the base of the infill. In both cases, the steepest slope will convey only little

information on the actual foot anatomy. This problem is most evident in several of the I1 footprints. Second, the steepest slope can rarely be followed along the whole outline; rather, it fades out frequently, causing the outline tracing to abruptly jump to a different height level. The latter problem might be solved by detecting the steepest slope on multiple points along the footprint margin, and approximating a single outline using splines or elliptic Fourier transforms.

Objective landmark positions resulting from the contour line approach were subjected to GPA and principal component analysis for all three trackways, reproducing the results given by the same analysis based on interpretative landmarks. Interpretative bias therefore cannot explain the observed variation patterns.

Causes of variability

In theory, footprint shape is determined by three factors, namely the anatomy of the trackmaker's foot, substrate properties, and behavior (*Falkingham, 2014*). Additional factors affecting footprint shape include pre-burial and recent alteration (e.g., *Henderson, 2006*; *Scott, Renaut & Owen, 2010*) as well as diagenesis (e.g., *Lockley, 1999*; *Schulp, 2002*; *Lockley & Xing, 2015*). The tracks were documented shortly after excavation, limiting exposure to the elements. The removal of the overburden using excavators frequently damaged the brittle tracking layer, contributing to the observed variability. However, digital comparisons of three footprint negatives with their casts (T3/44, T3/45 and T3/46) showed that shape differences due to material loss during excavation were minimal at least in these examples (*Wings, Lallensack & Mallison, in press*). Last but not least, subjectivity and noise introduced by interpreting the footprint outlines and determining the landmark points will inevitably contribute to the observed variability. Although subjectivity was reduced by applying specific criteria for the tracing of outlines, these criteria are not always applicable unambiguously. As discussed in 'Objective methods for the definition of footprint margins', a second geometric morphometric analysis using landmark positions derived from an objective approach was able to reproduce the observed patterns at least for the T3 and T2 trackways (Figs. S1 and S2), suggesting that interpretational bias, although considerably contributing to the observed variability, cannot explain the observed variation patterns.

A significant difference between left and right footprints was not observed in any of the three trackways. As foot anatomy does not change within a trackway, the substrate properties and the behavior are presumably the major causes of variability within the present trackways. Whether substrate or behavior is the major contributor to variability is generally difficult to assess, and depends on the footprint feature or measurement in question. Both theropod trackways differ from the ornithopod trackway in the pronounced variation patterns in the heel and lateral hypex areas. It is unclear whether these differences might be the result of locomotory differences in separate individuals, or even separate trackmaker groups such as ornithopods and theropods (*Lallensack, 2015*). Alternatively, the differences might be explained by the presumably higher body weight of the ornithopod, which might have resulted in a more regular impression of the heel and hypex areas. However, as the

absence of the distinctive variation pattern in the I1 trackway could also be a random effect given the small sample size, further research is needed to investigate these possibilities.

Variability of quantitative and qualitative track features

A wide array of quantitative and qualitative track features have been employed for the characterization of tracks (*Lockley, 1998*). The trackway pattern can be completely characterized by quantities, i.e., linear measurements such as pace- and stride lengths, and angular measurements such as pace angulation and footprint rotation. A comprehensive characterization of individual footprints encompasses both quantities and qualities (*Lockley, 1998*). The former include the number of digits and digital pads, linear measurements, such as the dimensions of the overall footprint and those of the individual digits and pads, and angular measurements, most importantly the interdigital angles. Qualities can include the shape, relative position, and orientation of parts of the footprint such as ungual impressions, the heel region, the hypices, or the pad impressions.

Linear measurements include both information on shape and size. Ichnotaxonomically meaningful comparisons are only possible when the influence of size is minimized, e.g., by using ratios. Nevertheless, mere size, usually approximated by footprint length, is commonly employed to distinguish ichnotaxa. For example, the ubiquitous ichnogenus *Grallator* is restricted to footprints less then 15 cm in length (*Olsen, Smith & McDonald, 1998*), while the newly described ichnogenus *Bellatoripes* was diagnosed to encompass footprints over 50 cm in length (*McCrea et al., 2014*). Other diagnoses make use of more general categories, such as "small size," "medium size" and "large size" (e.g., *Xing et al., 2013*; *Xing et al., 2014a*; *Lockley, Meyer & Dos Santos, 1998*). Employing size for the diagnosis of ichnotaxa appears questionable, as such categories are necessarily arbitrary. Such an approach can lead to an overestimate of the diversity present in a sample, as different ontogenetic stages of the same species would fall into separate ichnotaxa (*Bertling et al., 2006*). This is especially problematic since size difference between hatchlings and adult individuals is large, especially in larger dinosaurs.

Below, we review a selection of commonly employed qualitative and quantitative track features, and discuss their intratrackway variability based on the findings derived from the Münchehagen trackways.

Hypex positions and associated measurements. For excellently preserved footprints, hypices are rarely used as descriptors, since reference points based on well defined pad impressions are much more informative. Hypices become increasingly important for less well preserved material lacking discrete pad impressions, as useful reference points in such footprints are scarce. In the measurement scheme proposed by *Moratalla, Sanz & Jimenez (1988)*, which does not require the presence of pad impressions, 11 of the 18 measurements directly depend on the medial or lateral hypex (Fig. 8B). This includes commonly employed measurements such as the free lengths of digit impressions II, III, and IV, the heel-interdigital distances, and the digital widths, which also are important parameters in the discrimination of theropod and ornithopod footprints (e.g., *Moratalla, Sanz & Jimenez, 1988*). A qualitative feature, the relative position of the two hypices, is occasionally used to define new ichnotaxa (*Lockley et al., 2006*; *Lockley et al., 2007*; *Xing et al., 2014c*).

Belvedere (2008) observed that the hypices are the most variable of the six analyzed landmark positions in a theropod trackway from the Late Jurassic of Morocco, concluding that the hypices in general should not be used as features in ichnotaxonomy. In the Münchehagen footprints, the lateral hypex was determined the most variable of the six defined landmark positions in all three trackways (Fig. 13). Variability of the medial hypex is significantly lower, although still representing the second most variable landmark in the I1 and the third most variable landmark in the T3 trackway. The overall increased variability of the hypex landmarks is in accordance with the findings of *Belvedere (2008)*. In the Moroccan trackway, however, the medial hypex was found to be more variable than the lateral hypex (*Belvedere, 2008*), contrary to the condition in the Münchehagen tracks.

Intriguingly, the main variation in the medial and lateral hypex points appears in separate principal components in all three trackways, indicating that the lateral and medial hypex positions vary independently from each other. This suggests that the relative position of the hypices is a potentially very variable feature and is only informative if large sample sizes are available. Likewise, any measurements depending on the hypex positions should be used with caution. The free length of digit III can be determined by taking into account both the medial and lateral hypex, reducing extramorphological influences. On the other hand, measurements of the free lengths of digit impressions II and IV are necessarily based on only one of the two hypex positions, diminishing their informative value.

High variability in hypex positions in theropod footprints might result from different factors. First, hypices are non-compressed areas and as such are likely to be more influenced by variations caused by foot-sediment interactions than the highly loaded digit impressions (*Belvedere, 2008*). Furthermore, hypices can be expected to be influenced by trackmaker behavior, e.g., through changes in the interdigital angle and the degree to which the posterior part of the digits are impressed. Second, hypices are strongly influenced by preburial and recent erosion, especially when the interdigital angle is low, as the narrow sediment rims between the digit impressions are the first features to be eroded (*Henderson, 2006*). On the other hand, a preservation as undertracks less likely affects hypex positions according to *Henderson (2006)*. Last but not least, inferred hypex positions can very much vary when interpreted by separate researchers. In many of the Münchehagen footprints, the posterior end of the sediment bar separating the digit impressions fades out indistinctly into the base of the footprint, without showing a single distinct slope, making their identification highly subjective. As the result of an experiment, *Thulborn (1990)* illustrated eight different outline drawings drawn by separate persons based on the same photograph of a theropod footprint, in order to illustrate the influence of personal interpretation. Our examination of the outline drawings shows that in four interpretations the hypex of the right side is located posterior to the hypex on the left side, while the relative hypex positions are vice versa in two and equal in yet another two interpretations. As a conclusion, hypex positions in published outline drawings are probably not informative in most cases.

Heel region and associated measurements. The extension and morphology of the heel region is frequently employed in ichnotaxonomy (e.g., *Langston Jr, 1974*; *Gangloff, May & Storer, 2004*; *Lockley et al., 2014*; *Xing et al., 2014a*; *Díaz-Martínez et al., 2015*), as well as for discriminating between theropod and ornithopod (e.g., *Moratalla, Sanz & Jimenez, 1988*;

Pittman, 1989; *Thulborn, 1990*; *Mateus & Milán, 2008*; *Xing et al., 2014b*) and between left and right footprints (e.g., *Pittman, 1989*; *Thulborn, 1998*; *Marzola & Dalla Vecchia, 2014*). Several common measurements depend on this feature (Fig. 8B), most importantly the footprint and digit impression lengths. Footprint length is of crucial importance not only for describing overall footprint dimensions, but also for estimating hip height and locomotion speed of the trackmaker and associated paleobiological inferences (*Falkingham, in press*).

In both theropod trackways, the antero-posterior variation of the landmark on the heel constitutes the second largest "hotspot" of variability, only excelled by the landmark on the lateral hypex, which according to PC1 covaries with the heel landmark (Fig. 12). This covariation might be explained by variations in substrate properties or erosion. *Demathieu (1990)* suggested that the shape of the heel depends on the sinking depth of the foot, and thus on the sediment properties. This is not evident in the Münchehagen trackways, as PC1 does not significantly correlate with the maximum depth of the footprints. The hypex positions might be highly susceptible to changing substrate properties (*Belvedere, 2008*) or erosion (*Henderson, 2006*). However, in the T3 mean shape, the interdigital angle between digit impressions III and IV is larger than that between digit impressions II and III, resulting in a larger interdigital sediment bar that is less likely to be partially erased. The consistently higher variability in the lateral hypex thus appears counter-intuitive.

As an alternative explanation, PC1 might reflect behavioral differences of the animal, caused by variations in the degree to which the proximal part of digit IV was impressed. In recent ostrich (*Struthio camelus*) footprints, the presence of metatarsal impressions was suggested to be at least partly determined by behavior (*Belvedere & Mallison, 2014*), opening the possibility that the same holds true for tridactyl dinosaur footprints. Variations in the impression of the heel in a large tridactyl trackway from the Australian Lark Quarry have been suggested to result from different pedal postures, and thus, behavior (*Thulborn & Wade, 1984*; *Thulborn, 2013*; *Romilio & Salisbury, 2014*). Furthermore, it has been suggested that the degree to which the heel is impressed can vary with locomotion speed (and thus behavior), with running animals impressing only the distal parts of their digits (*Sarjeant, 1975*; *Thulborn & Wade, 1984*; *Lockley & Conrad, 1989*). However, foreshortened digit impressions and long stride lengths can in some cases be interpreted as swimming tracks (*Romilio, Tucker & Salisbury, 2013*). Contrary to the theropod outlines, the heel extent in the I1 outlines does not show an strongly increased variability, indicating a more constant impression of the heel pad.

The extent of the heel impression can vary not only due to an incomplete impression of the foot, but also due to the additional impression of the metatarsus. Although not preserved in the Münchehagen tracks, metatarsal traces are frequently found in footprints attributed to both theropods and ornithopods, and can be caused either by behavior or sinking depth of the foot into the sediment (e.g., *Kuban, 1989*; *Citton et al., 2015*; *Lallensack et al., 2015*; *Pérez-Lorente, 2015*). Several ichnotaxa are based on material including metatarsal impressions, causing ichnotaxonomical problems (e.g., *Díaz-Martínez et al., 2015*). In the light of the potential high variability in the extension and morphology, features and measurements related to the heel region should only be used when a full impression of the foot can be ascertained and a contribution of the metatarsus can be excluded.

The analyzed theropod footprints do not only show anteroposterior, but also mediolateral variation in the degree to which the heel is impressed. Thus, digit IV can be fully impressed while large parts of the proximal portion of digit II are not impressed, and vice versa. This results in a spectrum of different morphologies, including V-shaped, U-shaped, symmetrically bilobed and asymmetrically bilobed shapes. The I1 trackway, although showing a more constant heel pad impression, shows various different heel morphologies ranging from V-shaped or broadly arched to sub-rectangular; both width and position of the heel pad relative to digit impression III varies greatly. The consequences of the high variability in the heel on the differentiation between left and right footprints and on trackmaker identification are discussed below.

Morphology and dimensions of digit impressions. Morphology and dimensions of digit impressions are important characters in ichnotaxonomy (e.g., *Lockley, 1998*; *Lockley, 2009*; *Lockley et al., 2014*) as well as in the distinction between left and right footprints (e.g., *Pittman, 1989*; *Thulborn, 1990*) and between theropod and ornithopod footprints (e.g., *Farlow, 1987*; *Moratalla, Sanz & Jimenez, 1988*; *Thulborn, 1990*; *Romilio & Salisbury, 2011*; *Thulborn, 2013*; *Romilio & Salisbury, 2014*). Dimensions of the digit impressions can be described using the length-to-width ratio (e.g., *Moratalla, Sanz & Jimenez, 1988*), or by assessing the relative digit lengths, such as the projection of digit III beyond digits II and IV (e.g., *Lockley, 2009*), or the projection of digit IV relative to digit II (e.g., *Xing et al., 2014d*). Informative qualitative features include the tips of the digits, which may record the presence of claws or hooves.

In the T2 trackway, the tip of digit impression II generally extends beyond that of digit impression IV, as indicated by both the mean shape and well preserved footprints (Figs. 3 and 6). Landmark analysis indicates a slightly increased variability on digit impression II (Fig. 13). *Foster (2015)* discarded the relative extension of digits II and IV as an informative feature for *Hispanosauropus* tracks from the USA and Spain, as this feature was found to be very variable in these tracks.

Measurements of the length-to-width ratio can be problematic when digital pads are not well defined, as the variability in the heel (for measurements of overall digit lengths) and the hypices (for measurements of the digit free lengths) is difficult to assess. Furthermore, digit impression width varies greatly in the described footprints, especially in digit impression III. In the T2 trackway, the marked narrowness seen in the digit impressions of some footprints is possibly due to sediment being drawn inside the toe impression when the toe was withdrawn (*Thulborn, 1990*; *Gatesy et al., 1999*). A high degree of variability in the width of the digit impressions has been noted for other tracksites as well (e.g., *Farlow et al., 2007*).

Digit impression morphology remains relatively constant within both theropod trackways. The morphology of the distal tip is determined by the position of the claw. The mean shapes and best preserved footprints of both trackways indicate a central position of the claw of digit impression II, a medial position in digit impression III, and a lateral position in digit impression IV. Claw locations frequently deviate from this general position even in excellently preserved footprints, indicating behavioral variability. High variability in claw positions is a general feature in many theropod dinosaur footprints (*Thulborn, 1990*).

In the I1 trackway, digit impression morphology is more variable than in the theropod trackways; while appearing long and narrow in some examples, they approach a cloverleaf-shape in others. Digit impressions II and IV appear straight in some footprints, but show a bend at midlength in others, producing a pronounced inwards curvature. The foot anatomy in ornithopods generally allows some degree of mediolateral bending in digits II and IV—the combination of deformations in the digital joints and the soft parts during footprint formation might result in the observed morphology (T Hübner, pers. comm., 2016). Curvature of digit impressions can occur as a result of foot-substrate interactions even when the digits themselves are straight, as was recently demonstrated with computer simulated footprint formations, although at a much smaller scale (*Falkingham & Gatesy, 2014*). In conclusion, it is not clear to which degree the observed curvature reflects anatomical features. In both theropod trackways, digit impressions are generally straight, with the exception of digit impression IV in T3/47 (Fig. 5M), which shows a lateral bend. This bend is most pronounced in the distal third of the digit impression, where it probably results from a lateral orientation of the claw (cf. *Thulborn, 1990*).

Trackway parameters. Trackway parameters are commonly employed in ichnotaxonomy (e.g., *Lockley et al., 2014*; *Lockley, Meyer & Dos Santos, 1998*), despite the potential high influence of behavioral variability (*Díaz-Martínez et al., 2015*). They are also used to distinguish theropod and ornithopod trackmakers, with ornithopods tending to show shorter pace- and stride lengths, a lower pace angulation, and a stronger inward rotation (*Lockley, 1987*; *Farlow et al., 2007*; *Castanera et al., 2013*). Furthermore, the trackway pattern represents the most obvious criterion for the distinction between left and right footprints. All variables of the trackway configuration, regardless if describing the distance between footprints (pace and stride lengths), the width of trackway (e.g., pace angulation), or the pes rotation, are strongly influenced by the locomotion speed of the trackmaker (cf. *Alexander, 1976*; *Day et al., 2004*; *Kim & Huh, 2010*). As can be expected for an ornithopod, the I1 trackway shows shorter pace- and stride lengths and a higher pes rotation than both theropod trackways. However, pace angulation is slightly higher in the ornithopod trackway (167° on average) than in the T3 theropod trackway (165° on average); this parameter therefore cannot unambiguously differentiate between theropod and ornithopod footprints in the present tracks.

Stride lengths (and, consequently locomotion speeds) are relatively constant within all three trackways. The maximum locomotion speed of the T3 trackmaker of 1.93 m/s is in accordance with the independent estimate of 6.5 km/h (1.81 m/s) proposed by *Troelsen (2015)*. Our estimate for the T2 trackmaker (2.27 m/s or 8.18 km/h) however is lower than that of the latter study (12 km/h). As a whole, the T2 trackway appears very straight and regular, with only a slight bend to the left. The I1 trackway, apart from the abrupt turn to the left at footprint I1/29, is also reasonably straight and slightly sigmoidal. The T3 trackway, on the other hand, is more strongly sigmoidal, although its general course remains constant after the turn to the right between footprints T3/26 and T3/30. Similar sigmoidal trackways have been described by several authors for both theropod and ornithopod trackmakers (see *Pérez-Lorente, 2015* and references therein). The T2 trackway shows the smallest variability in all measured trackway parameters, possibly due to its straight course

and higher locomotion speed. Variability of the pace lengths is greater than that of the stride lengths in all three trackways.

For measuring trackway parameters, most studies utilize the tip of digit impression III as a corresponding reference point (*Thulborn, 1990*). Alternatively, the base of digit impression III might be used for this purpose (*Thulborn, 1990*). The divergence of results by the two approaches usually is negligible for trackways with long strides, as has been suggested by *Farlow (1989)* based on extant ostrich (*Struthio camelus*) trackways. The Münchehagen trackways, however, show a strong variability in footprint rotation, and, in case of the I1 trackway, a strong inward rotation, possibly significantly influencing results. Reference points on the tip of digit impression III give generally higher standard deviations than those on the base of that digit impression for all trackway parameters (Table S1). This suggests that measurements based on the digital bases are somewhat more informative since the influence of footprint rotation variability is reduced. Despite marked differences in standard deviation especially in the T3 trackway, average values derived from both approaches are very similar for most trackway parameters (Table S1). Average pace angulation in the I1 trackway is an exception, being increased by 10% when the tip rather than the base of digit impression III is used, a result of the strong inward rotation of the footprints in this trackway.

To our knowledge, systematic cross-over gait along most of the trackway course has not been reported in any other dinosaur trackway. When present, it is usually restricted to one single step, most frequently during turns (*Xing et al., 2014b*). A large tridactyl trackway from the Lark Quarry of the Upper Cretaceous of Queensland, Australia, shows a crossing of the trackway midline in probably four out of nine footprints, including two successive footprints with cross-over gait (*Thulborn & Wade, 1984*; *Romilio & Salisbury, 2014*). The reason for the observed cross-over gait in the T2 trackway is unclear, as muscular requirements caused by a mediolateral shift in the center of mass can be expected to be higher compared to a foot placement directly on the trackway midline (cf. *McClay & Cavanagh, 1994*). Given the apparent rarity of such a feature in dinosaur trackways, a biomechanical reason appears unlikely; rather, the cross-over gait might reflect peculiar behavior of the individual. A pathological explanation also cannot be ruled out. *Razzolini et al. (2016)* recently described an abnormal gait in an ornithopod trackway from the Lower Cretaceous of Spain, which can be attributed to a pathology in the pes of the animal recorded in the footprint morphology. In the T2 trackway, a statistically significant left–right asymmetry could not be detected neither in the footprint morphology nor in the trackway parameters.

Distinction between left and right footprints

The correct identification of a footprint as pertaining to the left or the right foot is crucial when descriptors related to footprint asymmetry are employed, such as any differences in divarication, morphology, and size between digit impression II and IV, relative orientation of digit- or heel-impressions, curvature of digit impressions, and orientation of the ungual impression, amongst others. The most straightforward criterion is the position of the footprint relative to the trackway midline – this criterion, however, is not infallible

even when long trackways are available, as shown below. Theropod tracks often show a pronounced asymmetry, allowing the assignment to the left or right foot even based on isolated footprints, while larger ornithopod tracks usually are subsymmetrical (*Díaz-Martínez et al., 2015*, but see below). For theropod footprints, left–right criteria include the configuration of the heel region, the curvature of digits, and the orientation of claw marks. Additional criteria might be employed occasionally, such as smear marks originating from the tips of the digit impressions (*Thulborn, 1998*), pressure release structures between digit impressions (*Martin et al., 2012*), or, if metatarsal impressions are present, the location of the hallux impression as well as the angling of the acropodial against the metapodial impression (*Pérez-Lorente, 1993*). In bird footprints, interdigital angles can be used as yet another criterion, as the angle between digits III and IV is often wider than between digits II and III (*Padian & Olsen, 1989*). This configuration appears to apply to many theropod footprints as well (*Farlow 1987*; *Pérez-Lorente 2015*, but see *Thulborn 1990* for a contrary statement).

Few attempts have been made to differentiate left and right footprints of larger ornithopods based on pes morphology (for exceptions, see e.g., *Currie, Nadon & Lockley, 1991*; *Hornung et al., 2012*), as such tracks generally display a high degree of symmetry (*Díaz-Martínez et al., 2015*). Contrary to this assumption, the mean shape of the I1 ornithopod footprint shows the subcircular heel pad being clearly displaced laterally with respect to digit impression III. Footprint asymmetry is highlighted by GPA-based comparisons of the T3, T2 and I1 mean shapes with their respective mirror images (Fig. 9D). Asymmetry is most pronounced in the T3 mean shape, with a Procrustes distance of 0.0089 between the mean shape and its mirror image, followed by the T2 mean shape (0.0045). Procrustes distance in the I1 mean shape is only slightly smaller, accounting for 0.0034. Below we test the three most important traditional criteria for the distinction between left and right footprints—the location of the footprint relative to the trackway midline, the heel configuration, and the orientation of digit III.

An asymmetric distal end of digit III can be seen in both theropod trackways, while in the ornithopod trackway digit III is symmetrical and thus not informative. Both the curvature and claw mark of digit III usually point to the inside of the trackway (*Pittman, 1989*; *Thulborn, 1990*). In the theropod footprints, asymmetry can result from both the position and orientation of the claw mark, usually towards the medial side. When the claw impression is not distinct, the termination of digit impression III is usually arched on the lateral and straight on the medial side. Of the 23 preserved footprints of the T2 trackway, asymmetry of digit impression III could be observed in 13 footprints. 11 footprints could be correctly classified as pertaining to either the left or right foot, while the classification was in error for 2 footprints (T2/1 and T2/3) in which asymmetry is only weakly expressed. The interpretation of footprint T2/17 is ambiguous, as the well preserved claw impression is located on the lateral side but tilted towards the medial side. In the T3 trackway, asymmetry could be observed in 15 footprints, all of them being classified correctly. In conclusion, the morphology of the distal end of digit III appears to be a reliable left–right criterion for footprints with well-developed asymmetry.

In theropod and smaller ornithopod footprints, digit IV is often impressed along its whole length including the metatarsophalangeal pad, while the proximal parts of digits II and III are held off the ground (*Baird, 1957*; *Farlow et al., 2000*). In the footprints, this condition often results in an indentation along the medial side of the footprint separating digit II from the metatarsophalangeal pad of digit IV (*Farlow et al., 2000*). Both the indentation of the medial side and the proximal extension of digit IV past digit impression II are commonly used to distinguish left and right footprints, even when the phalangeal pads are not visible (*Marzola & Dalla Vecchia, 2014*; *Pittman, 1989*; *Thulborn, 1998*). In the T2 trackway, 8 of the 23 footprints show a clearly asymmetric heel impression (most pronounced in T2/22), and all 8 footprints could be correctly classified as either left or right based on this feature. The T3 footprints, on the other hand, proved to be more ambiguous. In footprints preserving an impression of the metatarsophalangeal pad (best seen in T3/18), the heel varies from being strongly asymmetrical (e.g., T3/47) to being V-shaped, with only a slight tendency towards the lateral side and a quite weakly developed medial notch. The heel is clearly asymmetrical in 12 of the T3 footprints—while our classification was correct for nine of the footprints, it was incorrect for tree examples. All three incorrectly classified examples show a foreshortened digit impression IV being less extensive than digit impression II, resulting from an incomplete impression of the heel. These footprints, however, can be distinguished from examples showing a fully impressed heel in that the proximal ends of digits II and IV are more widely separated from each other, resulting in a much broader heel.

In the I1 trackway, distinction between left and right footprints is possible due to the asymmetric heel region, which proved to be a surprisingly reliable criterion. 18 footprints show a marked asymmetry in the heel, and all but one (I1/42) could be correctly classified as either left or right footprints based on this feature. A similar asymmetry appears to be present in several other ornithopod tracks from the Obernkirchen Sandstone (cf. *Lockley & Wright 2001*, Fig. 29.1B; cf. *Hornung et al. 2012*). The observed asymmetry probably results from an asymmetry in the foot anatomy of the trackmaker, and is possibly homologous to the asymmetric condition in theropods, which seems to represent the basal condition in dinosaurs (*Farlow et al., 2000*). Although metatarsal traces are frequently reported for ornithopod tracks (*Lockley, Young & Carpenter, 1983*; *Pérez-Lorente, 1993*; *Loza, Medrano & Lorente, 2006*; *Vela & Lorente, 2006*; *Lucas et al., 2011*; *Pérez-Lorente, 2015*), such traces tend to be angled medially with respect to the foot's long axis, contributing to the marked inward rotation of the foot (*Pérez-Lorente, 1993*; *Pérez-Lorente, 2015*). As the asymmetric heel pad is located laterally with respect to the foot's long axis, a significant contribution of the metatarsal shaft to the observed asymmetry appears unlikely.

Identification of left and right footprints based on their position relative to the trackway midline was expectedly unambiguous for the T3 and I1 footprints, but misleading for the T2 footprints. In the T3 trackway, all 20 measurable footprints are located on the expected site of the trackway, with only T3/39 being on-line with the preceding and subsequent footprint. The same holds true when the tip of digit impression III is chosen as the reference point. Likewise, in the I1 trackway, all 26 measured footprints fall on the expected side of the trackway midline, when the base of digit impression III is taken as the reference point.

However, when the tip of digit impression III is chosen as the reference point, 7 of the 26 measured footprints are located medial to the trackway midline, with an additional 5 being located on the trackway midline. This apparent overstepping results from the inward rotation of the footprints. In the T2 trackway, 12 of the 19 measured footprints show pronounced overstepping over the trackway midline, with only 6 footprints being located on the expected side and one directly on the midline. With the tip of digit impression III as the reference point, only five footprints fall on the expected side of the trackway, with two located directly on the trackway midline. This observation contradicts all other left–right criteria, including the heel configuration and the orientation and position of the claw of digit III. Examples with preserved phalangeal pads, such as T2/22 (Fig. 6G), confirm the presence of cross-over gait in most of the trackway.

Implications for the discrimination between ornithopod and theropod footprints

The distinction between ornithopod and theropod footprints can be difficult even when based on complete trackways (*Lockley, Foster & Hunt, 1998*; *Farlow et al., 2007*; *Romilio & Salisbury, 2011*; *Thulborn, 2013*; *Romilio & Salisbury, 2014*; *Hübner, in press*). The general appearance of the I1 differs considerably from the T2 and T3 mean shapes, most obviously in the heel region. However, direct comparison of the mean shapes reveals striking similarities in proportions (Figs. 9B and 9C), indicating that most traditional measurements might not be able to discriminate between footprints of both trackways. Important commonly employed criteria include the length-width ratio, assuming that theropod footprints in general are longer than wide, while ornithopod footprints are as wide as long or even wider (*Moratalla, Sanz & Jimenez, 1988*; *Thulborn, 1990*; *Farlow et al., 2007*; *Romilio & Salisbury, 2014*). Strikingly, in both the T3 and I1 mean shape, the length-width ratio is 0.91; the footprints thus are markedly wider than long, while the T2 mean shape is about as wide as long. Therefore, the length-width ratio is a misleading criterion for both the T2 and T3 mean shapes. A low length-width ratio appears to be not as uncommon in large theropod footprints as previously thought (*Lallensack et al., 2015*). While a high length-width ratio may still represent a reliable indicator for theropod footprints, the reverse, a low length-width ratio, might not be as reliable an indicator of ornithopod footprints as previously assumed.

Another criterion, the width of the digit impressions, assumes that digit impressions of theropod footprints tend to be narrower than those of ornithopods (*Moratalla, Sanz & Jimenez, 1988*; *Thulborn, 1990*; *Farlow et al., 2007*). In the present mean shapes, the relative widths of digit impressions II and IV are about equal in the T3 and I1 mean shape, with the impression of digit III even appearing wider in the T3 mean shape (Fig. 14B). Only digit impressions III and IV of the T2 mean shape show a reduced width when compared with the T3 and I1 mean shapes. Furthermore, as already discussed, digit proportions are amongst the most variable footprint features, especially in the I1 trackway, ranging from short and wide to long and narrow (Figs. 5–7), indicating that they do not fully correlate with the trackmaker's anatomy. A striking example of intratrackway variability of digit impression shape can be found in the Upper Jurassic Barkhausen tracksite, where a

tridactyl trackway shifts from a theropod-like to an ornithopod-like morphology along its course (*Lallensack et al., 2015*).

Other criteria for the distinction of ornithopod and theropod footprints include the shape of the digit terminations (*Thulborn, 1990*). Theropod footprints often show V-shaped terminations, while the terminations of ornithopod footprints are more U-shaped in outline; these differences are best seen in digit III (*Thulborn, 1990*). This feature is pronounced in many of the footprints (e.g., the cast of T3/18, and I1/36; Figs. 3B and 7F). In other footprints, ungual marks are absent due to poor preservation. *Thulborn (1990)* noted that the digit impression III of theropods is sometimes distinctly curved, while that of ornithopods is straight. Digit impression III is straight in all three mean shapes. An informative distinguishing criterion in the present tracks is the asymmetry of the digit impressions. In the theropod footprints, the tips of digit impressions II and IV tend to point towards the outside (away from the footprint midline), due to outwardly directed claw impressions. In the ornithopod footprints, this asymmetry is often reversed, with the tip located more towards the inside of the footprint (Fig. 10). Digit impression III tends to be symmetrical in the ornithopod footprint, but shows a markedly medially displaced tip in the theropod footprint, caused by the medially directed claw. In conclusion, most criteria based on the general shape of the footprints are not able to discriminate the present footprints, and that only anatomical details such as claw impressions and digital pads allow for an unambiguous determination of the trackmaker.

Moratalla, Sanz & Jimenez (1988) presented a multivariate approach to discriminate between theropod and ornithopod footprints. These authors carried out factor and discriminant analyses on 66 footprints previously ascribed to either theropods or ornithopods, in order to estimate the most informative parameters for the discrimination between these groups. From these parameters, nine bivariate ratios were defined. Threshold values were selected for each bivariate ratio, allowing for the classification of unknown material. Although the majority of the analyzed material stems from the Lower Cretaceous of La Rioja, Spain, this approach has recently been applied to classify footprints from different epochs of different parts of the world (*Mateus & Milán, 2008*; *Romilio & Salisbury, 2011*; *Schulp & Al-Wosabi, 2012*; *Therrien et al., 2015*). *Thulborn (2013)* recently questioned the use of this approach to classify contentious material, noting that (1) the threshold values are defined subjectively to provide the best separation between point clouds in the bivariate plots, (2) the analysis is essentially a set of bivariate plots and thus not a real multivariate analysis, (3) most of the employed ratios reflect the length-width ratio of the footprint, resulting in a high degree of redundancy, and that (4) all digital axes are required to originate from a single point on the heel outline and thus cannot appropriately describe the footprint shape in many examples.

Before discussing the results of the approach of *Moratalla, Sanz & Jimenez (1988)* applied to the present mean shapes, we need to point out some practical problems which might affect our results. First, the parameter "basal digit width" of digit impression III (WBIII) is defined as the connection line between the two hypices. Consequently, the value for WBIII will be enlarged when the two hypex positions differ in their anteroposterior position, which is frequently the case especially in theropod footprints (*Lockley, 1998*), including

Figure 14 Multivariate analysis of the T3, T2 and I1 mean shapes, adopting the approach of *Moratalla, Sanz and Jimenez (1988)* for the discrimination between ornithopod and theropod footprints. Red squares represent the T3 trackway (large theropod), blue circles the T2 trackway (mid-sized theropod) and the green triangles the I1 trackway (ornithopod). A clear separation between the theropod and the ornithopod trackways is not possible in this case. The graphical depiction follows *Romilio and Salisbury (2011)* and *Schulp and Al-Wosabi (2012)*. Measurements are indicated in Fig. 8.

the T3 footprints analyzed herein. Large WBIII values are considered an ornithopod-like feature by the discriminant analysis. According to both *Romilio & Salisbury* (*2011*, Fig. 3B) and *Thulborn (2013)*, the parameter "middle digit width" of digit impression III (WMIII) is measured parallel to WBIII. Again, differences in the relative positions of the hypices will result in a greater WMIII value, causing the bivariate ratio LIII/WBIII to suggest more ornithopod-like proportions. However, *Moratalla, Sanz & Jimenez (1988)* did not indicate the requirement of WMIII to be measured parallel to WBIII. In the present study, we measured WMIII at the shortest distance across the digit impression, which appears to be the most informative measurement approach. Second, the interpretation of the completed analysis is hampered as discriminant weights are only provided for the individual parameters, not for the ratios. This seems important, as weights for single parameters would be influenced by the size of the individual footprint, while the influence of size is reduced in the ratios. Thus, one cannot assess the relative importance of each of the nine ratios. Furthermore, no discriminating formula was provided, again suggesting that a classification is not possible when the result is not completely unambiguous.

When applied to the T3, T2 and I1 mean shapes, the approach of *Moratalla, Sanz & Jimenez (1988)* gives inconclusive or even misleading results (Fig. 14). For the T3 mean shape, only two of the nine ratios (L/K and L/M) fall within the theropod field. Of these, L/K plots very close to the threshold value, leaving L/M as the only ratio that unambiguously implies theropod affinities for the T3 trackway. Six ratios fall far inside the ornithopod's field, while another one (BL3/WMIII) equals the threshold value. In conclusion, the discriminant analysis favors an ornithopod affinity of the T3 trackway. For the T2 trackway, values are generally closer to the theropod's field. However, five of the nine ratios still indicate ornithopod affinities, two of which are very close to the threshold value. Only the I1 trackway could correctly be classified as ornithopod-like. All nine ratios plot inside the ornithopod's field, including three that are located very close to the threshold value. The three mean shapes tend to plot together, indicating that the footprint proportions are very similar and that the parameters as defined by *Moratalla, Sanz & Jimenez (1988)* are, in this case, insufficient to separate the ornithopod from the theropod mean shapes.

The only two ratios indicating theropod affinities of the T3 mean shape (L/K and L/M) include the total footprint length and the heel-interdigital distances. The hypices and the heel are the most variable regions in the T2 and T3 footprints, reducing the information content of the two ratios. This observation was confirmed by a PCA on the Procrustes-fitted landmark coordinates of all three trackways (Fig. 9A). Plotting the first against the second principal component reveals a weak separation of the T2, T3 and I1 shapes. The T3 shapes are best separated from the I1 shapes along the first principal component, which describes a posterior shift of the lateral hypex and an anterior shift in the heel – the very same shape differences are captured by the ratios L/K and L/M. However, both theropod trackways also greatly vary along the first principal component, causing significant overlap with the I1 point cloud. As the I1 shapes are restricted to low scores on the first principal component, footprints with shortened heel regions are unlikely to pertain to the ornithopod. The reverse may well be the case, as the heel regions of several of the T3 shapes are as extensive as in

average I1 shapes, causing great overlap. The T2 shapes are best separated, showing high scores on both the first and second principal components. The second principal component shows a more posterior position of the medial hypex and a reduced length-width ratio. Both the T2 and T3 confidence ellipses are elongated, while the I1 ellipse is more circular, indicating that the I1 shapes lack a distinctive variation pattern.

As expected, the separation reached by the CVA is significantly better than that of the PCA, with the T2 trackway being completely separated and a slight overlap between the I1 and T3 trackways (Fig. 9B). The best separation between the ornithopod and the two theropod trackways is reached by CV1. Large values on this axis describe a more posterior position of the hypices, a more anterior position in the heel, and an anteriorly extended digit impression III. CVA, however, is unstable with respect to sampling (*Reyment & Savazzi, 1999*). As the canonical vectors describe the best possible separation of the three trackways based on our sample, the separation reached by these vectors can be expected to be less clear when additional footprints are incorporated (*Reyment & Savazzi, 1999*). Consequently, the PCA (Fig. 9A) is the more prudent method to estimate the separation of the trackways.

Potentials of geometric morphometrics for the study of dinosaur footprints

Although the number of studies employing geometric morphometrics on dinosaur footprints increases (*Rasskin-Gutman et al., 1997*; *Rodrigues & Santos, 2002*; *Belvedere, 2008*; *Clark & Brett-Surman, 2008*; *Castanera et al., 2015*), the method still is not widely established in this field. In most cases, geometric morphometrics is used to differentiate footprints from different localities, with moderate success. In our study, we propose additional applications both for exploratory and statistical purposes. First, geometric morphometrics proved valuable in comparing different approaches for the definition of footprint margins. Individual tools of this method, such as GPA and elliptic Fourier transforms, may even be used to generate objective outlines. Second, GPA is a valuable tool for the comparison of separate shapes and the quantification of shape differences. In the present study, differences between mean shapes of the analyzed trackways and between left and right footprints are visualized using pair-wise GPA-based comparisons (Fig. 9C and 9D). Procrustes distances allow for the quantification of shape differences between individual shapes. Third, mean shapes are valuable quantifications of the average shape of a sample, as has already been shown for recent human and fossil hominin footprints (e.g., *Bennett et al., 2016*). Unlike selected single footprints considered as representative for a given sample, a mean shape minimizes the effects of intratrackway variability, thus revealing features that likely reflect the trackmaker's anatomy. A mean shape will necessarily show less detail than the best-defined examples of the sample. Nevertheless, they may reveal even subtle shape features, such as the slight medial bend in digit impression II or the constrictions that possibly delimit phalangeal pads in the T2 mean shape (Fig. 10B).

Furthermore, geometric morphometrics is able to exactly locate shape differences and variability within the footprint. With traditional linear measurements, it can be difficult to assess the origin of a shape difference, as these measurements depend on at least two

reference points, complicating their interpretation (e.g., are proportionally shorter digit impressions caused by a shortening of the digits, an elongation of the heel, a more distal position of the hypices, or a combination of these factors?). Likewise, the coefficient of variation can quantify variability of single measurements (*Dematthieu, 1987*; *Dematthieu, 1990*; *Weems, 1992*), but the footprint regions responsible for the shape variation are not immediately obvious. With geometric morphometric methods, shapes and mean shapes can be directly compared to visualize even subtle shape differences (*Rasskin-Gutman et al. 1997*; Fig. 9). This obviates the need for employing ratios of linear measurements, which otherwise would have been necessary to remove the effect of size differences. Variability can be assessed for each landmark position separately (Fig. 10), facilitating the understanding of the mechanisms responsible for the observed variability.

Last but not least, the ability of traditional quantitative measurements to discriminate between ornithopod and theropod footprints is shown to be limited, especially when footprint proportions are similar. Geometric morphometrics is able to capture more information on the footprint shape while limiting redundancy. Semi-landmarks allow to capture qualitative shape features (*sensu Lockley, 1998*) along the outline, including the heel morphology and the asymmetry of the terminations of the digit impressions, which we have shown to represent the most prominent differences between the analyzed ornithopod and theropod trackways. This reveals room for improvement of existing quantitative methods for the discrimination of trackmaker groups.

CONCLUSIONS

The three analyzed tridactyl dinosaur trackways are amongst the longest and best preserved in Germany. The I1 footprints, referable to an ornithopod trackmaker, show narrow digit impressions with symmetrical terminations and a bend at mid-length, and a rounded heel pad that is located lateral with respect to digit impression III. The T3 and T2 trackways can be ascribed to theropod trackmakers based on well preserved claw impressions. They probably represent two separate trackmaker taxa, as indicated by morphological differences evident from the calculated Procrustes mean shapes. The T2 footprints are more gracile than the T3 footprints, showing a narrower digit impression III, a greater projection of digit impression III beyond digit impressions II and IV, no offset in the hypex positions, and a distally elongated digit impression II that is slightly bended medially. In total, at least four trackmaker taxa have been recorded from the Münchehagen tracksite.

Trackway parameters are generally less variable when measured from the base of digit impression III rather than from the tip of that digit, suggesting that the former approach has to be preferred when footprint rotation is strong or variable. Pace lengths are more variable than stride lengths in all three trackways. The T2 trackway shows the least variability in all measured trackway parameters, possibly due to its higher locomotion speed. The T2 trackway is striking in showing cross-over gait along most of the trackway.

All three trackways exhibit a great amount of footprint shape variability. The major causes of variability can be narrowed down to variations in the substrate properties and the behavior of the trackmaker. The two theropod trackways show considerable

anteroposterior, but also mediolateral variation in the degree to which the heel is impressed, resulting in a large array of different heel morphologies within the same trackway. Although anteroposterior variability in the extent of the heel is much less pronounced in the ornithopod trackway, heel morphology is likewise variable. Digit impressions tend to retain their general shape but vary in thickness within the two theropod trackways. Digit impression morphology is most variable in the I1 trackway.

Geometric morphometrics proved to be of great value for locating and quantifying shape variability in the footprints. In both theropod trackways, variability of landmarks on the lateral hypex and the heel is markedly increased, while in the I1 trackway variability is more equally distributed amongst the landmarks. Any measurements depending on reference points on the heel or on the hypices should therefore be used with caution. Principal component analysis reveals covariation of separate landmarks. The pattern described by the first principal component is strikingly similar in the two theropod trackways, showing a more posterior position of the lateral hypex co-occurring with a more anterior position of the heel. This pattern might be interpreted to directly result from variations in the degree to which the posterolateral portion of the foot was impressed, although it cannot be excluded that this pattern is mainly the result of varying substrate properties. The anteroposterior positions of the two hypices vary independently from each other within all three trackways, suggesting that the relative hypex positions do not represent an informative feature when the sample size is small.

Given the high degree of interpretative subjectivity introduced during outline tracing, the development of objective means to measure footprint shapes is of crucial importance. Of two *a priori* defined objective approaches, the steepest slope approach resulted in a lesser variability of landmark positions than the contour line approach, and therefore is less influenced by intratrackway variability. Analyses of landmarks placed using this approach reproduced results derived from landmarks placed on interpretative outlines at least for the T2 and T3 trackways. An interpretational bias, therefore, can be excluded as a probable explanation for the observed variation patterns.

The observed high degree of variability raises the question how strongly criteria commonly employed to differentiate between left and right footprints of theropod trackmakers are affected. Asymmetry in the termination of digit impression III resulting from the position and orientation of the claw is shown to represent a reasonable reliable criterion for both the T3 and T2 trackways. This criterion is found to be misleading for 15% of the T2 footprints, while the T3 footprints could be assigned without any misclassification. Likewise, the heel morphology proved to represent a reliable criterion despite its substantial variability. No misclassifications occurred with the T2 footprints, while 25% of the T3 footprints were incorrectly classified. All incorrectly classified examples possess a much foreshortened and therefore very broad heel. Although ornithopod footprints described in the literature are generally considered to be rather symmetrical, our examination revealed marked asymmetry in the heel region in the I1 trackway. This asymmetry allowed for the correct classification of 17 of the I1 footprints, with only one misclassification, suggesting that assignment of isolated material is possible with a reasonable degree of confidence at least for the present type of ornithopod track. The location of the footprints relative to the

trackway midline is an expectedly unambiguous criterion for the T3 and I1 trackways. In the T2 trackway, however, 12 of 19 footprints fall on the other side of the trackway midline due to the pronounced cross-over gait, demonstrating that the relative placement of the footprints is not always an unambiguous left–right criterion.

Footprint shapes of the present theropod and ornithopod trackways, although appearing visually distinct, show strikingly similar proportions. Asymmetry in the terminations of the digit impressions proved to be one of the most informative distinguishing criteria. Applying the multivariate approach of *Moratalla, Sanz & Jimenez (1988)*, the three mean shapes tend to plot together, and only the ratio L/M (footprint length against the lateral heel-interdigital distance) was able to clearly separate the T3 from the I1 shape. The discriminative approach of *Moratalla, Sanz & Jimenez (1988)* tends to suggest ornithopod affinities for the T3 trackway, and is inconclusive regarding the T2 trackway. According to principal component analysis, the present theropod and ornithopod footprints are indeed best separated by the lateral heel-interdigital distance, although large variability of this parameter in the T3 trackway leads to significant overlap with the I1 footprints. Our results indicate that previous quantitative approaches are not suitable to differentiate the present ornithopod and theropod footprint shapes.

ACKNOWLEDGEMENTS

We wish to thank Pernille Troelsen for assistance in separating individual footprints of the photogrammetric models. P. Martin Sander, Sashima Läbe, Michael Buchwitz, and Tom Hübner are thanked for discussions on our technical procedure and interpretations. We furthermore are grateful to Ryan T. Tucker for helpful comments on an early version of the manuscript.

ADDITIONAL INFORMATION AND DECLARATIONS

Funding

Oliver Wings is currently funded in the Europasaurus-Project (grant no. 85 882) by the Volkswagen Foundation in the grant initiative "Research in Museums." The funders had no role in study design, data collection and analysis, decision to publish, or preparation of the manuscript.

Grant Disclosures

The following grant information was disclosed by the authors:
Europasaurus-Project: 85 882.

Competing Interests

The authors declare there are no competing interests.

Author Contributions

- Jens N. Lallensack conceived and designed the experiments, performed the experiments, analyzed the data, contributed reagents/materials/analysis tools, wrote the paper, prepared figures and/or tables, reviewed drafts of the paper.

- Anneke H. van Heteren and Oliver Wings conceived and designed the experiments, analyzed the data, contributed reagents/materials/analysis tools, wrote the paper, reviewed drafts of the paper.

Data Availability

The following information was supplied regarding data availability:

Data can be found in Figshare:
10.6084/m9.figshare.3027211
10.6084/m9.figshare.2972329
10.6084/m9.figshare.3025144
10.6084/m9.figshare.3026863
10.6084/m9.figshare.3027067
10.6084/m9.figshare.3027949
10.6084/m9.figshare.3027553
10.6084/m9.figshare.3027385
10.6084/m9.figshare.3029698.

Supplemental Information

Supplemental information for this article can be found online at http://dx.doi.org/10.7717/peerj.2059#supplemental-information.

REFERENCES

Alexander RM. 1976. Estimates of speeds of dinosaurs. *Nature* **261(5556)**:129–130 DOI 10.1038/261129a0.

Baird D. 1957. Triassic reptile footprint faunules from Milford, New Jersey. *Bulletin of the Museum of Comparative Zoology* **117(5)**:449–520.

Belvedere M. 2008. Ichnological researches on the Upper Jurassic dinosaur tracks in the Iouaridène area (Demnat, central High-Atlas, Morocco). PhD thesis, Università a degli studi di Padova.

Belvedere M, Farlow JO. A numerical scale for qantifying the quality of preservation of vertebrate tracks. In: Falkingham PL, Marty D, Richter A, eds. *Dinosaur tracks: the next steps*. Bloomington: Indiana University Press. In Press.

Belvedere M, Mallison H. 2014. Metatarsal impressions in modern ratites: gait, behaviour and posture influences. *Journal of Vertebrate Paleontology, Program and Abstracts*. page 89.

Bennett MR, Reynolds SC, Morse SA, Budka M. 2016. Laetoli's lost tracks: 3D generated mean shape and missing footprints. *Scientific Reports* **6**:21916.

Bertling M, Braddy SJ, Bromley RG, Demathieu GR, Genise J, Mikuláš R, Nielsen JK, Nielsen KS, Rindsberg AK, Schlirf M, Uchman A. 2006. Names for trace fossils: a uniform approach. *Lethaia* **39(3)**:265–286 DOI 10.1080/00241160600787890.

Castanera D, Colmenar J, Sauqué V, Canudo JI. 2015. Geometric morphometric analysis applied to theropod tracks from the Lower Cretaceous (Berriasian) of Spain. *Palaeontology* **58(1)**:183–200 DOI 10.1111/pala.12132.

Castanera D, Pascual C, Razzolini NL, Vila B, Barco JL, Canudo JI. 2013. Discriminating between medium-sized tridactyl trackmakers: tracking ornithopod tracks in the base of the Cretaceous (Berriasian, Spain). *PLoS ONE* **8(11)**:e81830 DOI 10.1371/journal.pone.0081830.

Citton P, Nicosia U, Nicolosi I, Carluccio R, Romano M. 2015. Elongated theropod tracks from the Cretaceous apenninic carbonate platform of southern Latium (central Italy). *Palaeontologia Electronica* **18(3)**:1–12.

Clark NDL, Brett-Surman MK. 2008. A comparison between dinosaur footprints from the Middle Jurassic of the Isle of Skye, Scotland, UK, and Shell, Wyoming, USA. *Scottish Journal of Geology* **44(2)**:139–150 DOI 10.1144/sjg44020139.

Currie PJ, Nadon GC, Lockley MG. 1991. Dinosaur footprints with skin impressions from the Cretaceous of Alberta and Colorado. *Canadian Journal of Earth Sciences* **28(1)**:102–115 DOI 10.1139/e91-009.

Day JJ, Norman DB, Gale AS, Upchurch P, Powell HP. 2004. A Middle Jurassic dinosaur trackway site from Oxfordshire, UK. *Palaeontology* **47(2)**:319–348 DOI 10.1111/j.0031-0239.2004.00366.x.

Demathieu GR. 1987. Use of statistical methods in palaeoichnology. In: Leonardi G, ed. *Glossary and manual of tetrapod footprint palaeoichnology, page 55*. Brasília: Publicação do Departemento Nacional da Produção Mineral Brasil, 117 pp.

Demathieu GR. 1990. Problems in discrimination of tridactyl dinosaur footprints, exemplified by the Hettangian trackways, the Causses, France. *Ichnos* **1(2)**:97–110 DOI 10.1080/10420949009386339.

Díaz-Martínez I, Pereda-Suberbiola X, Pérez-Lorente F, Canudo JI. 2015. Ichnotaxonomic review of large ornithopod dinosaur tracks: temporal and geographic implications. *PLoS ONE* **10(2)**:e0115477 DOI 10.1371/journal.pone.0115477.

Erbacher J, Hiss M, Luppold F, Mutterlose J. 2014. Deister-Formation. LithoLex [Online-Datenbank], record no. 2008154. *Available at http://www.bgr.bund.de/litholex* (accessed 25 May 2016).

Falkingham PL. 2010. Computer simulation of dinosaur tracks. PhD thesis, University of Manchester.

Falkingham PL. 2014. Interpreting ecology and behaviour from the vertebrate fossil track record. *Journal of Zoology* **292(4)**:222–228 DOI 10.1111/jzo.12110.

Falkingham PL. Applying objective methods to subjective track outlines. In: Falkingham PL, Marty D, Richter A, eds. *Dinosaur tracks: the next steps*. Bloomington: Indiana University Press. In Press.

Falkingham PL, Gatesy SM. 2014. The birth of a dinosaur footprint: subsurface 3d motion reconstruction and discrete element simulation reveal track ontogeny. *Proceedings of the National Academy of Sciences of the United States of America* **111(51)**:18279–18284 DOI 10.1073/pnas.1416252111.

Farlow JO. 1987. A guide to Lower Cretaceous dinosaur footprints and tracksites of the Paluxy River Valley, Somervell County, Texas. In: *Field trip guidebook, south-central section, Geological Society of America*. Waco: Baylor University, 50.

Farlow JO. 1989. Ostrich footprints and trackways: implications for dinosaur ichnology. In: Gillette DD, Lockley MG, eds. *Dinosaur tracks and traces*. Cambridge: Cambridge University Press, 243–248.

Farlow JO, Gatesy SM, Holtz TR, Hutchinson JR, Robinson JM. 2000. Theropod locomotion. *American Zoologist* **40(4)**:640–663.

Farlow JO, Langston Jr W, Deschner EE, Solis R, Ward W, Kirkland BL, Hovorka S, Reece TL, Whitcraft J. 2007. *Texas giants: dinosaurs of the Heritage Museum of the Texas Hill Country*. Canyon Lake: The Heritage Museum of the Texas Hill Country.

Fischer R. 1998. Das Naturdenkmal "Saurierfährten Münchehagen". *Mitteilungen aus dem Institut für Geologie und Paläontologie der Universität Hannover* **37**:125 pp.

Foster JR. 2015. Theropod dinosaur ichnogenus *Hispanosauropus* identified from the Morrison Formation (Upper Jurassic), western North America. *Ichnos* **22(3–4)**:183–191 DOI 10.1080/10420940.2015.1059335.

Gangloff RA, May KC, Storer JE. 2004. An early Late Cretaceous dinosaur tracksite in central Yukon Territory, Canada. *Ichnos* **11(3–4)**:299–309 DOI 10.1080/10420940490442269.

Gatesy SM, Middleton KM, Jenkins Jr FA, Shubin NH. 1999. Three-dimensional preservation of foot movements in Triassic theropod dinosaurs. *Nature* **399(6732)**:141–144 DOI 10.1038/20167.

Gierlinski GD, Ploch I, Gawor-Biedowa E, Niedzwiedzki G. 2008. The first evidence of dinosaur tracks in the Upper Cretaceous of Poland. *Oryctos* **8**:107–113.

Grabbe H. 1881. Neue Funde von Saurier-Fährten im Wealdensandsteine des Bückeberges. *Verhandlungen des naturhistorischen Vereines der preussischen Rheinlande und Westfalens, Correspondenzblatt* **38(1)**:161–164.

Hammer Ø, Harper D, Ryan P. 2001. Past: paleontological statistics software package for education and data analysis. *Palaeontologia Electronica* **4**:1–9.

Henderson DM. 2003. Footprints, trackways, and hip heights of bipedal dinosaurs—testing hip height predictions with computer models. *Ichnos* **10(2–4)**:99–114 DOI 10.1080/10420940390257914.

Henderson DM. 2006. Simulated weathering of dinosaur tracks and the implications for their characterization. *Canadian Journal of Earth Sciences* **43(6)**:691–704 DOI 10.1139/e06-024.

Hendricks A. 1981. Die Saurierfährte von Münchehagen bei Rehburg-Loccum (NW-Deutschland). *Abhandlungen aus dem Landesmuseum für Naturkunde zu Münster in Westfalen* **43**:1–22.

Hornung JJ, Böhme A, Lubbe TVD, Reich M, Richter A. 2012. Vertebrate tracksites in the Obernkirchen Sandstone (late Berriasian, Early Cretaceous) of northwest Germany—their stratigraphical, palaeogeographical, palaeoecological, and historical context. *Paläontologische Zeitschrift* **86(3)**:231–267 DOI 10.1007/s12542-012-0131-7.

Hübner T. Elusive ornithischian tracks in the famous Berriasian (Lower Cretaceous) Chicken Yard-tracksite of Northern Germany: quantitative differentiation between small tridactyl track makers. In: Falkingham PL, Marty D, Richter A, eds. *Dinosaur tracks: the next steps*. Indiana University Press. In Press.

Ishigaki S, Fujisaki T. 1989. Three dimensional representation of *Eubrontes* by the method of moiré topography. In: Gillette DD, Lockley MG, eds. *Dinosaur tracks and traces*. Cambridge: Cambridge University Press, 421–425.

Kim BS, Huh M. 2010. Analysis of the acceleration phase of a theropod dinosaur based on a Cretaceous trackway from Korea. *Palaeogeography, Palaeoclimatology, Palaeoecology* **293(1)**:1–8 DOI 10.1016/j.palaeo.2010.04.020.

Klingenberg CP. 2011. MorphoJ: an integrated software package for geometric morphometrics. *Molecular Ecology Resources* **11(2)**:353–357 DOI 10.1111/j.1755-0998.2010.02924.x.

Kuban GJ. 1989. Elongate dinosaur tracks. In: Gillette DD, Lockley GM, eds. *Dinosaur tracks and traces*. Cambridge: Cambridge University Press, 57–72.

Lallensack JN. 2015. Can we discriminate between theropod and ornithopod dinosaur trackways based on footprint shape variation patterns? A geometric morphometrics approach. In: *13th annual meeting of the European association of vertebrate palaeontologists, abstracts*, 47.

Lallensack JN, Sander PM, Knötschke N, Wings O. 2015. Dinosaur tracks from the Langenberg Quarry (Late Jurassic, Germany) reconstructed with historical photogrammetry: evidence for large theropods soon after insular dwarfism. *Palaeontologia Electronica* **18.2.24A**:1–34.

Langston Jr W. 1974. Nonmammalian comanchean tetrapods. *Geoscience and Man* **8**:77–102.

Leonardi G. 1987. Discussion of the terms and methods. In: Leonardi G, ed. *Glossary and manual of tetrapod footprint palaeoichnology, pages 43–51*. Brasília: Publicação do Departemento Nacional da Produção Mineral Brasil, 117 pp.

Lockley MG. 1987. Dinosaur footprints from the Dakota Group of eastern Colorado. *The Mountain Geologist* **24(4)**:107–122.

Lockley MG. 1998. Philosophical perspectives on theropod track morphology: blending qualities and quantities in the science of ichnology. *GAIA* **15**:279–300.

Lockley MG. 1999. *The eternal trail: a tracker looks at evolution*. New York: Perseus Books, 360 pp.

Lockley MG. 2009. New perspectives on morphological variation in tridactyl footprints: clues to widespread convergence in developmental dynamics. *Geological Quarterly* **53(4)**:415–432.

Lockley GM, Conrad K. 1989. The paleoenvironmental context, preservation and paleoecological significance of dinosaur tracksites in the western USA. In: Gillette DD, Lockley GM, eds. *Dinosaur tracks and traces*. Cambridge: Cambridge University Press, 121–134.

Lockley MG, Foster J, Hunt AP. 1998. A short summary of dinosaur tracks and other fossil footprints from the Morrison Formation. *Modern Geology* **23(2)**:277–290.

Lockley MG, Li R, Harris JD, Matsukawa M, Liu M. 2007. Earliest zygodactyl bird feet: evidence from Early Cretaceous roadrunner-like tracks. *Naturwissenschaften* **94(8)**:657–665 DOI 10.1007/s00114-007-0239-x.

Lockley GM, Matsukawa M, Sato Y, Polahan M, Daorerk V. 2006. A distinctive new theropod dinosaur track from the Cretaceous of Thailand: implications for theropod track diversity. *Cretaceous Research* **27(1)**:139–145 DOI 10.1016/j.cretres.2005.10.002.

Lockley MG, Meyer C, Dos Santos VF. 1998. *Megalosauripus* and the problematic concept of megalosaur footprints. *GAIA* **15**:313–337.

Lockley MG, Meyer CA, Moratalla JJ. 1998. *Therangospodus*: trackway evidence for the widespread distribution of a Late Jurassic theropod with well-padded feet. *GAIA* **15**:339–353.

Lockley MG, Wright JL. 2001. Trackways of large quadrupedal ornithopods from the Cretaceous: a review. In: Tanke D, Carpenter K, eds. *Mesozoic vertebrate life*. Bloomington: Indiana University Press, 428–442.

Lockley MG, Wright JL, Thies D. 2004. Some observations on the dinosaur tracks at Münchehagen (Lower Cretaceous), Germany. *Ichnos* **11(3–4)**:261–274 DOI 10.1080/10420940490428805.

Lockley MG, Xing L. 2015. Flattened fossil footprints: implications for paleobiology. *Palaeogeography, Palaeoclimatology, Palaeoecology* **426**:85–94 DOI 10.1016/j.palaeo.2015.03.008.

Lockley MG, Xing LD, Lockwood JA, Pond S. 2014. A review of large Cretaceous ornithopod tracks, with special reference to their ichnotaxonomy. *Biological Journal of the Linnean Society* **113(3)**:721–736 DOI 10.1111/bij.12294.

Lockley MG, Young BH, Carpenter K. 1983. Hadrosaur locomotion and herding behavior: evidence from footprints in the Mesaverde Formation, Grand Mesa Coal Field, Colorado. *The Mountain Geologist* **20(1)**:5–14.

Loza LER, Medrano NH, Lorente FP. 2006. La Pellejera: Descripción y aportaciones. Heterocronía y variabilidad de un yacimiento con huellas de dinosaurio de La Rioja (España). *Zubía* **18**:21–114.

Lucas SG, Sullivan RM, Jasinski SE, Ford TL. 2011. Hadrosaur footprints from the Upper Cretaceous Fruitland Formation, San Juan Basin, New Mexico, and the ichnotaxonomy of large ornithopod footprints. *New Mexico Museum of Natural History Bulletin* **53**:357–362.

Mallison H, Wings O. 2014. Photogrammetry in paleontology—a practical guide. *Journal of Paleontological Techniques* **12**:1–31.

Martin AJ, Rich TH, Hall M, Vickers-Rich P, Vazquez-Prokopec G. 2012. A polar dinosaur-track assemblage from the Eumeralla Formation (Albian), Victoria, Australia. *Alcheringa: An Australasian Journal of Palaeontology* **36(2)**:171–188 DOI 10.1080/03115518.2011.597564.

Marzola M, Dalla Vecchia FM. 2014. New dinosaur tracks from the Dolomia Principale (Upper Triassic) of the Carnic Prealps (Friuli-Venezia Giulia, NE Italy). *Bollettino Della Società Paleontologica Italiana* **53(1)**:1–18.

Mateus O, Milán J. 2008. Ichnological evidence for giant ornithopod dinosaurs in the Upper Jurassic Lourinhã Formation, Portugal. *Oryctos* **8**:47–52.

McClay IS, Cavanagh PR. 1994. Relationship between foot placement and mediolateral ground reaction forces during running. *Clinical Biomechanics* **9(2)**:117–123 DOI 10.1016/0268-0033(94)90034-5.

McCrea RT, Buckley LG, Farlow JO, Lockley MG, Currie PJ, Matthews NA, Pemberton SG. 2014. A 'terror of tyrannosaurs': the first trackways of tyrannosaurids and evidence of gregariousness and pathology in Tyrannosauridae. *PLoS ONE* **9(7)**:e103613 DOI 10.1371/journal.pone.0103613.

Moratalla JJ, Sanz JL, Jimenez S. 1988. Multivariate analysis on Lower Cretaceous dinosaur footprints: discrimination between ornithopods and theropods. *Geobios* **21(4)**:395–408 DOI 10.1016/S0016-6995(88)80042-1.

Mutterlose J. 1997. Münchehagen quarry. In: Mutterlose J, Wippich MGE, Geisen M, eds. *Cretaceous depositional environments of NW Germany*, vol. 46. Bochum: Bochumer geologische und geotechnische Arbeiten, 123–134.

Mutterlose J, Bodin S, Fähnrich L. 2014. Strontium-isotope stratigraphy of the Early Cretaceous (Valanginian–Barremian): implications for Boreal–Tethys correlation and paleoclimate. *Cretaceous Research* **50**:252–263 DOI 10.1016/j.cretres.2014.03.027.

Olsen PE, Smith JB, McDonald NG. 1998. Type material of the type species of the classic theropod footprint genera *Eubrontes*, *Anchisauripus*, and *Grallator* (Early Jurassic, Hartford and Deerfield basins, Connecticut and Massachusetts, USA). *Journal of Vertebrate Paleontology* **18(3)**:586–601 DOI 10.1080/02724634.1998.10011086.

Padian K, Olsen PE. 1989. Ratite footprints and the stance and gait of Mesozoic theropods. In: Gillette DD, Lockley GM, eds. *Dinosaur tracks and traces*. Cambridge: Cambridge University Press, 231–241.

Peabody FE. 1948. Reptile and amphibian trackways from the Lower Triassic Moenkopi Formation of Arizona and Utah. *California University, Bulletin Department of Geological Sciences* **27**:295–468.

Pérez-Lorente F. 1993. Dinosaurios plantígrados en la Rioja. *Zubía* **5**:189–228.

Pérez-Lorente F. 2015. *Dinosaur footprints and trackways of La Rioja*. Bloomington: Indiana University Press, 363 pp.

Petti FM, Avanzini M, Belvedere M, De Gasperi M, Ferretti P, Girardi S, Remondino F, Tomasoni R. 2008. Digital 3D modelling of dinosaur footprints by photogrammetry and laser scanning techniques: integrated approach at the Coste dell'Anglone tracksite (Lower Jurassic, Southern Alps, Northern Italy). *Studi Trentini di Scienze Naturali, Acta Geologica* **83**:303–315.

Pittman JG. 1989. Stratigraphy, lithology, depositional environment, and track type of dinosaur track-bearing beds of the Gulf Coastal Plain. In: Gillette DD, Lockley GM, eds. *Dinosaur tracks and traces*. Cambridge: Cambridge University Press, 135–153.

Pittman JG, Gillette DD. 1989. The Briar Site: a new sauropod dinosaur tracksite in Lower Cretaceous beds of Arkansas, USA. In: Gillette DD, Lockley MG, eds. *Dinosaur tracks and traces*. Cambridge: Cambridge University Press, 313–332.

Rasskin-Gutman D, Hunt G, Chapman RE, Sanz JL, Moratalla JJ. 1997. The shapes of tridactyl dinosaur footprints: procedures, problems and potentials. In: Wolberg DL,

Stump E, Rosenberg GD, eds. *Dinofest international: proceedings of a symposium held at Arizona State University*. Philadelphia: Academy of Natural Sciences, 377–383.

Razzolini NL, Vila B, Díaz-Martínez I, Manning PL, Galobart A. 2016. Pes shape variation in an ornithopod dinosaur trackway (Lower Cretaceous, NW Spain): new evidence of an antalgic gait in the fossil track record. *Cretaceous Research* **58**:125–134 DOI 10.1016/j.cretres.2015.10.012.

Reyment R, Savazzi E. 1999. *Aspects of multivariate statistical analysis in geology*. Amsterdam: Elsevier.

Rodrigues LA, Santos VF. 2002. Sauropod tracks—a geometric morphometric study. In: Elewa A, ed. *Morphometrics: applications in biology and paleontology*. Berlin, Heidelberg: Springer-Verlag, 129–142.

Rohlf FJ. 2003. Bias and error in estimates of mean shape in geometric morphometrics. *Journal of Human Evolution* **44(6)**:665–683 DOI 10.1016/S0047-2484(03)00047-2.

Rohlf FJ. 2014. *Tps series*. New York: Department of Ecology and Evolution, State University of New York at Stony Brook. *Available at http://life.bio.sunysb.edu/morph/*.

Romilio A, Salisbury SW. 2011. A reassessment of large theropod dinosaur tracks from the mid-Cretaceous (late Albian–Cenomanian) Winton Formation of Lark Quarry, central-western Queensland, Australia: a case for mistaken identity. *Cretaceous Research* **32(2)**:135–142 DOI 10.1016/j.cretres.2010.11.003.

Romilio A, Salisbury SW. 2014. Large dinosaurian tracks from the Upper Cretaceous (Cenomanian–Turonian) portion of the Winton Formation, Lark Quarry, central-western Queensland, Australia: 3D photogrammetric analysis renders the 'stampede trigger' scenario unlikely. *Cretaceous Research* **51**:186–207 DOI 10.1016/j.cretres.2014.06.003.

Romilio A, Tucker RT, Salisbury SW. 2013. Reevaluation of the Lark Quarry dinosaur Tracksite (late Albian–Cenomanian Winton Formation, central-western Queensland, Australia): no longer a stampede? *Journal of Vertebrate Paleontology* **33(1)**:102–120 DOI 10.1080/02724634.2012.694591.

Sarjeant WAS. 1975. Fossil tracks and impressions of vertebrates. In: Frey RW, ed. *The study of trace fossils*. Berlin, Heidelberg: Springer-Verlag, 283–324.

Schulp AS. 2002. The effects of tectonic deformation on dinosaur trackway morphology. *Sargetia. Acta Musei Devensis, Series Scientia Naturae, Deva* **19(27)**:e32.

Schulp AS, Al-Wosabi M. 2012. Telling apart ornithopod and theropod trackways: a closer look at a large, Late Jurassic tridactyl dinosaur trackway at Serwah, Republic of Yemen. *Ichnos* **19(4)**:194–198 DOI 10.1080/10420940.2012.710672.

Scott JJ, Renaut RW, Owen RB. 2010. Taphonomic controls on animal tracks at saline, alkaline Lake Bogoria, Kenya Rift Valley: impact of salt efflorescence and clay mineralogy. *Journal of Sedimentary Research* **80(7)**:639–665 DOI 10.2110/jsr.2010.057.

Therrien F, Zelenitsky DK, Quinney A, Tanaka K, Sues H-D. 2015. Dinosaur trackways from the Upper Cretaceous Oldman and Dinosaur Park formations (Belly River Group) of southern Alberta, Canada, reveal novel ichnofossil preservation style. *Canadian Journal of Earth Sciences* **52(8)**:630–641 DOI 10.1139/cjes-2014-0168.

Thulborn RA. 1990. *Dinosaur tracks*. London: Chapman and Hall.

Thulborn T. 1998. Australia's earliest theropods: footprint evidence in the Ipswich Coal Measures (Upper Triassic) of Queensland. *Gaia* **15**:301–311.

Thulborn RA. 2013. Lark Quarry revisited: a critique of methods used to identify a large dinosaurian track-maker in the Winton Formation (Albian–Cenomanian), western Queensland, Australia. *Alcheringa: An Australasian Journal of Palaeontology* **37(3)**:312–330 DOI 10.1080/03115518.2013.748482.

Thulborn RA, Wade M. 1984. Dinosaur trackways in the Winton Formation (mid-Cretaceous) of Queensland. *Memoirs of the Queensland Museum* **21(2)**:413–517.

Troelsen P. 2015. The speed of theropod dinosaurs: new data from trackways at Münchehagen, Germany. In: *13th annual meeting of the European association of vertebrate palaeontologists, abstracts*, 85.

Vela AJ, Lorente FP. 2006. El corral del Totico: dos nuevos yacimientos con pistas singulares. (Enciso, La Rioja. España). *Zubia* **18**:115–144.

Weems RE. 1992. A re-evaluation of the taxonomy of Newark Supergroup saurischian dinosaur tracks, using extensive statistical data from a recently exposed tracksite near Culpeper, Virginia. *Proceedings 26th Forum on the Geology of Industrial Minerals. Virginia Division of Mineral Resources Publication* **119**:113–127.

Wings O, Falk D, Knötschke N, Richter A. 2012. Excursion guide B1: the Early Cretaceous dinosaur trackways in Münchehagen (Lower Saxony, Germany)—the natural monument 'Saurierfährten Münchehagen' and the adjacent Wesling Quarry. In: *Dinosaur tracks 2011. An international symposium, Obernkirchen, April 14–17, 2011. Abstract volume and field guide to excursions*. Göttingen: Universitätsdrucke Göttingen, 113–142.

Wings O, Lallensack JN, Mallison H. The Early Cretaceous Dinosaur Trackways in Münchehagen (Lower Saxony, Germany)—3D photogrammetry as basis for geometric morphometric analysis of shape variation and evaluation of material loss during excavation. In: Falkingham PL, Marty D, Richter A, eds. *Dinosaur tracks: the next steps*. Bloomington: Indiana University Press. In Press.

Xing LD, Harris JD, Feng XY, Zhang ZJ. 2009. Theropod (Dinosauria: Saurischia) tracks from Lower Cretaceous Yixian Formation at Sihetun, Liaoning Province, China and possible track makers. *Geological Bulletin of China* **28(6)**:705–712.

Xing LD, Klein H, Lockley MG, Wetzel A, Li ZD, Li JJ, Gierlinski GD, Zhang JP, Matsukawa M, Divay JD, Zhou L. 2014d. *Changpeipus* (theropod) tracks from the Middle Jurassic of the Turpan Basin, Xinjiang, Northwest China: new discoveries, ichnotaxonomy, preservation and paleoecology. *Vertebrata PalAsiatica* **52**:233–259.

Xing LD, Lockley MG, Chen W, Gierliński G, Li J, Persons IV WS, Matsukawa M, Yong Y, Gingras MK, Wang C-W. 2013. Two theropod track assemblages from the Jurassic of Chongqing, China, and the Jurassic stratigraphy of Sichuan Basin. *Vertebrata PalAsiatica* **51(2)**:107–130.

Xing LD, Lockley MG, Klein H, Gierliński GD, Divay JD, Hu SM, Zhang JP, Ye Y, He YP. 2014a. The non-avian theropod track *Jialingpus* from the Cretaceous of the Ordos Basin, China, with a revision of the type material: implications

for ichnotaxonomy and trackmaker morphology. *Palaeoworld* **23(2)**:187–199 DOI 10.1016/j.palwor.2013.12.001.

Xing LD, Lockley MG, Zhang J, Klein H, Kim JY, Persons IV WS, Matsukawa M, Yu X, Li J, Chen G, Hu Y. 2014b. Upper Cretaceous dinosaur track assemblages and a new theropod ichnotaxon from Anhui Province, eastern China. *Cretaceous Research* **49**:190–204 DOI 10.1016/j.cretres.2014.03.003.

Xing LD, Lockley MG, Zhang J, Klein H, Marty D, Peng G, Ye Y, McCrea RT, Persons WS, Xu T. 2015. The longest theropod trackway from East Asia, and a diverse sauropod-, theropod-, and ornithopod-track assemblage from the Lower Cretaceous Jiaguan Formation, southwest China. *Cretaceous Research* **56**:345–362 DOI 10.1016/j.cretres.2015.05.008.

Xing LD, Lockley MG, Zhang J, Klein H, Persons WS, Dai H. 2014c. Diverse sauropod-, theropod-, and ornithopod-track assemblages and a new ichnotaxon *Siamopodus xui* ichnosp. nov. from the Feitianshan Formation, Lower Cretaceous of Sichuan Province, southwest China. *Palaeogeography, Palaeoclimatology, Palaeoecology* **414**:79–97 DOI 10.1016/j.palaeo.2014.08.011.

Supplemental Figures S1 and S2

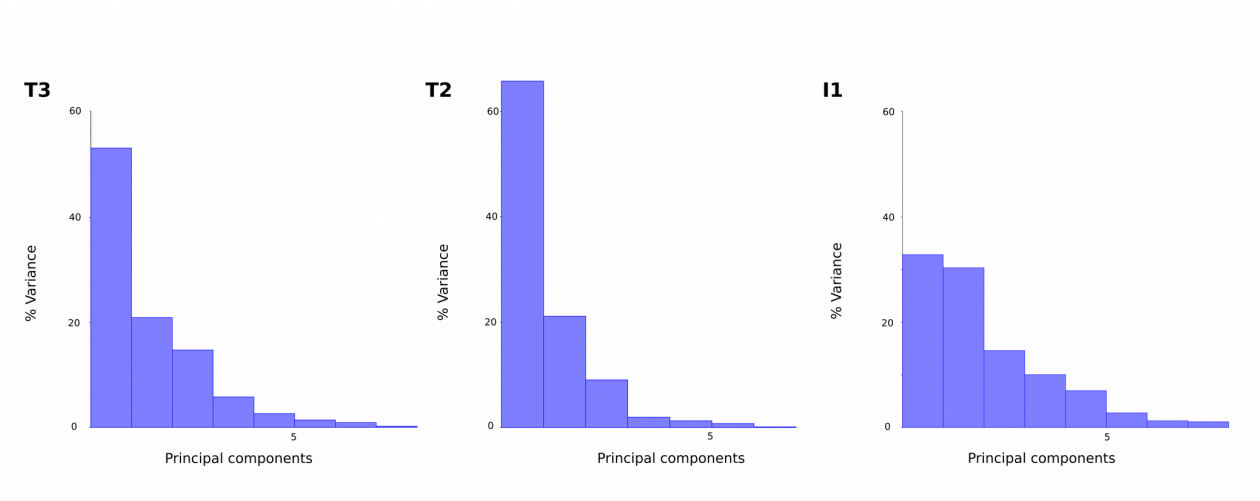

Figure S1: Loadings of the principal components of the T3, T2 and I1 trackways, based on objectively placed landmarks using the steepest slope approach. For the two theropod (T3 and T2) trackways, much of the variation is explained by the first principal component, while in the I1 trackway loadings are more equally distributed among the principal components. A similar pattern was derived from landmarks placed on interpretative outlines (compare with Fig. 9.)

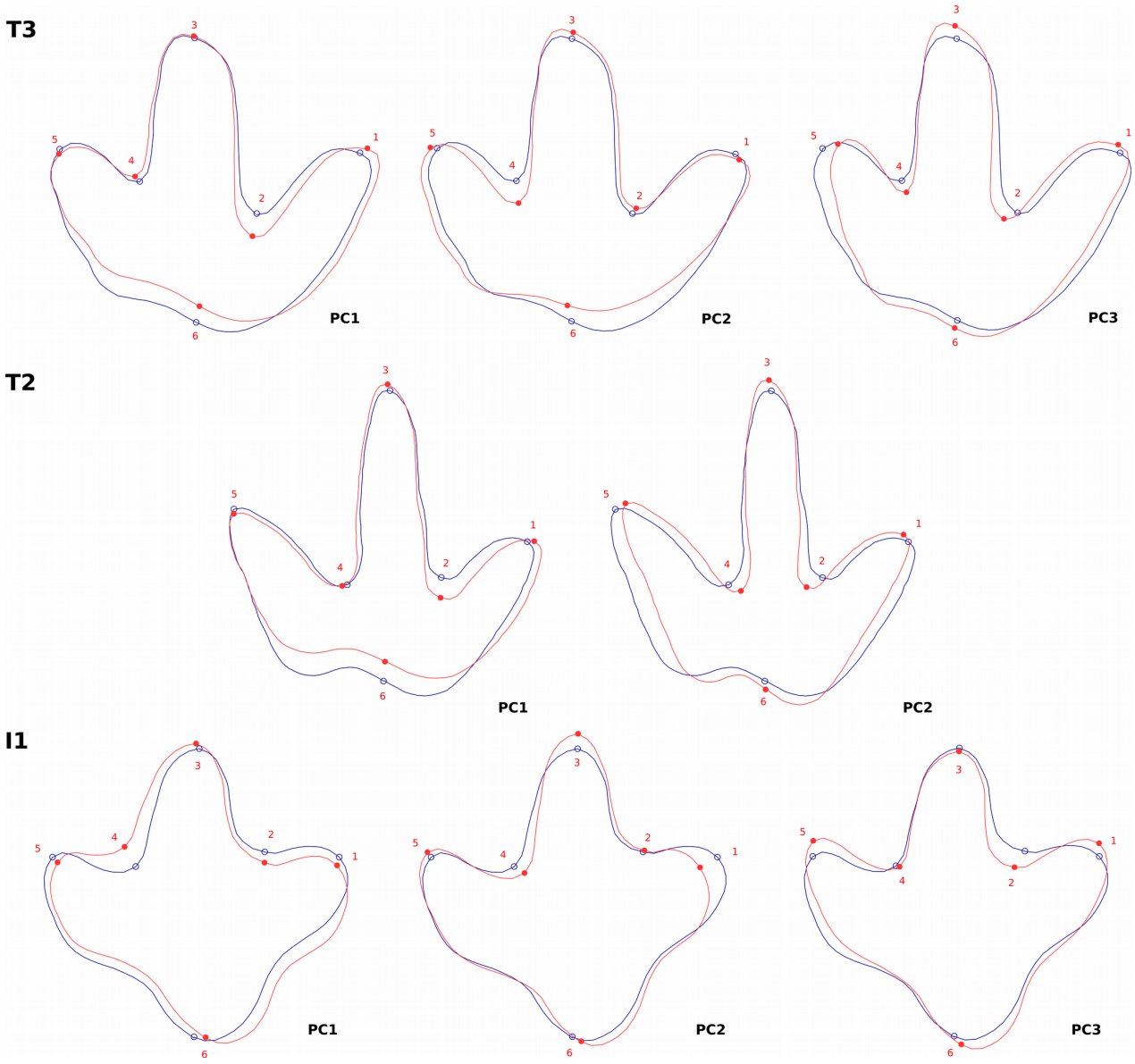

Figure S2: Shape changes described by principal components based on objectively placed landmarks using the steepest slope approach. The shape changes (red outlines, solid dots) are shown relative to the mean shapes (blue outlines, hollow dots) using warped outline drawings. Shape changes described by the first principal components of the T3 and T2 trackways are nearly identical to those derived from principal component analysis of landmarks placed on interpretative outlines; only for the I1 trackway both approaches give different results (compare with Fig. 10).

Supplemental table S1: Measurements of trackway parameters

Abbreviations:
db = measured based on reference points at the base of digit impression III (see article text for details)
dt = measured based on reference points at the tip of digit impression III (see article text for details)
PA = Pace angulation
FR = Footprint rotation

Trackway T3	**Footprint Nr.**	**left/right**	**Pace (db)** [cm]	**Pace (dt)** [cm]	**Stride (db)** [cm]	**Stride (dt)** [cm]	**PA (db)** [°]	**PA (dt)** [°]	**FR (db)** [°]	**FR (dt)** [°]
	T3/23	right								
	T3/24	left								
	T3/25	right								
	T3/26	left								
	T3/27	right								
	T3/28	left	115.31	115.15	229.48	229.37				
	T3/29	right	115.23	115.1	206.16	207.12	169.01	169.94	-0.61	-0.53
	T3/30	left	108.57	112.18	212.93	214.64	134.18	131.37	14.72	17.01
	T3/31	right	109.34	109.37			155.45	151.32	-6.89	-8.18
	T3/32	left			225.93	225.97				
	T3/33	right								
	T3/34	left	112.65	112.27	223.45	223.61				
	T3/35	right	113.02	112.9	227.21	227.85	163.91	166.5	-4.67	-3.68
	T3/36	left	118.24	118.99	228.83	228.23	158.52	158.55	4.54	5.13
	T3/37	right	113.43	113.1	229.43	228.9	162.05	159.06	-3.15	-2.2
	T3/38	left	119.03	120.39	231.5	233.74	161.47	157.24	16.26	16.15
	T3/39	right	112.46	113.36	228.87	205.83	179.91	179.07	-14.82	-17.17
	T3/40	left	116.86	93.08	231.7	231.2	172.79	171.15	4.81	7.77
	T3/41	right	115.08	139.4	234.45	258.48	174.81	167.71	-1.95	10.18
	T3/42	left	120.57	122.34	240.45	241.33	168.41	161.87	15.86	15.26
	T3/43	right	121.13	121.43	239.11	239.48	168.32	163.79	6.33	4.85
	T3/44	left	118.04	118.07	220.96	221.85	177.35	178.64	-6.07	-7.46
	T3/45	right	107.52	108.29	232.15	232.37	156.8	157.07	3.78	5.84
	T3/46	left	126.38	126.23	237.88	237.89	165.96	164.45	1.33	0.29
	T3/47	right	113.63	113.76			164.7	164.83	-2.8	-2.49
	T3/48	left								
AVERAGE			115.361	115.856	228.264	228.698	164.603	162.660	1.667	2.548
STANDARD DEVIATION			4.758	9.212	8.820	12.650	10.775	11.248	8.701	9.555
COEFFICIENT OF VARIATION			4.125	7.952	3.864	5.531				

Trackway T2	**Footprint Nr.**	**left/right**	**Pace (db)** [cm]	**Pace (dt)** [cm]	**Stride (db)** [cm]	**Stride (dt)** [cm]	**PA (db)** [°]	**PA (dt)** [°]	**FR (db)** [°]	**FR (dt)** [°]
	T2/1	right	101.7	102.66	210.35	209.73				
	T2/2	left	109.02	107.33	210.97	208.91	186.8	185.65	10.41	8.89
	T2/3	right	101.99	101.77	202.59	201.91	182.26	184.94	-9.22	-5.23
	T2/4	left	100.77	100.56	200.67	200.26	184.71	187.36	3.86	-1.09
	T2/5	right	101.27	101.84	206.77	208.29	193.36	196.66	-8.47	-10.86
	T2/6	left	105.66	106.82	213.31	211.79	184.52	186.79	0.74	3.62
	T2/7	right	108.11	105.4	209.48	208.27	172.48	172.68	5.28	6.54
	T2/8	left	101.38	102.91	210.7	211.88	181.12	182.15	-8.96	-6.33
	T2/9	right	109.36	108.97	210.65	210.23	177.73	179.5	7.53	2.63
	T2/10	left	101.74	101.48	203.16	202.87	172.51	174.63	0.47	1.11
	T2/11	right	101.59	101.73	206.43	206.05	184.73	186.67	-5.32	-4.5
	T2/12	left	105.8	105.6	209.39	208.84	191.03	192.72	3.18	3.28
	T2/13	right	103.99	103.86	212.69	212.16	187.09	188.76	1.62	-1.23
	T2/14	left	108.74	108.38	210.94	211.23	182.28	183.11	4.49	5.76
	T2/15	right	102.23	102.91	204.11	203.21	177.84	177.18	-0.42	2.19
	T2/16	left	102.29	100.6			187.29	186.28	1.37	1.43
	T2/17	right			208.14	210.27				
	T2/18	left								
	T2/19	right	104.46	103.15	206.8	204.64				
	T2/20	left	102.41	101.64	209.34	208.74	176.84	175.52	4.63	8
	T2/21	right	107.03	107.35	209.6	200.74	176.5	174.4	7.16	5.69
	T2/22	left	102.92	93.79	202.43	202.05	186.57	187.26	-5.79	-4.74
	T2/23	right	100.1	108.99			188.76	189.77	-5.1	-1.93
	T2/24	left								
AVERAGE			103.931	103.702	207.926	207.104	182.864	183.791	0.393	0.696
STANDARD DEVIATION			2.988	3.612	3.655	4.012	5.940	6.617	5.954	5.352
COEFFICIENT OF VARIATION			2.875	3.483	1.758	1.937				

Trackway I1	Footprint Nr.	left/right	Pace (db) [cm]	Pace (dt) [cm]	Stride (db) [cm]	Stride (dt) [cm]	PA (db) [°]	PA (dt) [°]	FR (db) [°]	FR (dt) [°]
	I1/17	right								
	I1/18	left								
	I1/19	right								
	I1/20	left								
	I1/21	right								
	I1/22	left								
	I1/23	right	74.25	75.49	141.56	141.42				
	I1/24	left	67.49	66.01	133.54	133.39	174.18	176.05	2.49	-4.2
	I1/25	right	67.56	67.65	132.86	132.99	162.88	172.64	-17.75	-17.89
	I1/26	left	65.3	65.66	133.26	134.19	179.6	187.97	-12.97	-12.13
	I1/27	right	69.31	69.38	125	125.19	163.8	167.09	6.9	8.33
	I1/28	left	55.88	55.81	117.01	118.3	173.7	179.55	-11.34	-14.5
	I1/29	right	66.12	65.12	132.31	132.53	147.02	155.96	0.9	2.74
	I1/30	left	66.7	67.41	135.6	136.7	170.05	179.11	-21.43	-23.45
	I1/31	right	69.22	69.31	133.85	134.14	172.17	182.15	-10.55	-8.79
	I1/32	left	65.38	65.06			167.8	173.2	-1.37	-0.82
	I1/33	right			133.02	132.78				
	I1/34	left								
	I1/35	right	63.55	62.93	127.62	127.08				
	I1/36	left	65.04	64.25	128.56	127.81	165.89	175.36	-9.62	-11.52
	I1/37	right	63.53	64.86	118.97	120.43	179.14	196.27	-24.65	-26.91
	I1/38	left	55.77	56.12	121.29	120.96	171.46	190.89	-17.67	-16.18
	I1/39	right	67.65	64.96	132.28	132.15	158.58	174.8	-7.54	-7.8
	I1/40	left	66.66	67.36	135.3	135.61	160.07	174.15	-26.65	-25.94
	I1/41	right	70.56	68.5	138.17	137.73	160.81	173.05	-3.6	-3.38
	I1/42	left	68.78	69.23	133.73	134.46	165.13	179.55	-25.52	-27.06
	I1/43	right	65.94	65.28	127.59	129.22	166.12	183.19	-16.43	-16.01
	I1/44	left	65.82	65.44	134.84	134.68	151.09	162.64	-12.37	-10.13
	I1/45	right	70.07	69.53	139.27	138.86	165.66	172.53	-9.07	-9.28
	I1/46	left	69.25	69.44	135.04	134.93	176.78	184.64	-12.77	-13.1
	I1/47	right	65.87	65.65	130.27	130.41	176	185.41	-6.75	-7.06
	I1/48	left	64.89	64.76	127.79	127.88	170.09	179.62	-12.5	-12.28
	I1/49	right	64.75	63.77	131.81	132.01	160.57	168.41	-1.68	-1.22
	I1/50	left	67.76	68.3	132.92	133.74	168.17	176.43	-17.07	-17.79
	I1/51	right	66.43	65.74	127.94	128.02	164.25	172.23	-2.97	-2.01
	I1/52	left	63.71	63.29			158.91	165.63	-18.16	-8.74
	I1/53	right								
AVERAGE			66.187	65.940	131.163	131.393	166.535	176.482	-11.159	-11.043
STANDARD DEVIATION			3.775	3.840	5.763	5.569	7.999	8.842	8.827	9.035
COEFFICIENT OF VARIATION			5.703	5.824	4.394	4.239				

Chapter 3

unpublished.

Lallensack, J.N., Engler, T., Barthel, H.J., unpubl. Shape variability in tridactyl dinosaur footprints: The significance of size and function. Doctoral thesis 2018 (chapter 3). Bonn, Germany. **p. 62–98.**

Supplementary Material:

- Supplementary Material S1: Data Sample. **p. 99–102.**
- Supplementary Material S2: Correlation coefficients and p-values. **p. 103.**

Author contributions:

- Jens N. Lallensack conceived the statistical analysis, collected data, analyzed the data, wrote the paper, prepared figures and tables, reviewed drafts of the paper.
- Thomas Engler and H. Jonas Barthel collected data, wrote the paper, and reviewed drafts of the paper.

Shape variability in tridactyl dinosaur footprints: The significance of size and function

Jens N. Lallensack[1], Thomas Engler[1], and H. Jonas Barthel[1]

[1] Division of Paleontology, Steinmann Institute, University of Bonn, Bonn, Germany

ABSTRACT

The functional anatomy of the hindlimb of bipedal dinosaurs has been intensively studied. Yet, surprisingly little work has been done concerning functional adaptations in the digits for terrestrial locomotion. This lack of research is probably reflecting the scarcity of complete and articulated pes skeletons in the fossil record. However, pes shape is abundantly recorded by the rapidly increasing record of fossil footprints, providing a complementary data source yielding great potential for the understanding of dinosaur locomotion. Here we aim to elucidate the significance of footprint shape for locomotion using a larger sample (n=303) of tridactyl dinosaur footprints from a broad range of geographic localities and time slots, taken from the literature. Shape variation is characterized separately for theropods and ornithischians, the two principal trackmaker taxa. The influence of size on shape is quantified, and an attempt made to analyze shape independent of size. The projection of digit III beyond digits II and IV is proposed to be correlated with cursorial ability. Increased interdigital angles are associated with a decrease in digital widths, and are hypothesized to represent an adaptation for stability.

INTRODUCTION

Understanding shape variation of fossil dinosaur footprints is fundamental for their interpretation. Yet, the influence of the separate factors leading to this variation are still poorly understood. Putting aside the difficult to avoid subjectivity of the observer in defining the footprint borders (Falkingham, 2016) as well pre- and postburial alteration, footprint shape is not only determined by the anatomy of the trackmaker, but also by its behavior (including foot kinematics) and the condition of the substrate, factors whose importance have been fully appreciated only recently (Falkingham, 2014). Variation referable to the anatomy of the trackmaker can be intraspecific, interspecific, or ontogenetic in nature. Even if variation can be assumed to be interspecific in origin, the question remains if it reflects the phylogeny of the trackmaker or if it arises from differing functional morphologies overprinting any phylogenetic signal. Footprint shape has often been interpreted to reflect phylogeny. On this basis, ichnotaxonomy is employed to classify footprints into morphotypes that ideally would correspond to a biological taxon at some level (e.g., Farlow et al., 2012b). Although ichnotaxonomy is employed by many, if not most, recently published ichnological research articles or contributions, the basic assumption of phylogenetic informativeness of widely used shape features has rarely been evaluated.

Olsen (1980) was the first to statistically demonstrate how dinosaur footprint shape can vary with size, based on a sample of the classical theropod ichnotaxa *Grallator*, *Anchisauripus,* and *Eubrontes* from the Newark Supergroup of New Jersey, US. Arguing that a continuous decrease in "toe extension" (the projection of digit III beyond digits II and IV, henceforth termed digit III projection) with increasing footprint size represents an allometric relationship, this author proposed that the three ichnotaxa might represent different ontogenetic stages, possibly of the same trackmaker species. Later, Olsen noted correlations with size also for both the footprint length-to-width ratio and the interdigital angle: Large tracks (*Eubrontes*) tend to be proportionally wider and show a larger interdigital angle as well as a relatively shorter digit III impression compared to small footprints (*Grallator*) (Olsen, 1995). It remains unclear, however, if these allometric relationships are intraspecific, interspecific, or both (cf. Olsen et al., 1998).

Lockley (2009) suggested that the same allometric relationships hold true for other, although not all, theropod taxa as well. According to this author, the Chinese ichnotaxon *Minisauripus* represents a notable exception—despite its minute size (2.5–6.1 cm), it shows a low digit III projection similar to much larger theropod tracks such as *Eubrontes* (Lockley, 2009; Lockley et al., 2008b). Discussed in a morphodynamic context, Lockley et al. (2008b) argued that this for its size unusual morphology in *Minisauripus* might be the result of heterochrony. Furthermore, Lockley (2009) suggested that similar allometric relationships of the length-to-width ratio and the digit III projection exist in ornithopods as well, as is exemplified by very large ornithopod tracks with very low digit III projection values (e.g., *Ornithopodichnus*; Kim et al., 2009). Exceptions from this trend—relatively small footprints with low projection values—have been discussed in subsequent reports (Lockley et al., 2012; Xing and Lockley, 2014). Statistical support for allometric trends outside the *Grallator–Anchisauripus–Eubrontes* plexus, however, has not been presented by any of these studies.

In the following, we explore gross shape variation in tridactyl dinosaur footprints. The influence of allometry on the shape as a whole and on separate shape features will be assessed, as will be covariation of separate shape features. We will furthermore evaluate the question if footprint shape holds a strong functional signal, and attempt to interpret the possible functional meaning of recurring shape variation patterns.

MATERIAL & METHODS

Data collection

The present study is based on data derived from illustrations published in the literature. Our sample encompasses 303 footprints taken from a total of 134 publications (Adams et al., 2010; Avanzini et al., 2012; Barco et al., 2005; Belvedere et al., 2010; Calvo, 1991; Castanera et al., 2013a, 2013b; Contessi, 2013; Currie et al., 1991; Dalla Vecchia et al., 2000; Dalman and Weems, 2013; Ellenberger, 1974, 1972; Fanti et al., 2013; Foster, 2015; Foster et al., 2000; Foster and Lockley, 2006; Fuentes Vidarte and Meijide Calvo, 1998; Fujita et al., 2007; Gand et al., 2005; Gaston et al., 2003; Gatesy et al., 1999; Gierliński, 1996a, 1991; Gierliński et al., 2009a, 2009b, 2008, 2004, 2001; Gierliński and Ahlberg, 1994; Gierliński and Sabath, 2008; Henderson, 2017; Herrero et al., 2016; Huh et al., 2003; Ishigaki and Fujisaki, 1989; Kellner et al., 2012; Kim et al., 2016, 2017; Lallensack et al., 2016, 2015; Leonardi, 1984, 1980; Leonardi and Dos Santos, 2004; Li et al., 2006, 2012, 2015; Lim et al., 2012; Lockley, 1987; Lockley et al., 2014a, 2014b, 2014c, 2014d, 2014e, 2014f, 2014g, 2014h, 2013, 2012, 2011, 2009, 2008a, 2008b, 2007, 2006a, 2006b, 2004, 2003, 2002, 2001, 2000, 1998a, 1998b, 1998c, 1996;

Lockley and Gierliński, 2006; Lockley and Hunt, 1994; Lockley and Matsukawa, 1998; Marty et al., 2017; Masrour et al., 2017; Mateus and Miguel, 2003; Matsukawa et al., 2006, 1997; McCrea et al., 2014a, 2014b; Meyer and Thuring, 2003; Milàn and Surlyk, 2015; Milner et al., 2006; Milner and Lockley, 2006; Niedźwiedzki and Pieńkowski, 2004; Olsen, 1980; Olsen et al., 1998; Olsen and Galton, 1984; Olsen and Rainforth, 2003; Pascual-Arribas et al., 2009; Pittman, 1989; Raath, 1972; Rainforth and Lockley, 1996; Razzolini et al., 2017; Rodríguez-de la Rosa et al., 2012; Salisbury et al., 2017; Santos et al., 2013; Shounan et al., 1989; Thulborn, 1994; Wagensommer et al., 2016, 2012; Wang et al., 2016; Weems, 2006; Xing et al., 2017a, 2017b, 2016a, 2016b, 2016c, 2016d, 2016e, 2016f, 2015a, 2015b, 2015c, 2015d, 2014a, 2014b, 2014c, 2014d, 2014e, 2014f, 2014g, 2014h, 2014i, 2013a, 2013b, 2011; Xing and Lockley, 2014; Zhen et al., 1986). A complete list of the used footprints can be found in Supplementary Material S1. In most cases the used illustrations represent outline tracings, but photographs and photogrammetric models were used in some instances when landmarks could be placed unambiguously. Care was taken that only the original tracings were included, and not redrawings published in subsequent publications. Only functional tridactyl footprints referred to Dinosauria were included. Birds were excluded as their ability to fly can be expected to result in very different functional requirements of their feet. Likewise, the footprints of clearly obligate quadrupedal dinosaurs (i.e., stegosaurs) were excluded. For each tracksite, at most four footprints per morphotype (as recognized in the respective publication) were included, and at most one footprint per trackway. We only selected footprints that were completely impressed, including all three digits; impressions of the metatarsal shaft were excluded. Illustrations were excluded when incompleteness of the outline did not allow for an unequivocal placement of all landmarks; when the scale was not given; when an identification of the footprint as pertaining to either the left or right foot was not possible; or when the resolution or scale of the tracings was not considered sufficient for accurate landmark placement. In order to restrict our sample to reasonably well preserved footprints (i.e., footprints that convey information on the foot anatomy), we only included footprints that show at least some of the phalangeal pads, although this criterion was somewhat relaxed for ornithischian footprints. This corresponds to grades 2 and 3 of the quality scale proposed by Belvedere and Farlow (2016). Although it might be argued that only footprints with well-defined pads and clear ungual marks (grade 3) should be used for statistical analysis, such a restrictive approach would exclude footprint types where pads are not distinct due to the soft-tissue anatomy of the trackmaker (e.g. Lockley et al., 1998c). Furthermore, the presence of anatomical details such as pad-, ungual-, and skin impressions in the footprint does not guarantee that the foot shape is faithfully captured, and even grade 3 footprints can be obviously distorted (cf. Currie et al., 1991, fig. 4).

In contrast to body fossils, footprints are generally documented in the field and remain uncollected in most cases, as removal is either undesirable (e.g., when single footprints are meaningful only in their spatial context) or impracticable (Bennett et al., 2013). Scientific access to specimens remaining in the field can be complicated given the remoteness of many sites and the degradation over time due to weathering. These circumstances often leave footprint workers little choice but to rely on published literature. The use of published footprint outlines in the present study allowed for the collection of a large and world-wide sample where single trackmaker genera, regions, or time slots are more unlikely to distort overall results. Our sample can therefore be considered representative for the fossil record of tridactyl dinosaur tracks as a whole. This literature-based approach, however, comes at a cost, as outline drawings are not objective and can differ considerably depending on the individual researcher (Falkingham, 2016). Furthermore, the accuracy of outline drawings is difficult to assess, and we were probably not always able to differentiate be-

tween accurate tracings and potentially imprecise sketches. Furthermore, we could not always ascertain whether footprint outlines were traced in the field using faithful recording techniques, or if they were simply traced on vertical photographs, which would introduce perspective distortion as an additional source of error. Despite these drawbacks, which probably added a significant degree of additional noise, we argue that the broad shape patterns observed in our study likely reflect the actual footprint record, as non-systematical sources of error are expected to be canceled out given the relatively large sample size.

Analytical approach

We here employ a combination of geometric and traditional morphometrics: Procrustes-fitted landmark configurations are not only treated as whole shapes, but also form the basis for linear and angular measurements. Both approaches come with their merits and drawbacks. For example, the possible relationship between digit III projection and interdigital angles cannot be easily assessed using simple linear and angular measurements, as an increase in interdigital angles would necessarily increase the projection, causing a spurious positive correlation. Geometric morphometric analysis, which considers the spatial position of all landmarks of the shape, allows for measuring the projection of digit III relative to the complete shape, showing that there might be, in fact, a negative relationship between both features at least in theropods (see below). On the other hand, linear and angular measurements are of practical value, allowing for comparisons with existing literature, and, last but not least, for the independent analysis of individual shape features.

Landmark placement

All outlines were exported to separate image files at sufficient resolution, all including a scale bar. The outlines were then rotated so that the axis of digit III, which can be considered the mid-axis of the footprint (Leonardi, 1987), is oriented vertically. All outlines were made sure to appear as footprints from the right foot (with digit IV on the right-hand side); left footprints were mirrored accordingly. Landmark selection was aimed at capturing most information present in an outline and at unequivocal placement on all shapes of our sample. Fine anatomical details such as the margins between phalangeal pads (e.g., Castanera et al., 2015) could not be used to define landmarks as these features are not present in all footprints of our sample. Furthermore, we avoided to define landmarks on features that have been demonstrated to be strongly influenced by behavior and substrate conditions, including claw marks and hypices (Belvedere, 2008; Lallensack et al., 2016).

Our landmark definitions rely on the mid-axes of the three functional digits, which are straight lines extending from the posterior margin of the posteriormost pad impression of the respective digit to the digit apex, excluding claw impressions. Landmarks 1 to 3 represent the distal ends of the digital axes, while landmark 4 represents the posteriormost point of the posterior metatarsophalangeal pad. Landmarks 5 to 20 capture the lateral and medial borders of the digit impressions at 1/8, 2/4, and 1/2 of the axis length measured from its distal end. A graphical template was defined a priori and fitted to each of the digits (green lines in Fig. 1A) to allow for fast and accurate landmark placement. For digit impression II, the template was scaled to the axis length of digit impression IV, assuring equal spacing between landmarks in digit impressions II and IV. This approach aims to increase comparability between the landmarks of the two digits, as digit II is often incompletely impressed, with only the two distalmost phalangeal pads im-

pressed in theropods. In addition to the 20 landmarks, we defined 14 reference marks (marks 21 to 34), which allow for some additional measurements, including the maximum footprint width, the maximum width of the digit impressions, the interdigital angles, and the length of the claw impressions. These reference marks are not necessarily homologous and thus are not incorporated in the Procrustes superimposition or any of the subsequent geometric morphometric analyses. Coordinates of both the landmarks and reference marks, as well as scaling information, were collected using the freeware tpsDig 2.17 (Rohlf, 2014).

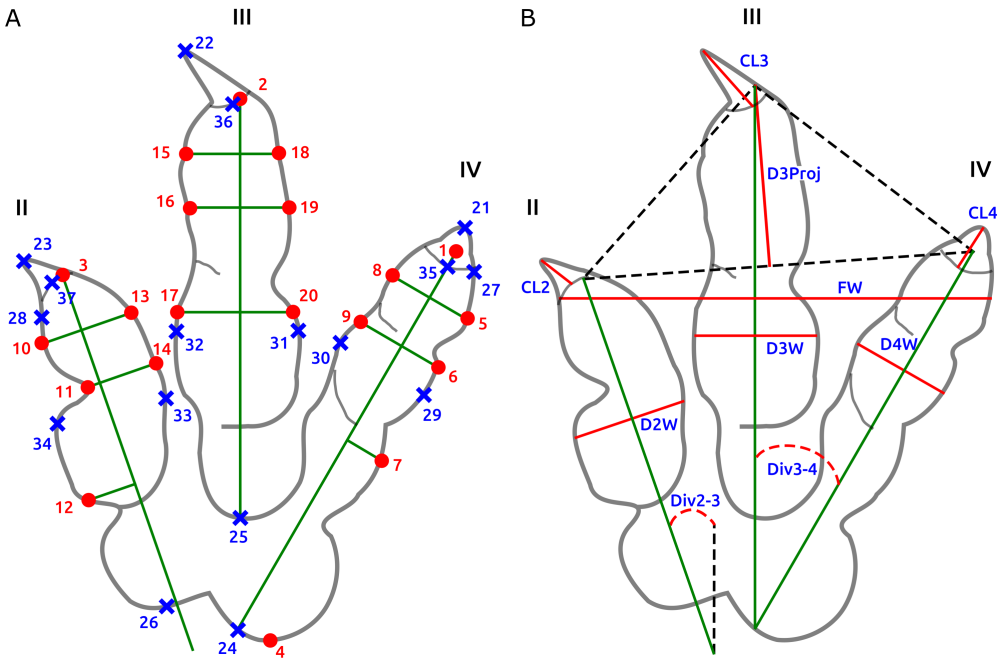

Fig. 1. Schematic footprint outline showing the placement of landmarks and reference points.

Statistical analysis

Geometric morphometric analyses were performed on the set of 20 landmarks using the free software MorphoJ 1.06c (Klingenberg, 2011). All analyses were performed after Procrustes fitting (GPA) and include Principal Component Analysis (PCA) on both the Procrustes coordinates and regression residuals, and regression analysis of separate PCs against log centroid size. The significance of all regression analyses was determined by performing a permutation test using 10000 randomization rounds. A separate analysis was performed using the free programming environment R 3.2.5 (R Core Team, 2016) in order to analyze individual linear and angular measurements. For the latter analysis, landmarks were subjected to Procrustes fitting using the R package Geomorph, by omitting the projection into Kendall's shape space. Reference mark coordinates were subsequently converted into the new coordinate system.

Measurements as defined in Fig. 1B were calculated based on distances between individual coordinates using standard trigonometric functions, and include footprint length; footprint width; the projection of digit

impression III beyond digit impressions II and IV (digit III projection); the widths of digit impressions II, III, and IV; as well as the interdigital angle of digit impressions II and III, III and IV, and II and IV. All measurements, until noted otherwise, exclude claw impressions. To assess the influence of shortcomings of the landmark definitions, some of the measured parameters, including digit III projection, footprint width, and the digit impression widths, were additionally measured using different sets of landmarks or reference marks. Digit III projection is defined as the height of a triangle spanned by the distal ends of the three digital axes, excluding the claw marks, and is therefore compatible with the length-to-width ratio of the anterior triangle (AT l/w) as defined by Lockley (2009). However, the exact positions of the distal ends of the digital axes cannot be unambiguously determined in all footprints of our sample, as a discrete margin between the distalmost phalangeal pad impression and the claw impression is often lacking, requiring interpolation to place the respective landmarks. Digit III projection was therefore additionally measured based on the tips of the digit impressions, including the claw impressions when such were present. While this approach is fully unambiguous, it suffers from the variable orientation and preservation of claw impressions due to substrate properties as well as trackmaker behavior and kinematics. Footprint and digit impression widths were measured between a pair of pre-defined landmarks, choosing the pair with the greatest distance. Additionally, widths were measured between reference marks (marks 27 to 34) that capture the maximum width of the impressions. Lengths of the claw impressions were taken for a subsample excluding footprints that do not preserve claw impressions on all digit impressions.

Correlation analyses were then performed to test for interdependence of individual measurements with log centroid size and other measurements. In this work, we employ the non-parametric Spearman rank correlation coefficient until otherwise noted; the parametric Pearson correlation coefficients are additionally given in Supplementary Material S2. For each variable, robust linear regressions against log centroid size were calculated using the R package MASS. Each regression was tested for heteroscedasticity employing the Breusch-Pagan test implemented in the R package lmtest. If present, heteroscedasticity was accounted for using a weighted least squares approach. For all other bivariate comparisons, standardized major axis regressions were calculated using the R package smatr. As apparent correlations between two measurement variables could be simply the result of correlations of both variables with size, we performed bivariate comparisons on the regression residuals to correct for size.

RESULTS

Sample statistics

Our sample includes a total of 303 footprints, of which 193 have been referred to theropod and 108 to ornithischian trackmakers; only for 2 footprints a classification within one of these two principal groups was not possible. Despite our efforts to include as many ornithischian footprints as possible, those of theropods dominate our sample, contrary to what the body fossil record would predict. This theropod dominance in the dinosaur track record was noted and discussed by several authors (e.g., Farlow, 1987; Thulborn, 1990), and plausible explanations include the greater activity and larger home ranges expected for theropods. This discrepancy is increased when only footprints are considered that are suitable for inclusion in our study, as these must be identifiable as either left or right; in the more symmetrical ornithischian footprint, this identification is often only possible when the footprint is part of a trackway.

Sample sizes for the Jurassic (n=138) and the Cretaceous (n=133) are similar, but the Late Triassic (n=16) is poorly represented. Sample size is largest for the Early Cretaceous (n=86) and Early Jurassic (n=75), followed by the Late Jurassic (n=48), Late Cretaceous (n=32), and Middle Jurassic (n=12). Footprints of our sample come from at least 169 separate tracksites from around the world. Although the sample was taken with the aim to include as many geographic regions as possible, it its unequally distributed among the continents and countries. Most footprints stem from Asia (n=102) and North America (n=87), closely followed by Europe (n=69). On the other hand, sample size is poor for Africa (n=28), South America (n=10), and Australia (n=7). Most footprints come from localities located in China (n=81) and the US (n=76), followed by Poland (n=20) and Spain (n=18). Although this unequal geographic distribution can be partly explained by the varying richness in fossil tracks of the geologic units of separate countries, it appears also to be biased by single researchers focusing on publishing large numbers of tracksite reports including high quality footprint tracings. Indeed, 49% of the analyzed footprints were taken from papers first-authored by only three researchers (Martin Lockley, n=64; Xing Lida, n=53; Gerard Gierliński, n=32), with the remaining 51% coming from papers first-authored by a total of 53 separate researchers.

68% of the footprints were assigned to one of 54 ichnogenera; the total number of ichnospecies included is 78. The most frequent ichnogenera are *Anomoepus* (n=19); *Grallator* (n=19); *Caririchnium* (n=15), *Eubrontes* (n=15), and *Megalosauripus* (n=13). 40 of the ichnogenera have been referred to theropod trackmakers in the respective papers and 15 to ornithischian trackmakers; only the affiliation of the ichnogenus *Coelurosaurichnus* is unknown.

	Theropoda	Ornithischia	Total
Total	193	108	303
Late Triassic	15	0	16
Early Jurassic	48	27	75
Middle Jurassic	9	3	12
Late Jurassic	40	8	48
Early Cretaceous	48	38	86
Late Cretaceous	17	14	32

Table 1. Number of theropod and ornithischian footprints of our sample by epoch. The numbers do not necessarily sum up to the value given in the "total" field since not all footprints can be referred to one of the epochs or groups.

Size and shape through time

Footprint size was quantified using both footprint length and centroid size as size proxies. While footprint length is the more accessible measurement, centroid size takes into account the precise shape of the foot-

print and therefore is a more precise proxy for body mass as a biological meaningful size measure. Footprint length in our sample averages at 25.20 cm (centroid size: 0.405) with positive skewness. The smallest footprint included in our sample, coming from the Late Cretaceous Jiaguan Formation of China and referred to the theropod ichnogenus *Minisauripus* (Lockley et al., 2008b), measures 2.46 cm in length (centroid size: 0.035). The largest theropod footprint of our sample measures 76.35 cm in length (centroid size: 1.173) and, based on its temporal and spatial context (Maastrichtian, US), was ascribed to the theropod *Tyrannosaurus* under the ichnotaxonomic label *Tyrannosauripus* (Lockley and Hunt, 1994). The largest ornithischian footprint is only slightly shorter at 74.22 cm, and is the largest footprint in terms of centroid size (1.334). Stemming from the Late Cretaceous of the US, it is of probable hadrosaurid origin (Lockley et al., 2003). The largest footprint from the Jurassic is 73.61 cm in length (centroid size: 1.083); this track comes from the Late Jurassic of Switzerland and was ascribed to the theropod ichnogenus *Jurabrontes* (Marty et al., 2017). Even larger Late Jurassic theropod footprints of more than 80 cm in length have been reported (Boutakiout et al., 2009; Rauhut et al., 2018), but are not included in this study.

Footprints from the Cretaceous (mean centroid size: 0.48) are significantly larger in centroid size ($p<0.001$) than footprints from the Jurassic (mean centroid size: 0.347). Over the whole Mesozoic, footprint centroid size is slightly smaller ($p<0.05$) in theropods than in ornithischians (0.39 vs. 0.44, respectively). However, in both the Early and Late Jurassic, theropod footprints are significantly larger than ornithischian footprints ($p<0.001$; o.37 vs. 0.20 and 0.43 vs. 0.27, respectively). In contrast, theropod prints are significantly smaller in centroid size than those of ornithischians in both the Early Cretaceous ($p<0.001$; 0.33 vs. 0.54) and Late Cretaceous ($p<0.05$; 0.47 vs. 0.72, respectively). The median centroid sizes of ornithischian footprints show a steady increase from the Late Triassic/Early Jurassic to the Late Cretaceous, while the median centroid sizes of theropods remain relatively constant in the four time slots, only showing a slight drop in the Early Cretaceous (Fig. 2).

Lockley (1999) suggested that interdigital angles are larger in Late Jurassic and Cretaceous theropods compared to earlier forms. Weems (2006) even proposed that some Early Jurassic tracks referred to *Kayentapus* that show a large interdigital angle III-IV in combination with a low interdigital angle II-III represent an intermediate stage in the evolution of larger interdigital angles. Our data does not show a significant increase in interdigital angles over time. However, there appears to be a slight increase from the Early Cretaceous to the Late Cretaceous, which does not reach statistical significance ($p=0.08$), possibly due to the limited sample size of Late Cretaceous tracks. In ornithischians, interdigital angles are significantly larger than those of theropods until the Late Jurassic, but are much decreased in the Cretaceous. Another feature of interest, the projection of digit III, does not show a significant trend from the Late Triassic/Early Jurassic to the Middle/Late Jurassic in both theropods and ornithischians; however, there is a significant decrease from the Late Jurassic to the Early Cretaceous in both groups.

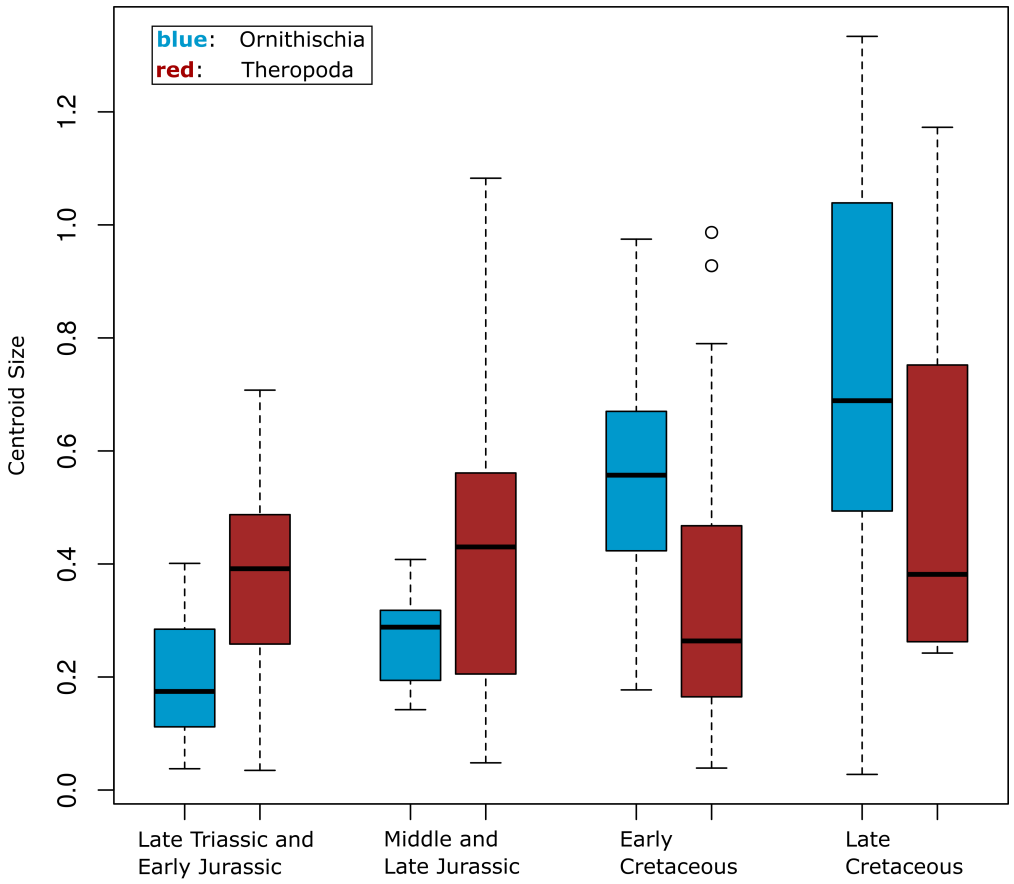

Fig. 2. Boxplot showing footprint sizes (using centroid size as proxy) of ornithischians (blue) and theropods (red) for four separate time slots (Late Triassic and Early Jurassic; Middle and Late Jurassic; Early Cretaceous; Late Cretaceous). Note that ornithischian footprints are smaller than theropod footprints in the earlier Mesozoic but larger in the Cretaceous.

Mean shapes

The 303 footprints in our sample are on average significantly longer (mean: 25.3 cm) than wide (mean: 21.0 cm; $p < 0.001$). Digit impression III is the most protruding, while digit impressions II and IV are equal in their anterior extension relative to the axis of digit impression III. Digit impression III is also significantly wider ($p < 0.001$), while the mean widths of digit impressions II and IV are not significantly different ($p > 0.87$). The interdigital angle between digit impressions II and IV averages at 48.2°. The angle between digit impressions III and IV (26.1°) is significantly larger ($p < 0.001$) than that between digit impressions II and III (22.1). The posteriormost point of the heel region is slightly displaced laterally. This general description holds true when theropods and ornithischians are analyzed separately (Table 1). However, the ornithischian footprints are not significantly longer than wide ($p > 0.6$), and digit impression III is not significantly wider than the other two digit impressions ($p > 0.2$).

The wireframe graphs of Fig. 2 capture digit tips by both the ends of the digital axes (landmarks 1, 2, and 3) and the distalmost points of the digits (reference marks 21, 22, and 23). The reference marks tend to deviate from the respective landmarks, most frequently due to the presence of claw impressions. In footprints without clear claw impressions, asymmetrical digit tips can still be the result of a medially or laterally deflected ungual impression (Lallensack et al., 2016). In the mean shapes of the complete sample and the theropod subsample, the tip of digit impression III and especially of digit impression II is deflected medially, indicating a medial orientation of the claw mark, which can be attributed to foot kinematics during footprint formation (Avanzini et al., 2012). The tip of digit impression IV, on the other hand, is slightly deflected laterally. Given these trends, therefore, claw orientations can serve as a criterion to assign isolated footprints to the left or right foot. In ornithischians, the slight deviation of the reference landmarks is more difficult to interpret but might be also influenced by the claw impressions, which are only present in some of the smaller footprints.

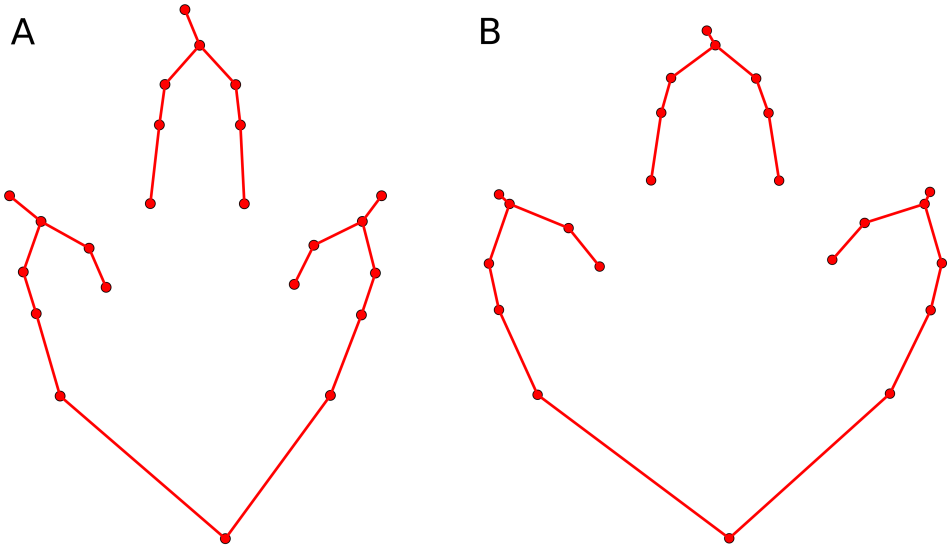

Fig. 3. Mean shapes of the theropod (**A**) and ornithischian (**B**) subsamples. The digit ends are represented by both the landmark on the end of the respective digital axis and by reference marks on the digit tip; deviation of both marks is mostly due to the presence of claw impressions which are excluded from the landmarks. All footprints shown in this paper represent footprints of the right foot. See text for a detailed description.

	Complete sample	Theropoda	Ornithischia
Length/Width	1.30 (0.28)	1.42 (0.26)	1.08 (0.15)
IDA (total) [°]	48.19 (19.91)	45.38 (15.64)	53.30 (25.18)

IDA II/III [°]	22.14 (10.79)	20.79 (9.32)	24.61 (12.76)
IDA III/IV [°]	26.06 (11.98)	24.59 (9.11)	28.69 (15.53)
Width digit III/II	1.25 (0.36)	1.29 (0.40)	1.16 (0.25)
Width digit III/IV	1.25 (0.31)	1.39 (0.33)	1.16 (0.23)

Table 2. Average measurements and standard deviations (in brackets) taken from the complete sample (n=303) and from the theropod (n=193) and ornithischian (n=108) subsamples.

Discrimination between theropod and ornithischian footprints

Discriminant function analysis could separate both groups only with a large degree of overlap. Ornithischian footprints can be best distinguished from those of theropods based on their smaller length-to-width ratio, the less protruding digit impression III, the moderately broader digit impression III, the much broader digit impressions II and IV, and the more central position of the posteriormost extension of the heel region. Additionally, we subdivided the dataset into three equal size bins for theropod and ornithischian footprints each, using centroid size as proxy, and performed CVA as well as pair-wise discriminant analyses on these six groups. Mid-sized and large ornithischians are best separated from theropods and small ornithischians by high loadings on CV1, which is associated with a low length-to-width ratio, a weak digit III projection, and significant digit thickening. Especially large ornithischians are well separated from theropods and small ornithischians, with minimal overlap. Small ornithischians are best separated from small theropods by low loadings on CV2, with associated shape changes including the weaker digit III projection, the larger interdigital angle, the slightly longer digits II and IV, and the less elongated and more symmetrical heel region. Interestingly, small ornithischians can be better distinguished from small theropod footprints than from medium-sized and, especially, large theropod footprints. Furthermore, the pairwise discriminant analyses reveal that the shape features allowing for the best possible separation between ornithischians and theropods are different between size bins: For the small-size bin, the interdigital angle (higher in ornithischians) is an important discriminant factor, but is less applicable to the mid-size bin and especially the large-size bin. Conversely, the shape and width of the digits (broader and more rounded in ornithischians) is an important discriminator for the large-size bin and, to a lesser degree, the medium-size bin, but not for the small-size bin.

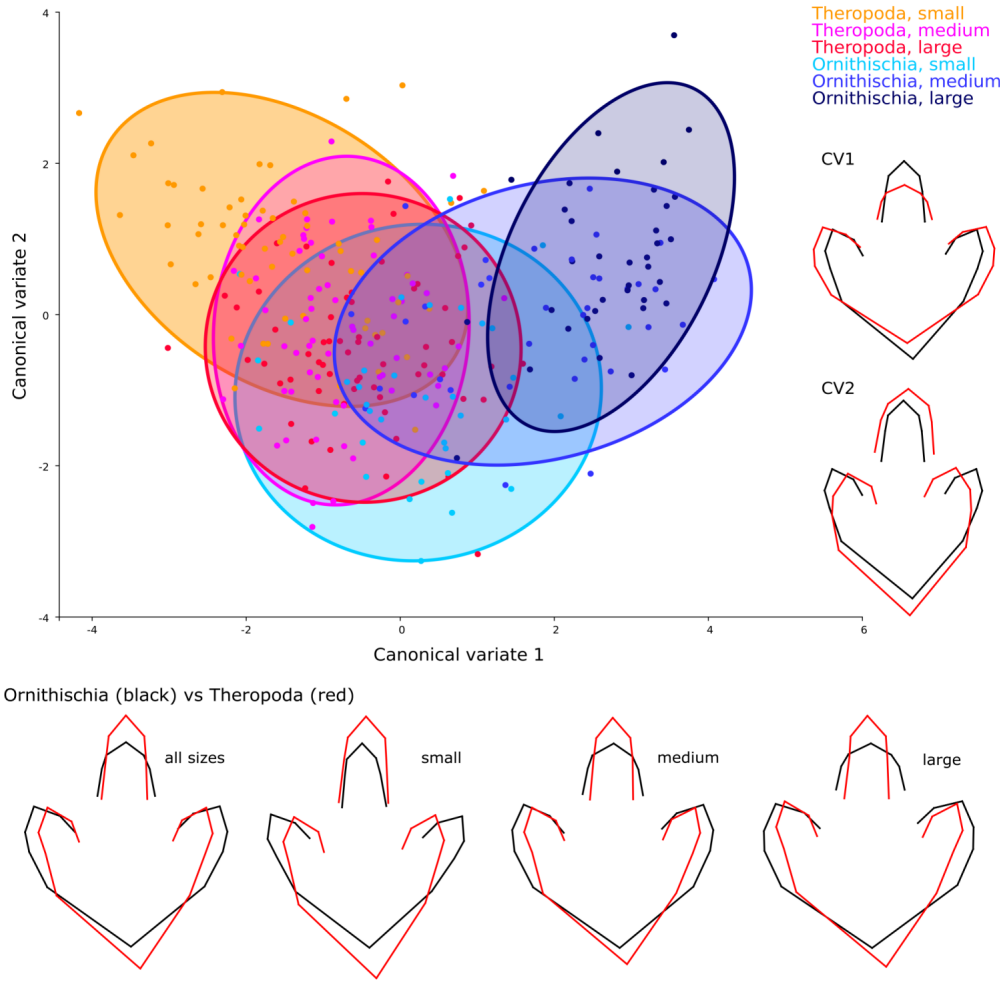

Fig. 4. Discrimination between theropod and ornithischian footprints. **Top**. Canonical variate analysis on three equal size bins for theropods and ornithischians, respectively, using centroid size as size proxy. The scatter plot shows the loadings of footprints of the separate groups (highlighted by color and 80% confidence ellipses) on CV1 and CV2. The shape changes associated with the canonical variates are shown on the right, with the black wireframe graphs representing the starting shape (low loadings) and the red ones the target shape (high loadings), using a scale factor of 4 (the scale factor is identical to the values on the axes of the scatter plot). While large ornithischians are well separated from theropods due to their high loadings on CV1, small ornithischians share an extensive overlap with theropods. Interestingly, small ornithischians can be best distinguished from small theropods but to increasingly lesser degrees from medium-sized and large sized theropods. **Bottom**. Wireframe graphs showing the shape features differentiating ornithischian (black) from theropod (red) footprints of all sizes and the three size bins. The comparison shows that differentiating features change with size: the interdigital angle is an important discriminant only at smaller sizes, and digit width only at larger sizes.

Principal component analysis

PCA was performed as an exploratory method to identify major patterns of shape variation. PC1 (38.3% of total variability) suggests that a more elongated overall footprint shape is associated with a reduced interdigital angle, a larger digit III projection, and a decreased width of digit impressions II and IV. PC2 (22.0% of total variability) indicates that a high interdigital angle is associated with a shortening of the heel region (and, thus, a smaller footprint length), a larger digit III projection (due to the more posterior positions of the tips of digit impressions II and IV), and a reduced width of all three digit impressions. Theropod footprints mostly vary along PC1, while most of the variability within the ornithischian footprints is described by PC2. Very low scores on PC1 are dominated by ornithischian footprints, while higher values are occupied by theropod footprints. A regression of PC1 against log centroid size pooled by groups is significant ($p<0.0001$) and describes 19.0% of the total variation, suggesting that high values on PC1 are associated with smaller sizes. On the other hand, the regression of PC2 against log centroid size does not appear to be significant ($p>0.5$). These results hold generally true when the non-parametric Spearman rank correlation coefficient is employed, which suggests that 17.7% of the total variation of PC1 and 1.1% of PC2 can be explained by size ($p<0.0001$ and $p=0.068$, respectively). PC3 (13.0% of total variability) is related to footprint asymmetry, and is unrelated to size.

PCA was additionally performed on the theropod and ornithischian subsamples (Fig. 7). The principal components of the theropod subsample are similar in composition to those of the complete sample (Fig. 5), which can be attributed to the dominance of theropod footprints in the sample. High loadings on PC1 are associated with more slender shapes. The relative length of digit III is greater, while digits II and IV are shorter. Both interdigital angles are reduced, while the heel region is more extensive. Digit widths, however, remain relatively constant. PC1 is strongly correlated with size; a regression of PC scores against log centroid size explains 21.7% of the variability ($p<0.0001$). PC2 describes shape variation towards a shorter footprint with more slender toes. Digit impression III is moderately reduced in width, while digit impressions II and IV are markedly more narrow. Both interdigital angles are increased, while the heel region is less extensive. The projection of digit III is increased, which however is largely due to the reduced relative lengths and greater interdigital angles of digit impressions II and IV, with only a slight increase of the relative length of digit impression III. Shapes with high loadings on PC2 also appear to be more asymmetrical, which is seen in the laterally displaced heel; in the reduced extension of digit impression IV compared to II; and in the larger interdigital angle between digit impressions III and IV compared to II and III. The regression of PC2 against size is insignificant. PC3 is mostly related to asymmetry, where high loadings indicate that interdigital angle II-III is much enlarged while the interdigital angle III-IV is reduced and digit impression IV more protruding than digit impression II. PC3 is correlated with size, a regression explains 3.1% of the variance ($p=0.02$).

The ornithischian subsample gives different results. Here, PC1 closely resembles PC2 of the theropod subsample: high loadings indicate an increased interdigital angle, while the width of all three digit impressions is reduced. Digit impression III is more protruding, while digit impressions II and IV are less protruding, and the heel less extensive. High loadings are furthermore associated with increased asymmetry similar to, but not as pronounced as in PC2 of the theropod subsample. All three digit impressions display straight medial and lateral borders at high loadings, but, and in contrast to PC2 of the theropod subsample, rounded borders at low loadings. Different to PC2 of the theropod subsample, the regression against size is

significant (p<0.0001), explaining 16.1% of the variability. PC2 is similar to PC1 of the theropod subsample in showing an increased projection of digit III as well as a reduced interdigital angle and an extended heel at high loadings. PC2 also describes asymmetry, with the interdigital angle III-IV being smaller than that of II-III; digit impression IV more protruding than digit impression II; and a medially displaced heel, which however appears to have been exaggerated by Procrustes fitting due to the asymmetry in digit impressions II and IV. A regression of PC2 against size is significant (p=0.0003) and explains 11.5% of the variability. PC3 shows wider and more rounded digit impressions at high loadings, which are associated with asymmetry, with the interdigital angle II-III being larger than that of III-IV, and digit impression IV more extensive. A regression of PC3 against size fails to reach significance.

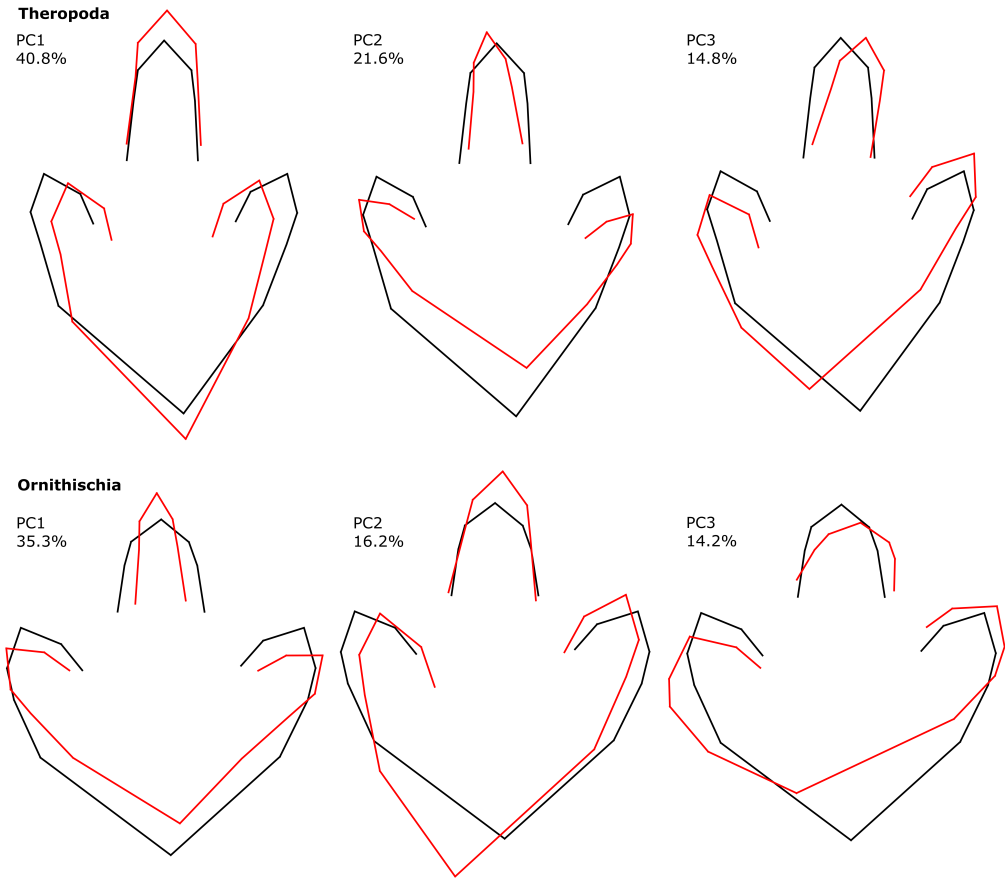

Fig. 5. PCA on Procrustes coordinates. Wireframe diagrams show shape changes associated with the respective PC for the complete sample and the theropod and ornithischian subsamples. The black line represents lower loadings and the red line higher loadings on the respective PC. Percentage values indicate the variation described by the respective PC. Not to scale.

Correlation analysis on individual shape parameters

Shape features of interest identified by PCA were quantified as linear and angular parameters measured on the Procrustes fitted shapes and tested for correlations with log centroid size and correlations between selected pairs of measurements, for both the theropod and ornithischian subsamples (Fig. 6; Table 4). Correlation of individual measurements with size confirms results derived from the PCA. The footprint length-to-width ratio is significantly negatively correlated with size in both theropods (R=-42) and ornithischians (R=-26). The projection of digit III, measured from the ends of the digital axes, is negatively correlated with size in both theropods and ornithischians (R=-0.38 and R=-0.47, respectively); this correlation is stronger when the projection is measured from the claw tips (R=-0.44 and R=-0.60, respectively). A striking difference between the theropod and ornithischian subsets, the digit impression widths are strongly correlated with size in ornithischians (R=0.58, 0.56 and 0.57 for impressions II, III, and IV, respectively), while no correlation is evident in theropods (R=0.09, -0.06, and -0.01, respectively). The interdigital angle is moderately negatively correlated in ornithischians (R=-0.29). In theropods, there appears to be a slight correlation of opposite sign (R=0.18), which is, however, partly spurious, as an increased interdigital angle would necessarily increase footprint width and thus centroid size. Repeating the analysis using footprint length as size proxy recovered a much weaker (R=0.09) and insignificant correlation. The asymmetry between the two interdigital angles is slightly positively correlated with size in theropods (R=0.18), but fails to reach significance in ornithischians. The asymmetry of the lengths of digit impressions II and IV is not significantly correlated with size. For theropods, claw impressions were analyzed using a reduced dataset (n=96), suggesting a negative correlation of claw impression length with size (R=-0.41).

	Theropoda	Ornithischia
FL/FW	-0.42***	-0.26**
FW	0.40***	0.19
D3Proj (from axes)	-0.38***	-0.47***
D3Proj (from claw tips)	-0.44***	-0.60***
D2W	0.09	0.58***
D3W	-0.06	0.56***
D4W	-0.01	0.57***
DWR	-0.05	0.45
IDA	0.18*	-0.29**
Asym IDA	0.17*	-0.18
Asym DL	0.13	-0.09
CL	-0.41*** (n=96)	–

Table 4. Correlation values of selected measurements against log centroid size for the theropod (n=193) and ornithischian (n=108) subsamples. Table gives the Spearman rank correlation coefficient R. Stars indicate level of significance, with $p < 0.001$, ***; $p < 0.01$, **; $p < 0.05$, *. **Abbreviations**: **FW**, footprint width. **FL**, footprint length. **D3Proj**, projection of digit impression III. **D2W**, width of digit II. **D3W**, width of digit III. **D4W**, width of digit IV. **DWR**, ratio between with of digit III and the widths of digits II and IV. **IDA**, interdigital angle between digits II and IV. **Asym DL**, difference between the anterolateral extents of digits IV and II, measured along the footprint midline. **Asym IDA**, the difference between interdigital angles II-III and III-IV. **CL**, average length of claw impressions of digits II, III and IV.

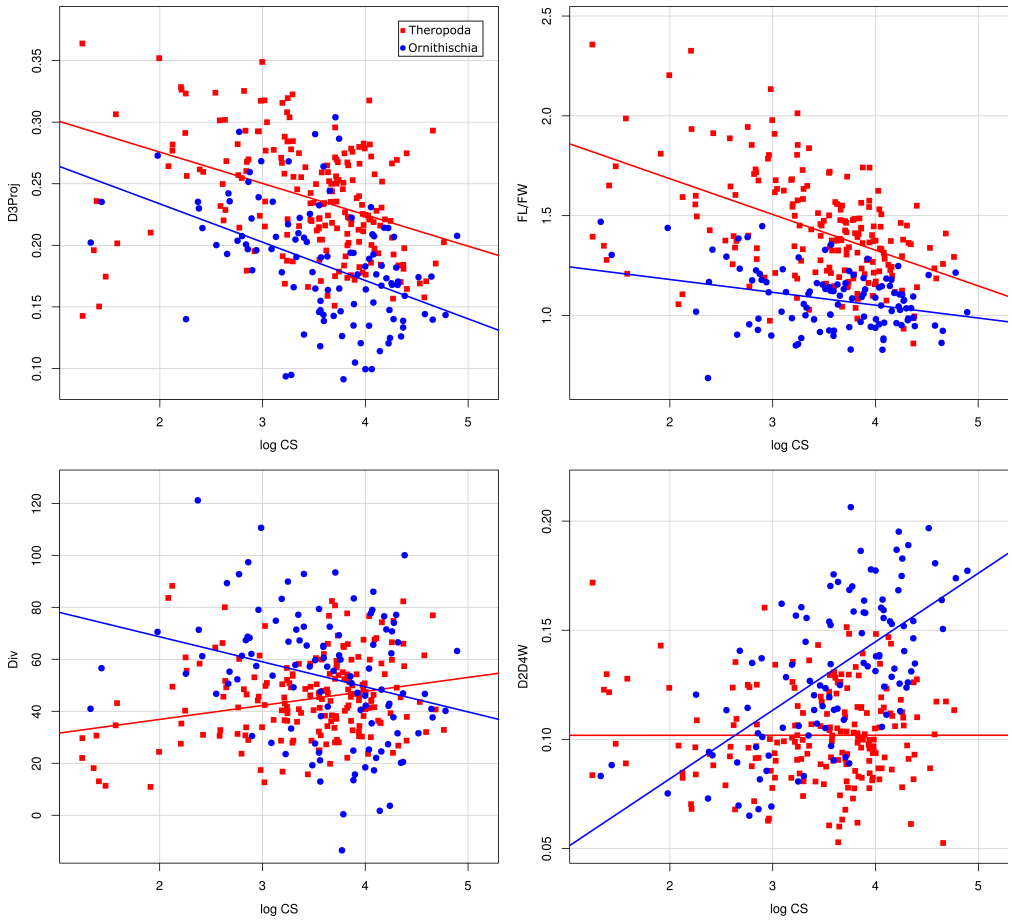

Fig. 6. Scatter plots showing the correlations of selected measurements (the projection of digit III; the footprint width; the interdigital angle; and the average of the widths of digits II and IV) against log centroid size, which is used as size proxy. Regression lines were plotted for theropods (red squares) and ornithischians (blue dots) separately.

As most of the analyzed parameters were found to be significantly correlated with size, we performed pairwise correlation analysis on both the plain measurements and on residuals of the regression of the individual parameter against log centroid size, in order to remove or lessen the influence of size. Both approaches

As most of the analyzed parameters were found to be significantly correlated with size, we performed pairwise correlation analysis on both the plain measurements and on residuals of the regression of the individual parameter against log centroid size, in order to remove or lessen the influence of size. Both approaches led to similar correlation coefficients that for all selected pairs of measurements agree in sign (Table 3). As already suggested by PCA, the negative correlation between footprint width and digit III projection is highly significant in both subgroups but partly spurious, as a longer digit III will necessarily decrease relative footprint width. The negative correlation of digit III projection against the average widths of digits II and IV, again, proved to be significant; the correlation is stronger in ornithischians than in theropods. The negative correlation between digit III projection and digit III width is likewise substantial in ornithischians, but weak and insignificant in theropods. The digital width ratio is significantly correlated with digit III projection in theropods but not in ornithischians. The average width of digits II and IV is negatively correlated with the interdigital angle in ornithischians, although correlation is weaker when based on regression residuals, suggesting that this correlation is exaggerated by the fact that both variables show a clear correlation with size. For theropods, the correlation is only significant when the residuals are analyzed. Again, digit III differs in its variation pattern from that of digits II and IV; the correlation between digit III and the interdigital angle is significant in both theropods and ornithischians, although stronger in the latter. The digital width ratio is strongly negatively correlated with the interdigital angle in both theropods and ornithischians. The two employed asymmetry measures (the differences between the lengths of digits II and IV, and between the interdigital angles II-III and III-IV) are strongly correlated with each other in both groups.

	Theropoda	Theropoda (residuals)	Ornithischia	Ornithischia (residuals)
FW vs D3Proj	-0.63***	-0.59***	-0.48***	-0.46***
D3Proj vs D2D4W	-0.35***	-0.37***	-0.55***	-0.44***
D3Proj vs D3W	-0.10	-0.13	-0.58***	-0.46***
D3Proj vs DWR	0.24***	0.25***	-0.07	-0.11
IDA vs FL	-0.68***	-0.67***	-0.27**	-0.46***
D2D4W vs IDA	-0.13	-0.14*	-0.32***	-0.24***
D3W vs IDA	-0.29***	-0.29***	-0.55***	-0.53***
DWR vs IDA	-0.29***	-0.29***	-0.35***	-0.40***
Asym DL vs Asym IDA	0.54***	0.51***	0.58***	0.59***

Table 3. Correlation values of selected pairs of footprint features for the theropod (n=193) and ornithischian (n=108) subsamples. Columns 2 and 4 give correlation values performed on the regression residuals, which lessen the influence of size. Values represent the Spearman rank correlation coefficient (R). Stars indicate level of significance, with $p < 0.001$, ***; $p < 0.01$, **; $p < 0.05$, *. **Abbreviations**: **FW**, footprint width. **D3Proj**, projection of digit impression III. **D2D4W**, average of the widths of digit II and IV. **IDA**, interdigital angle between digits II and IV. **Asym DL**, difference between the anterolateral extents of digits IV and II, measured along the footprint midline. **Asym IDA**, the difference between interdigital angles II-III and III-IV.

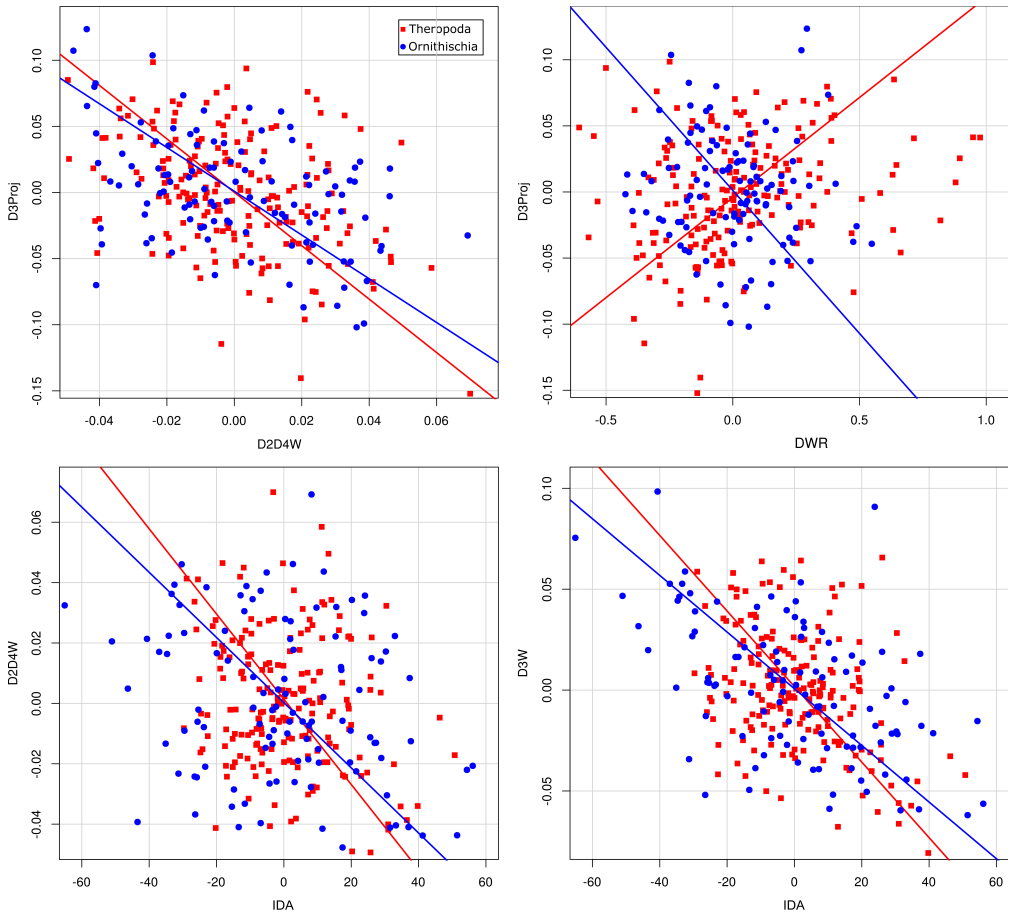

Fig. 7. Bivariate plots showing correlations between residuals of selected measurements (D2D4W vs D3Proj; DWR vs D3Proj; IDA vs D2D4W, IDA vs D3W). Model 2 regression lines were plotted for theropods (red squares) and ornithischians (blue dots) separately.

DISCUSSION

The influence of size

Body size is one of the most crucial factors determining the biology of an animal. As stresses acting on bones and muscles increase in proportion to body mass$^{1/3}$, modifications of the pes in response to increased stresses, as well as increasingly constrained locomotory abilities can be expected to have a significant impact on footprint shape. Our analysis confirms significant correlations with footprint size (using log centroid size as a size proxy) for the digit III projection and the footprint length-to-width ratio in both theropods and ornithischians (Table 4). These allometric relationships, which had already been statistically demonstrated for theropod tracks of the Newark Supergroup (Olsen, 1995; Olsen et al., 1998), can therefore be confirmed to hold true for non-avian tridactyl dinosaur tracks as a whole. For other parameters, possible allometric relationships are more equivocal. Ornithischians show a strong correlation between size and the widths of digits impressions II, III, and IV, but this correlation is virtually absent in theropods. This difference between ornithischian and theropod tracks might relate to the more columnar foot structure developed in hadrosaurids (Moreno et al., 2007). The positive correlation between footprint size and interdigital angles previously proposed for the Newark Supergroup sample (Olsen, 1995; Olsen et al., 1998) appears to be absent in our theropod sample. Ornithischians, on the other hand, show a negative correlation between size and the interdigital angles. This becomes evident when comparing the often widely splayed, small *Anomoepus* tracks with larger ornithopod tracks, where the distal parts of digits II and IV are frequently bended inwards and thus sub-parallel to digit III.

Although some of the most important shape parameters (i.e., digit III projection, footprint length-to-width ratio, digit widths in ornithischians) are correlated with size, the latter does account only for parts of the detected variability, suggesting that there might be additional factors to consider. Indeed, when a size-corrected correlation analysis is performed on the regression residuals, correlation values are generally similar to those obtained from the uncorrected analysis, and in all cases agree in sign (Table 3). In other words, shape features covary across the whole size spectrum in the same way as they covary among footprints of similar sizes. Similar shape continua can be found in both theropods and ornithischians, with PC1 and PC2 of the theropod sample closely corresponding to PC2 and PC1 of the ornithischian sample, respectively.

As expected, parameters with significant allometry (i.e., digit III projection; footprint length-to-width ratio; and, in ornithischians, digit widths) are correlated which each other. The correlation between the footprint length-to-width ratio and digit III projection, which has been suggested previously (Lockley, 2009), is strongly supported. Kim et al. (2009) suggested the presence of a polarity in ornithischians between gracile feet with strong mesaxony and robust feet with weak mesaxony. Indeed, when digit III projection is employed as a proxy for mesaxony, and digit impression width as a proxy for robustness, there appears to be a strong negative correlation in ornithischians, both for the widths of digits II and IV and for the width of digit III. A somewhat weaker but significant negative correlation between the widths of digits II and IV and digit III projection can be also found in theropods, although digit III in theropods does not correlate significantly.

Although some of the most important shape parameters (i.e., digit III projection, footprint length-to-width ratio, digit widths in ornithischians) are correlated with size, the latter does account only for parts of the

detected variability, suggesting that there might be additional factors to consider. Indeed, when a size-corrected correlation analysis is performed on the regression residuals, correlation values are generally similar to those obtained from the uncorrected analysis, and in all cases agree in sign (Table 3). In other words, shape features covary across the whole size spectrum in the same way as they covary among footprints of similar sizes. The close resemblance of the variation patterns in theropods and ornithischians independent of size indicate that footprint shape is primarily determined by functional requirements. Furthermore, the correlations between individual shape features and size might often be interpreted as instances where function, and thus shape, is constrained by size.

Functional interpretations of footprint shape are currently hampered by the scarcity of studies regarding the functional anatomy of tridactyl dinosaur and bird feet. Ambiguity of any functional interpretations based on our data also arises from the inability to determine the length of the digits relative to the whole leg based on footprints, and from the exclusion of trackway data such as stride lengths and step angles, which would allow for independent clues about locomotory adaptations. With these caveats in mind, we offer preliminary interpretations of the possible functional meaning of the variation patterns described above.

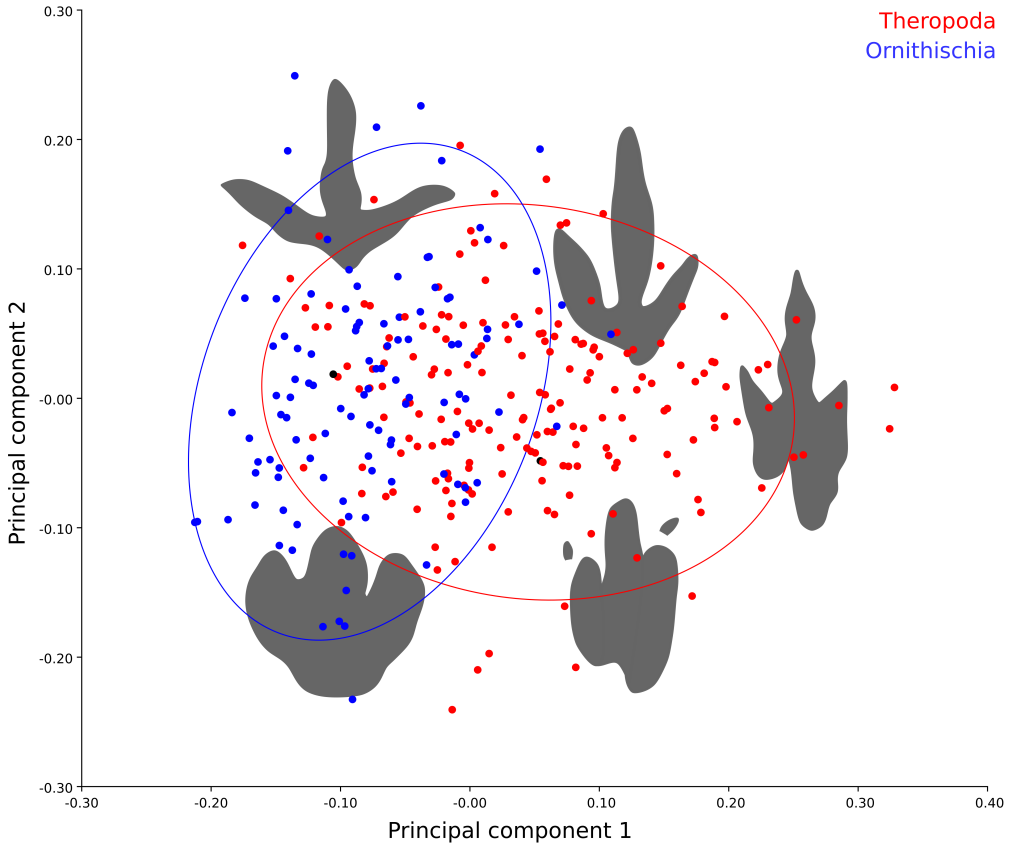

Fig. 8. PCA results of the complete sample (n=300), along with functional interpretations of major shape trends. The scatterplot shows the loadings on PC1 and PC2, with ornithischians shown as blue and

theropods as red dots. As shown by the orientation of the 90% confidence ellipses, theropod footprints mostly vary along PC1, and ornithischian footprints along PC2.

Cursorial adaptations in modern ratites and non-avian theropods

Modern birds, and especially the large, flightless ratites, provide the closest modern analog to non-avian dinosaurs regarding the functional significance of foot shape, and thus can provide valuable clues about the possible functional meaning of the observed footprint shape variation. In birds, such functional adaptations can be related to cursoriality, graviportality, wading, and walking over soft ground (Storer, 1971). Of these, only adaptations for cursoriality in ratites have been analyzed in greater detail (Schaller, 2008; Schaller et al., 2011).

Cursorial ratites and other cursorial taxa tend to shorten or lose non-central digits (e.g., Lull, 1904; Patak and Baldwin, 1998; Schaller et al., 2011). The functional advantage of this relative shortening probably lies in the lightening of the distal limb, optimizing swing dynamics and allowing for higher stride frequencies (Schaller et al., 2011). While a complete loss of non-central digits only occurs in some quadrupedal mammals, bipedal cursors retain at least two functional digits for stability reasons (Schaller et al., 2011). Pressure distributions on the digits in running ostriches indicate that digit IV does not significantly contribute to propulsion, but serves primarily as an outrigger, stabilizing the animal during rapid locomotion (Schaller et al., 2011). Likewise, in the emu, digit II bears less load as speed increases, suggesting that digit IV is the crucial element ensuring stability while running. Stability gained by increased interdigital angles, however, comes at the cost of an increased injury potential, as the digits can more easily be over-abducted while running, in particular at larger body sizes. In the ostrich, over-abduction is prevented by a ligament running from the proximal phalanx of digit III to the second phalanx of digit IV, restricting the interdigital angle to 34° (Schaller et al., 2011). Besides reducing non-central digits, cursors tend to decrease the length of the central digit (and thus, footprint length) in relation to overall leg length in order to minimize traction surface (Storer, 1971). In the ostrich, traction surface is further reduced as the proximal phalanx of both digits is permanently lifted above the ground. This feature has also been argued to function in storage and release of elastic energy as well as in shock absorption (Schaller et al., 2011).

Cursorial adaptations in the pes of modern ratites open the possibility that similar adaptations have been present in some non-avian theropod dinosaurs. Trackways of running dinosaurs, however, are surprisingly rare. (Pérez-Lorente, 2015) concluded that of the vast track record of La Rioja, Spain, only 0.23% of the theropod trackways can be interpreted as running. As suggested by this author, this fraction reflects the fraction of time these dinosaurs spend running throughout their lives. It thus might be argued that the relative absence of running behavior in the track record renders it unlikely that cursorial adaptations are responsible for a large fraction of the observed shape variability. Cursorial limb proportions, however, can be found in a broad array of theropod taxa (Holtz, 2012). It is well possible that the rareness of running trackways is the result of a bias in the track record, as the reduced traction area of the foot while running would require firm ground, which is unsuited for footprint registration.

Functional significance of the projection of digit III

The projection of digit III beyond digits II and IV is among the most variable shape features in our sample. Digit III projection is the most common measure of mesaxony (i.e., the dominance of the central digits over outer digits) in footprints (Lockley, 2009; Olsen, 1980; Weems, 1992), although mesaxony can also be increased by enlarging the width of the middle digit compared to the remaining digits. Digit III projection can be increased either by 1) relative shortening of the non-central digits; 2) relative elongation of digit III, or 3) increased interdigital angles. In the theropod subsample, PC1 shows that high digit III projection values are associated with reduced interdigital angles. Thus, digit III projection values in theropods are mainly controlled by the relative lengths of the digits and only to a lesser degree by interdigital angles. Given the nature of our dataset, however, we are unable to determine if shortening of non-central digits or elongation of digit III is responsible for the observed variation. In the ornithischian subsample, on the other hand, variation in the interdigital angles appears to be the most important determinant of digit III projection, as shown by PC1, while the variation determined by relative digit lengths only occurs on PC2.

In order to allow for preliminary comparisons, we measured digit III projection relative to digit III length on published skeletal diagrams of pes skeletons of four modern ratite birds and various tridactyl dinosaurs. In ratites, the most extreme degree of cursorial adaptations can be found in the ostrich (*Struthio camelus*), which only retains digits III and IV. Digit III is substantially shorter than the latter, with the digit III projection accounting for 70% of its length (Schaller et al., 2011, fig. 1). A pronounced digit III projection is also observed in the highly cursorial Emu (*Dromaius novaehollandiae*), measured at 69% (Milàn, 2006), and Greater Rhea (*Rhea americana*), measured at 59% (Padian and Olsen, 1989). Within non-avian dinosaurs, the highest digit III projection values are found within the ornithomimosaurs *Nqwebasaurus* (59%; Sereno, 2017, fig. 22.2), *Gallimimus* (57%; Osmólska et al., 1972, plate L) and *Struthiomimus* (54%, Makovicky et al., 2004 fig. 6.5G), with at least the latter two genera being commonly interpreted as highly cursorial (Makovicky et al., 2004). To a somewhat lesser degree, it is also obvious in *Coelophysis* (48%; Colbert, 1989, fig. 87) and *Caudipteryx* (49%, Zhou and Wang, 2000, fig. 3), which have been interpreted as being cursorial (Colbert, 1989; Jones et al., 2000; Zhou and Wang, 2000). While there appears to be a clear trend for cursorial species showing high digit III projection values, not all species fit this scheme, indicating that there are probably additional factors influencing this measurement. For example, digit III projection is not particularly strongly pronounced in *Hypsilophodon* (43%; Galton, 1971, fig. 2e), although it had been interpreted as one of the most cursorial ornithischians (Galton, 1971).

The foregoing comparisons suggest that digit III projection might present a proxy for cursorial ability, at least in cases where digit impressions are not widely splayed. High projection vales caused by shortening of digits II and IV would come with the benefit of lightening the foot, reduction of traction surface, and reduced risk of injury, as over-abduction is less likely to happen when the laterally and medially splayed digits are short. It would also have minimized the fraction of time that digits II and IV are in contact with the ground during running, reducing overall ground contact. The shortening of digits II and IV becomes possible once these digits neglect their function in active motion and instead function primarily as dynamic stabilizers.

In the triangular morphospace described by PC1 and PC2 (Fig. 8), footprint shapes with high digit III projection values are distributed across the upper edge of the triangle, ranging from extreme loadings on PC2 to extreme values on PC1 at the upper and right corner, respectively. In footprints plotting at extreme val-

ues of PC2, digit III projection is primarily caused by the much increased interdigital angles. In those plotting at extreme values of PC1, on the other hand, digit III projection is caused by a digit III that is much longer than digits II and IV and shifted anteriorly relative to the latter. Footprint shapes consistent with those of modern cursorial ratites are found in-between these extremes, while those on extreme loadings on both PC1 and PC2 differ in important aspects. In other words, shapes predicted to represent cursorial adaptations are not directly associated with neither PC1 nor PC2, but with a combination of both. This opens the question if PC1 and PC2 themselves reflect functional adaptation, and to which functions shapes at extreme loadings on these PCs would have been adapted for.

Elongated footprints with low interdigital angles

At positive loadings, PC1 describes a decrease in interdigital angles and an increase in the length-to-width ratio as well as digit III projection values, resulting in more elongated footprints. This trend culminates in some footprints attributed to the ichnogenus *Grallator* that are extremely slender, with the three digits arranged almost parallel to each other. The high projection values and low interdigital angles indicate that the use of digits II and IV for motion was reduced, with most of the forward thrust generated by digit III. This would have made thrust generation more efficient but would also have reduced the ability of varied motion—all features to be expected in cursors. However, two features associated with high values of PC1, the low interdigital angles and the elongated shape, are unseen in footprints of modern terrestrial birds.

It might be argued that the very elongated shapes associated with high loadings on PC1 would have impeded running ability, as is the case for elongated digits in modern birds. Theropods, however, tend to lift the posterior portion of the foot above the ground while running (Sarjeant, 1975; Thulborn, 1990; Viera and Torres, 1995), shortening the footprint. Therefore, the strongly elongated shapes might have merely occurred at lower speeds when an increased traction surface is of advantage, and thus are not necessarily incompatible with cursoriality. In fact, when partially elevated, the digits might have functioned as an additional spring for storage and release of elastic energy, as has been suggested for the permanently elevated posterior digit portions in the ostrich.

Modern cursorial ratites show interdigital angles markedly larger than that of the mean shape of our sample, ranging between 61° to 102° in the emu (Milàn, 2006) and 78° to 101° in the rhea (Padian and Olsen, 1989). Low interdigital angles would have reduced the risk of over-abduction of digits II and IV while running, but also their ability to stabilize, which was identified as the most important function of digit IV in the ostrich (Schaller et al., 2011). It is possible that such low interdigital angles were only possible due to the long tail present in non-avian dinosaurs. In non-avian theropods, tails show a pronounced transition point, dividing the tail into two separate functional units, with the posterior portion being thinner and more rigid (Gauthier, 1986; Russell, 1972). This posterior portion has been interpreted as a dynamic stabilizer during locomotion, especially during turning (Farlow et al., 2000; Gauthier, 1986). Furthermore, it is possible that wings presumably present in some theropods (e.g., *Ornithomimus)* provided an additional aid in stabilization and maneuverability during running, as is the case in the ostrich (Zelenitsky et al., 2012).

The low interdigital angles indicate that functional requirements differed from those of the more splayed footprints of modern ratites. Low angles would have reduced stability while running, which would be most severe at high speeds and body sizes. It is therefore possible that PC1 reflects adaptations for an increased

efficiency in terrestrial locomotion but not for largely increased locomotion speeds. The negative correlation of PC1 (and, for ornithischians, PC2) with body size might result from constrains on cursorial ability imposed by increased body sizes.

Cursoriality at small body sizes

Minute theropod footprints attributed to the ichnogenus *Minisauripus* show that a cursorial lifestyle is not necessarily reflected in the shape of the footprints, and thus requires further discussion. These footprints show an unusually weak mesaxony for their size, but have been suggested to represent the trace of a cursorial trackmaker based on high velocities estimated from its trackways (Xing et al., 2016f). Likewise, the modern roadrunner (*Geococcyx*), although being famous for its cursoriality, features zygodactyl feet similar to those of its arboreal relatives, without apparent cursorial adaptations (Kaiser, 2010). In both cases, cursorial features are possibly absent due to the small body sizes, where constraints imposed by body size are less severe. Indeed, Carrano (1999) demonstrated that cursorial features are generally difficult to distinguish at small body sizes, and that larger dinosaurian cursors display a higher degree of cursorial adaptations than smaller ones. The shapes of these minute-sized footprints could thus be more determined by other functional requirements, phylogeny, or ontogeny. It is currently unclear to what degree dinosaur feet grew isometrically (Farlow et al., 2012a), in which case foot shape of juvenile individuals would be expected to be determined by functional requirements at adult size, where constraints imposed by body size are most severe. This possibility might explain the occurrence of graviportal features in some small (footprint length <15 cm) ornithopod footprints assigned to the ichnogenus *Ornithopodichnus* (Lockley et al., 2012; Xing and Lockley, 2014). However, most *Minisauripus* footprints analyzed here fall outside the morphospace occupied by other tridactyl dinosaur footprints of our sample. Therefore, the possibility that they represent juveniles of a trackmaker with isometrically growing feet appears to be more unlikely.

Alternatively, the disparate footprint shapes in large and minute cursors might be simply due to the fact that behaviors are not exactly comparable across different body sizes. As pointed out by Storer (1971), modern cursorial birds may be divided into two principal groups: Birds of small size, such as the Sanderling (*Calidris alba*), that typically run only over short distances, and larger species that are adapted for sustained running. It is possible that the same dichotomy holds true for non-avian theropods.

Graviportality reflected by footprint shape

At the lower-left corner of the morphospace described by PC1 and PC2, shapes are characterized by a weak digit III projection, an increased footprint width, increased digital widths, and small interdigital angles. This trend probably reflects the transition from the plesiomorphic digitigrade pes towards the subunguligrade, columnar pes structure seen in hadrosaurids, and thus indicates graviportality (Moreno et al., 2007). Similar pes structures can be found in other clades reaching large body sizes such as sauropods, ceratopsians, stegosaurs, and large mammals, and can be interpreted as adaptations for supporting higher body masses at the cost of reduced flexibility and resistance to torsion (Moreno et al., 2007). Thus, the low digit III projection values would have lead to a more equal distribution of stresses across the weight-bearing digits. Comparable pes structures are absent even in large theropods, probably due to selection pressures in favor of cursoriality and maneuverability. Theropods footprints, however, do show proportionally

shorter claw impressions as size increases, possibly reflecting a greater specialization of the feet for locomotion while their secondary function in attacking prey is more and more transferred to the jaws.

Recurrent "bird-like" shapes and their functional implications

High interdigital angles of around 110°–120° and narrow toe impressions are commonly regarded as criteria for the identification of Mesozoic bird footprints, leading to speculations about possible avian affinities of Late Triassic and Early Jurassic footprints (e.g., De Valais and Melchor, 2008; Lockley et al., 1992). This characteristic morphology is not as uncommon in non-avian dinosaur tracks as often assumed, and frequently occurs in some probable theropod (e.g., Farlow et al., 2000) as well as in early ornithischian footprints referred to the ichnogenus *Anomoepus* (G. Gierliński, 1996; Thulborn, 1990; Xing et al., 2017a). As some of the bird-like *Anomoepus* footprints are part of quadrupedal trackways, an avian affinity can be excluded. In fact, this avian-like shapes appear to be the end member of the shape continuum that ranges from very low interdigital angles associated with wider digits to very high angles associated with narrow digits. This shape continuum can be found in both the theropod and ornithischian subsamples. The recurrence of this shape continuum in both groups suggests that avian-like shapes possibly reflect functional adaptations.

The negative correlation between the interdigital angle and digit III width is highly significant in both groups, although weaker in theropods (R=-0.28) than in ornithischians (R=-0.55). On the other hand, the negative correlation between interdigital angle and the widths of digits II and IV are less strong in both groups, and does not reach significance in theropods. This suggests that digit III tends to be more equal in width to digits II and IV with increasing interdigital angle. In ornithischians, the correlation is weaker and less significant when performed on regression residuals, indicating that it can be partly explained with the evolution of graviportality in hadrosaurids, which combine large body sizes with thicker outer digits and low interdigital angles.

The functional advantage of a highly spread foot might lie in the increased mediolateral stability, which can be of importance, e.g., in long-legged animals with a high center of mass position. The small digit widths conceivably bring the advantage of lightening the foot, which would be of obvious relevance especially in flying birds. Possibly, this digit narrowing is enabled by the higher interdigital angles, since broader digits would be necessary to maintain mediolateral stability when interdigital angles are small. Slender and widely splayed digits might also have been adaptations to increase footprint area, providing better support while walking on soft substrates (Storer, 1971; Farlow, 2000). As widely splayed, elongated digits would have restricted running ability (Storer, 1971), such shapes can be expected in animals which do not rely on the latter, most evidently flighted birds.

Limits of study and future research

The study of footprint shapes in the light of functional morphology has great potential for the study of fossil ecosystems. Although we suggest possible links between recurrent shape patterns and specific functions —cursoriality, graviportality and stability—our inferences are limited as we could not include trackway and skeletal morphology data, nor detailed assessments of foot function in modern birds. The inclusion of trackway data would allow for testing of hypotheses proposed herein, as cursorial adaptations in footprint

shape can be expected to be correlated with relative stride length (which are a proxy for trackmaker speed), and as an increased need for stability can be expected to be correlated with step angle (and thus, trackway width). Although the inclusion of skeletal data is hampered by the scarcity of complete pes skeletons in the fossil record, analysis of existing examples would allow to test if foot shape is correlated to overall limb morphology, and how foot shape relates to foot length in relation to the whole limb. Finally, more comprehensive analyses of the functional morphology of feet in modern birds are a prerequisite for detecting possible analogues shapes and functions in dinosaur feet. While research on overall limb function is abundant, the functional morphology of bird feet is surprisingly poorly known, despite its obvious potential in understanding bird and dinosaur biology.

CONCLUSIONS

As direct evidence for animal activity, fossil footprints hold great value for the understanding of dinosaurs. We analyzed a larger (n=303) sample of tridactyl footprints from around the world taken from the literature using an approach combining geometric morphometrics with traditional linear and angular measurements. Included footprints stem from at least 169 tracksites and 134 publications. Although inherent subjectivity of published outline tracings is necessarily included in the present analysis, it is argued that the gross shape patterns observed reflect the actual track record giving the size and diversity of the sample. Ornithischians are demonstrated to show a steady increase in footprint size from the Early Jurassic to the Late Cretaceous, a trend not observable in theropods. Ornithischian tracks are significantly smaller than theropod tracks in the Jurassic but significantly larger in the Cretaceous. Discriminant analysis reveals that features differentiating between theropods and ornithischians change with size, and that small ornithischian footprints are most similar in shape to large theropod footprints.

Both the digit III projection and the footprint length-to-width ratio could be confirmed to correlate significantly with size in both theropods and ornithischians. Digit impression widths show a positive correlation with size in ornithischians but not in theropods. The positive correlation between footprint size and interdigital angles previously proposed for a theropod footprint sample from the Newark Supergroup (Olsen, 1995; Olsen et al., 1998) is absent from our sample; this correlation is negative in ornithischians. Claw impression lengths are negatively correlated with size in theropods.

Although size is demonstrated to be an important determinant of footprint shape, it is only able to explain parts of the variability, and results from size-corrected correlations are similar to those of uncorrected correlations. It is hypothesized that footprint shape is strongly influenced by both size and functional requirements, both of which are tightly interconnected. We argue that footprint shape analysis has great potential for understanding the functional anatomy of dinosaurs, and consequently provide an attempt to infer function from footprint shape. The projection of digit impression III is suggested to be an indicator for cursoriality. Wide interdigital angels are found to be correlated with narrower digits in both theropods and ornithischians, possibly representing an adaptation for maximizing stability while lightening the foot. Weak digit III projection, increased digital widths, and small interdigital angles are interpreted as adaptations for graviportality.

ACKNOWLEDGMENTS

We wish to thank Paul E. Olsen, James O. Farlow, Michael Buchwitz, and Sashima Läbe for discussions, and P. Martin Sander for comments on an early version of this work.

REFERENCES

Adams, T.L., Strganac, C., Polcyn, M.J., Jacobs, L.L., 2010. High resolution three-dimensional laser-scanning of the type specimen of *Eubrontes* (?) *glenrosensis* Shuler, 1935, from the Comanchean (Lower Cretaceous) of Texas: implications for digital archiving and preservation. Palaeontologia Electronica 13, 1–11.

Avanzini, M., Piñuela, L., Garcia-Ramos, J.C., 2012. Late Jurassic footprints reveal walking kinematics of theropod dinosaurs. Lethaia 45, 238–252.

Barco, J.L., Canudo, J.I., Ruiz-Omeñaca, J.I., Rubio, J.L., 2005. Evidencia icnológica de un dinosaurio terópodo gigante en el Berriasiense (Cretácico Inferior) de Laurasia (Las Villasecas, Soria, España). Revista Española de Paleontología, número extraordinario 10, 59–71.

Belvedere, M., 2008. Ichnological researches on the Upper Jurassic dinosaur tracks in the Iouaridène area (Demnat, central High-Atlas, Morocco) (Unpublished PhD thesis). Università a degli studi di Padova.

Belvedere, M., Farlow, J.O., 2016. A numerical scale for qantifying the quality of preservation of vertebrate tracks, in: Falkingham, P.L., Marty, D., Richter, A. (Eds.), Dinosaur Tracks: The Next Steps. Indiana University Press, pp. 92–98.

Belvedere, M., Mietto, P., Ishigaki, S., 2010. A Late Jurassic diverse ichnocoenosis from the siliciclastic Iouaridene Formation (Central High Atlas, Morocco). Geological Quarterly 54, 367–380.

Bennett, M.R., Falkingham, P., Morse, S.A., Bates, K., Crompton, R.H., 2013. Preserving the impossible: Conservation of soft- sediment hominin footprint sites and strategies for three-dimensional digital data capture. PLoS ONE 8, e60755.

Boutakiout, M., Hadri, M., Nouri, J., Díaz-Martínez, I., Pérez-Lorente, F., 2009. Rastrilladas de icnitas therópodas gigantes del Jurásico Superior (Sinclinal de Iouaridène, Marruecos). Revista Española de Paleontología 24, 31–46.

Calvo, J.O., 1991. Huellas de dinosaurios en la Formación Río Limay (Albiano-Cenomaniano?), Picún Leufú, provincia de Neuquén, República Argentina. (Ornithischia-Saurischia: Sauropoda-Theropoda). Ameghiniana 28, 241–258.

Carrano, M.T., 1999. What, if anything, is a cursor? Categories versus continua for determining locomotor habit in mammals and dinosaurs. Journal of Zoology 247, 29–42.

Castanera, D., Colmenar, J., Sauqué, V., Canudo, J.I., 2015. Geometric morphometric analysis applied to theropod tracks from the Lower Cretaceous (Berriasian) of Spain. Palaeontology 58, 183–200.

Castanera, D., Pascual, C., Razzolini, N.L., Vila, B., Barco, J.L., Canudo, J.I., 2013a. Discriminating between medium-sized tridactyl trackmakers: tracking ornithopod tracks in the base of the Cretaceous (Berriasian, Spain). PloS one 8, e81830.

Castanera, D., Vila, B., Razzolini, N.L., Falkingham, P.L., Canudo, J.I., Manning, P.L., Galobart, À., 2013b. Manus track preservation bias as a key factor for assessing trackmaker identity and quadrupedalism in basal ornithopods. PLoS One 8, e54177.

Colbert, E.H., 1989. The triassic dinosaur *Coelophysis*. Museum of Northern Arizona Bulletin 57, 1–160.

Contessi, M., 2013. A new dinosaur ichnofauna from Tunisia: Implications for the palaeobiogeography of peri-Adriatic carbonate platforms in the mid-Cretaceous. Palaeogeography, Palaeoclimatology, Palaeoecology 392, 302–311.

Currie, P.J., Nadon, G.C., Lockley, M.G., 1991. Dinosaur footprints with skin impressions from the Cretaceous of Alberta and Colorado. Canadian Journal of Earth Sciences 28, 102–115.

Dalla Vecchia, F.M., Tarlao, A., Tunis, G., Venturini, S., 2000. New dinosaur tracksites in the Albian (Early Cretaceous) of the Istrian Peninsula (Croatia)—Part II—Paleontology. Memorie di Scienze Geologiche 52, 227–292.

Dalman, S.G., Weems, R.E., 2013. A new look at morphological variation in the ichnogenus *Anomoepus*, with special reference to material from the Lower Jurassic Newark Supergroup: implications for ichnotaxonomy and ichnodiversity. Bulletin of the Peabody Museum of Natural History 54, 67–124.

De Valais, S., Melchor, R.N., 2008. Ichnotaxonomy of bird-like footprints: an example from the Late Triassic-Early Jurassic of Northwest Argentina. Journal of Vertebrate Paleontology 28, 145–159.

Ellenberger, P., 1974. Contribution à la classification des pistes de vertébrés du Trias: Les types du Stormberg d´Afrique du Sud (II éme partie: Le Stormberg Superieur - I. Le biome de la zona B/1 ou niveau de Moyeni: ses biocénoses). Palaeovertebrata, Memoire Extraordinaire 1–143.

Ellenberger, P., 1972. Contribution à la classification des pistes de vertébrés du Trias: Les types du Stormberg d´Afrique du Sud (I). Palaeovertebrata, Memoire Extraordinaire 1–152.

Falkingham, P.L., 2016. Applying objective methods to subjective track outlines, in: Falkingham, P.L., Marty, D., Richter, A. (Eds.), Dinosaur Tracks: The Next Steps. Indiana University Press, pp. 72–81.

Falkingham, P.L., 2014. Interpreting ecology and behaviour from the vertebrate fossil track record. Journal of Zoology 292, 222–228.

Fanti, F., Bell, P.R., Sissons, R.L., 2013. A diverse, high-latitude ichnofauna from the Late Cretaceous Wapiti Formation, Alberta, Canada. Cretaceous Research 41, 256–269.

Farlow, J.O., 1987. A guide to Lower Cretaceous dinosaur footprints and tracksites of the Paluxy River Valley, Somervell County, Texas. Field Trip Guidebook, South-Central Section, Geological Society of America, Baylor University, Waco, Texas 50.

Farlow, J.O., Bonnan, M.E., Rainforth, E.C., Benson, J., Shearer, K., 2012a. Emus, alligators, and *Eubrontes*: assessing intraspecific and interspecific variability in foot and footprint shape, in: Richter, A., Reich, M. (Eds.), Dinosaur Tracks 2011, An International Symposium, Obernkirchen, April 14–17, 2011. Abstracts Volume and Field Guide to Excursions. Universitätsdrucke Göttingen, p. 21.

Farlow, J.O., Chapman, R.E., Breithaupt, B.H., Matthews, N.A., 2012b. The Scientific Study of Dinosaur Footprints, in: Brett-Surman, M.K., Holtz, T.R., Farlow, J.O. (Eds.), The Complete Dinosaur. Indiana University Press, pp. 712–759.

Farlow, J.O., Gatesy, S.M., Holtz, T.R., Hutchinson, J.R., Robinson, J.M., 2000. Theropod locomotion. American Zoologist 40, 640–663.

Foster, J.R., 2015. Theropod dinosaur ichnogenus *Hispanosauropus* identified from the Morrison Formation (Upper Jurassic), Western North America. Ichnos: an international journal of plant & animal traces 22, 183–191.

Foster, J.R., Hamblin, A.H., Lockley, M.G., 2000. The oldest evidence of a sauropod dinosaur in the Western United States and other important vertebrate trackways from Grand Staircase-Escalante National Monument, Utah. Ichnos: an international journal of plant & animal traces 7, 169–181.

Foster, J.R., Lockley, M.G., 2006. The vertebrate ichnological record of the Morrison Formation (Upper Jurassic, North America), in: Foster, J.R., Lucas, S.G. (Eds.), Paleontology and Geology of the Upper Jurassic Morrison Formation, New Mexico Museum of Natural History and Science Bulletin. pp. 203–216.

Fuentes Vidarte, C., Meijide Calvo, M., 1998. Icnitas de dinosaurios terópodos en el Weald de Soria (España). Nuevo icnogénero Kalohipus. Estudios geológicos 54, 147–152.

Fujita, M., Azuma, Y., Lee, Y., Lu, J., Dong, Z., Noda, Y., Urano, K., 2007. New theropod track site from the Upper Jurassic Tuchengzi Formation of Liaoning Province, northeastern China. Memoir of the Fukui Prefectural Dinosaur Museum 6, 17–25.

Galton, P.M., 1971. *Hypsilophodon*, the cursorial non-arboreal dinosaur. Nature 231, 159.

Gand, G., Demathieu, G., Grancier, M., Sciau, J., 2005. Les traces dinosauroïdes du Trias supérieur français: discrimination, interprétation et comparaison. Bulletin de la Société géologique de France 176, 69–80.

Gaston, R., Lockley, M.G., Lucas, S.G., Hunt, A.P., 2003. *Grallator*-dominated fossil footprint assemblages and associated enigmatic footprints from the Chinle Group (Upper Triassic), Gateway area, Colorado. Ichnos: an international journal of plant & animal traces 10, 153–163.

Gatesy, S.M., Middleton, K.M., Jenkins Jr, F.A., Shubin, N.H., 1999. Three-dimensional preservation of foot movements in Triassic theropod dinosaurs. Nature 399, 141–144.

Gauthier, J., 1986. Saurischian monophyly and the origin of birds. Memoirs of the California Academy of sciences 8.

Gierliński, G.D., 1996a. Dinosaur ichnotaxa from the Lower Jurassic of Hungary. Geological Quarterly 40, 119–128.

Gierliński, G.D., 1996b. Avialian theropod tracks from the Early Jurassic strata of Poland. Zubia 14, 79–87.

Gierliński, G.D., 1991. New dinosaur ichnotaxa from the Early Jurassic of the Holy Cross Mountains, Poland. Palaeogeography, Palaeoclimatology, Palaeoecology 85, 137–148.

Gierliński, G.D., Ahlberg, A., 1994. Late Triassic and Early Jurassic dinosaur footprints in the Höganäs Formation of southern Sweden. Ichnos: an international journal of plant & animal traces 3, 99–105.

Gierliński, G.D., Menducki, P., Janiszewska, K., Wicik, I., Boczarowski, A., 2009a. A preliminary report on dinosaur track assemblages from the Middle Jurassic of the Imilchil area, Morocco. Geological Quarterly 53, 477–482.

Gierliński, G.D., Niedźwiedzki, G., Nowacki, P., 2009b. Small theropod and ornithopod footprints in the Late Jurassic of Poland. Acta Geologica Polonica 59, 221–234.

Gierliński, G.D., Niedźwiedzki, G., Pieńkowski, G., 2001. Gigantic footprint of a theropod dinosaur in the Early Jurassic of Poland. Acta Palaeontologica Polonica 46, 441–446.

Gierliński, G.D., Pieńkowski, G., Niedźwiedzki, G., 2004. Tetrapod Track Assemblage in the Hettangian of Sołtyków, Poland, and its Paleoenvironmental Background. Ichnos: an international journal of plant & animal traces 11, 195–213.

Gierliński, G.D., Ploch, I., Gawor-Biedowa, E., Niedźwiedzki, G., 2008. The first evidence of dinosaur tracks in the Upper Cretaceous of Poland. Oryctos 8, 107–113.

Gierliński, G.D., Sabath, K., 2008. Stegosaurian footprints from the Morrison Formation of Utah and their implications for interpreting other ornithischian tracks. Oryctos 8, 29–46.

Henderson, D.M., 2017. The first evidence of iguanodontids (Dinosauria: Ornithischia) in Alberta, Canada – a fossil footprint from the Early Cretaceous. Cretaceous Research 76, 28–33.

Herrero, C., Herrero, E., Martín-Chivelet, J., Pérez-Lorente, F., 2016. Contribution to knowledge of the last dinosaur footprints in Europe. Persistence of ornithopods in the upper Maastrichtian of SE Spain. Cretaceous Research 57, 490–507.

Holtz, T.R., 2012. Theropods, in: Brett-Surman, M.K., Holtz, T.R., Farlow, J.O. (Eds.), The Complete Dinosaur. Indiana University Press, pp. 347–378.

Huh, M., Hwang, K.G., Paik, I.S., Chung, C.H., Kim, B.S., 2003. Dinosaur tracks from the Cretaceous of South Korea: Distribution, occurrences and paleobiological significance. Island Arc 12, 132–144.

Ishigaki, S., Fujisaki, T., 1989. Three dimensional representation of *Eubrontes* by the method of Moiré topography, in: Gillette, D.D., Lockley, M.G. (Eds.), Dinosaur Tracks and Traces. Cambridge University Press, Cambridge, pp. 421–425.

Jones, T.D., Farlow, J.O., Ruben, J.A., Henderson, D.M., Hillenius, W.J., 2000. Cursoriality in bipedal archosaurs. Nature 406, 716.

Kaiser, G.W., 2010. The inner bird: anatomy and evolution. UBC Press.

Kellner, A.W.A., Dalla Vecchia, F.M., Ataabadi, M.M., Silva, H. de P., Khosravi, E., 2012. Review of the dinosaur record from Iran with the description of new material. Rivista Italiana di Paleontologia e Stratigrafia (Research In Paleontology and Stratigraphy) 118, 261–275.

Kim, J.Y., Lockley, M.G., Chun, H.Y., 2016. New dinosaur tracks from the Lower Cretaceous (Valanginian-Hauterivian) Saniri Formation of Yeongdong area, central Korea. Cretaceous Research 61, 5–16.

Kim, J.Y., Lockley, M.G., Kim, H.M., Lim, J.-D., Kim, K.S., 2009. New dinosaur tracks from Korea, *Ornithopodichnus masanensis* ichnogen. et ichnosp. nov. (Jindong Formation, Lower Cretaceous): implications for polarities in ornithopod foot morphology. Cretaceous Research 30, 1387–1397.

Kim, K.S., Lim, J.D., Lockley, M.G., Xing, L., Ha, S.J., Kim, C.B., Paik, I.S., Ahn, J.H., Mun, S.C., 2017. First reports of a distinctive theropod track assemblage from the Jinju Formation (Lower Cretaceous) of Korea provides strong correlations with China. Cretaceous Research 81, 26–35.

Klingenberg, C.P., 2011. MorphoJ: an integrated software package for geometric morphometrics. Molecular Ecology Resources 11, 353–357.

Lallensack, J.N., Sander, P.M., Knötschke, N., Wings, O., 2015. Dinosaur tracks from the Langenberg Quarry (Late Jurassic, Germany) reconstructed with historical photogrammetry: Evidence for large theropods soon after insular dwarfism. Palaeontologia Electronica 18.2.24A, 1–34.

Lallensack, J.N., van Heteren, A.H., Wings, O., 2016. Geometric morphometric analysis of intratrackway variability: a case study on theropod and ornithopod dinosaur trackways from Münchehagen (Lower Cretaceous, Germany). PeerJ 4, e2059.

Leonardi, G., 1987. Discussion of the terms and methods, in: Leonardi, G. (Ed.), Glossary and Manual of Tetrapod Footprint Palaeoichnology. Publicação do Departemento Nacional da Produção Mineral Brasil, Brasília, pp. 43–51.

Leonardi, G., 1984. Le impronte fossili di dinosauri, in: Bonaparte, J.F., Colbert, E.H., Currie, P.J., Ricqlès, A. de, Kielan-Jaworowska, Z., Leonardi, G., Morello, N., Taquet, P. (Eds.), Sulle Orme Dei Dinosauri, Esplorazioni e Ricerche. Erizzo, Venezia, pp. 163–186.

Leonardi, G., 1980. Dez novas pistas de dinossauros (Theropoda Marsh, 1881) na bacia do Rio do Peixe, Paraíba, Brasil. Actas II Congreso Argentino de Paleontología y Bioestratigrafía y I Congreso Latinoamericano de Paleontología 1.

Leonardi, G., Dos Santos, M. de F.C.F., 2004. New dinosaur tracksites from the Sousa Lower Cretaceous basin (Paraíba, Brasil). Studi trentini di scienze naturali - Acta Geologica 81, 5–21.

Li, D., Azuma, Y., Fujita, M., Lee, Y., Arakawa, Y., 2006. A preliminary report on two new vertebrate track sites including dinosaurs from the Early Cretaceous Hekou Group, Gansu Province, China. Journal of the Paleontological Society of Korea 22, 29.

Li, J., Lockley, M.G., Yuguang, Z., Songmei, H., Masaki, M., Zhiqiang, B., 2012. An important ornithischian tracksite in the Early Jurassic of the Shenmu Region, Shaanxi, China. Acta Geologica Sinica (English Edition) 86, 1–10.

Li, R., Lockley, M.G., Matsukawa, M., Liu, M., 2015. Important Dinosaur-dominated footprint assemblages from the lower cretaceous Tianjialou Formation at the Houzuoshan Dinosaur Park, Junan County, Shandong province, China. Cretaceous Research 52, 83–100.

Lim, J.-D., Lockley, M.G., Kong, D.-Y., 2012. The trackway of a quadrupedal ornithopod from the Jindong Formation (Cretaceous) of Korea. Ichnos: an international journal of plant & animal traces 19, 101–104.

Lockley, M.G., 2009. New perspectives on morphological variation in tridactyl footprints: clues to widespread convergence in developmental dynamics. Geological Quarterly 53, 415–432.

Lockley, M.G., 1999. The eternal trail: a tracker looks at evolution. Basic Books.

Lockley, M.G., 1987. Dinosaur footprints from the Dakota Group of Eastern Colorado. The Mountain Geologist 24, 107–122.

Lockley, M.G., Cart, K., Prunty, R., Houck, K., Hups, K., Lim, J.-D., Kim, K.S., Gierliński, G., 2014a. A bonanza of new tetrapod tracksites from the Cretaceous Dakota Group, Western Colorado: Implications for paleoecology, in: Lockley, M.G., Lucas, S.G. (Eds.), Fossil Footprints of Western North America. pp. 393–409.

Lockley, M.G., Foster, R.H., Foster, J., Cart, K., Gerwe, S., 2014b. Early Jurassic track assemblages from the Granite Creek Area of Eastern Utah, in: Lockley, M.G., Lucas, S.G. (Eds.), Fossil Footprints of Western North America. pp. 205–210.

Lockley, M.G., Garcia-Ramos, J.C., Piñuela, L., Avanzini, M., 2008a. A review of vertebrate track assemblages from the Late Jurassic of Asturias, Spain with comparative notes on coeval

ichnofaunas from the western USA: implications for faunal diversity in siliciclastic facies assemblages. Oryctos 8, 53–70.

Lockley, M.G., Gierliński, G.D., 2006. Diverse vertebrate ichnofaunas containing *Anomoepus* and other unusual trace fossils from the Lower Jurassic of the western United States: implications for paleoecology and palichnostratigraphy, in: Harris, J.D., Lucas, S.G., Spielmann, J.A., Lockley, M.G., Milner, A.R.C., Kirkland, J.I. (Eds.), The Triassic-Jurassic Terrestrial Transition., New Mexico Museum of Natural History and Science Bulletin. Albuquerque, pp. 176–191.

Lockley, M.G., Gierliński, G.D., Dubicka, Z., Breithaupt, B.H., Matthews, N.A., Lockley, M.G., Lucas, S.G., 2014c. A preliminary report on a new dinosaur tracksite in the Cedar Mountain Formation (Cretaceous) of Eastern Utah, in: Fossil Footprints of Western North America. pp. 279–285.

Lockley, M.G., Gierliński, G.D., Houck, K., Lim, J.-D., Kim, K.S., Kim, D.Y., Kim, T.K., Kang, S.-H., Hunt Foster, R., Li, R., 2014d. New excavations at the Mill Canyon Dinosaur Track Site (Cedar Mountain Formation, Lower Cretaceous) of Eastern Utah, in: Lockley, M.G., Lucas, S.G. (Eds.), Fossil Footprints of Western North America, New Mexico Museum of Natural History and Science Bulletin 62. Albuquerque, pp. 287–300.

Lockley, M.G., Gierliński, G.D., Martin, J., Kent, C., 2014e. An unusual theropod tracksite in the Cretaceous Dakota Group, western Colorado: implications for ichnodiversity, in: Lockley, M.G., Lucas, S.G. (Eds.), Fossil Footprints of Western North America, New Mexico Museum of Natural History and Science Bulletin 62. Albuquerque, pp. 411–415.

Lockley, M.G., Gierliński, G.D., Titus, A.L., Albright, B., 2006a. An introduction to thunderbird footprints at the Flag Point pictograph-track site-preliminary observations on Lower Jurassic theropod tracks from the Vermillion Cliffs area, southwestern Utah, in: Harris, J.D., Lucas, S.G., Spielmann, J.A., Lockley, M.G., Milner, A.R.C., Kirkland, J.I. (Eds.), The Triassic-Jurassic Terrestrial Transition., New Mexico Museum of Natural History and Science Bulletin. Albuquerque, pp. 310–314.

Lockley, M.G., Honda, K.K., Simmons, B., 2014f. A new dinosaur tracksite in the Dakota Group (Cretaceous) of the historic Stone City area, Colorado, in: Lockley, M.G., Lucas, S.G. (Eds.), Fossil Footprints of Western North America. pp. 205–210.

Lockley, M.G., Houck, K., Green, C., Caldwell, M., 2014g. New fossil footprints from the Dakota Group (Cretaceous) Roxborough State Park, Colorado, in: Lockley, M.G., Lucas, S.G. (Eds.), Fossil Footprints of Western North America. pp. 373–383.

Lockley, M.G., Huh, M., Kim, B.S., 2012. *Ornithopodichnus* and pes-only sauropod trackways from the Hwasun tracksite, Cretaceous of Korea. Ichnos: an international journal of plant & animal traces 19, 93–100.

Lockley, M.G., Hunt, A.P., 1994. A track of the giant theropod dinosaur *Tyrannosaurus* from close to the Cretaceous/Tertiary boundary, northern New Mexico. Ichnos: an international journal of plant & animal traces 3, 213–218.

Lockley, M.G., Hunt, A.P., Meyer, C., Rainforth, E.C., Schultz, R.J., 1998a. A survey of fossil footprint sites at glen canyon national recreation area (western USA): A case study in documentation of trace fossil resources at a national preserve. Ichnos: an international journal of plant & animal traces 5, 177–211.

Lockley, M.G., Janke, P., Theisen, L., 2001. First reports of bird and ornithopod tracks from the Lakota Formation (Early Cretaceous), Black Hills, South Dakota, in: Tanke, D.H., Carpenter, K., Skrepnick, M.W.. (Eds.), Mesozoic Vertebrate Life: New Research Inspired by the Paleontology of Philip J. Currie. Indiana University Press, pp. 443–452.

Lockley, M.G., Kent, C., Martin, J., Milner, A.R.C., 2011. New theropod tracksites from the Upper Cretaceous "Mesaverde" Group, western Colorado: implications for ornithomimosaur track morphology, in: Sullivan, R.M., Lucas, S.G., Spielmann, J.A. (Eds.), Fossil Record 3.Sullivan et Al., Eds., 2011, Fossil Record 3., New Mexico Museum of Natural History and Science Bulletin. Albuquerque, pp. 321–329.

Lockley, M.G., Kim, J.Y., Kim, K.S., Kim, S.H., Matsukawa, M., Rihui, L., Jianjun, L., Yang, S.-Y., 2008b. *Minisauripus*—the track of a diminutive dinosaur from the Cretaceous of China and South Korea:

implications for stratigraphic correlation and theropod foot morphodynamics. Cretaceous Research 29, 115–130.
Lockley, M.G., King, M., Howe, S., Sharp, T., 1996. Dinosaur tracks and other archosaur footprints from the Triassic of South Wales. Ichnos: an international journal of plant & animal traces 5, 23–41.
Lockley, M.G., Li, J.-J., Rihui, L.I., Matsukawa, M., Harris, J.D., Xing, L.-D., 2013. A review of the tetrapod track record in China, with special reference to type ichnospecies: implications for ichnotaxonomy and paleobiology. Acta Geologica Sinica (English Edition) 87, 1–20.
Lockley, M.G., Lucas, S.G., Hunt, A.P., 2000. Dinosaur tracksites in New Mexico: a review. New Mexico Museum of Natural History Bulletin 17, 9–16.
Lockley, M.G., Matsukawa, M., 1998. Lower Cretaceous vertebrate tracksites of east Asia. Lower and Middle Cretaceous Terrestrial Ecosystems. New Mexico Museum of Natural History and Science Bulletin 14, 135–142.
Lockley, M.G., Matsukawa, M., Sato, Y., Polahan, M., Daorerk, V., 2006b. A distinctive new theropod dinosaur track from the Cretaceous of Thailand. Cretaceous Research 27, 139–145.
Lockley, M.G., McCrea, R.T., Matsukawa, M., 2009. Ichnological evidence for small quadrupedal ornithischians from the basal Cretaceous of SE Asia and North America. Geological Society, London, Special Publications 315, 255–269.
Lockley, M.G., Meyer, C.A., Dos Santos, V.F., 1998b. *Megalosauripus* and the problematic concept of megalosaur footprints. Gaia 15, 313–337.
Lockley, M.G., Meyer, C.A., Moratalla, J.J., 1998c. *Therangospodus*: trackway evidence for the widespread distribution of a Late Jurassic theropod with well-padded feet. Gaia 15, 339–353.
Lockley, M.G., Mitchell, L., Odier, G.P., 2007. Small theropod track assemblages from Middle Jurassic eolianites of eastern Utah. Ichnos: an international journal of plant & animal traces 14, 131–142.
Lockley, M.G., Nadon, G., Currie, P.J., 2003. A diverse dinosaur-bird footprint assemblage from the Lance Formation, Upper Cretaceous, Eastern Wyoming: implications for ichnotaxonomy. Ichnos: an international journal of plant & animal traces 11, 229–249.
Lockley, M.G., Schulp, A.S., Meyer, C.A., Leonardi, G., Kerumba Mamani, D., 2002. Titanosaurid trackways from the Upper Cretaceous of Bolivia: evidence for large manus, wide-gauge locomotion and gregarious behaviour. Cretaceous Research 23, 383–400.
Lockley, M.G., Triebold, M., Janke, P.R., 2014h. Dinosaur tracks from the Hell Creek Formation (Upper Cretaceous, Maastrichtian), South Dakota, in: Lockley, M.G., Lucas, S.G. (Eds.), Fossil Footprints of Western North America. pp. 459–468.
Lockley, M.G., Wright, J.L., Thies, D., 2004. Some observations on the dinosaur tracks at Münchehagen (Lower Cretaceous), Germany. Ichnos: an international journal of plant & animal traces 11, 261–274.
Lockley, M.G., Yang, S.Y., Matsukawa, M., Fleming, F., Lim, S.K., 1992. The track record of Mesozoic birds: evidence and implications. Phil. Trans. R. Soc. Lond. B 336, 113–134.
Lull, R.S., 1904. Adaptations to aquatic, arboreal, fossorial and cursorial habits in mammals. IV. Cursorial adaptations. The American Naturalist 38, 1–11.
Makovicky, P.J., Kobayashi, Y., Currie, P.J., 2004. Ornithomimosauria, in: Weishampel, D.B., Dodson, P., Osmólska, H. (Eds.), The Dinosauria. University of California Press, Berkeley, pp. 137–150.
Marty, D., Belvedere, M., Razzolini, N.L., Lockley, M.G., Paratte, G., Cattin, M., Lovis, C., Meyer, C.A., 2017. The tracks of giant theropods (*Jurabrontes curtedulensis* ichnogen. & ichnosp. nov.) from the Late Jurassic of NW Switzerland: palaeoecological & palaeogeographical implications. Historical Biology 0, 1–29.
Masrour, M., Lkebir, N., Pérez-Lorente, F., 2017. Anza palaeoichnological site. Late Cretaceous. Morocco. Part II. Problems of large dinosaur trackways and the first African *Macropodosaurus* trackway. Journal of African Earth Sciences 134, 776–793.
Mateus, O., Miguel, T.A., 2003. A new dinosaur tracksite in the Lower Cretaceous of Portugal. Ciências da Terra (UNL) 15, 253–262.

Matsukawa, M., Hamuro, T., Mizukami, T., Fujii, S., 1997. First trackway evidence of gregarious dinosaurs from the Lower Cretaceous Tetori Group of eastern Toyama prefecture, central Japan. Cretaceous Research 18, 603–619.

Matsukawa, M., Lockley, M.G., Li, J.-J., 2006. Cretaceous terrestrial biotas of East Asia, with special reference to dinosaur-dominated ichnofaunas. Cretaceous Research 27, 3–21.

McCrea, R.T., Buckley, L.G., Farlow, J.O., Lockley, M.G., Currie, P.J., Matthews, N.A., Pemberton, S.G., 2014a. A "terror of tyrannosaurs": the first trackways of tyrannosaurids and evidence of gregariousness and pathology in Tyrannosauridae. PloS one 9, e103613.

McCrea, R.T., Buckley, L.G., Plint, A.G., Currie, P.J., Haggart, J.W., Helm, C.W., Pemberton, S.G., 2014b. A review of vertebrate track-bearing formations from the Mesozoic and earliest Cenozoic of Western Canada with a description of a new theropod ichnospecies and reassignment of an avian ichnogenus, in: Lockley, M.G., Lucas, S.G. (Eds.), Fossil Footprints of Western North America. pp. 5–93.

Meyer, C.A., Thuring, B., 2003. The first iguanodontid dinosaur tracks from the Swiss Alps (Schrattenkalk Formation, Aptian). Ichnos: an international journal of plant & animal traces 10, 221–228.

Milàn, J., 2006. Variations in the morphology of emu (*Dromaius novaehollandiae*) tracks reflecting differences in walking pattern and substrate consistency: ichnotaxonomic implications. Palaeontology 49, 405–420.

Milàn, J., Surlyk, F., 2015. An enigmatic, diminutive theropod footprint in the shallow marine Pliensbachian Hasle Formation, Bornholm, Denmark. Lethaia 48, 429–435.

Milner, A.R.C., Lockley, M.G., 2006. The story of the St. George Dinosaur Discovery Site at Johnson Farm: an important new Lower Jurassic dinosaur tracksite from the Moenave Formation of southwestern Utah, in: Harris, J.D., Lucas, S.G., Spielmann, J.A., Lockley, M.G., Milner, A.R.C., Kirkland, J.I. (Eds.), The Triassic-Jurassic Terrestrial Transition., New Mexico Museum of Natural History and Science Bulletin. Albuquerque, pp. 329–345.

Milner, A.R.C., Vice, G.S., Harris, J.D., Lockley, M.G., 2006. Dinosaur tracks from the Upper Cretaceous Iron Springs Formation, Iron County, Utah, in: Lucas, S.G., Sullivan, R.M. (Eds.), Late Cretaceous Vertebrates from the Western Interior., New Mexico Museum of Natural History and Science Bulletin. Albuquerque, pp. 105–113.

Moreno, K., Carrano, M.T., Snyder, R., 2007. Morphological changes in pedal phalanges through ornithopod dinosaur evolution: A biomechanical approach. Journal of Morphology 268, 50–63.

Niedźwiedzki, G., Pieńkowski, G., 2004. A dinosaur track association from the Early Jurassic deltaic deposits of Podole near Opatów, Poland. Geological Quarterly 48, 333–338.

Olsen, P.E., 1995. Paleontology and paleoenvironments of Early Jurassic age strata in the Walter Kidde Dinosaur Park (New Jersey, USA), in: Baker, J.E.B. (Ed.), Field Guide and Proceedings of the Twelfth Annual Meeting of the Geological Association of New Jersey. Geological Association of New Jersey, William Patterson College, pp. 156–190.

Olsen, P.E., 1980. Fossil great lakes of the Newark Supergroup in New Jersey, in: Field Studies in New Jersey Geology and Guide to Field Trips. pp. 352–398.

Olsen, P.E., Galton, P.M., 1984. A review of the reptile and amphibian assemblages from the Stormberg of southern Africa, with special emphasis on the footprints and the age of the Stormberg. Palaeontologica Africana 25, 87–110.

Olsen, P.E., Rainforth, E.C., 2003. The Early Jurassic ornithischian dinosaurian ichnogenus *Anomoepus*. The great rift valleys of Pangea in eastern North America 2, 314–367.

Olsen, P.E., Smith, J.B., McDonald, N.G., 1998. Type material of the type species of the classic theropod footprint genera *Eubrontes*, *Anchisauripus*, and *Grallator* (Early Jurassic, Hartford and Deerfield basins, Connecticut and Massachusetts, USA). Journal of Vertebrate Paleontology 18, 586–601.

Padian, K., Olsen, P.E., 1989. Ratite footprints and the stance and gait of Mesozoic theropods, in: Gillette, D.D., Lockley, G.M. (Eds.), Dinosaur Tracks and Traces. Cambridge University Press, pp. 231–241.

Pascual-Arribas, C., Hernández Medrano, N., Latorre Macarrón, P., Sanz Pérez, E., 2009. El icnogénero *Iguanodontipus* en el yacimiento de "Las Cuestas I" (Santa Cruz de Yanguas, Soria, España). Studia Geologica Salmanticensia 45, 105–128.

Patak, A.E., Baldwin, J., 1998. Pelvic limb musculature in the emu *Dromaius novaehollandiae* (Aves: Struthioniformes: Dromaiidae): Adaptations to high-speed running. Journal of Morphology 238, 23–37.

Pérez-Lorente, F., 2015. Dinosaur Footprints and Trackways of La Rioja. Indiana University Press.

Pittman, J.G., 1989. Stratigraphy, lithology, depositional, environment, and track type of dinosaur track-bearing beds of the Gulf Coastal Plain, in: Gillette, D.D., Lockley, M.G. (Eds.), Dinosaur Tracks and Traces. Cambridge University Press, Cambridge, pp. 135–153.

R Core Team, 2016. R: A Language and Environment for Statistical Computing. R Foundation for Statistical Computing, Vienna, Austria.

Raath, M.A., 1972. First record of dinosaur footprints from Rhodesia. Arnoldia (Rhodesia) Series of miscellaneous publications National Museums of Rhodesia 5, 1–5.

Rainforth, E.C., Lockley, M.G., 1996. Tracking life in a Lower Jurassic desert: vertebrate tracks and other traces from the Navajo Sandstone. Museum of Northern Arizona Bulletin 60, 285–289.

Rauhut, O.W., Piñuela, L., Castanera, D., García-Ramos, J.-C., Cela, I.S., 2018. The largest European theropod dinosaurs: remains of a gigantic megalosaurid and giant theropod tracks from the Kimmeridgian of Asturias, Spain. PeerJ 6, e4963.

Razzolini, N.L., Belvedere, M., Marty, D., Paratte, G., Lovis, C., Cattin, M., Meyer, C.A., 2017. *Megalosauripus transjuranicus* ichnosp. nov. A new Late Jurassic theropod ichnotaxon from NW Switzerland and implications for tridactyl dinosaur ichnology and ichnotaxomy. PloS one 12, e0180289.

Rodríguez-de la Rosa, R.A., Bravo-Cuevas, V.M., Carrillo-Montiel, E., Ortiz-Ubilla, A., 2012. Lower Cretaceous Dinosaur Tracks from Puebla, Mexico. Journal of Geological Research 2012, 1–7.

Rohlf, F.J., 2014. Tps series. Department of Ecology and Evolution, State University of New York at Stony Brook, New York. http://life.bio.sunysb.edu/morph/.

Russell, D.A., 1972. Ostrich dinosaurs from the Late Cretaceous of western Canada. Canadian Journal of Earth Sciences 9, 375–402.

Salisbury, S.W., Romilio, A., Herne, M.C., Tucker, R.T., Nair, J.P., 2017. The dinosaurian ichnofauna of the Lower Cretaceous (Valanginian–Barremian) Broome Sandstone of the Walmadany area (James Price Point), Dampier Peninsula, Western Australia. Journal of Vertebrate Paleontology 36, 1–152.

Santos, V.F., Callapez, P.M., Rodrigues, N.P.C., 2013. Dinosaur footprints from the Lower Cretaceous of the Algarve Basin (Portugal): New data on the ornithopod palaeoecology and palaeobiogeography of the Iberian Peninsula. Cretaceous Research 40, 158–169.

Sarjeant, W.A.S., 1975. Fossil tracks and impressions of vertebrates, in: The Study of Trace Fossils. Springer, pp. 283–324.

Schaller, N.U., D'Août, K., Villa, R., Herkner, B., Aerts, P., 2011. Toe function and dynamic pressure distribution in ostrich locomotion. Journal of Experimental Biology 214, 1123–1130.

Shounan, Z., Jianjun, L., Chenggang, R., Mateer, N.J., Lockley, M.G., 1989. A review of dinosaur footprints from China, in: Gillette, D.D., Lockley, M.G. (Eds.), Dinosaur Tracks and Traces. Cambridge University Press, Cambridge, pp. 187–197.

Storer, R.W., 1971. Adaptive radiation of birds, in: Avian Biology. Academic Press, New York and London, pp. 149–188.

Thulborn, R.A., 1994. Ornithopod dinosaur tracks from the Lower Jurassic of Queensland. Alcheringa 18, 247–258.

Thulborn, R.A., 1990. Dinosaur tracks. Chapman and Hall, London; New York.

Viera, L.I., Torres, J.A., 1995. Análisis comparativo sobre dos rastros de dinosaurios theropodos. Forma de marcha y velocidad. Munibe Ciencias Naturales 47, 53–56.

Wagensommer, A., Latiano, M., Leroux, G., Cassano, G., D'Orazi Porchetti, S., 2012. New dinosaur tracksites from the Middle Jurassic of Madagascar: ichnotaxonomical, behavioural and palaeoenvironmental implications. Palaeontology 55, 109–126.

Wagensommer, A., Latiano, M., Mocke, H.B., D'Orazi, P., 2016. Dinosaur diversity in an Early Jurassic African desert: the significance of the Etjo Sandstone ichnofauna at the Otjihaenamaparero locality (Namibia). Neues Jahrbuch für Geologie und Paläontologie – Abhandlungen 281, 155–182.

Wang, B., Li, J.-J., Bai, Z., Gao, J., Dong, S., Hu, B., Zhao, S., Chang, J., 2016. Research on Dinoasur Footprints in Zizhou, Shaanxi Province, China. Acta Geologica Sinica (English Edition) 90, 1–18.

Weems, R.E., 2006. The manus print of *Kayentapus minor*; its bearing on the biomechanics and ichnotaxonomy of Early Mesozoic saurischian dinosaurs, in: Harris, J.D., Lucas, S.G., Spielmann, J.A., Lockley, M.G., Milner, A.R.C., Kirkland, J.I. (Eds.), The Triassic-Jurassic Terrestrial Transition., New Mexico Museum of Natural History and Science Bulletin. Albuquerque, pp. 369–378.

Weems, R.E., 1992. A re-evaluation of the taxonomy of Newark Supergroup saurischian dinosaur tracks, using extensive statistical data from a recently exposed tracksite near Culpeper, Virginia. Proceedings 26th forum on the geology of industrial minerals. Virginia Division of Mineral Resources Publication 119, 113–127.

Xing, L., Abbassi, N., Lockley, M.G., Klein, H., Jia, S., McCrea, R.T., IV, W.S.P., 2017a. The first record of *Anomoepus* tracks from the Middle Jurassic of Henan Province, Central China. Historical Biology 29, 223–229.

Xing, L., Harris, J.D., Jia, C.-K., Luo, Z.-J., Wang, S.-N., An, J.-F., 2011. Early Cretaceous bird-dominated and dinosaur footprint assemblages from the northwestern margin of the Junggar Basin, Xinjiang, China. Palaeoworld 20, 308–321.

Xing, L., Klein, H., Lockley, M.G., Wang, S.-L., Chen, W., Ye, Y., Matsukawa, M., Zhang, J.-P., 2013a. Earliest records of theropod and mammal-like tetrapod footprints in the Upper Triassic of Sichuan Basin, China. Vertebrata PalAsiatica 51, 184–198.

Xing, L., Klein, H., Lockley, M.G., Wetzel, A., Li, Z.-D., Li, J.-J., Gierliński, G.D., Zhang, J.-P., Matsukawa, M., Divay, J.D., Zhou, L., 2014a. *Changpeipus* (theropod) tracks from the Middle Jurassic of the Turpan Basin, Xinjiang, Northwest China: review, new discoveries, ichnotaxonomy, preservation and paleoecology. Vertebrata PalAsiatica 4, 233–259.

Xing, L., Li, D., Lockley, M.G., Zhang, J.-P., You, H., Klein, H., Marty, D., Persons IV, W.S., Peng, C., 2014b. Theropod and sauropod track assemblages from the Lower Cretaceous Hekou group of Zhongpu, Gansu Province, China. Acta Palaeontologica Sinica 53, 381–391.

Xing, L., Liu, Y.Q., Kuang, H.W., Klein, H., Zhang, J.P., Burns, M.E., Chen, J., Wang, M.W., Hu, J., 2014c. Theropod and possible ornithopod track assemblages from the Jurassic–Cretaceous boundary Houcheng Formation, Shangyi, northern Hebei, China. Palaeoworld 23, 200–208.

Xing, L., Lockley, M.G., 2014. First report of small *Ornithopodichnus* trackways from the Lower Cretaceous of Sichuan, China. Ichnos: an international journal of plant & animal traces 21, 213–222.

Xing, L., Lockley, M.G., Gierliński, G.D., Persons IV, W.S., Matsukawa, M., Ye, Y., Gingras, M.K., Wang, C.-W., 2013b. Two theropod track assemblages from the Jurassic of Chongqing, China, and the Jurassic stratigraphy of Sichuan Basin. Vertebrata PalAsiatica 51, 107–130.

Xing, L., Lockley, M.G., Hu, S., Li, Q., Persons IV, W.S., 2016a. Early Jurassic *Anomoepus* tracks from the Fengjiahe Formation of northern Central Yunnan, China, in: Sullivan, R.M., Lucas, S.G. (Eds.), Fossil Record 5. New Mexico Museum of Natural History and Science Bulletin. pp. 327–330.

Xing, L., Lockley, M.G., Klein, H., Falkingham, P.L., Kim, J.Y., Mccrea, R.T., Zhang, J., Persons, W.S., Wang, T., Wang, Z., 2016b. First Early Jurassic Small Ornithischian Tracks from Yunnan Province, Southwestern China. PALAIOS 31, 516–524.

Xing, L., Lockley, M.G., Klein, H., Gierliński, G.D., Divay, J.D., Hu, S.M., Zhang, J.-P., Ye, Y., He, Y.P., 2014d. The non-avian theropod track *Jialingpus* from the Cretaceous of the Ordos Basin, China, with a revision of the type material. Palaeoworld 23, 187–199.

Xing, L., Lockley, M.G., Klein, H., Zhang, J.-P., Persons IV, W.S., 2016c. A new ornithischian-dominated and theropod footprint assemblage from the Lower Jurassic Lufeng formation of Yunnan province,

China, in: Sullivan, R.M., Lucas, S.G. (Eds.), Fossil Record 5, New Mexico Museum of Natural History and Science Bulletin. Albuquerque, pp. 331–338.

Xing, L., Lockley, M.G., Li, D., Klein, H., Ye, Y., Scott Persons, W., Ran, H., 2017b. Late Cretaceous ornithopod-dominated, theropod, and pterosaur track assemblages from the Nanxiong Basin, China: new discoveries, ichnotaxonomy, and paleoecology. Palaeogeography, Palaeoclimatology, Palaeoecology 466, 303–313.

Xing, L., Lockley, M.G., Marty, D., Klein, H., Yang, G., Zhang, J., Peng, G., Ye, Y., Persons, W.S., Yin, X., Xu, T., 2016d. A diverse saurischian (theropod–sauropod) dominated footprint assemblage from the Lower Cretaceous Jiaguan Formation in the Sichuan Basin, southwestern China: a new ornithischian ichnotaxon, pterosaur tracks and an unusual sauropod walking pattern. Cretaceous Research 60, 176–193.

Xing, L., Lockley, M.G., Marty, D., Zhang, J., Wang, Y., Klein, H., McCrea, R.T., Buckley, L.G., Belvedere, M., Mateus, O., Gierliński, G.D., Piñuela, L., Persons IV, W.S., Wang, F., Ran, H., Dai, H., Xie, X., 2015a. An ornithopod-dominated tracksite from the Lower Cretaceous Jiaguan Formation (Barremian–Albian) of Qijiang, South-Central China: new discoveries, ichnotaxonomy, preservation and palaeoecology. PloS one 10, e0141059.

Xing, L., Lockley, M.G., Tang, Y., Klein, H., Zhang, J., IV, W.S.P., Dai, H., Ye, Y., 2015b. Theropod and ornithischian footprints from the Middle Jurassic Yanan Formation of Zizhou County, Shaanxi, China. Ichnos: an international journal of plant & animal traces 22, 1–11.

Xing, L., Lockley, M.G., Wang, Q.-F., Li, Z.-D., Klein, H., Persons IV, W.S., Ye, Y., Matsukawa, M., 2014e. Earliest records of dinosaur footprints in Xinjiang, China. Vertebrata PalAsiatica 52, 340–348.

Xing, L., Lockley, M.G., Wang, Y., Pole, M.S., Klein, H., Peng, G., Xie, X., Zhang, G., Deng, C., Burns, M.E., 2016e. New Middle Jurassic dinosaur track record from northeastern Sichuan Province, China. Swiss J Palaeontol 1–6.

Xing, L., Lockley, M.G., Yang, G., Cao, J., Benton, M., Xu, X., Zhang, J., Klein, H., Persons, W.S., Kim, J.Y., Peng, G., Ye, Y., Ran, H., 2016f. A new *Minisauripus* site from the Lower Cretaceous of China: Tracks of small adults or juveniles? Palaeogeography, Palaeoclimatology, Palaeoecology 452, 28–39.

Xing, L., Lockley, M.G., Zhang, J.-P., Klein, H., Kim, J.Y., Persons IV, W.S., Matsukawa, M., Yu, X., Li, J.-J., Chen, G., Hu, Y., 2014f. Upper Cretaceous dinosaur track assemblages and a new theropod ichnotaxon from Anhui Province, eastern China. Cretaceous Research 49, 190–204.

Xing, L., Lockley, M.G., Zhang, J.-P., Klein, H., Persons IV, W.S., Dai, H., 2014g. Diverse sauropod-, theropod-, and ornithopod-track assemblages and a new ichnotaxon *Siamopodus xui* ichnosp. nov. from the Feitianshan Formation, Lower Cretaceous of Sichuan Province, southwest China. Palaeogeography, Palaeoclimatology, Palaeoecology 414, 79–97.

Xing, L., Peng, G.-Z., Lockley, M.G., Ye, Y., Klein, H., McCrea, R.T., Zhang, J.-P., Persons IV, W.S., 2015c. Saurischian (theropod–sauropod) track assemblages from the Jiaguan Formation in the Sichuan Basin, Southwest China. Historical Biology 28, 1003–1013.

Xing, L., Peng, G.-Z., Lockley, M.G., Ye, Y., Klein, H., Zhang, J., Persons IV, W.S., 2015d. Early Cretaceous sauropod and ornithopod trackways from a stream course in Sichuan Basin, Southwest China. New Mexico Museum of Natural History and Science Bulletin 68, 319–325.

Xing, L., Peng, G.-Z., Ye, Y., Lockley, M.G., Klein, H., Persons IV, W.S., Zhang, J.-P., Shu, C., Hao, B., 2014h. Sauropod and small theropod tracks from the Lower Jurassic Ziliujing Formation of Zigong City, Sichuan, China, with an overview of Triassic–Jurassic dinosaur fossils and footprints of the Sichuan Basin. Ichnos: an international journal of plant & animal traces 21, 119–130.

Xing, L., Peng, G.-Z., Ye, Y., Lockley, M.G., McCrea, R.T., Currie, P.J., Zhang, J.-P., Burns, M.E., 2014i. Large theropod trackway from the Lower Jurassic Zhenzhuchong Formation of Weiyuan County, Sichuan Province, China. Palaeoworld 23, 285–293.

Zelenitsky, D.K., Therrien, F., Erickson, G.M., DeBuhr, C.L., Kobayashi, Y., Eberth, D.A., Hadfield, F., 2012. Feathered Non-Avian Dinosaurs from North America Provide Insight into Wing Origins. Science 338, 510–514.

Zhen, S., Li, J., Rao, C., 1986. Dinosaur footprints of Jinning, Yunnan. Beijing natural history museum 33, 1–19.

Zhou, Z.-H., Wang, X.L., 2000. A new species of *Caudipteryx* from the Yixian Formation of Liaoning, northeast China. Vertebrata PalAsiatica 38, 113–130.

Supplementary Material S1: Data Sample

Reference	Figure	Ichnogenus	Period	Epoch	Group	Centroid Size	FL (cm)
Adams et al., 2010	Fig. 6	NA	Cretaceous	Cretaceous, Early	Theropoda	92.773	61.464
Avanzini et al., 2012	Fig. 1A	Anchisauripus	Jurassic	Jurassic, Late	Theropoda	19.719	15.577
Avanzini et al., 2012	Fig. 1B	NA	Jurassic	Jurassic, Late	Theropoda	33.771	20.23
Barco et al., 2005	Fig. 3	Iberosauripus	Cretaceous	Cretaceous, Early	Theropoda	98.666	62.669
Belvedere et al., 2010	Fig. 5B	Megalosauripus	Jurassic	Jurassic, Late	Theropoda	44.783	29.964
Belvedere et al., 2010	Fig. 8D	NA	Jurassic	Jurassic, Late	Theropoda	35.058	23.397
Belvedere et al., 2010	Fig. 4B	NA	Jurassic	Jurassic, Late	Ornithischia	40.8	23.089
Calvo, 1991	Fig. 9	Abelichnus	Cretaceous	NA	Theropoda	63.095	39.16
Calvo, 1991	Fig. 4 (left)	Limayichnus	Cretaceous	NA	Ornithischia	91.584	57.296
Castanera et al., 2013a	Fig. 4D	NA	Cretaceous	Cretaceous, Early	Ornithischia	37.908	21.974
Castanera et al., 2013a	Fig. 7D	NA	Cretaceous	Cretaceous, Early	Ornithischia	37.713	22.281
Castanera et al., 2013b	Fig. 6A (first track)	NA	NA	NA	Ornithischia	35.453	23.167
Castanera et al., 2013b	Fig. 9B	NA	NA	NA	Ornithischia	18.152	12.672
Contessi, 2013	Fig. 5K	NA	Cretaceous	Cretaceous, Late	Theropoda	24.911	17.271
Currie et al., 1991	Fig. 4	Caririchnium	Cretaceous	NA	Ornithischia	78.844	45.745
Currie et al., 1991	Fig. 5	Hadrosauropodus	Cretaceous	Cretaceous, Late	Ornithischia	105.142	54.261
Dalla Vecchia et al., 2000	Fig. 8C (PUII-T1-4)	NA	Cretaceous	Cretaceous, Early	Theropoda	28.122	20.322
Dalla Vecchia et al., 2000	Fig. 8D (SOLI-T1-7)	NA	Cretaceous	Cretaceous, Early	Theropoda	27.126	19.281
Dalla Vecchia et al., 2000	Fig. 8P (SOLII-189)	NA	Cretaceous	Cretaceous, Early	Theropoda	24.062	17.542
Dalman and Weems, 2013	Fig. 7B	Anomoepus	Jurassic	Jurassic, Early	Ornithischia	3.77	2.652
Dalman and Weems, 2013	Fig. 43	Anomoepus	Jurassic	Jurassic, Early	Ornithischia	4.195	2.811
Ellenberger, 1972	Planche II (23)	Boisutrisauropus	Triassiv	Triassic, Late	Theropoda	64.219	38.747
Ellenberger, 1972	Planche IV (44 A)	Deuterotrisauropus	Jurassic	Jurassic, Early	Theropoda	49.176	30.475
Ellenberger, 1972	Planche IV (44 B)	Deuterotrisauropus	Triassic	Triassic, Late	Theropoda	57.793	39.729
Ellenberger, 1972	Planche IV (45 A)	Mafatrisauropus	Jurassic	Jurassic, Early	Theropoda	59.756	37.483
Ellenberger, 1974	Planche A (right)	Neotrisauropus	Jurassic	Jurassic, Early	Theropoda	33.026	22.9
Ellenberger, 1974	Planche C (right)	Moyenisauropus	Jurassic	Jurassic, Early	Ornithischia	35.284	19.229
Ellenberger, 1974	Planche D (left)	Moyenisauropus	Jurassic	Jurassic, Early	Ornithischia	30.873	18.737
Ellenberger, 1974	Planche E (bottom right)	Moyenisauropus	Jurassic	Jurassic, Early	Ornithischia	28.459	16.975
Ellenberger, 1974	Planche E (top middle)	Moyenisauropus	Jurassic	Jurassic, Early	Ornithischia	17.086	10.902
Ellenberger, 1974	Planche J (top right)	Neotrisauropus	Jurassic	Jurassic, Early	Theropoda	29.233	20.263
Ellenberger, 1974	Planche K (bottom left)	Moyenisauropus	Jurassic	Jurassic, Early	Ornithischia	17.396	9.055
Ellenberger, 1974	Planche N (bottom middle)	Masitisisauropus	Jurassic	Jurassic, Early	Theropoda	14.117	9.189
Fanti et al., 2013	Fig. 5B	NA	Cretaceous	Cretaceous, Late	Theropoda	79.707	43.275
Foster et al., 2000	Fig. 4A	NA	Jurassic	Jurassic, Middle	Theropoda	63.442	42.122
Foster and Lockley, 2006	Fig. 5A	NA	Jurassic	Jurassic, Late	Theropoda	16.762	11.762
Foster and Lockley, 2006	Fig. 6C	NA	Jurassic	Jurassic, Late	Theropoda	63.907	40.06
Foster and Lockley, 2006	Fig. 3 (track 4)	NA	Jurassic	Jurassic, Late	Ornithischia	14.578	9.035
Foster, 2015	Fig. 3B	Hispanosauropus	Jurassic	Jurassic, Late	Theropoda	74.2	49.431
Fuentes Vidarte and Meijide Calvo, 1998	Fig. 3	Kalohipus	Cretaceous	Cretaceous, Early	Theropoda	10.892	7.309
Fuentes Vidarte and Meijide Calvo, 1998	Fig. 3	Kalohipus	Cretaceous	Cretaceous, Early	Theropoda	9.604	6.744
Fujita et al., 2007	Fig. 5 (A43-sketch)	NA	Jurassic	Jurassic, Late	Theropoda	4.815	3.61
Fujita et al., 2007	Fig. 6 (B1-sketch)	NA	Jurassic	Jurassic, Late	Theropoda	17.496	12.855
Fujita et al., 2007	Fig. 6 (C14-sketch)	NA	Jurassic	Jurassic, Late	Theropoda	20.53	14.912
Gand et al., 2005	Fig. 1 (21)	Coelurosaurichnus	Triassic	Triassic, Late	NA	13.866	9.061
Gand et al., 2005	Fig. 2 (13)	Grallator	Triassic	Triassic, Late	Theropoda	26.5	16.411
Gand et al., 2005	Fig. 2 (18)	Eubrontes	Triassic	Triassic, Late	Theropoda	42.079	25.743
Gaston et al., 2003	Fig. 6 (7)	Grallator	Triassic	Triassic, Late	Theropoda	8.364	5.992
Gaston et al., 2003	Fig. 6 (4)	Grallator	Triassic	Triassic, Late	Theropoda	9.508	6.727
Gatesy et al., 1999	Fig. 1A	Grallator	Triassic	Triassic, Late	Theropoda	26.094	17.379
Gierliński, 1991	Fig. 2A	Eubrontes	Jurassic	Jurassic, Early	Theropoda	30.448	18.482
Gierliński, 1991	Fig. 2B	Eubrontes	Jurassic	Jurassic, Early	Theropoda	41.44	24.527
Gierliński, 1991	Fig. 3 (lowest)	Anomoepus	Jurassic	Jurassic, Early	Ornithischia	22.158	13.898
Gierliński, 1991	Fig. 4 (lowest)	Moyenisauropus	Jurassic	Jurassic, Early	Ornithischia	40.107	24.216
Gierliński and Ahlberg, 1994	Fig. 3	Eubrontes	Triassic	Triassic, Late	Theropoda	45.781	26.914
Gierliński and Ahlberg, 1994	Fig. 4B	Eubrontes	Jurassic	Jurassic, Ealry	Theropoda	41.775	24.443
Gierliński, 1996	Fig. 2	Grallator	Jurassic	Jurassic, Ealry	Theropoda	28.614	21.319
Gierliński, 1996	Fig. 4	Kayentapus	Jurassic	Jurassic, Ealry	Theropoda	40.689	24.78
Gierliński et al., 2001	Fig. 3A	Megalosauripus	Jurassic	Jurassic, Late	Theropoda	57.048	36.903
Gierliński et al., 2001	Fig. 3B	Megalosauripus	Jurassic	Jurassic, Early	Theropoda	44.529	29.46
Gierliński et al., 2004	Fig. 8A	Kayentapus	Jurassic	Jurassic, Ealry	Theropoda	47.525	32.453
Gierliński et al., 2004	Fig. 8B	Eubrontes	Jurassic	Jurassic, Ealry	Theropoda	46.362	32.071
Gierliński et al., 2004	Fig. 8C	NA	Jurassic	Jurassic, Ealry	Theropoda	69.807	48.239
Gierliński et al., 2004	Fig. 11A	Anchisauripus	Jurassic	Jurassic, Ealry	Theropoda	22.388	15.76
Gierliński et al., 2004	Fig. 11B	Grallator	Jurassic	Jurassic, Ealry	Theropoda	7.344	5.582
Gierliński et al., 2004	Fig. 12A	Anomoepus	Jurassic	Jurassic, Ealry	Ornithischia	18.907	12.017
Gierliński et al., 2008	Fig. 3	NA	Cretaceous	Cretaceous, Late	Ornithischia	75.078	42.379
Gierliński et al., 2008	Fig. 5A	Iguanodontipus	Cretaceous	Cretaceous, Early	Ornithischia	59.046	29.378
Gierliński et al., 2008	Fig. 5B	Caririchnium	Cretaceous	NA	Ornithischia	47.256	25.161
Gierliński et al., 2008	Fig. 5C	Amblydactylus	Cretaceous	Cretaceous, Early	Ornithischia	70.366	37.353
Gierliński and Sabath, 2008	Fig. 7B	Dinehichnus	Jurassic	Jurassic, Late	Ornithischia	34.825	20.477
Gierliński et al., 2009b	Fig. 5B	Jialingpus	Jurassic	Jurassic, Late	Theropoda	15.756	12.457
Gierliński et al., 2009b	Fig. 7A	Dinehichnus	Jurassic	Jurassic, Late	Ornithischia	30.052	16.413
Gierliński et al., 2009b	Fig. 7B	Dinehichnus	Jurassic	Jurassic, Late	Ornithischia	27.177	15.306
Gierliński et al., 2009b	Fig. 7C	Dinehichnus	Jurassic	Jurassic, Late	Ornithischia	28.821	16.865
Gierliński et al., 2009b	Fig. 8A	Dinehichnus	Jurassic	Jurassic, Late	Ornithischia	24.224	13.136
Gierliński et al., 2009b	Fig. 8B	NA	Jurassic	Jurassic, Late	Ornithischia	30.035	16.712
Gierliński et al., 2009a	Fig. 2 B	Changpeipus	Jurassic	Jurassic, Middle	Theropoda	48.178	31.634
Gierliński et al., 2009a	Fig. 3 E	NA	Jurassic	Jurassic, Middle	Ornithischia	33.552	20.655

Reference	Figure	Ichnogenus	Period	Epoch	Group	Centroid Size	FL (cm)
Gierliński et al., 2009a	Fig. 3 D	Therangospodus	Jurassic	Jurassic, Middle	Theropoda	41.246	26.175
Gierliński et al., 2009a	Fig. 3 C	Carmelopodus	Jurassic	Jurassic, Middle	Theropoda	19.537	10.365
Gierliński et al., 2009a	Fig. 3 B	Jialingpus	Jurassic	Jurassic, Middle	Theropoda	13.978	10.567
Henderson, 2017	Fig. 4B	NA	Cretaceous	Cretaceous, Early	Ornithischia	78.824	42.939
Herrero et al., 2016	Fig. 12	NA	Cretaceous	Cretaceous, Late	Ornithischia	49.371	29.859
Huh et al., 2003	Fig. 4A (first track)	NA	Cretaceous	NA	Ornithischia	72.161	41.931
Huh et al., 2003	Fig. 4B (first track)	Caririchnium	Cretaceous	Cretaceous, Late	Ornithischia	69.361	39.535
Ishigaki and Fujisaki, 1989	Fig. 48.1	Eubrontes	Jurassic	Jurassic, Early	Theropoda	54.797	33.925
Kellner et al., 2012	Fig. 5 A2 (NV/UHUL-T1-2)	NA	Jurassic	Jurassic, Early	Theropoda	53.501	36.846
Kellner et al., 2012	Fig. 5 I1 (NV/LHLL-T1-1)	NA	Jurassic	Jurassic, Early	Theropoda	31.982	20.746
Kim et al., 2016	Fig. 2E	Caririchnium	Cretaceous	Cretaceous, Early	Ornithischia	62.863	38.859
Kim et al., 2017	Fig. 6A (left)	Grallator	Cretaceous	Cretaceous, Early	Theropoda	20.004	14.892
Kim et al., 2017	Fig. 6E	Asianopodus	Cretaceous	Cretaceous, Early	Theropoda	34.765	25.902
Kim et al., 2017	Fig. 7B (HTD 011)	Corpulentatpus	Cretaceous	Cretaceous, Early	Theropoda	24.954	15.46
Lallensack et al., 2015	Fig. 7	NA	Jurassic	Jurassic, Late	Theropoda	79.12	43.361
Lallensack et al., 2016	Fig. 3A	NA	Cretaceous	Cretaceous, Early	Theropoda	41.216	26.842
Lallensack et al., 2016	Fig. 3B	NA	Cretaceous	Cretaceous, Early	Theropoda	60.788	35.781
Lallensack et al., 2016	Fig. 4 (upper left)	NA	Cretaceous	Cretaceous, Early	Ornithischia	57.644	32.35
Leonardi, 1980	FIg. 1	NA	NA	NA	Theropoda	45.013	25.922
Leonardi, 1980	Fig. 2	NA	NA	NA	Theropoda	44.077	27.211
Leonardi, 1980	Fig. 6 (lowest)	NA	NA	NA	Theropoda	46.033	26.46
Leonardi, 1980	Fig. 11	NA	NA	NA	Theropoda	34.049	21.252
Leonardi, 1980	Fig, 4	NA	NA	NA	Theropoda	26.944	18.202
Leonardi, 1984	Fig. 9 (35)	NA	Cretaceous	Cretaceous, Early	Theropoda	34.74	21.774
Leonardi and Dos Santos, 2004	Fig. 4A	NA	Cretaceous	Cretaceous, Early	Theropoda	78.99	38.675
Li et al., 2006	Fig. 15	NA	Cretaceous	Cretaceous, Early	Ornithischia	50.572	33.273
Li et al., 2011	Fig. 9D	Corpulentapus	Cretaceous	NA	Theropoda	27.916	15.915
Li et al., 2012	Fig. 11B (second pes)	Shenmuichnus	Jurassic	Jurassic, Early	Ornithischia	58.098	35.788
Li et al., 2012	Fig. 12A (right)	Shenmuichnus	NA	Triassic, Late	Ornithischia	42.287	25.953
Li et al., 2012	Fig. 12D (second track)	Anomoepus	Jurassic	NA	Ornithischia	25.864	16.597
Li et al., 2012	Fig. 12E (first track)	Anomoepus	Jurassic	NA	Ornithischia	18.563	11.96
Li et al., 2015	Fig. 5B (second track)	NA	Cretaceous	Cretaceous, Early	Ornithischia	42.914	20.831
Li et al., 2015	Fig. 6A (right, second track)	NA	Cretaceous	Cretaceous, Early	Ornithischia	54.597	30.149
Li et al., 2015	Fig. 13 T1 (track 2)	Asianopodus	Cretaceous	Cretaceous, Early	Theropoda	25.508	15.378
Li et al., 2015	Fig. 18 (bottom, first track)	NA	Cretaceous	Cretaceous, Early	Ornithischia	44.113	29.331
Lim et al., 2012	Fig. 2	Caririchnium	Cretaceous	Cretaceous, Late	Ornithischia	60.705	36.217
Lockley, 1987	Fig. 5D (track 7)	NA	Cretaceous	Cretaceous, Late	Ornithischia	73.753	41.625
Lockley, 1987	Fig. 5A (track 1)	Caririchnium	Cretaceous	Cretaceous, Late	Ornithischia	68.427	39.344
Lockley and Hunt, 1994	Fig. 2	Tyrannosauripus	Cretaceous	Cretaceous, Late	Theropoda	117.269	76.347
Lockley et al., 1996	Fig. 9 (upper right)	Grallator	Triassic	Triassic, Late	Theropoda	13.24	10.05
Lockley and Matsukawa, 1998	Fig. 5B	NA	NA	NA	Theropoda	12.682	8.19
Lockley et al., 1998b	Fig. 11 (left)	Megalosauripus	Jurassic	Jurassic, Late	Theropoda	57.45	40.064
Lockley et al., 1998b	Fig. 8 (upper right)	Megalosauripus	Jurassic	Jurassic, Late	Theropoda	59.644	39.688
Lockley et al., 1998b	Fig. 8 (lower left)	Megalosauripus	Jurassic	Jurassic, Late	Theropoda	51.562	38.326
Lockley et al., 1998b	Fig. 8 (lower right)	Megalosauripus	Jurassic	Jurassic, Late	Theropoda	77.022	52.666
Lockley et al., 1998c	Fig. 1A	Therangospodus	Jurassic	Jurassic, Late	Theropoda	32.055	22.126
Lockley et al., 1998c	Fig. 6E	Therangospodus	Jurassic	Jurassic, Late	Theropoda	34.775	24.299
Lockley et al., 1998c	Fig. 6F	Therangospodus	Jurassic	Jurassic, Late	Theropoda	36.919	26.095
Lockley et al., 1998c	Fig. 6G	Therangospodus	Jurassic	Jurassic, Late	Theropoda	34.994	26.068
Lockley et al., 1998c	Fig. 9	Therangospodus	Jurassic	Jurassic, Late	Theropoda	36.508	21.967
Lockley et al., 1998a	Fig. 8	Grallator	NA	NA	Theropoda	17.229	11.208
Lockley et al., 2000	Fig. 7 left (second track)	NA	Cretaceous	NA	Ornithischia	32.626	19.441
Lockley et al., 2001	Fig. 30.4 (left, first track)	NA	Cretaceous	Cretaceous, Early	Ornithischia	74.76	39.884
Lockley et al., 2001	Fig. 30.4 (upper right)	NA	Cretaceous	Cretaceous, Early	Ornithischia	69.002	39.978
Lockley et al., 2001	Fig. 30.4 (lower right, second)	NA	Cretaceous	Cretaceous, Early	Ornithischia	58.462	28.211
Lockley et al., 2002	Fig. 6A (uppermost track)	NA	Cretaceous	Cretaceous, Late	NA	32.212	16.326
Lockley et al., 2003	Fig. 8 (first track)	Hadrosauropodus	Cretaceous	Cretaceous, Late	Ornithischia	133.36	72.722
Lockley et al., 2004	Fig. 7 (upper right, track 2)	Iguanodontipus	Cretaceous	Cretaceous, Early	Ornithischia	56.641	30.175
Lockley and Gierliński, 2006	Fig. 5A (second track)	Grallator	Jurassic	Jurassic, Early	Theropoda	26.971	19.32
Lockley et al., 2006b	Fig. 5A	Siamopodus	Cretaceous	Cretaceous, Early	Theropoda	47.724	29.791
Lockley et al., 2006b	Fig. 7A	NA	Cretaceous	Cretaceous, Early	Theropoda	66.018	39.275
Lockley et al., 2006a	Fig. 6B	Kayentapus	Jurassic	Jurassic, Early	Theropoda	70.761	41.875
Lockley et al., 2006a	Fig. 6C	Eubrontes	Jurassic	Jurassic, Early	Theropoda	53.695	37.222
Lockley et al., 2007	Fig. 7B	Grallator	Jurassic	Jurassic, Early	Theropoda	9.077	7.254
Lockley et al., 2007	Fig. 7B	Grallator	Jurassic	Jurassic, Early	Theropoda	9.122	6.948
Lockley et al., 2008	Fig. 4D	NA	Jurassic	Jurassic, Late	Theropoda	17.003	12.409
Lockley et al., 2008	Fig. 4G	NA	Jurassic	Jurassic, Late	Theropoda	20.466	15.656
Lockley et al., 2008	Fig. 7B	Hispanosauropus	Jurassic	Jurassic, Late	Theropoda	50.184	32.211
Lockley et al., 2008	Fig. 7F	Hispanosauropus	Jurassic	Jurassic, Late	Theropoda	81.632	56.967
Lockley et al., 2008	Fig. 3	Minisauripus	Cretaceous	Cretaceous, Late	Theropoda	3.484	2.457
Lockley et al., 2008	Fig. 6 (left detail)	Minisauripus	Cretaceous	Cretaceous, Early	Theropoda	4.362	3.35
Lockley et al., 2008	Fig. 6 (right detail)	Minisauripus	Cretaceous	Cretaceous, Early	Theropoda	4.091	3.179
Lockley et al., 2008	Fig. 10 (A)	Minisauripus	Cretaceous	Cretaceous, Early	Theropoda	6.757	5.131
Lockley et al., 2009	Fig. 7A (third track)	NA	NA	NA	Ornithischia	33.494	21.541
Lockley et al., 2009	Fig. 8 (right; upper left, track 6)	Neoanomoepus	Cretaceous	Cretaceous, Early	Ornithischia	18.033	11.406
Lockley et al., 2009	Fig. 8 (right, upper right, track 2)	Neoanomoepus	Cretaceous	Cretaceous, Early	Ornithischia	17.719	10.664
Lockley et al., 2009	Fig. 7 (upper, first track)	Dinehichnus	Jurassic	Jurassic, Early	Ornithischia	36.323	21.1
Lockley et al., 2009	Fig. 7 (lower, first track)	Dinehichnus	Jurassic	Jurassic, Early	Ornithischia	19.319	11.531
Lockley et al., 2011	Fig. 10A	Ornithomimipus	Cretaceous	Cretaceous, Late	Theropoda	70.705	44.687
Lockley et al., 2011	Fig. 10B (7)	Ornithomimipus	Cretaceous	Cretaceous, Late	Theropoda	38.359	22.904
Lockley et al., 2011	Fig. 10B (8)	Ornithomimipus	Cretaceous	Cretaceous, Late	Theropoda	37.965	25.306

Reference	Figure	Ichnogenus	Period	Epoch	Group	Centroid Size	FL (cm)
Lockley et al., 2011	Fig. 10B (14)	Ornithomimipus	Cretaceous	Cretaceous, Late	Theropoda	45.782	25.256
Lockley et al., 2012	Fig. 5	Ornithopodichnus	Cretaceous	Cretaceous, Late	Ornithischia	26.54	13.704
Lockley et al., 2013	Fig. 2C	Changpeipus	Jurassic	Jurassic, Early	Theropoda	47.47	32.749
Lockley et al., 2013	Fig. 2P	Weiyuanpus	Jurassic	Jurassic, Early	Theropoda	51.478	35.487
Lockley et al., 2013	Fig. 2N	Jinlijingpus	Jurassic	Jurassic, Early	Theropoda	40.471	25.749
Lockley et al., 2013	Fig. 3A	Yangtzepus	Jurassic	Jurassic, Early	Theropoda	31.22	23.275
Lockley et al., 2013	Fig. 5E	Chapus	Cretaceous	Cretaceous, Early	Theropoda	34.895	22.544
Lockley et al., 2014d	Fig. 8B	Irenesauripus	Cretaceous	Cretaceous, Early	Theropoda	57.927	38.912
Lockley et al., 2014e	Fig. 3F	Irenesauripus	Cretaceous	NA	Theropoda	35.409	22.687
Lockley et al., 2014e	Fig. 3E	Irenesauripus	Cretaceous	NA	Theropoda	41.201	27.597
Lockley et al., 2014e	Fig. 3D, upper	Irenesauripus	Cretaceous	NA	Theropoda	53.157	31.571
Lockley et al., 2014e	Fig. 5 (O7)	Caririchnium	Cretaceous	NA	Ornithischia	59.439	30.514
Lockley et al., 2014b	Fig. 6	Eubrontes	Jurassic	Jurassic, Early	Theropoda	51.361	34.5
Lockley et al., 2014c	Fig. 8B (first track)	NA	Cretaceous	Cretaceous, Early	Ornithischia	65.59	37.961
Lockley et al., 2014f	Fig. 3 (no. 1)	NA	Cretaceous	NA	Ornithischia	38.625	21.758
Lockley et al., 2014g	Fig. 4b (track 1)	NA	Cretaceous	NA	Ornithischia	48.635	29.898
Lockley et al., 2014a	Fig. 3a (detail, track 1)	NA	Cretaceous	NA	Ornithischia	80.077	42.857
Lockley et al., 2014a	Fig. 4 (track 53)	NA	Cretaceous	NA	Ornithischia	63.953	35.624
Lockley et al., 2014h	Fig. 10 (left)	NA	Cretaceous	Cretaceous, Late	Theropoda	105.358	63.832
Marty et al., 2017	Fig. 5B	Jurabrontes	Jurassic	Jurassic, Late	Theropoda	81.814	49.661
Marty et al., 2017	Fig. 6K	Jurabrontes	Jurassic	Jurassic, Late	Theropoda	108.262	73.609
Masrour et al., 2017	Fig. 7 (3.1ANZ15.1)	NA	Cretaceous	Cretaceous, Late	Theropoda	24.236	17.825
Masrour et al., 2017	Fig. 7 (4.1ANZ1.1)	NA	Cretaceous	Cretaceous, Late	Theropoda	37.338	24.886
Mateus and Miguel, 2003	Fig. 4A	NA	Cretaceous	Cretaceous, Early	Theropoda	56.67	35.157
Mateus and Miguel, 2003	Fig. 4P	NA	Cretaceous	Cretaceous, Early	Ornithischia	68.166	43.446
Matsukawa et al., 1997	Fig. 3A	Toyamasauripus	Cretaceous	Cretaceous, Early	Theropoda	13.925	9.071
Matsukawa et al., 1997	Fig. 3H	Toyamasauripus	Cretaceous	Cretaceous, Early	Theropoda	8.035	4.634
Matsukawa et al., 1997	Fig. 3H	Toyamasauripus	Cretaceous	Cretaceous, Early	Theropoda	8.35	4.752
Matsukawa et al., 2006	Fig. 3 (upper right)	NA	NA	NA	Ornithischia	48.843	26.638
Matsukawa et al., 2006	Fig. 4B (second track)	NA	Cretaceous	Cretaceous, Late	Theropoda	25.611	18.531
Matsukawa et al., 2006	Fig. 4B (second track)	NA	Cretaceous	Cretaceous, Late	Theropoda	26.87	19.495
Matsukawa et al., 2006	Fig. 9B (upper right)	NA	Cretaceous	Cretaceous, Early	Theropoda	45.805	28.715
Matsukawa et al., 2006	Fig. 9C (lower right)	NA	Cretaceous	Cretaceous, Early	Theropoda	71.816	37.425
McCrea et al., 2014a	Fig. 8 (track 2)	Bellatoripes	Cretaceous	Cretaceous, Late	Theropoda	96.946	59.216
McCrea et al., 2014	Fig. 74	NA	Cretaceous	Cretaceous, Late	Theropoda	39.472	22.505
Meyer and Thuring, 2003	Fig. 5B (TR1 R2)	Iguanodontipus	Cretaceous	Cretaceous, Early	Ornithischia	42.334	22.423
Milàn and Surlyk, 2015	Fig. 3	NA	Jurassic	Jurassic, Early	Theropoda	4.881	2.975
Milner et al., 2006	Fig. 4D	NA	Cretaceous	Cretaceous, Late	Ornithischia	54.541	31.17
Milner et al., 2006	Fig. 4H	NA	Cretaceous	Cretaceous, Late	Ornithischia	119.165	74.218
Milner and Lockley, 2006	Fig. 17A	Eubrontes	Jurassic	Jurassic, Early	Theropoda	54.676	36.093
Niedźwiedzki and Pieńkowski, 2004	Fig. 3A	Anchisauripus	Jurassic	Jurassic, Early	Theropoda	25.568	19.163
Niedźwiedzki and Pieńkowski, 2004	Fig. 3B	Kayentapus	Jurassic	Jurassic, Ealry	Theropoda	25.457	14.552
Olsen, 1980	Fig. 5G	Grallator	Triassic	Triassic, Late	Theropoda	9.461	6.582
Olsen, 1980	Fig. 20A (a)	Grallator	Jurassic	Jurassic, Early	Theropoda	3.476	2.796
Olsen, 1980	Fig. 20A (d)	Grallator	Jurassic	Jurassic, Early	Theropoda	16.385	12.573
Olsen, 1980	Fig. 20A (g)	Grallator	Jurassic	Jurassic, Early	Theropoda	31.968	22.17
Olsen, 1980	Fig. 20B (lowest)	Anomoepus	Jurassic	Jurassic, Early	Ornithischia	16.442	10.16
Olsen and Galton, 1984	Fig. 3I (c)	Grallator	Triassic	Triassic, Late	Theropoda	32.345	22.342
Olsen and Galton, 1984	Fig. 3I (e)	Grallator	Triassic	Triassic, Late	Theropoda	48.281	36.516
Olsen and Galton, 1984	Fig. 4B (e)	Anchisauripus	Jurassic	Jurassic, Early	Theropoda	38.932	27.474
Olsen et al., 1998	Fig. 5A	Eubrontes	Jurassic	Jurassic, Early	Theropoda	47.543	35.072
Olsen and Rainforth, 2003	Fig. 19.11 B (second track)	Anomoepus	Jurassic	Jurassic, Early	Ornithischia	11.181	7.422
Olsen and Rainforth, 2003	Fig. 19.20 B (second pes)	Anomoepus	Jurassic	Jurassic, Early	Ornithischia	7.235	4.894
Olsen and Rainforth, 2003	Fig. 19.24 B (third pes)	Anomoepus	Jurassic	Jurassic, Early	Ornithischia	12.806	8.545
Olsen and Rainforth, 2003	Fig. 19.29 B (second pes)	Apatichnus	Jurassic	Jurassic, Early	Ornithischia	22.867	13.517
Olsen and Rainforth, 2003	Fig. 19.23 D	Anomoepus	Jurassic	Jurassic, Early	Ornithischia	15.732	10.82
Pascual-Arribas et al., 2009	Fig. 4 (left, second track)	Iguanodontipus	Cretaceous	Cretaceous, Early	Ornithischia	54.837	29.819
Pascual-Arribas et al., 2009	Fig. 4 (middle, first track)	Iguanodontipus	Cretaceous	Cretaceous, Early	Ornithischia	59.021	29.22
Pascual-Arribas et al., 2009	Fig. 4 (right, third track)	Iguanodontipus	Cretaceous	Cretaceous, Early	Ornithischia	67.002	35.152
Pittman, 1989	Fig. 15.8 A	NA	Cretaceous	Cretaceous, Early	Theropoda	75.287	51.389
Pittman, 1989	Fig. 15.8 J	NA	Cretaceous	Cretaceous, Early	Theropoda	71.465	48.024
Pittman, 1989	Fig. 15.8 F	NA	Cretaceous	Cretaceous, Early	Theropoda	57.664	38.091
Raath, 1972	Fig. 1B	NA	NA	NA	Theropoda	13.616	8.28
Rainforth and Lockley, 1996	Fig. 1A	Eubrontes	NA	NA	Theropoda	42.209	28.544
Razzolini et al., 2017	Fig. 4A	Megalosauripus	Jurassic	Jurassic, Late	Theropoda	46.201	30.808
Razzolini et al., 2017	Fig. 4F	Megalosauripus	Jurassic	Jurassic, Late	Theropoda	51.324	36.425
Razzolini et al., 2017	Fig. 4G	Megalosauripus	Jurassic	Jurassic, Late	Theropoda	51.403	35.974
Razzolini et al., 2017	Fig. 4B	Megalosauripus	Jurassic	Jurassic, Late	Theropoda	56.103	40.422
Razzolini et al., 2017	Fig. 4C	Megalosauripus	Jurassic	Jurassic, Late	Theropoda	45.83	31.299
Razzolini et al., 2017	Fig. 4N	Megalosauripus	Jurassic	Jurassic, Late	Theropoda	52.838	35.643
Rodríguez-de la Rosa et al., 2012	Fig. 7B	NA	Cretaceous	Cretaceous, Early	Ornithischia	47.779	27.489
Salisbury et al., 2017	Fig. 19G	Megalosauropus	Cretaceous	Cretaceous, Early	Theropoda	43.842	30.725
Salisbury et al., 2017	Fig. 21C	Yangtzepus	Cretaceous	Cretaceous, Early	Theropoda	41.457	30.001
Salisbury et al., 2017	Fig. 37C	Wintonopus	Cretaceous	Cretaceous, Early	Ornithischia	25.726	12.112
Salisbury et al., 2017	Fig. 39C	Wintonopus	Cretaceous	Cretaceous, Early	Ornithischia	31.819	15.718
Salisbury et al., 2017	Fig. 42C	Walmadanyichnus	Cretaceous	Cretaceous, Early	Ornithischia	97.477	51.46
Salisbury et al., 2017	Fig. 43F	Walmadanyichnus	Cretaceous	Cretaceous, Early	Ornithischia	70.83	41.457
Santos et al., 2013	Fig. 6A (fourth track)	NA	Cretaceous	Cretaceous, Early	Ornithischia	71.815	40.694
Shounan et al., 1989	Fig. 19.3 D	Changpeipus	Jurassic	NA	Theropoda	39.474	28.383
Shounan et al., 1989	Fig. 19.3 F	Youngichnus	Jurassic	Jurassic, Early	Theropoda	38.768	27.171
Thulborn, 1994	Fig. 4A	Anomoepus	Jurassic	Jurassic, Early	Ornithischia	10.806	6.554

Reference	Figure	Ichnogenus	Period	Epoch	Group	Centroid Size	FL (cm)
Wagensommer et al., 2012	Fig. 6H	Kayentapus	Jurassic	Jurassic, Middle	Theropoda	56.702	38.8
Wagensommer et al., 2012	Fig. 6S	Kayentapus	Jurassic	Jurassic, Middle	Theropoda	54.282	31.6
Wagensommer et al., 2016	Fig. 7a	Kayentapus	Jurassic	Jurassic, Early	Theropoda	39.16	26.88
Wagensommer et al., 2016	Fig. 12d	Eubrontes	Jurassic	Jurassic, Early	Theropoda	40.653	29.779
Wang et al., 2016	Fig. 8	Pengxianpus	Jurassic	Jurassic, Early	Theropoda	35.705	24.073
Weems, 2006	Fig. 4	Kayentapus	Triassic	Triassic, Late	Theropoda	40.652	27.588
Weems, 2006	Fig. 4	Eubrontes	Triassic	Triassic, Late	Theropoda	61.893	40.548
Xing et al., 2011	Fig. 9.G	NA	Cretaceous	Cretaceous, Early	Theropoda	17.133	12.896
Xing et al., 2011	Fig 10C	NA	Cretaceous	Cretaceous, Early	Theropoda	25.638	19.159
Xing et al., 2011	Fig 10D	NA	Cretaceous	Cretaceous, Early	Theropoda	19.181	14.461
Xing et al., 2011	Fig 9E	Kayentapus	Cretaceous	Cretaceous, Early	Theropoda	20.581	12.639
Xing et al., 2011	Fig 9F	Asianopodus	Cretaceous	Cretaceous, Early	Theropoda	41.051	28.13
Xing et al., 2013b	Fig. 4, V1394-1	Chongqingpus	Jurassic	Jurassic, Late	Theropoda	38.629	25.984
Xing et al., 2013b	Fig. 6. C	Chongqingpus	Jurassic	Jurassic, Late	Theropoda	37.628	26.819
Xing et al., 2013b	Fig. 8 JJ4	NA	Jurassic	Jurassic, Late	Theropoda	36.196	24.615
Xing et al., 2013a	Fig. 4. B	Pengxianpus	Triassic	Triassic, Late	Theropoda	51.036	30.481
Xing et al., 2014c	Fig. 4b	NA	NA	NA	Theropoda	24.825	16.35
Xing et al., 2014c	Fig. 7d	NA	NA	NA	Ornithischia	21.907	12.284
Xing et al., 2014i	Fig. 4B	Eubrontes	Jurassic	Jurassic, Early	Theropoda	59.181	39.303
Xing et al., 2014g	Fig. 6. A	Caririchnium	Cretaceous	Cretaceous, Early	Ornithischia	48.649	29.443
Xing et al., 2014g	Fig. 6 C lower track	Caririchnium	Cretaceous	Cretaceous, Early	Ornithischia	43.524	26.308
Xing et al., 2014g	Fig. 9. ZJIIN-T1-L2	NA	Cretaceous	Cretaceous, Early	Theropoda	35.822	24.089
Xing et al., 2014a	Fig. 9 B (SSIB59)	Changpeipus	Jurassic	Jurassic, Middle	Theropoda	46.755	33.153
Xing et al., 2014a	Fig. 12E (ZLJ-ZQK2)	Changpeipus	Jurassic	Jurassic, Early	Theropoda	37.94	25.512
Xing et al., 2014d	Fig. 5 (XYT1)	Jialingpus	Cretaceous	Cretaceous, Early	Theropoda	15.854	10.702
Xing et al., 2014d	Fig. 5 (XYT2)	Jialingpus	Cretaceous	Cretaceous, Early	Theropoda	13.735	9.297
Xing et al., 2014d	Fig. 5 (DJP4)	Jialingpus	Cretaceous	Cretaceous, Early	Theropoda	20.689	15.166
Xing et al., 2014d	Fig. 7 (XYT7)	Jialingpus	Cretaceous	Cretaceous, Early	Theropoda	20.958	14.814
Xing et al., 2014d	Fig. 8 (IVPP DT2)	Jialingpus	Jurassic	Jurassic, Late	Theropoda	25.481	19.071
Xing et al., 2014d	Fig. 8 (IVPP DT1)	Jialingpus	Jurassic	Jurassic, Late	Theropoda	19.368	14.499
Xing et al., 2014d	Fig. 8 (CU 199-36)	Jialingpus	Jurassic	Jurassic, Late	Theropoda	11.266	8.65
Xing et al., 2014h	Fig. 5 A	NA	Jurassic	Jurassic, Early	Theropoda	13.329	9.882
Xing et al., 2014f	Fig. 6 F	Paracorpulentapus	Cretaceous	Cretaceous, Late	Theropoda	28.631	15.985
Xing et al., 2014f	Fig. 6 D	NA	Cretaceous	Cretaceous, Late	Theropoda	24.343	16.775
Xing et al., 2014b	Fig. 2	NA	Cretaceous	Cretaceous, Early	Theropoda	17.207	11.439
Xing et al., 2014b	Fig. 3 B	NA	Jurassic	Jurassic, Early	Theropoda	16.015	9.849
Xing and Lockley, 2014	Fig. 7	Ornithopodichnus	Cretaceous	Cretaceous, Early	Ornithischia	25.164	12.599
Xing et al., 2015c	Fig. 5B	NA	Cretaceous	Cretaceous, Early	Theropoda	37.77	25.525
Xing et al., 2015a	Fig. 6 (upper left)	Caririchnium	Cretaceous	Cretaceous, Early	Ornithischia	56.59	33.775
Xing et al., 2015a	Fig. 6 (upper middle)	Caririchnium	Cretaceous	Cretaceous, Early	Ornithischia	34.804	18.578
Xing et al., 2015a	Fig. 6 (middle, left)	Caririchnium	Cretaceous	Cretaceous, Early	Ornithischia	63.814	38.64
Xing et al., 2015a	Fig. 6 (upper right)	Caririchnium	Cretaceous	Cretaceous, Early	Ornithischia	77.264	42.614
Xing et al., 2015d	Fig. 7B	Caririchnium	Cretaceous	Cretaceous, Early	Ornithischia	35.258	21.194
Xing et al., 2015b	Fig. 5 HI3	NA	Jurassic	Jurassic, Middle	Theropoda	53.682	33.997
Xing et al., 2015b	Fig. 7B (bottom)	Anomoepus	Jurassic	Jurassic, Middle	Ornithischia	14.22	7.546
Xing et al., 2016d	Fig. 3 B (O9-L1)	Caririchnium	Cretaceous	Cretaceous, Early	Ornithischia	52.185	28.24
Xing et al., 2016c	Fig. 6 (left)	Shenmuichnus	Jurassic	Jurassic, Early	Ornithischia	36.461	19.076
Xing et al., 2016c	Fig. 6 (right)	Shenmuichnus	Jurassic	Jurassic, Early	Ornithischia	36.31	18.587
Xing et al., 2016c	Fig. 7 (right, center)	Changpeipus	Jurassic	Jurassic, Early	Theropoda	53.192	33.815
Xing et al., 2016a	Fig. 2c	Anomoepus	Jurassic	Jurassic, Early	Ornithischia	9.532	5.529
Xing et al., 2017a	Fig. 4C	Anomoepus	Jurassic	Jurassic, Early	Ornithischia	10.706	4.329
Xing et al., 2017a	Fig. 5C	Anomoepus	Jurassic	Jurassic, Early	Ornithischia	15.995	8.18
Xing et al., 2016e	Fig. 3 (first track)	Anomoepus	Jurassic	Jurassic, Middle	Ornithischia	14.406	9.672
Xing et al., 2016b	Fig. 6B	Anomoepus	Jurassic	Jurassic, Early	Ornithischia	19.82	10.027
Xing et al., 2016b	Fig. 7 (O2-R1)	Anomoepus	Jurassic	Jurassic, Early	Ornithischia	17.492	9.599
Xing et al., 2016f	Fig. 3B (YMZ-T11-L2)	Minisauripus	Cretaceous	Cretaceous, Early	Theropoda	3.995	2.642
Xing et al., 2016f	Fig. 3B (YMZ-T13-R1)	Minisauripus	Cretaceous	Cretaceous, Early	Theropoda	3.887	2.651
Xing et al., 2016f	Fig. 5B (bottom)	NA	Cretaceous	Cretaceous, Early	Theropoda	24.423	17.766
Xing et al., 2017b	Fig. 6F	NA	Cretaceous	Cretaceous, Late	Ornithischia	103.892	51.518
Xing et al., 2017b	Fig. 7B (second track)	NA	Cretaceous	Cretaceous, Late	Ornithischia	35.177	19.582
Zhen et al., 1986	Fig. 5	Schizograllator	Jurassic	Jurassic, Early	Theropoda	44.372	27.214

Supplementary Material S2: Correlation coefficients and p-values

(for abbreviations see Table 4 in main text)

Complete Sample (n=303)

	R-Pearson	p-Pearson	R-Spearman	p-Spearman	R-Pearson (Residuals)	p-Pearson (Residuals)	R-Spearman (Residuals)	p-Spearman (Residuals)
FW	0.3604	0	0.3249	0	-	-		
FL	-0.3559	0	-0.3481	0	-	-		
Length-to-width ratio	-0.3936	0	-0.345	0	-	-		
D3Proj (measured from digit axes)	-0.3641	0	-0.4006	0	-	-		
D3Proj (measured from clawtips)	-0.4117	0	-0.4711	0	-	-		
D3W	0.2207	0.0001	0.2093	0.0003	-	-		
D2W	0.2756	0	0.2865	0	-	-		
D4W	0.2288	0.0001	0.2533	0	-	-		
D2D4W	0.2707	0	0.2913	0	-	-		
DWR	-0.0552	0.3381	-0.0663	0.2494	-	-		
IDA (III-IV)	0.0375	0.516	0.0148	0.798	-	-	-	
IDA (II-III)	-0.015	0.7946	-0.0258	0.6539	-	-	-	
IDA (total)	0.0144	0.803	-0.0092	0.8727	-	-	-	
AsymLOD	0.1209	0.0354	0.0538	0.3506	-	-	-	
AsymDIV	0.055	0.3399	0.0405	0.482	-	-	-	
D3Proj-vs-FW	-0.717	0	-0.6877	0	-0.5683	0	-0.5308	0
D3Proj-vs-LtW	0.6242	0	0.5873	0	0.404	0	0.3521	0
D3Proj-vs-D2D4W	-0.5792	0	-0.5673	0	-0.4106	0	-0.3746	0
D3Proj-vs-D3W	-0.4228	0	-0.3781	0	-0.28	0	-0.2422	0
D3Proj-vs-DWR	0.2229	0.0001	0.2295	0.0001	0.1217	0.0348	0.1287	0.0256
IDA-vs-DWR	-0.2744	0	-0.2656	0	-0.2593	0	-0.2522	0
D3Proj-vs-IDA	0.1789	0.0018	0.1524	0.0079	0.3314	0	0.2975	0
FL-vs-IDA	-0.5148	0	-0.5054	0	-0.5674	0	-0.5736	0
D2D4W-vs-IDA	-0.1619	0.0047	-0.1267	0.0275	-0.2202	0.0001	-0.1719	0.0028
D3W-vs-IDA	-0.3802	0	-0.3196	0	-0.4394	0	-0.3863	0
FW-vs-D2D4W	0.4736	0	0.4747	0	0.2875	0	0.2792	0
FW-vs-D3W	0.2025	0.0004	0.2048	0.0003	-0.004	0.9455	-0.0074	0.8982
AsymLOD-vs-AsymDiv	0.5548	0	0.5525	0	0.5436	0	0.538	0

Theropod Sample (n=193)

	R-Pearson	p-Pearson	R-Spearman	p-Spearman	R-Pearson (Residuals)	p-Pearson (Residuals)	R-Spearman (Residuals)	p-Spearman (Residuals)
FW	0.4224	0	0.4014	0	-	-	-	
FL	-0.4068	0	-0.4211	0	-	-	-	
Length-to-width ratio	-0.4542	0	-0.4226	0	-	-	-	
D3Proj (measured from digit axes)	-0.3266	0	-0.3676	0	-	-	-	
D3Proj (measured from clawtips)	-0.3506	0	-0.4372	0	-	-	-	
D3W	-0.0331	0.6476	-0.0618	0.3932	-	-	-	
D2W	0.0443	0.5411	0.0907	0.2094	-	-	-	
D4W	-0.1162	0.1075	-0.0072	0.9204	-	-	-	
D2D4W	-0.0368	0.6111	0.0488	0.5001	-	-	-	
DWR	-0.0119	0.8691	-0.055	0.4475	-	-	-	
IDA (III-IV)	0.2832	0.0001	0.2509	0.0004	-	-	-	
IDA (II-III)	0.1021	0.1578	0.0936	0.1952	-	-	-	
IDA (total)	0.2258	0.0016	0.1823	0.0112	-	-	-	
AsymLOD	0.2143	0.0028	0.1281	0.0759	-	-	-	
AsymDIV	0.167	0.0203	0.1739	0.0157	-	-	-	
D3Proj-vs-FW	-0.6693	0	-0.6329	0	-0.622	0	-0.5948	0
D3Proj-vs-LtW	0.5607	0	0.4891	0	0.4914	0	0.4529	0
D3Proj-vs-D2D4W	-0.3575	0	-0.3498	0	-0.3927	0	-0.3657	0
D3Proj-vs-D3W	-0.1409	0.0506	-0.1042	0.1492	-0.1612	0.0251	-0.1251	0.0831
D3Proj-vs-DWR	0.2028	0.0047	0.2388	0.0008	0.2074	0.0038	0.2511	0.0004
IDA-vs-DWR	-0.1941	0.0068	-0.175	0.015	-0.1957	0.0064	-0.1607	0.0257
D3Proj-vs-IDA	0.0895	0.2159	0.0911	0.2076	0.1747	0.0151	0.1462	0.0426
FL-vs-IDA	-0.7077	0	-0.6849	0	-0.6922	0	-0.6736	0
D2D4W-vs-IDA	-0.2044	0.0044	-0.1277	0.0767	-0.2003	0.0052	-0.1426	0.0479
D3W-vs-IDA	-0.3521	0	-0.2947	0	-0.3535	0	-0.2921	0
FW-vs-D2D4W	0.2265	0.0015	0.2325	0.0012	0.2688	0.0002	0.2533	0.0004
FW-vs-D3W	-0.0657	0.3639	-0.0932	0.197	-0.0561	0.4385	-0.0813	0.2609
AsymLOD-vs-AsymDiv	0.5318	0	0.5441	0	0.5151	0	0.5167	0

Ornithischian Sample (n=108)

	R-Pearson	p-Pearson	R-Spearman	p-Spearman	R-Pearson (Residuals)	p-Pearson (Residuals)	R-Spearman (Residuals)	p-Spearman (Residuals)
FW	0.2546	0.0078	0.1857	0.0545	-	-	-	
FL	-0.3294	0.0005	-0.2701	0.0048	-	-	-	
Length-to-width ratio	-0.3447	0.0003	-0.2567	0.0075	-	-	-	
D3Proj (measured from digit axes)	-0.43	0	-0.4675	0	-	-	-	
D3Proj (measured from clawtips)	-0.5431	0	-0.5993	0	-	-	-	
D3W	0.5435	0	0.5585	0	-	-	-	
D2W	0.5913	0	0.5803	0	-	-	-	
D4W	0.601	0	0.5722	0	-	-	-	
D2D4W	0.6369	0	0.6167	0	-	-	-	
DWR	-0.0898	0.3552	-0.0476	0.6244	-	-	-	
IDA (III-IV)	-0.2773	0.0037	-0.3108	0.0011	-	-	-	
IDA (II-III)	-0.2258	0.0188	-0.2321	0.0158	-	-	-	
IDA (total)	-0.2855	0.0027	-0.2901	0.0024	-	-	-	
AsymLOD	-0.0616	0.5267	-0.0882	0.3637	-	-	-	
AsymDIV	-0.108	0.266	-0.1796	0.0631	-	-	-	
D3Proj-vs-FW	-0.5077	0	-0.4828	0	-0.4556	0	-0.392	0
D3Proj-vs-LtW	0.3011	0.0015	0.3045	0.0014	0.1792	0.0635	0.1428	0.1402
D3Proj-vs-D2D4W	-0.5817	0	-0.5536	0	-0.4422	0	-0.3936	0
D3Proj-vs-D3W	-0.5858	0	-0.5833	0	-0.4638	0	-0.4309	0
D3Proj-vs-DWR	-0.046	0.6364	-0.0698	0.472	-0.0939	0.3339	-0.1153	0.2343
IDA-vs-DWR	-0.3765	0.0001	-0.3475	0.0002	-0.4215	0	-0.4021	0
D3Proj-vs-IDA	0.5823	0	0.5823	0	0.5305	0	0.5338	0
FL-vs-IDA	-0.3234	0.0006	-0.2657	0.0056	-0.4594	0	-0.4317	0
D2D4W-vs-IDA	-0.3613	0.0001	-0.321	0.0007	-0.2429	0.0113	-0.2234	0.0203
D3W-vs-IDA	-0.5814	0	-0.5501	0	-0.5302	0	-0.5024	0
FW-vs-D2D4W	0.4352	0	0.4294	0	0.3662	0.0001	0.3569	0.0002
FW-vs-D3W	0.2311	0.0161	0.2757	0.004	0.1148	0.2367	0.1418	0.1431
AsymLOD-vs-AsymDiv	0.5911	0	0.5752	0	0.5882	0	0.5883	0

Chapter 4

unpublished.

Lallensack, J.N., unpubl. Automatic generation of objective footprint outlines. Doctoral thesis 2018 (chapter 4). Bonn, Germany. **p. 105–114.**

Supplementary Material:

- Supplementary Material S1: oboutline function (R-script). **p. 115–125.**
- Supplementary Material S2: 3D models of footprints used as examples (available from DVD only)

Automatic generation of objective footprint outlines

Jens N. Lallensack[1]

[1] Division of Paleontology, Steinmann Institute, University of Bonn, Bonn, Germany

ABSTRACT

The objective definition of footprint margins poses a central problem in ichnology. The transition from the footprint to the surrounding sediment is often continuous, and the footprint wall complex, requiring interpolation, approximation, and a priori assumptions about trackmaker anatomy to arrive at feasible interpretations of footprint shapes. The degree of subjectivity introduced in such interpretations is substantial, and outlines produced by separate researchers can differ greatly. As a consequence, statistical shape analysis, regardless if based on linear and angular measurements or on the shape as a whole, are neither fully repeatable nor objective.

Here I present an algorithm implemented in the programming environment R that is able to generate continuous footprint outlines based on three-dimensional models—fully automatically, objectively, and repeatable. The approach, which is based on contour lines extracted from the model, traces the outline at the point where the slope of the track wall is maximized. The resulting outlines tend to correspond with human-made interpretative drawings regarding the overall shape, although faint anatomical details such as claw impressions are often not recorded. While not suited as a full replacement of interpretative drawings in many cases, computed outlines can form the objective basis for such interpretations, and open possibilities for fully objective analyses of footprint shapes.

INTRODUCTION

Fossil footprints are an important supplement to the body fossil record, given their abundance and their nature as life traces that directly record behavior and locomotion. Yet, the potential of analyses combining footprint and body fossil data is not yet exhausted, partly due to the slow advancement of objective and quantitative methodology in ichnology. A central problem in applying such methods to track data is the inability to objectively define the margins of a footprint, especially when the footprint indistinctly grades into the surrounding sediment. Falkingham (2016) showed that the length of a footprint can vary as much as 27% depending on the height level chosen for measurement. Various criteria for the identification of the footprint margin have been proposed, including the point of inflexion of the footprint wall, the minimum outline, and the selection of a single contour line, amongst others (Falkingham 2016). However, none of these criteria is feasibly applicable to a wider range of different footprints, which typically show multiple inflexion points and often do not show distinct minimum outlines (Falkingham 2016; Lallensack et al. 2016). Adding to the problem, the vast majority of ichnological publications does not specify the criteria

used for defining the footprint margins. The inability to define footprint margins objectively is highly problematic especially when objective quantitative methods are to be applied to analyze footprint shape, since such analyses can only generate fully objective results when based on objective data (Falkingham 2016).

The problem persists when not only linear and angular measurements but a complete outline representing the shape of the footprint is to be extracted. The outlines of one and the same footprint, when drawn by separate researchers, can differ considerably from each other (Thulborn 1990), repeatedly leading to calls for caution in interpreting such data (e.g., Sarjeant 1975; Thulborn 1990; Falkingham 2010, 2016). Furthermore, their high degree of simplification has been criticized, proposing that instead the full three-dimensional profile should be taken into account (e.g., Ishigaki and Fujisaki 1989; Belvedere et al. 2018). Nevertheless, outline drawings remain the most widely used means for distributing footprint shape data, also because most anatomical information of the footprint is contained in its outline.

Recent efforts to increase objectivity in footprint research rely on 3D-digitization techniques, most importantly photogrammetry, which allow for the fast and cost-effective capturing of footprint morphologies in high resolution (e.g., Falkingham 2012; Mallison and Wings 2014; Matthews et al. 2016). A relatively new set of methods, these techniques promise to solve critical problems of collection and dissemination of footprint data, and have been widely accepted as best practice in the documentation of fossil footprints (Falkingham et al. 2018). Thus, the availability of such models can be expected to increase greatly in the future.

Although a number of methods for the analysis of 3D footprint data exist, none can effectively solve or circumvent the problem of the definition of footprint margins. 3D geometric morphometric approaches in principle allow for the analysis of the entire 3D morphology, but will include both the footprint and the surrounding sediment unless the footprint margin has been defined a priori. Furthermore, capturing of the full internal footprint morphology adds significant noise, as the footprint interior tends to be affected by differing substrate properties more strongly than the footprint outline. Three-dimensional mean shapes based on two or more tracks can reduce variability unrelated to the anatomy of the trackmaker (Bennett et al. 2016; Belvedere et al. 2018). However, the registration of the separate footprints still requires user-defined landmarks that often cannot be placed unequivocally, especially when a footprint is not well defined. Furthermore, 3D mean shapes are feasible only when foot posture, most importantly the interdigital angles, is constant, as otherwise regions of the footprint may get averaged with surrounding sediment.

The algorithm presented herein allows for the fully objective and automatic generation of continuous outlines based on 3D surface models of footprints. The method relies on the steepness of the footprint slope, the probably most commonly used criterium for the definition of footprint margins (Ishigaki and Fujisaki 1989).

METHODS

The presented approach was implemented in the free programming environment R, which was designed for statistical computing, thus representing the ideal solution for the present problem. Many required functions have been already implemented in the wealth of packages available for R; these were used whenever possible, reducing the script to approximately 650 lines of code. The implemented R function, named

"oboutline", will perform the import of the 3D model, calculation of the outline, and export of graphics automatically in a single step, without requiring human input.

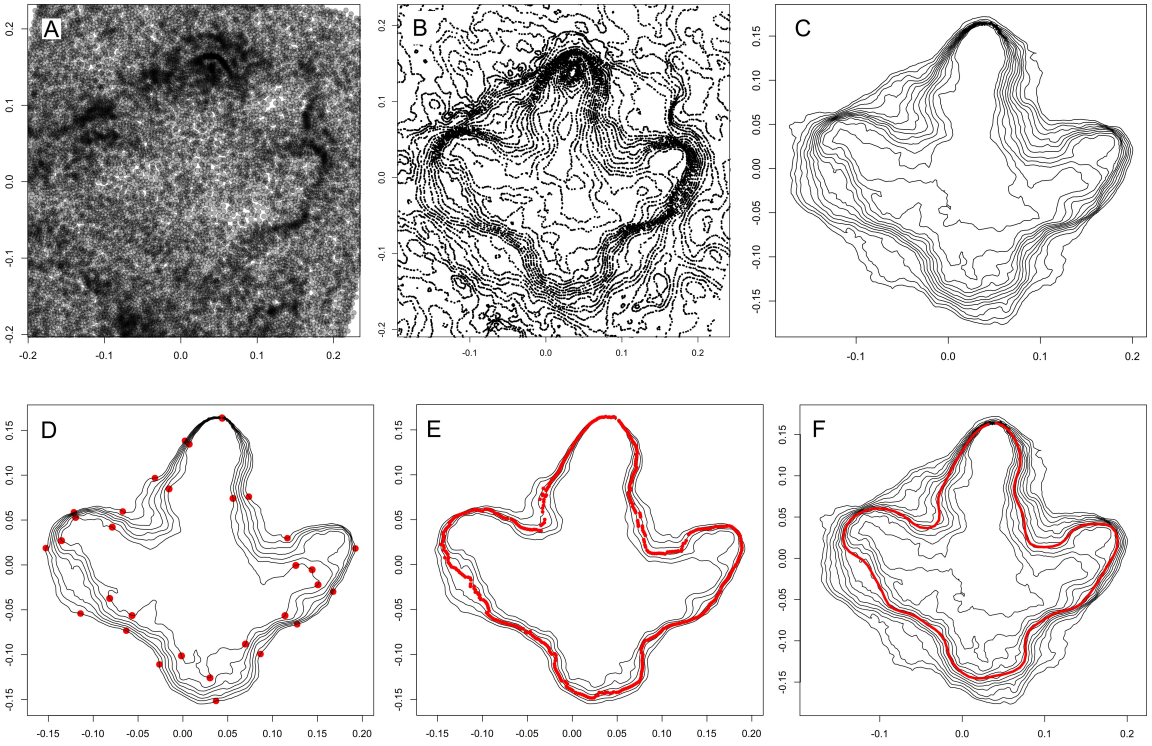

Fig. 1: Procedure of calculating objective outlines of footprints from 3D models, using ornithopod footprint I1-31 from the Lower Cretaceous of Münchehagen, Germany (Lallensack et al. 2016) as example. All six steps are carried out automatically. Axes scales are in meters, and all plots are in z-direction (top view). Plots can be reproduced using the script and the 3D-model provided in Supp. 1 and 2. **A.** The xyz point cloud is extracted from the submitted PLY mesh, and subjected to principal component analysis (PCA) for fitting to the horizontal plane. **B.** Contour lines for 30 height levels are extracted based on the point cloud (xyz-coordinates of contours are shown). **C.** Incomplete and short contours are removed. **D.** Further contours are removed based on Procrustes distances (i.e., shape similarities). In order to establish correspondence between points of separate outlines, bottleneck points are determined along the outlines (red points). Sections in-between bottleneck points are resampled to equal numbers of equidistant points for each contour, so that each point of a contour has homologous counterparts on the other contours. **E.** The location of the steepest slope is computed for each set of homologous points. Multiple slopes are taken into account by taking weighted means of the coordinates. **F.** Elliptical Fourier transforms are used to fit an approximating curve to the succession of points, providing a smooth, continuous outline.

Model import, orientation, and contour line generation

Import of 3D-models is achieved using the vcgImport function of the Rvcg package, which supports commonly used formats including the PLY format. The supplied 3D-model should contain only a single complete footprint as well as a margin of surrounding surface. The exact extent of the surrounding margin will

not alter results except when an increased margin size includes additional large-scale continuous contours that enclose the footprint. The orientation of the supplied 3D-model in the xyz-plane may be arbitrary, as it will be automatically fitted to the horizontal plane of the mesh and rotated.

After import, xyz-coordinates of the vertex points of the mesh will be extracted. In order to fit the extracted point cloud to the horizontal plane (i.e., the tracking surface on which the animal walked), principal component analysis (PCA) is performed on the coordinates using the prcomp function of the "stats" R package (Fig. 1A). PCA on three variables (x,y,z) will detect three orthogonal axes along which variation is maximized; PC1 is defined as the axis with the greatest variation, followed by PC2 and PC3. In most situations, PC1 and PC2 will therefore represent the horizontal plane, and PC3 the relief (i.e., the deviation from the horizontal plane). Problematically, the point cloud can get mirror-inverted during PCA fitting as the signs of the columns of the rotation matrix are arbitrary, a problem also occurring in respective implementations in 3D-mesh software like Meshlab (tested with version v2016.12) or CloudCompare (tested with version 2.9). As a workaround, the present function calculates the Procrustes distance (a measure of shape difference) of a subset of points of the model before and after the PCA fit. If Procrustes distances are unequal zero, the point cloud is assumed to have been mirrored, and will be mirrored back by inverting the sign of the x variable. Procrustes distances are calculated using the "procdist" function of the shapes R package.

All subsequent computations are based on a set of 30 equally spaced contour lines extracted using the "getContourLines" function of the contoureR R package (Fig. 1B). Contour lines reduce the complex three-dimensional problem to a simpler and easier-to-handle two-dimensional one, and form the natural basis for 2D footprint outlines. Before the objective outline can be extracted, a number of additional steps are required, including 1) the removal of contours not representative for the footprint wall and 2) the establishment of homology between the points of separate contours.

Contours not representative for the footprint wall are excluded based on simple criteria. First, all open contours are removed, eliminating structures that continue beyond the margins of the model. Second, only the longest contour of each height level is selected and kept, respectively, with all others removed. This results in a stack of continuous contours, with one contour per height level. Third, all contours less than 50% of the length of the longest contour are removed, while assuring that no gaps within the stack are being created. This approach eliminates smaller structures within the footprint that are unlikely to contain relevant information on the footprint wall (Fig. 1C). Fourth, all contours external to the contour stack are removed. The resulting stack of contours may still include a number of contours that convey little or no information on the footprint wall, including roundish contours around the actual footprint. To eliminate these contours as well, a more complex approach is employed involving the homologization of contours (as described below) and calculation of Procrustes distances to quantify the shape differences between individual contours. Starting from the middle contour of the stack, the Procrustes distances of each contour with its next lowest (or highest) neighbor are compared; if the Procrustes distance between two contours exceeds a pre-defined threshold-value, the upper (or lower) of this contour and all following contours are removed (Fig. 1D).

Homologization of contours

Even if the starting point would correspond between all contours and if each contour would contain the same number of equidistant points (requirements not fulfilled a priori), the individual points of the separate contours would tend to deviate from each other when far from the starting point, as the shapes of the contours are not identical. Because of this reason, when producing a simple mean shape, points will be averaged oblique rather than perpendicular to the footprint wall, leading to erroneous results. The implemented solution detects a number of "bottlenecks"—pairs of points with minimum distance between the inner and outer contour. Points forming the bottleneck will be considered homologous (define a line that is assumed to be perpendicular to the footprint wall), and the points in-between the bottlenecks will be interpolated by resampling.

First, all contours are resampled to the same number of equidistant points, which is achieved using the "sp-sample" function provided by the sp R package. Per default, a number of n=500 points per contour is used. The resulting resampled contours can be variously oriented clockwise or counter-clockwise. To assure uniform clockwise orientation, the orientation is tested at four points sampled around the outline, while checking if following and preceding points continue in the expected direction. If a counter-clockwise orientation is detected, the respective contour is reversed using the "rev" function of the base R package.

Second, Euclidean distances between all possible pairs of the inner and outer contour of the stack are calculated and stored in a matrix with the dimensions n x n. The pair with the minimum distance, the first bottleneck, is then extracted, and those points of the intermediate contours are detected that are closest to a line defined by the bottleneck points. The resulting set of homologous points is then defined as the starting point of the contours.

Third, additional bottlenecks are detected to establish homology. The implemented algorithm first detects a second bottleneck on the side of the footprint opposite to the first bottleneck; two additional bottlenecks are then found on each side between the first and second bottleneck. More bottlenecks are detected within the intermediate sections if the latter are long enough. In all cases, bottlenecks in proximity to existing bottlenecks are prevented, assuring a roughly equal distribution of bottlenecks along the outline (Fig. 1D). Finally, the individual sections between the bottlenecks are resampled to equal numbers of equidistant points, which can now be considered homologous.

Tracing of the steepest slope and rotation to an upright position

The objective outline will be traced along the steepest slope of the track wall. For each point within each set of homologous points, the minimum distance between the neighboring contours is measured. A set of homologous points is not always fully perpendicular to the footprint wall, especially when the section between the bottleneck points is long and contours differ substantially in shape. For this reason, the algorithm does not simply compute the distances within the set of homologous points, but the distances between each of the homologous points and all nearby points within and outside of the set. The steepest slope computed this way is seldom continuous along the whole outline, but rather tends to fade out and continue on a different height level, frequently leading to abrupt steps in the outline that are obviously incompatible with human interpretations. For this reason, the algorithm does not only detect the steepest point, but takes into account the steepness of all other points. The final coordinate of the steepest slope is

then computed as the weighted arithmetic mean of all of these points. Points will receive equal weight only when the steepness is equal; the lower the steepness compared to the steepest slope, the less weight is given.

Last but not least, an approximating function is applied to the resulting set of points, producing a continuous and smooth final outline. Of various tested options, including B-splines and Bézier curves, elliptic Fourier transforms were found to produce results most similar to those expected from a human interpreter (Fig. 1F, 2). Elliptic Fourier transforms are performed using the "efourier" function of the R package Momocs using 25 harmonics and 10 smoothing iterations.

As the resulting objective outline and contour stack will be rotated arbitrarily, an algorithm is implemented that rotates both outline and stack into an upright orientation. In a first step, the circular mean of the angles between all points of the objective outline is computed, and the shape rotated by this mean angle. In elongated shapes, the resulting mean orientation can be assumed to approximate the orientation of the long axis of the shape. In footprints that are not elongated, the points describing the digital impressions tend to be angled roughly parallel to the respective digital long axes. Provided that the digital impressions are sufficiently defined and reflect the orientation of the foot, the shape will be correctly rotated even when it is somewhat broader than long. For tridactyl footprints, this approach is only precise if the digital impressions are symmetrical; unequal digit lengths or interdigital angles will result in slightly oblique orientations (Fig. 2A–B). In a second step, it is determined whether the shapes have to be rotated by 180° to have the digital impressions facing upwards. To make this decision, the standard deviation is computed of Euclidean distances between the centroid coordinate and all points of the outline, both for points with y-values greater than that of the centroid and for ones with smaller y-values. The standard deviation can be expected to be higher in the half containing the digital impressions due to the curved profile of the latter, and the shape rotated accordingly. The second step is only reliable if digital impressions are sufficiently captured by the objective outline. Despite its drawbacks, the present rotation algorithm leads to acceptable results in most cases, and is generally applicable without relying on additional a priori assumptions on footprint shapes.

DISCUSSION

Comparison with human-made interpretational drawings and applications

Human-made interpretational drawings aim to capture shape and dimensions of footprints as faithfully as possible. Although slope steepness is the most important criterion, the steepest slope will frequently fade out along the footprint wall to continue at a different height level, making interpolation unavoidable. If no single distinct slope can be identified, a best-guess approach is needed, which, however, can lead to greatly differing results when performed by separate researchers, introducing a substantial degree of subjectivity. Furthermore, humans tend to apply additional criteria based on a priori assumptions about trackmaker anatomy to arrive at their interpretational drawings. Thus, extramorphological features—features unrelated to the foot anatomy of the trackmaker—can be excluded whenever feasible. At the same time, anatomical features of interest, including pad impressions and digital terminations such as claw marks, are usually emphasized in interpretational drawings even when weakly impressed.

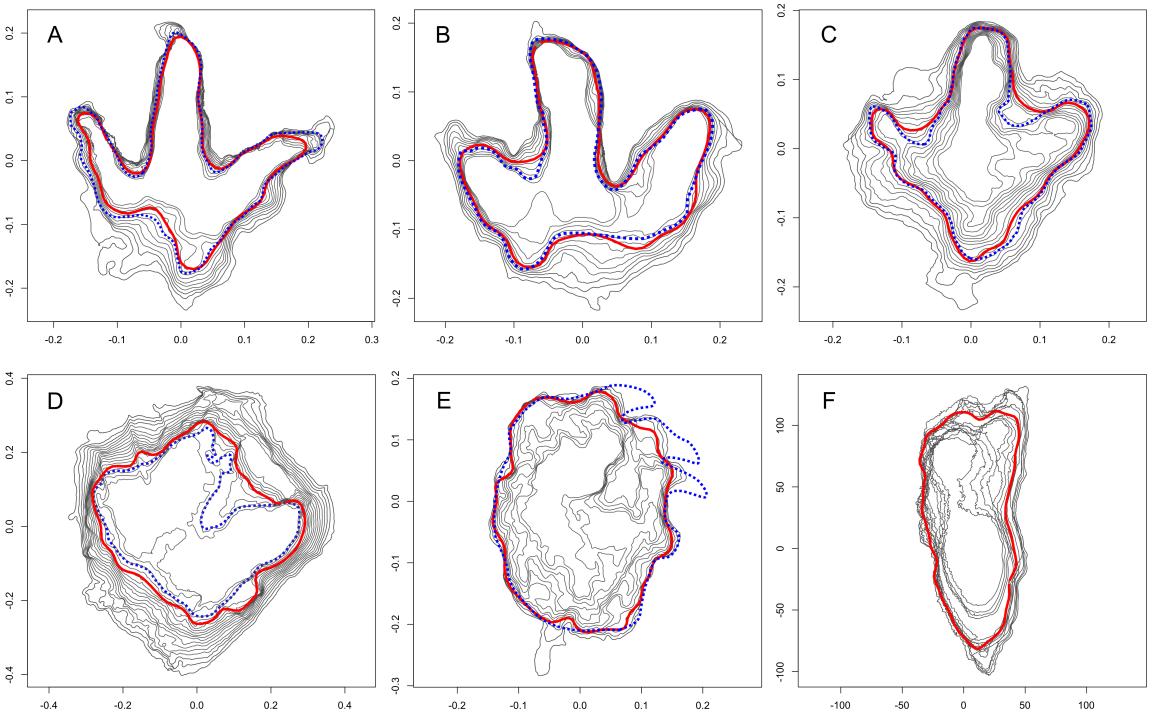

Fig. 2: Objective outlines calculated for various footprints (continuous red lines), with published interpretational drawings (dotted blue lines) for comparison (not available for F). **A–C**: Footprints of theropod trackway T3 (A: T3/47; B: T3/37) and ornithopod trackway I1 (I1/35; C) from the Lower Cretaceous Münchehagen locality, Germany (Lallensack et al. 2016). **D:** Footprint of a large tridactyl trackmaker (specimen QM F10322) from the Upper Cretaceous of Lark Quarry, Australia (Romilio and Salisbury 2014). The interpretive outline was based on a selected contour line. 3D-model provided by Anthony Romilio. **E:** Sauropod pedal footprint from the Upper Triassic of Greenland (Lallensack et al. 2017). Note that the faint impressions of the claws are not recorded by the present approach. **F.** Hominin footprint G1-33 from the Pliocene of Laetoli, Tanzania (Bennett 2013).

The present algorithm is successful in detecting and interpolating outlines even when the steepest parts of the slope are indistinct (Fig. 2). However, it does not include any a priori assumptions on trackmaker anatomy (although steps in this direction are planned for future versions, as discussed below). The exclusion of such assumptions keeps the algorithm simple and predictable, and applicable to a wide range of footprint types, and potentially even other topographic features defined by the steepest slope. On the other hand, such outlines expectedly tend to provide less information on the presumed foot anatomy than interpretative drawings.

The approach is demonstrated using six fossil footprints previously published in the literature (Fig. 2), for which 3D-models are freely available. All footprints were processed using the same script version and parameters. The first five of these examples are compared with published interpretative drawings that had been produced based on the same 3D-models. Footprints T3/47, T3/37, and I1-35 (Fig. 2A–C, respectively) come from the Lower Cretaceous of Münchehagen, Germany (Lallensack et al. 2016; Wings et al. 2016). All

three footprints were left by the right foot. T3/47 and T3/37 were part of a larger theropod and I1/35 (Fig. 2C) of an ornithopod trackway, both showing a pronounced intratrackway variability. The objective outlines (red continuous lines) are generally in accordance with published interpretational drawings (dotted blue lines). However, the sediment bars between the digital impressions tend to be less extensive than in the interpretational drawings, because the latter had been drawn not strictly according to the position of the steepest slope, but also in order to maximize the free length of digital impressions (Lallensack et al. 2016). In T3/47, digital impression IV is abbreviated in the objective outline due to sediment infilling in the distal tip of the impression, displacing the steepest slope proximally.

QM F10322 (Fig. 2D) is a replica of a latex cast made around 1977 from the right pedal impression of a large tridactyl trackway from the Upper Cretaceous of Lark Quarry in Queensland, Australia (Thulborn and Wade 1984; Romilio and Salisbury 2011, 2014). This trackway became famous after it was suggested to have been left by a large theropod causing a dinosaur stampede (Thulborn and Wade 1984), a hypothesis that has been discussed controversially in recent years (Romilio and Salisbury 2011, 2014; Romilio et al. 2013; Thulborn 2013, 2017), with the identification of the large tridactyl trackmaker constituting a major point of disagreement. This discussion is instructive in showing how much interpretative outlines can differ when produced by separate researchers with different preconceptions about the responsible trackmaker species. Well aware of this problem, Romilio and Salisbury (2014) did not produce a traditional subjective outline drawing but selected a single contour line from the 3D model they considered representative to increase objectivity. Still, this approach is not completely objective, as separate contours can differ greatly in shape and dimensions (Falkingham 2016). The single selected contour corresponds well with the fully objective contour produced using the present algorithm, except for the right interdigital sediment bar, which is faint and was thus largely omitted by the objective approach. A sauropod pedal footprint (Fig. 2E) of the Late Triassic of Greenland (S1-RP1, Lallensack et al. 2017) once again shows a good correspondence with the interpretive outline published. However, the faint claw impressions, which are barely visible on photographs but clearly discernible on photogrammetric depth-color maps (Lallensack et al. 2017), are not described by the selected set of landmarks and thus not included into the objective outline. Finally, a hominin footprint from the famous Laetoli tracksite of Tanzania (Leakey and Hay 1979; data from Bennett 2013) demonstrates that the present approach is equally well applicable to non-dinosaurian footprints.

Current limitations and further work

Several limitations of the presented approach are currently restricting its application, and are planned to be resolved in future versions:

1) The footprint has to be continuous (i.e., outlines have to describe the whole impression). In future versions, discontinuous footprints are planned to be processed by finding separate outlines for separate parts.

2) Only information within the set of selected continuous outlines is taken into account.

3) Separate parts of the footprint are not treated separately, although they may require different parameters. Consequently, the present approach is not able to trace the full extent of digital impressions in cases where the distalmost point is not coinciding with the position of the steepest slope,

resulting in abbreviated digits in the final outline. Solving this problem will require introduction of a priori assumptions on the anatomy of separate trackmaker taxa.

4) The present algorithm for outline rotation, although universally applicable, does not allow for precise alignment especially in tridactyl footprints, resulting in slightly differing rotation angles in separate footprints. A prerequisite for geometric morphometric analysis, shapes are required to be aligned into an uniform orientation. Resolving this problem does again require a priori assumptions on trackmaker anatomy.

CONCLUSIONS

The lack of widely applicable, objective means for defining the footprint margin is among the most vexing problems in the research of fossil footprints. The present algorithm automatically generates continuous objective footprint outlines by employing the criterium of the steepest slope. Although these outlines tend to correspond with human interpretations, extramorphological features unrelated to the foot anatomy may be incorporated, and anatomical detail not captured by the steepest slope may be excluded. While not a fully appropriate replacement for human-made drawings in most cases, computed outlines may be used as an objective basis for the production of interpretational drawings, reducing interpretational bias. Most importantly, the approach paves the way for fully objective analyses of footprint shape.

ACKNOWLEDGEMENTS

I like to thank Michael Buchwitz, Karl Bernhardi and Vincent Bonhomme for discussions, ideas, and help with writing the presented software. Antony Romilio and Matthew Bennett provided additional 3D models that were important in testing this software.

REFERENCES

Belvedere, M., Bennett, M.R., Marty, D., Budka, M., Reynolds, S.C. and Bakirov, R. 2018. Stat-tracks and mediotypes: powerful tools for modern ichnology based on 3D models. *PeerJ* 6: e4247.

Bennett, M.R. 2013. *Bournemouth Fossil Footprint Archive*. Downloaded from http://footprints.bournemouth.ac.uk/ on 29 June 2018.

Bennett, M.R., Reynolds, S.C., Morse, S.A. and Budka, M. 2016. Laetoli's lost tracks: 3D generated mean shape and missing footprints. *Scientific reports* 6.

Falkingham, P.L. 2010. Computer simulation of dinosaur tracks. Unpublished PhD thesis, University of Manchester, 201pp.

Falkingham, P.L. 2012. Acquisition of high resolution three-dimensional models using free, open-source, photogrammetric software. *Palaeontologia Electronica* 15 (1).

Falkingham, P.L., 2016. Applying Objective Methods to Subjective Track Outlines, in: Falkingham, P.L., Marty, D., Richter, A. (Eds.), Dinosaur Tracks: The Next Steps. Indiana University Press, Bloomington, pp. 72–81.

Falkingham, P.L., Bates, K.T., Avanzini, M., Bennett, M., Bordy, E.M., Breithaupt, B.H., Castanera, D., Citton, P., Díaz-Martínez, I., Farlow, J.O., Fiorillo, A.R., Gatesy, S.M., Getty, P., Hatala, K.G., Hornung, J.J., Hyatt, J.A., Klein, H., Lallensack, J.N., Martin, A.J., Marty, D., Matthews, N.A., Meyer, C.A., Milàn, J., Minter, N.J., Razzolini, N.L., Romilio, A., Salisbury, S.W., Sciscio, L., Tanaka, I., Wiseman, A.L.A., Xing, L.D. and Belvedere, M. 2018. A standard protocol for documenting modern and fossil ichnological data. *Palaeontology* 61 (4): 469–480.

Ishigaki, S. and Fujisaki, T. 1989. Three dimensional representation of *Eubrontes* by the method of moiré topography. *In*: Gillette, D.D. and Lockley, M.G. (eds.), *Dinosaur Tracks and Traces*, 421–425.

Lallensack, J.N., van Heteren, A.H. and Wings, O. 2016. Geometric morphometric analysis of intratrackway variability: a case study on theropod and ornithopod dinosaur trackways from Münchehagen (Lower Cretaceous, Germany). *PeerJ* 4: e2059.

Lallensack, J.N., Klein, H., Milàn, J., Wings, O., Mateus, O. and Clemmensen, L.B. 2017. Sauropodomorph dinosaur trackways from the Fleming Fjord Formation of East Greenland: evidence for Late Triassic sauropods. *Acta Palaeontologica Polonica* 62 (4): 833–843.

Leakey, M.D. and Hay, R.L. 1979. Pliocene footprints in the Laetolil Beds at Laetoli, northern Tanzania. *Nature* 278 (5702): 317–323.

Mallison, H. and Wings, O. 2014. Photogrammetry in paleontology – a practical guide. *Journal of Paleontological Techniques* 12: 1–31.

Matthews, N.A., Noble, T. and Breithaupt, B.H. 2016. Close-Range Photogrammetry for 3-D Ichnology: The Basics of Photogrammetric Ichnology. *In*: Falkingham, P.L., Marty, D. and Richter, A. (eds.), *Dinosaur Tracks: The Next Steps*. Indiana University Press, Bloomington, pp. 28–55.

Romilio, A. and Salisbury, S.W. 2011. A reassessment of large theropod dinosaur tracks from the mid-Cretaceous (late Albian–Cenomanian) Winton Formation of Lark Quarry, central-western Queensland, Australia: A case for mistaken identity. *Cretaceous Research* 32 (2): 135–142.

Romilio, A. and Salisbury, S.W. 2014. Large dinosaurian tracks from the Upper Cretaceous (Cenomanian–Turonian) portion of the Winton Formation, Lark Quarry, central-western Queensland, Australia: 3D photogrammetric analysis renders the 'stampede trigger' scenario unlikely. *Cretaceous Research* 51: 186–207.

Romilio, A., Tucker, R.T. and Salisbury, S.W. 2013. Reevaluation of the Lark Quarry dinosaur Tracksite (late Albian–Cenomanian Winton Formation, central-western Queensland, Australia): no longer a stampede? *Journal of Vertebrate Paleontology* 33 (1): 102–120.

Sarjeant, W.A.S. 1975. Fossil Tracks and Impressions of Vertebrates. *In*: Frey, R.W. (ed.), *The Study of Trace Fossils*, 283–324. Springer Berlin Heidelberg.

Thulborn, R.A. 1990. *Dinosaur tracks*. Chapman and Hall, London, New York, .

Thulborn, R.A. 2013. Lark Quarry revisited: a critique of methods used to identify a large dinosaurian track-maker in the Winton Formation (Albian–Cenomanian), western Queensland, Australia. *Alcheringa: An Australasian Journal of Palaeontology* 37 (3): 312–330.

Thulborn, R.A. and Wade, M. 1984. Dinosaur trackways in the Winton Formation (mid-Cretaceous) of Queensland. *Memoirs of the Queensland Museum* 21 (2): 413–517.

Thulborn, T. 2017. Behaviour of Dinosaurian Track-Makers in the Winton Formation (Cretaceous, Albian–Cenomanian) at Lark Quarry, Western Queensland, Australia: Running or Swimming? *Ichnos* 24 (1): 1–18.

Wings, O., Lallensack, J.N. and Mallison, H. 2016. The Early Cretaceous Dinosaur Trackways in Münchehagen (Lower Saxony, Germany) – 3D photogrammetry as basis for geometric morphometric analysis of shape variation and evaluation of material loss during excavation. *In*: Falkingham, P.L., Marty, D. and Richter, A. (eds.), *Dinosaur Tracks: The Next Steps*, Indiana University Press.

```r
#Objective Footprint Outline Tool v. 0.2
#Jens N. Lallensack, 2018

#### Readme ####
# This script requires a number of additional R packages that need to be installed first:
#
install.packages(c("Momocs","Rvcg","contoureR,"rlist","sp,"shapes","circular","tools","SDMTools"))
# Run program with
# oboutline("mesh.ply")
# Beforehand, the 3D-model should be cropped so that the footprint is filling most of the model.
# The 3D-model can have any orientation; orienting to the horizontal plane will be done automatically by the script.
# Due to current limitations, only a single outline can be created; the impression therefore has to be deep enough.
# If the footprint is a natural cast, the resulting images needs to be mirror-inverted.
# Two types of objective outlines will be produced; the median shape and the steepest slope. The median shape tends to preserve the shape best, but can be affected by abbreviated digits.

oboutline <- function(x){
  require(Momocs)
  require(Rvcg)
  require(contoureR)
  require(rlist)
  require(sp)
  require(shapes)
  require(spdep)    #Rotate function
  require(circular)
  require(SDMTools)
  require(tools)
  start_time <- Sys.time()  #for benchmark
  n <- 500  #number of points per contoure
  print("Importing and orientating mesh …")
  mesh <- meshimport(x)
  print("Extracting and cleaning contours …")
  cleaned <- trackclean(mesh)
  for(i in 1:(length(cleaned)-1)){   #remove contours outside of the stack
   inpoly <- pnt.in.poly(matrix(cleaned[[i]][1,],ncol=2),cleaned[[i+1]])
   if(inpoly[,3] == 0){cleaned[(i+1):length(cleaned)] <- NULL; break}
  }
  filtered <- kickout(cleaned,100)
  print("Rotating contours")
  sampled <- samplepoints(filtered,n=500)
  #rotated <- samplepoints(filtered,n=500)
  #rotated <- rotate(sampled)
  angle <- rotangle(sampled)
  rotated <- rotate(sampled,angle)
  print("Calculating distances between points …")
  outerproduct <- distOuter(rotated[[1]],rotated[[length(rotated)]])
  starting <- startingpoint(rotated,outerproduct)
  #outerproductA <- adjustouter(filtered,starting,outerproduct)
  outerproduct <- distOuter(starting[[1]],starting[[length(starting)]])
  print("Finding bottleneck points …")
  mdist <- corresponding(starting,outerproduct)
  print("Align contours to make points homologous …")
  homologous <- ContourAlignStack(starting,mdist,outerproduct)
  print("Calculate median shape")
  medianshape <- mshape(homologous,median)
  r180 <- rot180(medianshape)
  if(r180 == TRUE) {
    homologous <- controt(homologous,r180)
    starting <- controt(starting,r180)
    medianshape <- Rotation(medianshape,pi)
  }
  meanshape <- mshape(homologous,mean)
```

```
  print("Tracing steepest slope …")
  slope <- slope(homologous)
  plotf(starting,cleaned,mdist,angle,medianshape,meanshape,slope,r180)
  end_time <- Sys.time()    #for benchmark
  print("Done. Processing time:")
  end_time - start_time #time difference processing time
}

#Calculates equidistant points for a single polyline, returns object of class SpatialPoints
# x: Single polyline (as data frame)
# n: desired number of points per contour
equi <- function(x,n){
  rownames(x) <- NULL   #workaround to avoid warnings of funktion sp for duplicate row names
  equis <- spsample(SpatialLines(list(Lines(Line(x),ID=1))), n=n, "regular")@coords
  rownames(equis) <- 1:nrow(equis)
  return(equis)
}

rad2deg <- function(rad) {(rad * 180) / (pi)}
deg2rad <- function(deg) {(deg * pi) / (180)}

alpha <- function(a,b,c){
  acos((-0.5*a^2+0.5*b^2+0.5*c^2)/(b*c))}

beta <- function(a,b,c){
  acos((0.5*a^2-0.5*b^2+0.5*c^2)/(a*c))}

rotangle <- function(x){
  #rotate stack of contours so that digit impression III is pointing upwards
  RA <- deg2rad(90)
  RA <- deg2rad(90)
  l <- nrow(x[[1]])
  angme <- sapply(x,function(q) {
    ang <- vector()
    for (i in 1:(l-1)) {
      pair <- rbind(q[i,],q[i+1,])
      my <- max(q[i,2],q[i+1,2])
      miy <- min(q[i,2],q[i+1,2])
      mywhich <- which(pair[,2] == max(pair[,2]))
      miywhich <- which(pair[,2] == min(pair[,2]))
      C <- pair[mywhich,]
      B <- pair[miywhich,]
      A <- c(diff(c(B[1],C[1])),C[2]-B[2])
      b <- C[2]-B[2]
      a <- ed(B,C)
      angle <- asin(b/a)
      angle <- ifelse(pair[mywhich,1] > pair[miywhich,1],angle <- pi-angle, angle <- angle)
      ang <- c(ang,angle)
    }
    anglecircle <- ang*2
    angci<- circular(anglecircle)
    angle <- mean(angci)
    angle <- angle/2
    angl <- angle-RA
    return(angl)
  })
  angci <- circular(angme)
  angle <- mean(angci)
  return(angle)
}
rotate <- function(x,angle){
  lapply(x,function(w) {
    Rotation(w,angle)
  })}

rot180 <- function(m) {
```

```r
  #returns TRUE if shape has to be rotated 180 degrees to have digits pointing up
  CTP <- coo_centpos(m)
  mupper <- subset(m, m[,2] > CTP[2])
  mlower <- subset(m, m[,2] < CTP[2])
  upper <- sd(apply(mupper,1,function(x){ed(x,CTP)}))
  lower <- sd(apply(mlower,1,function(x){ed(x,CTP)}))
  ifelse(lower > upper,TRUE,FALSE)
}

controt <- function(x,r180) {
  lapply(x,function(w) {
    Rotation(w,pi)
  })}

#As "equi"", but for list of contours/polylines
samplepoints <- function(x,n){
  lapply(x, function(g){
    e <- equi(g,n)
    miny <- which(e[,2] == min(e[,2])); maxy <- which(e[,2] == max(e[,2]))
    minx <- which(e[,1] == min(e[,1])); maxx <- which(e[,1] == max(e[,1]))
    l <- c(n*0.05,n*0.09,-(n*0.05),-(n*0.09))
    #detect if points are sorted clockwise, and reverse if not
    reverse <- 0; keep <- 0
    reve <- function(k,l,o,w){if(w==0){if(l<0){op <- ">"} else {op <- "<"}}
    else{if(l<0){op <- "<"} else {op <- ">"}};
      eval(call(op,e[k,o],e[k+l,o]))}
    if(miny > n*0.1 & miny < n*0.9)
      {s <- sum(unlist(lapply(l,function(g){reve(miny,g,1,0)}))); reverse <-
      reverse+s; keep <- keep+(length(l)-s)}  #x axis, bottom
    if(maxy > n*0.1 & maxy < n*0.9)
     {s <- sum(unlist(lapply(l,function(g){reve(maxy,g,1,1)}))); reverse <- reverse
     +s; keep <- keep+(length(l)-s)} #x axis, top
    if(minx > n*0.1 & minx < n*0.9)
    {s <- sum(unlist(lapply(l,function(g){reve(minx,g,2,0)}))); reverse <- reverse
    +s; keep <- keep+(length(l)-s)} #y axis, left
    if(maxx > n*0.1 & maxx < n*0.9)
    {s <- sum(unlist(lapply(l,function(g){reve(maxx,g,2,1)}))); reverse <- reverse
    +s; keep <- keep+(length(l)-s)} #y axis, right
    if(reverse > keep) {e[,1] <- rev(e[,1]); e[,2] <- rev(e[,2])}
    return(e)
  })
}

closest <- function(x,min){
  #find closest points to line
  #x: stack of sampled contours
  #m: vector of two, with [1] position of minimum of outer, and [2] of inner
  outline
  n <- nrow(x[[1]])             #number of points per contour
  outer <- x[[length(x)]]       #outer contour
  inner <- x[[1]]               #inner contour
  between <- x[-(length(x))]; between <- between[-1]
  mininner <- min[2]
  minouter <- min[1]
  coinner <- inner[mininner,]
  coouter <- outer[minouter,]
  pointsonline <- sapply(between,function(q){
    dat <- as.data.frame(q)
    distmatrix <- apply(dat,1,function(y) { ed(y,coinner) + ed(y,coouter) } )
    mindistma <- which(distmatrix == min(distmatrix))
    point <- which(q[,1] == dat[mindistma,1])
    return(point)
  })
  pointsonlinea <- c(mininner,pointsonline,minouter)
  return(pointsonlinea)
}

#Set same starting point for all outlines
#x: list of contours sampled with "samplepoints" function
```

```
#outer product (between inner and outer contour)
startingpoint <- function(x,o){
  n <- nrow(x[[1]])
  minpoint <- which(o == min(o), arr.ind = TRUE)        #gives vector with two values, with [1] row number of outer and [2] of inner contour
  close <- closest(x,minpoint)
  stack <- list()
  for(i in 1:length(x)) {
    cont <- x[[i]]
    mp <- close[i]
    cut <- cont[1:(mp-1),]
    cont <- cont[-(1:(mp-1)),]
    stack <- list.append(stack,rbind(cont,cut))
  }
  return(stack)
}

ContourAlignStack <- function(x,m,o){
  # as "ContourAlign", but on whole contour stack
  # x: Stack of contours (with same starting point)
  # m: mdist table
  # o: outerproduct matrix
  n <- nrow(x[[1]])
  closelist <- list()
  for (i in 2:nrow(m)) {
    close <- closest(x,m[i,])
    closelist <- list.append(closelist,close)
  }
  means <- round(sapply(closelist,mean))
  contlist <- list()
  for (t in 1:length(x)) {
    for (g in 1:length(closelist)) {
      if (g == 1) {
        cut <- x[[t]][1:closelist[[g]][t],]
        cont <- equi(cut,means[g])
      } else {
        cut2 <- x[[t]][closelist[[g-1]][t]:closelist[[g]][t],]
        ave <- means[g]-means[g-1]
        cutRe <- equi(cut2,ave)
        cont <- rbind(cont,cutRe)
      }
    }
    cut3 <- x[[t]][closelist[[length(closelist)]][t]:n,]
    ave <- n-means[length(means)]
    cutRe <- equi(cut3,ave)
    cont <- rbind(cont,cutRe)
    contlist <- list.append(contlist,cont)
  }
  return(contlist)
}

meshimport <- function(x){
  p <- TRUE
  if(file_ext(x) == "ASC"){    #ASC file support
    ASC <- TRUE
    mesh <- read.csv(x,sep="")
    cont <- mesh[,1:3]
  }else{
    ASC <- FALSE
    mesh <- vcgImport(x,clean=T)                    #import 3D data. Common formats, including .ply, are supported.
    cont <- t(mesh$vb[1:3,])                        #subset data to get matrix with xyz values of vertices
  }
    contH <- prcomp(cont)$x                         #perform PCA to have z axis exactly vertical to the horizontal plane of the model
    #Detect if mould or cast, and revert if needed
    centerXa <- min(contH[,1]) + ((max(contH[,1])-min(contH[,1]))*0.25) #select central forth of xy plane, to detect if negative or positive
```

```
254     centerXb <- min(contH[,1]) + ((max(contH[,1])-min(contH[,1]))*0.75)
255     centerYa <- min(contH[,2]) + ((max(contH[,2])-min(contH[,2]))*0.25)
256     centerYb <- min(contH[,2]) + ((max(contH[,2])-min(contH[,2]))*0.75)
257     contC <- contH[contH[,1] > centerXa,]; contC <- contC[contC[,2] > centerYa,]
        #the central area
258     contC <- contC[contC[,1] < centerXb,]; contC <- contC[contC[,2] < centerYb,]
259     if(mean(contC[,3]) > 0){Zorientation <- FALSE} else {Zorientation <- TRUE}
        #Check if the center quater of the model is lower than the rest
260     if(p != Zorientation) {contH[,3] <- -contH[,3]; contH[,1] <- -contH[,1];
        print("Z axis inverted")}   #and revert the sign of the z values if different
        from supplied p Parameter
261     #Detect if model got mirror-inverted during PCA fit, and revert if needed
262     testor <- cont[1:4,]    #four points of original mesh
263     testaft <- contH[1:4,]  #four points after PCA-fit
264     prdist <- round(procdist(as.matrix(testor),as.matrix(testaft)),4)   #compute
        Procrustes distance between both samples
265     if(prdist != 0) {contH[,1] <- -contH[,1]; print("xy mirrored")} #if mirrored,
        the Procrustes distance is expected to be unequal to zero; if so, mirror back
266     if(ASC==FALSE){mesh$vb[1:3,] <- t(contH)                        #Write fitted
        coordinates back to mesh file
267     vcgPlyWrite(mesh,"mesh-aligned.ply",binary=T)}  #Export fitted mesh
268     cont <- contH
269   return(cont)
270 }
271
272 trackclean <- function(x){
273   conts <- getContourLines(x, nlevels=30)       #Compute 30 equally spaced contour
      lines. Returns dataframe
274   #where conts$LID is the contour level, and conts$GID the individual contour
275   maxLID <- max(conts$LID)                      #Number of contour levels (i.e.
      height levels)
276   conList <- list()
277   for (i in 1:maxLID){
278     contsL <- conts[conts$LID==i,]                  #For each contour level, select
        respective data
279     maxGID <- max(contsL$GID)                       #Number of contours for each
        contour level
280     z <- 1
281     for (t in 0:maxGID){
282       contsG <- contsL[contsL$GID==t,]              #For each contour within an
          level, select respective data
283       contsG <- contsG[,5:6]                            #select xy values only
284       if(contsG[1,1]==contsG[nrow(contsG),1]) {     #if the first and last
          coordinate of a contour is identical, we have a closed contour
285         if(z==1){length <- nrow(contsG)} else {         #If closed, write number of
            points
286           length <- c(length,nrow(contsG))}
287       }
288       else {
289         if(z==1){length <- 0} else {                    #If open, set number of
            points to 0 to have it filtered in the next step
290           length <- c(length,0)
291         }
292       }
293       z <- z+1
294     }
295
296     GIDselected <- (which.max(length))-1            #Select longest contour per
        height level
297     consel <- contsL[contsL$GID==GIDselected,]      #Select data of longest contour
        of respective height level
298     conList <- list.append(conList,consel[,5:6])    #Write to list. Only the
        longest contour was selected, with all open contours removed
299   }
300   conList <- conList[sapply(conList,nrow)>(max(sapply(conList,nrow))*0.5)]  #Remove
      all contours less than 50% of longest
301   return(conList)
302 }
303
```

```
304 distOuter <- function(x,y) {apply(x,1,function(x){apply(y,1,function(z)
    {ed(x,z)})})}
305 #Calculates euclidean distance for all combination of pairs of points in two
    matrices (x and y)
306
307 corresponding <- function(x,o){
308   #Stack of contours <- x
309   #Outerproduct matrix, distances between inner and outer outline <- o
310
311   x <- x[[1]]    #inner contour
312   y <- x[[length(x)]]    #outer contour
313   n <- nrow(x)    #number of points per contour
314   min1 <- c(1,1)  #the already homologous starting point is the first bottleneck,
    min1
315
316   #min2 (opposing side)
317   interval2 <- 0; interval2a <- 0; interval2b <- 0
318   min2.interval.min <- min1[1] + (n*0.4); min2.interval.max <- min1[1] + (n*0.6)
319
320   if(min2.interval.max <= n){interval2 <- o[min2.interval.min:min2.interval.max,];
    poss <- 1
321   } else {
322     if(min2.interval.min > n){interval2 <- o[(min2.interval.min-n):
    (min2.interval.max-n),]; poss <- 2
323     } else {
324       interval2a <- o[(min2.interval.min:n),]; interval2b <- o[1:
      (min2.interval.max-n),]; poss <- 3
325     }}
326   if(poss == 3){interval2 <- rbind(interval2a,interval2b)}
327
328   min2 <- which(interval2 == min(interval2), arr.ind = TRUE)
329   rminrow <- which(rownames(o) == rownames(min2))
330   min2 <- c(rminrow[1],min2[2])
331   mindist <- rbind(min1,min2)
332   mindist <- ifelse(mindist>n,mindist-n,mindist) #workaround
333
334   #min3 (min1:min2), left of min1 -> min2
335
336   if(mindist[2,1] > mindist[1,1]){interval3 <- o[((mindist[1,1])+(n*0.1)):
    ((mindist[2,1])-(n*0.1)),]
337   } else {
338     interval3a <- o[((mindist[1,1]):n),]; interval3b <- o[1:(mindist[2,1]),];
339     interval3ab <- rbind(interval3a,interval3b)
340     interval3 <- interval3ab[(n*0.1):(nrow(interval3ab)-(n*0.1)),]
341   }
342   min3 <- which(interval3 == min(interval3), arr.ind = TRUE)
343   rminrow <- which(rownames(o) == rownames(min3))
344   min3 <- c(rminrow[1],min3[2])
345   mindist <- rbind(mindist,min3)
346
347   #min4 (min2:min1), right of min1 -> min2
348   if(mindist[2,1] < mindist[1,1]){interval4 <- o[(mindist[2,1]+(n*0.1)):
    (mindist[1,1]-(n*0.1)),]
349   } else {
350     interval4a <- o[((mindist[2,1]):n),]; interval4b <- o[1:(mindist[1,1]),];
351     interval4ab <- rbind(interval4a,interval4b);
352     interval4 <- interval4ab[(n*0.1):(nrow(interval4ab)-(n*0.1)),]
353   }
354   min4 <- which(interval4 == min(interval4), arr.ind = TRUE)
355   rminrow <- which(rownames(o) == rownames(min4))
356   min4 <- c(rminrow[1],min4[2])
357   mindist <- rbind(mindist,min4)
358   mindist <- ifelse(mindist>n,mindist-n,mindist) #workaround
359   mindist <- mindist[c(1,c(3,2),4),] #resort matrix
360
361   #min N, between min1 and min3
362   bottleneck <- function(x,y,p){
363     q <- p/2
364     if(x[1] < y[1]){intervalN <- o[(x[1]+(n*q)):(y[1]-(n*q)),]
```

```
365     } else {
366       intervalNa <- o[(x[1]:n),]; intervalNb <- o[(1:y[1]),];
367       intervalNab <- rbind(intervalNa,intervalNb);
368       intervalN <- intervalNab[(n*q):(nrow(intervalNab)-(n*q)),]
369     }
370     minN <- which(intervalN == min(intervalN), arr.ind = TRUE)
371     rminrow <- which(rownames(o) == rownames(minN))
372     minN <- c(rminrow[1],minN[2])
373     ifelse(minN > n, minN-n, minN); #workaround
374   }
375
376   #e.g. for bottleneckSub: x = mindist[1,], y = mindist[2,]
377   bottleneckSub <- function(x,y,p){
378     #p: minimum distance to existing bottlenecks
379     if(x[1] < y[1]){
380       if((y[1] - x[1]) > (n*p)){
381         mindist <- bottleneck(x,y,p)}
382     }else{
383       if(((n-x[1])+y[1]) > (n*p)){
384         mindist <- bottleneck(x,y,p);
385       }
386     }
387   }
388
389   mindistA <- mindist
390   for(i in 1:nrow(mindist)){
391     if(i == nrow(mindist)){
392       mindistA <- rbind(mindistA,(bottleneckSub(mindist[i,],mindist[1,],0.1)))
393     }else{
394       mindistA <- rbind(mindistA,(bottleneckSub(mindist[i,],mindist[i+1,],0.1)))
395     }
396   }
397   mindistA <- mindistA[order(mindistA[,1]),]
398
399   mindistB <- mindistA
400   for(i in 1:nrow(mindistA)){
401     if(i == nrow(mindistA)){
402       mindistB <- rbind(mindistB,(bottleneckSub(mindistA[i,],mindistA[1,],0.1)))
403     }else{
404       mindistB <- rbind(mindistB,(bottleneckSub(mindistA[i,],mindistA[i+1,],0.1)))
405     }
406   }
407   mindistB <- mindistB[order(mindistB[,1]),]
408
409   mindistC <- mindistB
410   for(i in 1:nrow(mindistB)){
411     if(i == nrow(mindistB)){
412       mindistC <- rbind(mindistC,(bottleneckSub(mindistB[i,],mindistB[1,],0.1)))
413     }else{
414       mindistC <- rbind(mindistC,(bottleneckSub(mindistB[i,],mindistB[i+1,],0.1)))
415     }
416   }
417   mindistC <- mindistC[order(mindistC[,1]),]
418
419   mindistD <- mindistC
420
421   if (n > 200) {
422     for(i in 1:nrow(mindistC)){
423       if(i == nrow(mindistC)){
424         mindistD <- rbind(mindistD,(bottleneckSub(mindistC[i,],mindistC[1,],0.1)))
425       }else{
426         mindistD <- rbind(mindistD,(bottleneckSub(mindistC[i,],mindistC[i+1,],
          0.1)))
427       }}
428     mindistD <- mindistD[order(mindistD[,1]),]
429   }
430   #Check if any of the bottle necks has the same coordinate on the inner contour
431   while (any(duplicated(mindistD[,2])))
432   {
```

```
433     duplicate <- which(duplicated(mindistD[,2]) == TRUE)
434     mindistD[duplicate,2] <- mindistD[duplicate,2]+1
435   }
436   return(mindistD)
437 }
438
439 ContourAlign <- function(b,o,m){
440   # Align two contours, so that points are corresponding and directly comparable
441   # b: Inner contour
442   # o: Outer contour
443   # m: mindist table
444   n <- nrow(b)
445   q <- 0
446   ioc <- vector()
447   for (i in 1:(nrow(m))){
448     q <- q+1;
449     q1 <- q+1;
450     if(q == nrow(m)){q1 <- 1}
451     if((m[(q1),1]) > m[q,1]){
452       interval.outer <- o[m[q,1]:m[q1,1],];
453     } else {
454       interval.outer1 <- o[((m[q,1]):n),]; interval.outer2 <- o[1:(m[(q1),1]),];
455       interval.outer <-
      rbind(matrix(interval.outer1,ncol=2),matrix(interval.outer2,ncol=2));
456     }
457     if((m[(q1),2]) > m[q,2]){
458       interval.inner <- b[(m[q,2]:m[q1,2]),];
459     } else {
460       interval.inner1 <- b[((m[q,2]):n),]; interval.inner2 <- b[1:(m[(q1),2]),];
461       interval.inner <-
      rbind(matrix(interval.inner1,ncol=2),matrix(interval.inner2,ncol=2));
462     }
463     npoints.outer <- nrow(interval.outer); npoints.inner <- nrow(interval.inner);
464     npoints <- mean(npoints.outer,npoints.inner);
465     equi.outer <- equi(interval.outer,npoints); equi.inner <-
    equi(interval.inner,npoints);
466     ioca <- cbind(equi.outer,equi.inner); ioc <- rbind(ioc,ioca)
467   }
468   return(ioc)
469 }
470
471 pdists <- function(x){
472   #n: desired number of points per contour
473   t <- 1
474   for (i in 1:(length(x)-1)){
475     z <- list(x[[i]],x[[i+1]])
476     op <- distOuter(z[[1]],z[[2]])
477     KickCorresponding <- corresponding(z,op)
478     equidist <- ContourAlign(z[[1]],z[[2]],KickCorresponding)
479     j <- cbind(equidist[,1],equidist[,2])
480     k <- cbind(equidist[,3],equidist[,4])
481     pdista <- procdist(j,k,type="partial")
482     if(t==1) {Dists <- pdista} else {Dists <- c(Dists,pdista)}
483     t <- t+1
484   }
485   return(Dists)
486 }
487
488 kickout <- function(x,n){
489   #x: List of contours
490   #n: desired number of points per contour
491   b <- samplepoints(x,n)
492   pdist <- pdists(b)
493   sdev <- 0.1
494   contlist <- x
495   for (i in (round(length(contlist)/2)+1):(length(contlist)-1)){
496     if(pdist[i] > sdev){contlist <- contlist[-((i+1):length(contlist))]; break}}
497   for (i in (length(contlist)-3):1){if(pdist[i] > sdev){contlist <- contlist[-(i:
    1)]; break}}
```

```r
  lc <- length(contlist)
  if(lc > 8) {
    b <- samplepoints(contlist,n)
    pdist <- pdists(b)
    sdev <- sd(pdist)*1.5
    for (i in (round(lc/2)+2):lc-1){
      if(pdist[i] > sdev)
      {contlist2 <- contlist[-((i+1):lc)];
      if(length(contlist2) > 5) {contlist <- contlist2}; break}}
    for (i in (lc-2):0){
      if(pdist[i] > sdev){contlist2 <- contlist[-(i:1)]
      if(length(contlist2) > 5) {contlist <- contlist2} ;break}}
  }
  lc <- length(contlist)
  if(lc > 8) {
    b <- samplepoints(contlist,n)
    pdist <- pdists(b)
    sdev <- sd(pdist)*1.2
    for (i in (round(lc/2)+2):lc-1){
      if(pdist[i] > sdev)
      {contlist2 <- contlist[-((i+1):lc)];
      if(length(contlist2) > 5) {contlist <- contlist2}; break}}
    for (i in (lc-2):0){
      if(pdist[i] > sdev){contlist2 <- contlist[-(i:1)]
      if(length(contlist2) > 5) {contlist <- contlist2} ;break}}
  }
  #write.csv(pdist,file="pdists.csv")
  return(contlist)
}

mshape <- function(x,type){
  #x: set of contours with homologous points
  #type: can be "mean" or "median"
  for (i in 1:length(x)){
    if (exists("xaxis")) {xaxis <- cbind(xaxis,x[[i]][,1])} else {xaxis <- x[[i]][,1]}
    if (exists("yaxis")) {yaxis <- cbind(yaxis,x[[i]][,2])} else {yaxis <- x[[i]][,2]}
  }
  meanx <- apply(xaxis,1,type)
  meany <- apply(yaxis,1,type)
  meanshape <- cbind(meanx,meany)
  ef <- meanshape %>% efourier(nb.h=25) %>% efourier_i()
  return(ef)
}

plotf <- function(x,cleaned,mdist,angle,medianshape,meanshape,slope,r180){
  fullcontsRot <- rotate(cleaned,angle)
  if(r180 == TRUE) {
    fullcontsRot <- controt(fullcontsRot,r180)
  }
  par(pty="s")          #set graphics parameter to make plot region square
  svg("bottlenecks.svg")
  plot(x[[length(x)]],type="l",asp=1,col="white")       #asp: aspect ratio, for equal axes
  #points(meanshape,col="green",pch=19)
  lines(medianshape,col="blue",lwd=3)
  points(x[[1]][mdist[,2],],col="magenta",pch=19)
  points(x[[length(x)]][mdist[,1],],col="magenta",pch=19)
  sapply(x,lines)
  dev.off()

  svg("combined.svg")
  area <-
  rbind(fullcontsRot[[length(fullcontsRot)]],fullcontsRot[[length(fullcontsRot)-1]],fullcontsRot[[length(fullcontsRot)-2]]) #set plot area
  plot(area,type="l",asp=1,col="white")     #asp: aspect ratio, for equal axes
  sapply(fullcontsRot,function(x){lines(x,col="gray48")})
  lines(medianshape,col="blue",lwd=3)
```

```
562   lines(meanshape,col="green",lwd=3)
563   lines(slope,col="red",lwd=3)
564   dev.off()
565
566   svg("objective-outline.svg")
567   plot(area,type="l",asp=1,col="white")
568   sapply(fullcontsRot,lines)
569   lines(slope,col="red",lwd=4)
570   dev.off()
571 }
572
573 slope <- function(h){
574   #x stack of homologous contours
575   sections <- which(rownames(h[[1]]) == "1")            #sections between
    bottlenecks
576   sections <- c(sections,nrow(h[[1]]))
577   Slope <- vector()
578   for (i in 1:(length(sections)-1)) {
579     sec <- lapply(h,function(a) {a[sections[i]:(sections[(i+1)]-1),]})
580     ioc <- cbind(sec[[1]],sec[[length(sec)]])
581     contsbetw <- sec[2:(length(sec)-1)]
582     #Calculate which points are closest to vertical lines
583     dista <- apply(ioc,1,function(q){           #for each vertical row
584       lapply(contsbetw,function(w){             #for each contour
585         apply(w,1,function(e){                  #for each point
586           ed1 <- ed(e,q[1:2]); ed2 <- ed(e,q[3:4])
587           ed1 + ed2
588         })})
589     })
590     CON <- lapply(dista,function(x){lapply(x,function(x){which(x == min(x))})})
591     #returns sco variable containing minimum distances for each point on each
    contour
592     for (o in nrow(ioc)) {
593       n <- 1:nrow(ioc) #point, e.g. 1:10
594       m <- 1:length(contsbetw) #Contour, e.g. C2:C12
595       sco <- sapply(seq_along(n),function(x){sapply(seq_along(m),function(y){
596         pos <- unlist(CON[[x]][y]);
597         curc <- sec[[y+1]][pos,];
598         intnex <- sec[[y+2]];
599         intprev <- sec[[y]];
600         min(apply(intprev,1,function(z){ed(z,curc)})) + min(apply(intnex,
    1,function(z){ed(z,curc)}));
601       })})
602     }
603     mins <- function(r) {
604       n <- 1:length(r)
605       lapply(seq_along(n),function(v){
606         con <- unlist(CON[[v]][r[v]]);
607         sec[[(r[v])+1]][con,]
608       })
609     }
610     lse <- length(sec)
611     N <- ceiling((lse/2)-1)
612     mind1 <- apply(sco,2,function(x){which(x == min(x))})
613     mindlist <- list(); mindlist <- list.append(mindlist,unlist(mind1))
614     if(lse > 3) {
615       for (p in 1:N) {
616         mind <- apply(sco,2,function(x){
617           n <- length(x); sorted <- -sort(-x,partial=n-p)[n-p]; which(x ==
    sorted)})
618         mindlist <- list.append(mindlist,mind)
619       }}
620     coords <- lapply(mindlist,function(x) {t(sapply(mins(x),as.matrix))})
621     distmat <- sapply(mindlist, function(x){
622       dist <- vector()
623       for (s in 1:length(x)) {
624         dist <- c(dist,sco[x[s],s])
625       }
626       return(dist)
```

```
627     })
628     scores <- t(round(apply(distmat,1,function(x) {
629       scor <- vector()
630       for (d in 2:length(x)) {
631         scor <- c(scor,20-((x[d]/x[1])*10))
632       }
633       return(scor)
634     })))
635     scores[scores<0] <- 0
636     #scores: Matrix with two colums containing scores for the second and third
        steepest slope, respectively;
637     #the steepest slope is set at 10.
638     for (f in 1:nrow(coords[[1]])) {
639       xvalues <- vector()
640       yvalues <- vector()
641       xvalues <- c(xvalues,rep(coords[[1]][f,1],10))
642       yvalues <- c(yvalues,rep(coords[[1]][f,2],10))
643       for (a in 1:(length(coords)-1)) {xvalues <- c(xvalues,rep(coords[[a+1]][f,
        1],scores[f,a]))}
644       for (a in 1:(length(coords)-1)) {yvalues <- c(yvalues,rep(coords[[a+1]][f,
        2],scores[f,a]))}
645       Slope <- rbind(Slope,cbind(mean(xvalues),mean(yvalues)))
646     }
647   }
648   write.csv(Slope,file="slopecoords.csv")
649   ef <- Slope %>% efourier(nb.h=25, smooth.it=10) %>% efourier_i()
650   par(pty="s")
651   svg("objoutline-rawdata.svg")
652   plot(h[[length(h)]],col="white",asp=1)
653   sapply(h,function(y){lines(y)})
654   points(Slope,col="green")
655   lines(ef,col="red",lwd=3)
656   dev.off()
657   return(ef)
658 }
659
```

Chapter 5

accepted for publication in “Journal of Vertebrate Paleontology”.

Lallensack, J.N., Ishigaki, S., Lagnaoui, A., Buchwitz, M., Wings, O., accepted. Forelimb orientation and locomotion of sauropod dinosaurs: insights from the Middle Jurassic Tafaytour Tracksite (Argana Basin, Morocco). Journal of Vertebrate Paleontology. **p. 127–160.**

Author contributions:

- Jens N. Lallensack collected data, analyzed the data, wrote the paper, prepared figures and/or tables, reviewed drafts of the paper.
- Shinobu Ishigaki, Oliver Wings, and Abdelouahed Lagnaoui collected data, prepared figures, reviewed drafts of the paper.
- Michael Buchwitz analyzed the data, reviewed drafts of the paper.

Supplementary Material:

- Supplemental Data 1:
  - Detailed description of trackway configurations and footprint morphologies. **p. 161–172.**
  - Fig 1S–9S: additional diagrams and sitemaps. **p. 173–181.**
- Supplemental Data 2: Data Sample. **p. 182.**
- Supplemental Data 3: Trackway measurements. **p. 183.**
- Supplemental Data 4: Mean configuration calculator (ODF spreadsheet, available from DVD only)
- Photogrammetric 3D data (available from DVD or Figshare, see Table 1 in main text).

Forelimb orientation and locomotion of sauropod dinosaurs: insights from the ?Middle Jurassic Tafaytour Tracksites (Argana Basin, Morocco)

Jens N. Lallensack,[1] Shinobu Ishigaki,[2] Abdelouahed Lagnaoui,[3, 4] Michael Buchwitz,[5] and Oliver Wings[6]

[1]Division of Paleontology, Steinmann Institute, University of Bonn, Nussallee 8, 53115 Bonn, Germany;

[2]Okayama University of Science, Biosphere – Geosphere Science, Ridai-cho 1-1, Kita-ku, Okayama, 700-0005 Japan;

[3]CONICET, Instituto de Ciencias de la Tierra y Ambientales de La Pampa – INCITAP, Facultad de Ciencias Exactas y Naturales – Universidad Nacional de La Pampa, Av. Uruguay 151, 6300 Santa Rosa, La Pampa, Argentina.

[4]Laboratory of Stratigraphy of Oil-and-Gas Bearing Reservoirs, Department of Paleontology and Stratigraphy, Institute of Geology and Petroleum Technologies, Kazan (Volga Region) Federal University, Kremlyovskaya str. 18, 420008, Kazan, Russia;

[5]Museum für Naturkunde Magdeburg, Otto-von-Guericke-Str. 68-73, 39104 Magdeburg;

[6]Zentralmagazin Naturwissenschaftlicher Sammlungen (ZNS), Martin-Luther-Universität Halle-Wittenberg, Domplatz 4, 06108 Halle (Saale), Germany

ABSTRACT

Forelimb posture in sauropod dinosaurs is still poorly understood. Although a laterally directed (semi-supinated) manus is the plesiomorphic condition in sauropodomorphs, the sauropod track record prevailingly shows anterolateral to anterior manus orientations, suggesting a high degree of manus pronation. The ?Middle Jurassic Tafaytour tracksites described herein preserve at least ten trackways, nine of which show laterally, and in two examples even posterolaterally oriented manual impressions. Located in the Argana Basin of the Western High Atlas, Morocco, the tracksite yields hundreds of footprints on a highly bioturbated surface, including examples with well-preserved digit and claw impressions. Footprint morphology and trackway configuration vary greatly between trackways.

A literature review indicates that laterally directed manual impressions are restricted to small and medium-sized trackmakers. Statistical analysis was performed on a larger sample (n = 79) of small sauropod trackways from around the world, indicating that lateral manual orientations are correlated with low locomotion speeds and narrow trackway gauges. Manus pronation in sauropods is hypothesized to occur when the forelimb is actively contributing to the propulsion of the animal, which would be the case at faster speeds or at wider trackway gauges where the center of mass is located more anteriorly.

We present new approaches to the quantitative analysis of trackway data. Mean configuration plots allow for direct graphical comparisons of different trackways. Two types of trackway asymmetries are defined and quantified. The apparent glenoacetabular distance (GAD) represents a feasible proxy for body size, at least for the smaller sauropod trackmakers analyzed herein.

INTRODUCTION

One of the most notable events in the evolution of herbivorous non-avian dinosaurs is the transformation from the plesiomorphic obligatory bipedal to a quadrupedal mode of locomotion. Such secondary quadrupedalism is rare in tetrapod evolution, occurring only in silesaurids and in several dinosaurian lineages, including thyreophorans, ornithopods, ceratopsians, and sauropodomorphs (Remes, 2008; Maidment and Barrett, 2012; VanBuren and Bonnan, 2013). The plesiomorphic condition in the tetrapod forearm is semi-supination, i.e., animals with a parasagittal limb posture would show a laterally facing manus, if it was not for additional anatomical adaptations that rotate the manus to a more anterior orientation (Bonnan, 2003). Therian mammals possess the ability to actively pronate their forearm by pivoting the radius around the ulna; as a result, the radius crosses the ulna in anterior view (Darcus and Salter, 1953; Bonnan, 2003). Pronation allows for anteriorly directed digits, which can be used to generate forward thrust during quadrupedal locomotion (Bonnan and Senter, 2007). In dinosaurs and all other tetrapod groups apart from mammals and chameleons, full pronation is not possible (Bonnan, 2003; VanBuren and Bonnan, 2013; Hutson, 2014). Indeed, bipedal dinosaurs such as basal sauropodomorphs and theropods probably were unable to rotate their manus in a way so that the palm of the hand is facing ventrally (e.g. Bonnan, 2003; Bonnan and Senter, 2007; Milner et al., 2009; Mallison, 2010a, 2010b), raising the question if, and how, an anterior manus orientation was achieved in secondarily quadrupedal dinosaurs.

Reconciling sauropod forelimb osteology with manual print orientations has proved to be difficult (Bonnan, 2003). Articulation of the limb elements would suggest a semi-supinated manus orientation, as proposed by Borsuk-Bialynicka (1977) for the titanosaur *Opisthocoelicaudia*. Such a manus orientation, however, is at odds with the track record, which indicates a much more pronated manus (Bonnan, 2003). According to Bonnan (2003), the manual supination angle ranges from as little as 5–10° to as much as 55° in known sauropod trackways. Trackway evidence for a semi-supinated manus was lacking until recently. In the few existing reports (Ishigaki, 1985, 2007, 2009; Marty, 2008; Xing et al., 2010, 2013, 2014a, 2015a, 2015b, 2016a; Kim and Lockley, 2012; Zhang et al., 2012; Marty et al., 2013; Enniouar et al., 2014; Mazin et al., 2016), this conspicuous feature was often considered a mere curiosity, and comparisons with similar tracks from other parts of the world have rarely been made.

The ?Middle Jurassic Tafaytour tracksites in Morocco described herein yield at least ten trackways of small to small medium-sized sauropod trackmakers, including nine trackways with unusually high manual supination angles, exceeding 100° in three examples. This indicates that these sauropods walked with semi-supinated forelimbs, which is the plesiomorphic condition in dinosaurs. Here we aim to provide a detailed description of the Tafaytour sauropod trackways based on high-resolution photogrammetric data. Statistical analyses were performed on the Tafaytour trackways and other small to small medium-sized (pedal impression length < 60 cm) sauropod trackways (n = 79) from around the world, in order to test for covariation of independent trackway parameters, with special emphasis on the manual supination angles. Fur-

thermore, we present and discuss new approaches for the quantitative study of sauropod dinosaur trackways.

LOCALITY

The present site consists of two, nearly vertically oriented roadcut surfaces along the national road between Agadir and Marrakech, near Tafaytour, approximately 14 km WSW of Imi-N-Tanout (Fig. 1). The site is located within the Argana Basin, a 70 × 20 km large, NNE–SSW trending depositional area on the southwestern margin of the Western High Atlas mountain range, which exposes Permian, Triassic and Jurassic continental deposits (Tixeront, 1974). The tracksites have been referred to the Ameskroud Formation, which is between 100 to 500 m in thickness and can be divided into two members, the lower Imerhrane Member, and the upper Ait Mbarek Member (Enniouar et al., 2014). The Imerhrane Member is around 70 m in thickness and consists of playa mudstones, siltstones and sandstones. The Ait Mbarek Member consists of quartzite conglomerates deposited by braided river systems (Enniouar et al., 2014). The present tracksites have been generally considered to be part of the Imerhrane Member, which is Middle Jurassic in age (Jenny, 1981; Ishigaki, 2007, 2009; Enniouar, 2014). However, a possible Lower Cretaceous age of the tracksites cannot be excluded at present (Soulaimani and Ouanaimi, 2011; A. Fekkak, pers. comm., November 2017).

Discovered during construction of the road in 1980 or 1981, the tracks were briefly reported by Jenny et al. (1981). The tracksites were studied by one of us (SI) in 1984, 1988 and 2009, when six trackways were identified (Ishigaki, 1985, 2007, 2009). Enniouar et al. (2014) provided illustrations and a brief description of the two clearest trackways (herein, Trackways A1 and A2, as explained below). The majority of footprints, and nine of the ten trackways, occur at Tracksite A (31° 6' 52'' N, 8° 58' 55'' W), which is 54 m in length and up to 6 m in height. The layers dip at approximately 80° towards the north. The bed containing the tracks is 15 cm in thickness, consists of red or gray-white fine sandstone and is sandwiched between massive red siltstone beds (Ishigaki, 2007). Tracksite B, located 750 m east of Tracksite A (31° 6' 49'' N, 8° 58' 28'' W), is only 1.5 m in length and 5 m in height, and contains a single trackway (Ishigaki, 2007). As in Tracksite A, the track-bearing layer is a fine sandstone sandwiched between red and massive siltstone beds dipping at approximately 80° towards the north; the sandstone is gray-white in color and 50 cm in thickness (Ishigaki, 2007). Henceforth, we refer to the nine trackways of Tracksite A as Trackways A1–A9, with the numbering based on the position of the trackways from west to east, and to the single trackway of Tracksite B as Trackway B1.

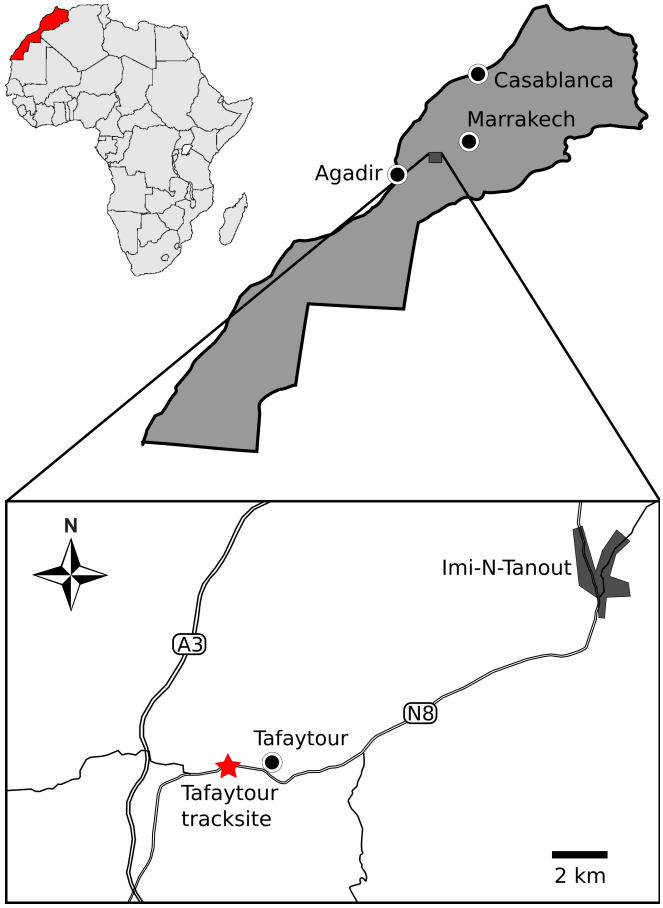

FIGURE 1. Geographic location of the Tafaytour Tracksites in Morocco.

Díaz-Martínez et al. (2010) provided several examples of dinosaur tracksites in the Central High Atlas of Morocco that had been degraded by weathering and erosion in recent years. Degradation can occur as continuous and gradual weathering of the whole surface, slowly erasing the topography of the tracks (Henderson, 2006b), or as patchy, localized erosion of larger pieces. In order to assess alteration of Tracksite A, we compared photographs taken by one of us (SI) in 1988 with our more recent data from 2015. While effects of gradual weathering are not apparent, the site was affected by localized mechanical removal of parts of the tracking layer. Destroyed parts include a large section measuring 140 × 60 cm in area, which contained the excellently preserved fifth left manual impression (LM5) of Trackway A1 (Supplementary Data 1, Fig. 8S), as well as a smaller area measuring 60 × 25 cm, which previously contained LM1 of Trackway A1. The shape and location of both now missing impressions have been reconstructed based on the 1988 data. Erosion, however, also uncovered many new footprints at the base of the roadcut since 1988, including one new trackway (Trackway A9). The vulnerability of ichnological sites highlights the value of three-dimensional digitalization techniques such as photogrammetry, which allow for securing large amounts of scientific data in short amounts of time (e.g., Bennett et al., 2013).

MATERIAL AND METHODS

Terminology

Terminology in this work follows, until otherwise noted, that of Leonardi (1987) and Marty (2008). 'Small-sized' sauropod footprints are defined to be <50 cm in length following Marty (2008), whereas 'small medium-sized' tracks are 50–60 cm in length. A variety of terms exist to describe the rotation of a footprint relative to the direction of travel (Thulborn, 1990). The term 'positive rotation' describes a rotation away from the trackway midline, whereas 'negative rotation' refers to a footprint pointing towards the trackway midline (Leonardi et al., 1987). Although commonly used, these terms are ambiguous and are often used in the converse sense (Thulborn, 1990). The alternative terms 'inward rotation' and 'outward rotation' are unambiguous. For dinosaur manual prints, however, they may lead to the wrong perception that the manus has been rotated away from an originally anterior (pronated) orientation, despite the fact that a lateral (supinated) manual orientation is plesiomorphic for quadrupedal dinosaurs. We here follow Bonnan (2003) in employing the term 'supination angle' for sauropod manual tracks, where the fully pronated, and thus anteriorly directed manus, has a supination angle of 0°. In inwards rotated manual tracks, the manual supination angle is negative. The terms 'anterior', 'posterior', medial', and 'lateral', are used to describe location and orientation of footprints relative to the trackway midline, but refer to the footprint axis when the morphology of the footprints themselves is described.

Gait terminology in this work follows that of Hildebrand (e.g., Hildebrand, 1965, 1980, 1989; see also Biknevicius and Reilly, 2006 for a review), which, according to Pfau et al. (2011), reflects the current consensus in studies dealing with different groups of tetrapods. It has to be noted that studies on fossil tracks often use a different terminology, which frequently becomes a source of confusion. The 'primitive alternate pace' and the 'amble', as defined in Leonardi (1987:48), is, respectively, termed a 'walking trot' and a 'pace' in Hildebrand's classification scheme.

Description	Size	URL
Photographs used for 3D model generation	2.96 GB	http://dx.doi.org/10.0.23.196/m9.figshare.5766348
Photogrammetric 3D-Models (.ply)	458 MB	http://dx.doi.org/10.6084/m9.figshare.5766366
Orthophoto	186 MB	http://dx.doi.org/10.6084/m9.figshare.5766372
High-resolution sitemaps	209 MB	http://dx.doi.org/10.6084/m9.figshare.5766384

TABLE 1. Additional data available via Figshare.

Photogrammetry and Measurements

Tracksite A was photogrammetrically documented by two of us (JNL and OW) during the field trip of the First International Congress on Continental Ichnology, held in El Jadida in April 2015. Our description of Tracksite B is based on data collected by one of us (SI) in 1988. For the photogrammetry of Tracksite A, two sets of photographs made by two separate cameras (a Sony DSC-RX100M2 and a Canon EOS 70D) were taken simultaneously, each aiming to cover the whole track surface. The photographs were taken under stable light conditions without direct sunlight, and approximately perpendicular to the track surface; a camera extension pole was used to reach the higher sections of the surface. The model was scaled based on two meter sticks placed on opposite ends of the surface. The on-site photogrammetric documentation was completed within one hour. Our photogrammetric model was calculated based on a total of 383 photographs (data provided via Figshare, see Table 1). Despite the two independent sets of photographs, a small region at the base of the surface remained poorly resolved as the result of insufficient coverage by close-up photographs. The inclusion of additional photographs made at the same time by other members of the field trip improved the resolution, whereas photographs made at different dates lead to a diminished model quality, probably due to different light conditions. For future work, we suggest taking at least three independent sets of photographs at larger track sites to avoid insufficient photograph coverage. Poorly resolved regions in models generated using the first set can then be easily improved by including matching photographs from subsequent sets of photographs.

The photogrammetric model itself as well as orthophotos were generated using Agisoft PhotoScan Professional 1.0.4 (www.agisoft.com), following the general procedure outlined in Mallison and Wings (2014). The horizontal plane of the model was automatically determined using the free software CloudCompare 2.6 (www.cloudcompare.org). Depth-color maps were generated using the free software Paraview 5.0 (www.paraview.org). A combination of orthophotos and depth-color maps highlighted both the topography and the texture of the track surface, allowing for the detection of trackways that had not been noted before, as well as for the generation of a detailed sitemap (Fig. 2–3; Supplementary Data 1, Fig. 2S–6S). Photogrammetric models, orthophotos, and depth-color maps used for analysis are available in full resolution via Figshare (Table 1).

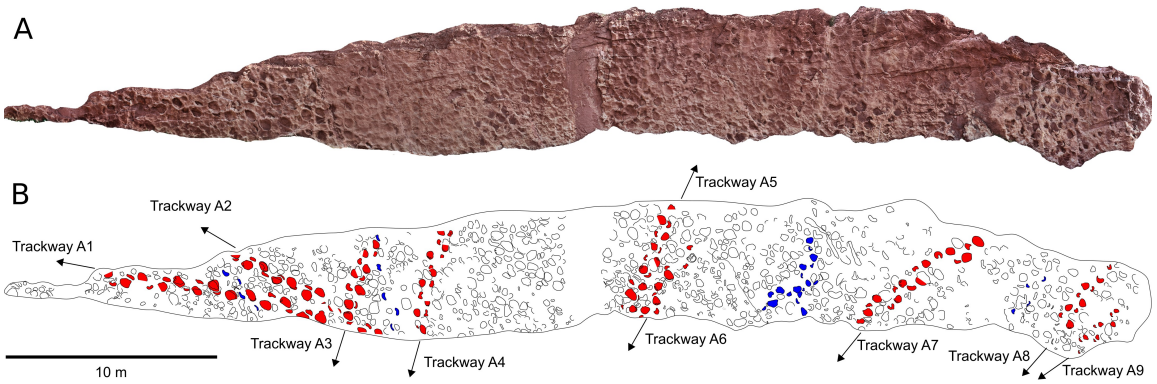

FIGURE 2. Photogrammetric orthophoto and sitemap of Tafaytour Tracksite A, showing Trackways A1–A9, five possible, unnumbered trackways, and many footprints without a clear trackway association; **A**, photogrammetric orthophoto; **B**, interpretative sitemap with recognized trackways highlighted in red, and possible additional trackways in blue.

Trackway parameters and footprint dimensions were calculated based on xy coordinates taken from the combined depth-color maps and the sitemap using the free software Inkscape 0.48 (www.inkscape.org). Five coordinates were defined for each footprint, describing the footprint length, footprint width, and the footprint center (usually the intersection between both lines), with the latter being used as the reference point for calculating trackway parameters. The coordinates were then processed with a specially designed spreadsheet written in the free software LibreOffice Calc 5.1 (www.libreoffice.org), in order to automatically calculate all footprint and trackway parameters employed herein, as well as to calculate mean-configuration coordinates (see below).

All measurements are defined as indicated in Fig. 4. We make a distinction between the 'manus-pes distance' (MPD) as defined in Farlow et al. (1989), which is measured between the reference points of manual and pedal prints of a couplet, and the parallel manual-pedal print distance (MPDp) defined herein, which removes the effects of divergent mediolateral positions of the pedal and manual prints. Although Marty (2008) defined the pedal rotation and manual supination angles based on the stride line towards the subsequent track only, we here calculate footprint rotation based on the subsequent, the precedent, and the opposite stride line, and take the mean of these three values. In order to quantify the medial to lateral position of the manual prints relative to the pedal print of a given set, we define a new parameter, the pedal-manual print angle (PMA), which is measured between the line connecting the pedal prints with the following manual print and the adjacent stride line (see section 'Trackway asymmetries'). Absolute locomotion speed is calculated according to Alexander (1976), using the formula $v \approx 0.25g^{0.5}SL^{1.67}h^{-1.17}$, where v = locomotion speed [m/s], g = gravitational constant (9.81 m/s^2), SL = stride length [m], and h = hip height [m], which can be estimated as four times pedal print length. Given the marked variability in pedal print lengths in the present tracksites, we here employ the apparent glenoacetabular distance (GAD) as an inde-

pendent proxy for trackmaker body size. Three separate formulae have been suggested to calculate GAD in sauropods, each assuming a different gait of the trackmaker (see section 'Trackway-based body size estimators' for details). Although these different approaches give differing estimations of total body size, they are here found to provide reliable estimates of relative body size. When not indicated otherwise, we measured GAD according to the formula MPDp + 3/4SL.

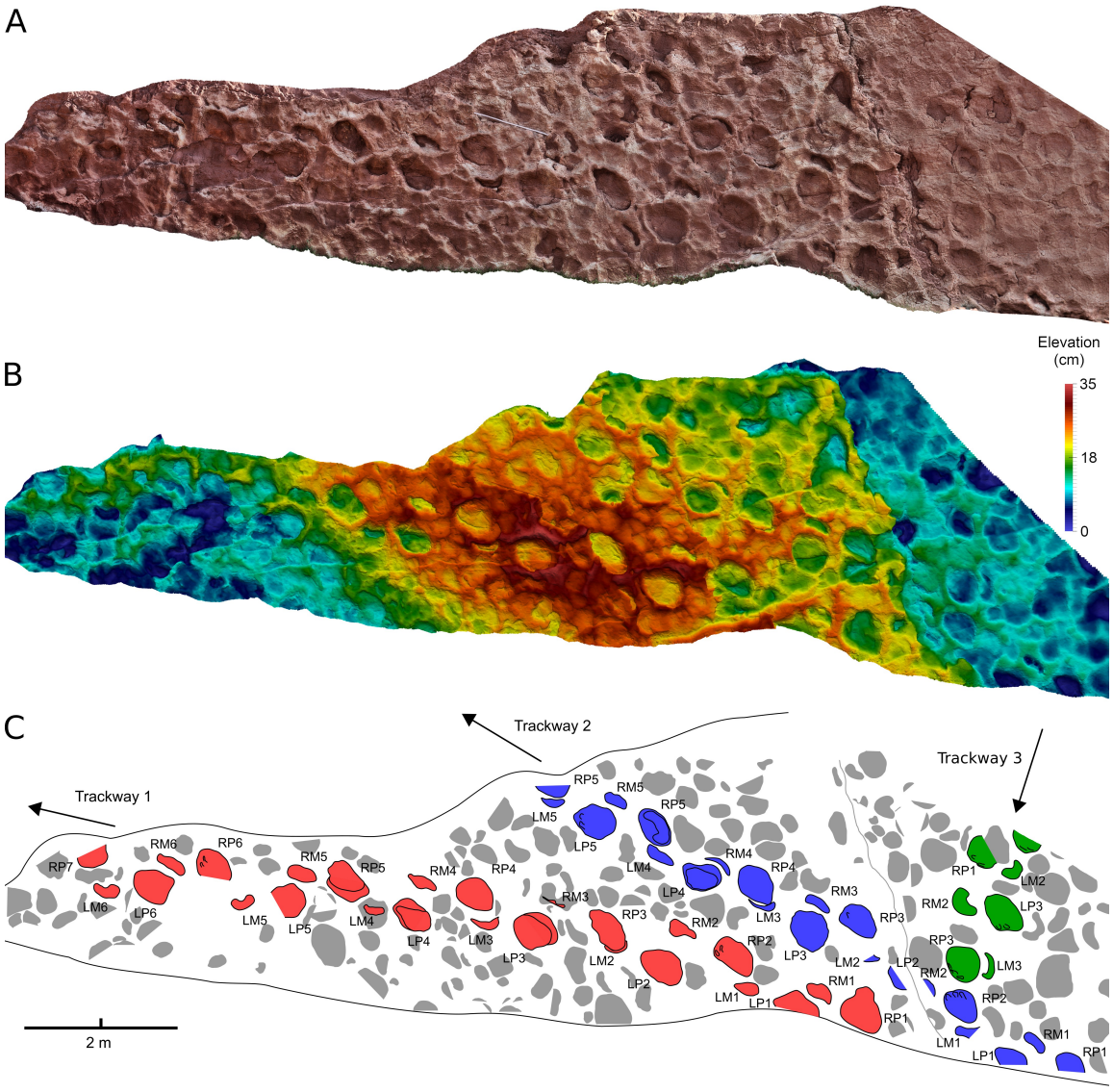

FIGURE 3. Detail of the easternmost section of Tafaytour Tracksite A, showing Trackways A1 and A2 in detail; A, photogrammetric orthophoto; B, photogrammetric depth-color map, where the deepest parts are shown in blue and the highest in red; C, interpretative sitemap, with Trackways 1 and 2 as well as part of Trackway 3 highlighted. [planned for whole page width]

Statistical analysis

Statistical tests were performed in the free programming environment R 3.2.5 (R Development Core Team, 2016) using a significance level of p=0.05, and include the Shapiro-Wilk test for normal distribution, the F-test for equality of variances, and the Student's t-test for the equality of means (see Hammer and Harper, 2006 for an overview). Mean configuration coordinates (see below) were calculated using LibreOffice Calc and plotted using the free software GnuPlot 4.6 (www.gnuplot.info).

In our comparative statistical analysis, we analyzed the 10 Tafaytour trackways as well as other small sized sauropod trackways based on data taken from the literature (Lockley et al., 1986, 2002b, 2004, 2006, 2014; Lim et al., 1989; Lockley and Santos, 1993; Dalla Vecchia, 1994; Meyer et al., 1994; Gierliński and Sawicki, 1998; Lee et al., 2000; Dalla Vecchia et al., 2001; Lockley et al., 2002a; Huh et al., 2003; Pérez-Lorente, 2003; Day et al., 2004; Nicosia et al., 2007; Marty, 2008; González Riga and Calvo, 2009; Castanera et al., 2011; Xing et al., 2011, 2013, 2014a, 2014b, 2014c, 2015a, 2016b, 2016c, 2016d, 2016e; Kim and Lockley, 2012; Fernández-Baldor, 2015; Marty et al., 2013; Mazin et al., 2016), resulting in a total of 79 trackways (Supplementary Data 2). Besides Morocco, the included trackways come from Switzerland, Germany, England, France, Italy, Croatia, Spain, Portugal, China, Korea, the US, Argentina, and Bolivia, and range from the Lower Jurassic to the Upper Cretaceous. We restricted the analysis to small-sized and small medium-sized trackways (pedal print length < 60 cm), in order to lessen the influence of possible constrains imposed by large body sizes. Measurements were taken directly from the literature when based on the measurement scheme of Marty (2008); parameters for all other trackways were calculated based on xy-coordinates taken from published trackway drawings. The analyzed data is provided in Supplementary Data 3 and can be directly imported into R.

Correlation tables were produced using the R package Hmisc 3.17 (Harrell Jr., 2016), employing both the parametric Pearson correlation coefficient and the Spearman rank-order correlation coefficient as a robust, non-parametric correlation measure. The Spearman coefficient was preferred when one of the variables cannot be considered normally distributed, as is the case in the absolute and relative measures for locomotion speed, and when relationships are not linear. Scatterplot matrices including frequency distribution plots were generated using the R package car 2.1 (Fox and Weisberg, 2011). Correlation analysis was carried out on 16 partly redundant variables. These include indicators of speed (the stride length/pes length ratio and the stride length/GAD ratio using all three GAD measures); of trackway gauge (the WAP/PL-ratio, the manual and pedal pace angulations, the average of the manual and pedal pace angulations, and the difference between the manual and pedal pace angulation); of body size (pedal print length and the three GAD measures); as well as the pedal rotation and manual supination angles. MANOVA as well as linear models using one dependent and n independent variables were carried out using PAST 3.14 (Hammer et al., 2001).

Principal Component Analysis (PCA) was carried out on five selected variables, namely the manual supination and pedal rotation angles; the average of the manual and pedal pace angulation, as an indicator for trackway width; the difference between the manual and pedal pace angulation; and the stride length/GAD ratio, as an indicator for relative speed. Variable selection was aimed to both minimize redundancy and maximize information content, and to reduce noise. Data values were standardized by subtracting the

mean of the variable and dividing the result by the standard deviation of the respective variable. PCA then was performed and plotted using the 'prcomp' and 'biplot' core functions of R.

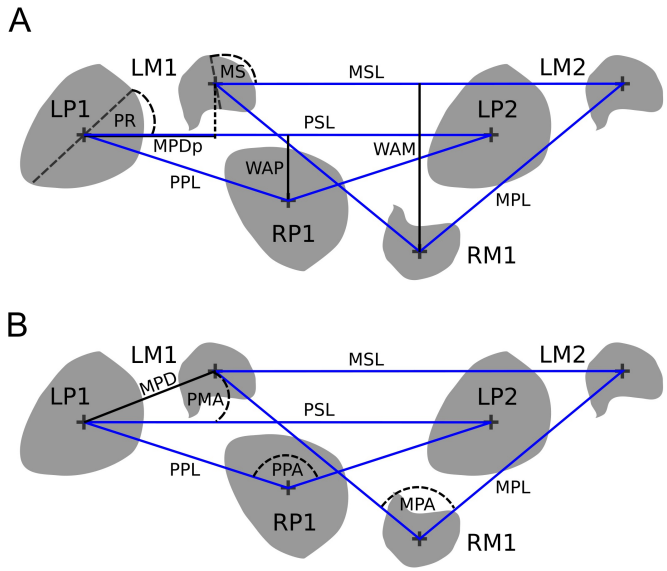

FIGURE 4. Measurements employed in this study, shown on a schematic diagram based on the mean configuration of Trackway A6, which shows a pronounced difference between the manual and pedal trackway width; **A,** diagram showing the pedal rotation and manual supination angles, the manual-pedal print distances and the widths of the angulation patterns; **B,** diagram showing the pace angulations as well as the pedal-manual print angle, which is introduced herein. **Abbreviations**: **P**, pedal print; **M**, manual print; **L**, left; **R**, right; **PP**, pedal pace length; **MPL**, manual print pace length; **PSL**, pedal print stride length; **MSL**, manual stride length; **PR**, pedal rotation angle; **MS**, manual supination angle; **PPA**, pedal pace angulation; **MPA**, manual pace angulation; **WAP**, width of the pedal print angulation pattern; **WAM**, width of the manual print angulation pattern; **MPD**, manual-pedal print distance; **MPDp**, parallel manual-pedal print distance; **PMA**, pedal-manual print angle.

RESULTS

In the following, we briefly discuss how trackways and their walking directions were identified, and summarize general observations on footprint morphology and trackway configurations. Detailed descriptions of the individual trackways, along with discussions on how individual footprints were assigned to their respective trackways, are provided in Supplementary Data 1.

Trackway Configurations

Trackways were identified based on the position, orientation, preservation, depth, size, and shape of successions of footprints. Walking directions can be difficult to determine due to the generally high supination angles of the manual prints, and in the case of Trackways A1 and A2 deserve further discussion. Data presented by Ishigaki (2007, 2009) was based on an assumed walking direction of both trackmakers towards

the east, whereas Enniouar et al., 2014 proposed the opposite, a walking direction towards the west. Footprints RP2 of Trackway A1 and RP2, RP3 and RP4 of Trackway A2 feature depressions that are consistent with claw marks in their position and orientation, suggesting a walking direction towards the east. Although the mean manual supination angles would be, in this case, unusually high for both trackways (>100°), the supination angle is even higher in Trackway A5, whose walking direction is unambiguous due to well preserved claw impressions. pedal print orientation and morphology is also in accordance with a direction to the east in most footprints but in LP2 and LP4 of Trackway A1 and LP1 of Trackway A2. Lack of detail and high morphological variability of the latter footprints indicate that the observed differences are the result of deformations and do not necessarily reflect the original orientation of the foot of the trackmaker. Consequently, Trackways A1 and A2 are here interpreted as leading towards the east.

The ten identified Tafaytour trackways derive from small to small medium-sized sauropod trackmakers, with an average pedal print length ranging from 23 to 54 cm and a GAD from 95 to 191 cm (Table 2). Trackway gauge is extremely variable amongst the trackways, ranging from very narrow to wide gauge (Fig. 3; Fig. 6A), and can differ considerably between the manual and pedal prints of a single trackway. Pedal pace angulation is significantly larger than the manual pace angulation in Trackways A1 ($p=0.0142$), A5 ($p=0.0016$), A6 ($p=0.005$) and A9 ($p=0.0054$); in Trackway A6, this difference is most extreme, accounting for 43° (Fig. 6B). Extremely narrow pedal trackway gauges were measured in Trackways A6 and A2, with pace angulation values of 143° and 141° and WAP/PL-ratios of 0.51 and 0.56, respectively. Trackway A2 also shows a high manual pace angulation averaging at 139°, rendering this trackway one of the narrowest sauropod trackways known. At the other extreme, the aberrant Trackway A9 is wide gauged with a pedal pace angulation of only 106° and a WAP/PL-ratio as high as 1.5 (Fig. 6A).

Pedal rotation varies from 14° to 38°. Strikingly, the manual supination angle varies between 0.6° in Trackway A9, indicating an anteriorly facing manus, and 106° in Trackway A5, indicating a posterolaterally facing manus (Fig. 6A). Supination angles are very high in the remaining trackways (70°–104°). Trackway asymmetries proved to be statistically significant in several cases. The left and right manual print pace lengths are significantly different in Trackway A1 ($p=0.0101$). Discrepancy between the left and right pedal print pace lengths reaches significance in Trackway A2 ($p=0.009$), Trackway A4 ($p=0.0498$) and Trackway A8 ($p=0.0343$). Manual prints can be displaced laterally relative to the pes footprints. The left and right pedal-manual print angles are significantly different in Trackway A4 ($p=0.03$) and Trackway A5 ($p=0.02$).

Trackway	A1	A2	A3	A4	A5	A6	A7	A8	A9	B1
PL (cm)	54	52	46	36	43	44	43	49	23	45
GAD (cm)	191	176	152	155	152	143	159	147	95	158
PR (°)	14	21	29	22	38	37	36	29	34	17
MS (°)	101	104	71	91	106	93	78	70	0.6	75
PSL (cm)	173	158	120	134	126	133	142	127	96	147
MSL (cm)	171	157	131	134	126	132	141	128	94	143
PP (cm)	93	83	72	80	73	70	86	75	59	80
MP (cm)	96	84	85	76	83	87	91	75	64	86
PPA (°)	136	141	115	113	121	143	112	115	106	134
MPA (°)	125	139	103	122	100	100	104	117	93	115
MPD (cm)	62	59	61	54	59	47	53	51	28	50
PMA (°)	2.3	-0.1	3.7	-3.4	7.3	15.2	5	-4.4	13.2	7

TABLE 2. Selected average measurements of the described Tafaytour trackways. For abbreviations see Fig. 3.

Footprint Morphology

Pedal print impression morphology at the Tafaytour Tracksites is typically sub-triangular, with a straight medial margin, a broad anterior margin facing anterolaterally, and a convex lateral margin. Digital traces are present in seven of the trackways as well as in isolated pedal impressions (Fig. 5A–B), and can be referred to digits I, II, III and IV. Claw impressions are frequently discernible within digital impressions I–III, but not for digital impression IV, which is less protruding and well-separated from digital impression III by a sedimentary bar (e.g., Fig. 5A–B; Trackway A6). If present, claw impressions are either directed anterolaterally (e.g, Fig. 5A–B), or deflected posterolaterally (e.g., Trackway A3 and A6), depending on the degree of digital flexion. The impression of digit I is usually the broadest and most salient, forming the leading edge of the footprint. In some footprints, however, the impression of digit II is the most salient (e.g., Fig. 5A–B); this variation can occur even within the same trackway (Trackway A4).

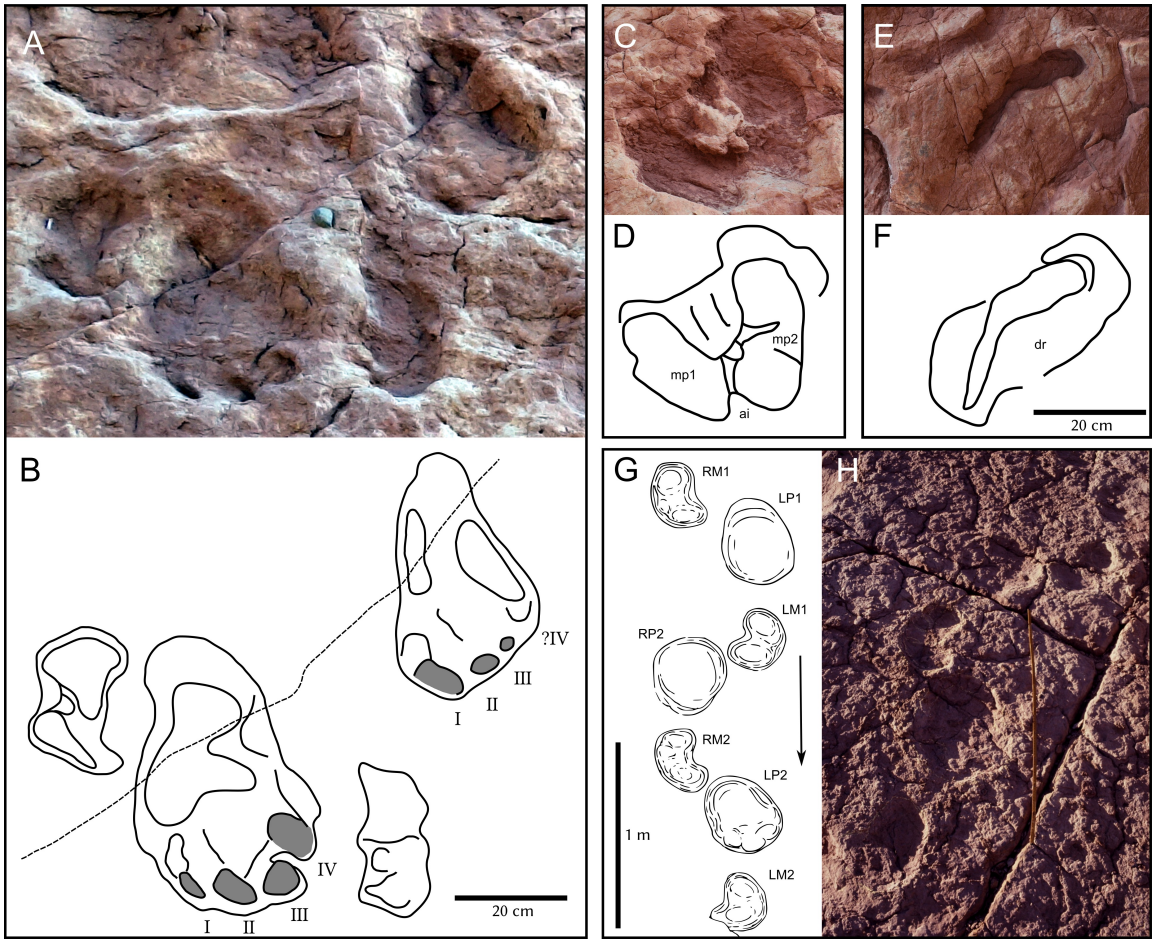

FIGURE 5. Details of Tafaytour Tracksites A and B. **A**; photograph in oblique view of footprints without an obvious associated trackway pattern in Tracksite A. Two pes impressions are elongated and display well-preserved claw and digital impressions. Manual impressions are subdivided into two pads; **B**, interpretative drawing of the detail shown in A, drawn in top view based on photogrammetric data (see Supplementary Data 1); **C,** close-up of a manual impression LM4 of Trackway 7, showing a pronounced horseshoe-shape; **D,** interpretative drawing of C, drawn in top view based on photogrammetric data; **E**, manual impression showing a slit-like morphology, Tracksite A; **F**, interpretative drawing of E based on photogrammetric data; **G**, interpretative drawing of Trackway B1 of Tracksite B drawn by one of us (SI) based on data collected in 1988. The arrow shows the direction of travel of the trackmaker; **H**, photograph of Trackway B1 (SI, 1988). **Abbreviations: I-V**, digital impressions I, II, III, and IV; **mp**, manual pad impression; **ai**, anterior indentation; **dr**, displacement rim; **R**, right; **L**, left, **P**, pedal print; **M**, manual print.

Manual print shapes are highly variable, especially in their anterior to posterior length, ranging from very narrow, slightly curved to crescent-shaped slits (Fig. 3, 5E–F) to oval, dumbbell-, or semicircle-shaped impressions (Fig. 5A–B, G–H) as well as tightly-bond horseshoe-like shapes that are almost as long as wide

(Fig. 5C–D). This variation in manual print morphology might be the result of variable substrate conditions, as is discussed below. In five of the trackways (Trackways A4, A6–A8, B1; Fig. 5G-H; Supplementary Data 1, Fig. 9S) and numerous isolated footprints (e.g., Fig. 5A–B), the manual print is subdivided into two separate oval-shaped impressions that are arranged in a "V"-shape and separated by an axial bulge on the floor of the footprint and/or a constriction formed by the anterior and posterior footprint margin. Such a subdivision is not evident in trackways where the anterior to posterior length of the manual print is strongly reduced (Trackways A1, A2, and A5). Several manual impressions of these trackways (RM2 and RM4 of Trackway A1; LM4 of Trackway A2; LM4 of Trackway A5) show a distinctly broadened medial half, possibly indicating the presence of a similar subdivision. Manual prints often show a spur-like expansion at the posteromedial edge. Although often assigned to sauropod pollex impressions in the literature (e.g., Castanera et al., 2016), it is not present in well-preserved horseshoe-shaped impressions. If the manual print morphologies observable at the tracksites are indeed preservational variants of the tracks of a single taxon, this spur-like extension would likely be an artifact of footprint deformation.

Statistical Analysis of Small-Sized Sauropod Trackways Globally

Locomotion speed in our sample (n=79) varies from 0.43 to 2.7 m/s, averaging at 0.9 m/s. The frequency distribution has a strong positive skew (Supplementary Data 1, Fig. 1S), suggesting that locomotion speeds usually fall within the lower third of their possible range, with trackways showing faster relative locomotion speeds becoming progressively rarer. This distribution is similar to, but more pronounced, than those observed by previous studies for both bipedal dinosaur (Thulborn, 1984) and sauropod trackways (Marty, 2008). The average pedal pace angulation is significantly greater than the average manual pace angulation (116° vs. 102°, $p<0.0001$). Frequency distributions of both the pedal rotation and manual supination angles show a broad peak, indicating marked variability (Supplementary Data 1, Fig. 1S). The pes is generally rotated outwards, with an average rotation of 21°, a minimum of -4° and a maximum of 44°. Manual supination is generally high, averaging at 43° in the complete sample, and is 38° when Tafaytour trackways are excluded. The minimum value is -6°, indicating an individual with fully pronated manus, whereas the maximum value is as high as 106°, indicating a posterolaterally oriented manus. Very low rotation values (i.e., near-anterior orientations), however, are as rare or even rarer as very high values in both the manual and pedal prints (Supplementary Data 1, Fig. 1S).

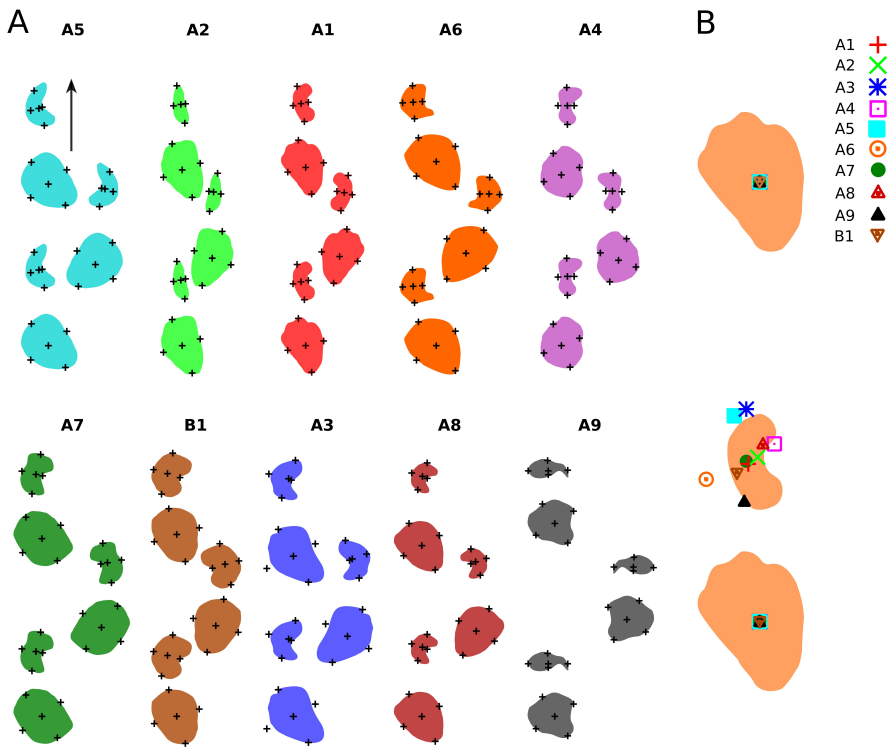

FIGURE 6. Trackway mean configurations; **A**, mean configuration plots of the Tafaytour trackways calculated from mean trackway parameters and scaled to the same GAD (see text for details). Silhouettes are added to aid visual identification, and represent selected footprints of the respective trackway. Trackways are arranged in descending order according to their manual supination angle; **B**, mean configuration plot of the Tafaytour trackways scaled to the same stride length, highlighting the average position of the manual prints relative to the two pedal prints of a stride.

Correlation analysis of the variables reveals the degree of correlation between trackway gauge, locomotion speed, body size, pedal rotation and manual supination (Tables 3–4). As expected, the manual pace angulation is positively correlated with the pedal pace angulation (R=0.47, Spearman). The difference between the manual and pedal pace angulation values is significantly negatively correlated with measures of trackway gauge, i.e., the wider the trackway, the greater the discrepancy between the pedal and manual pace angulation. Correlation between pedal rotation and manual supination is weak or absent (R=0.09, Spearman). Pedal rotation is not significantly correlated with any other variable. Manual supination is negatively correlated with all employed proxies for relative locomotion speed ($p<0.001$, respectively, Spearman), including the three St/GAD ratios (Fig. 7A) and the St/PL ratio (Fig. 7B). The Spearman coefficient suggests a stronger and more significant correlation than the Pearson coefficient (Tables 3–4), indicating that the relationships are not linear. Besides relative speed, manual supination is negatively correlated with a second variable, the WAP/PL-ratio, which is a measure for trackway gauge width ($p<0.01$, Spearman). A linear model, in which the St/GAD and WAP/PL ratios are the independent and manual supination is the dependent variable, describes 20% of the variability.

	WAP/PL	GAD	PL	St/PL	St/GAD	PA	PPA	MPA	PR
GAD	-0.02								
PL	-0.26*	0.82***							
St/PL	0.43***	0.23*	-0.16						
St/GAD	0.18	0.01	0.1	0.50***					
PA	-0.42***	0.33**	0.16	0.41***	0.2				
PPA	-0.65***	0.22	0.13	0.27*	0.15	0.80***			
MPA	-0.11	0.37***	0.15	0.42***	0.12	0.84***	0.47***		
PR	0.08	0.04	0.05	-0.01	-0.04	-0.04	-0.14	0.04	
MS	-0.33**	0.05	0.08	-0.41***	-0.41***	0.09	0.19	0.02	0.09

TABLE 3. Correlation table showing the Spearman rank correlation coefficient for selected parameters (n=72). Stars indicate significance level, with * = p<0.05; ** = p<0.01, and *** = p<0.001.

	WAP/PL	GAD	PL	St/PL	St/GAD	PA	PPA	MPA	PR
GAD	-0.01								
PL	-0.23*	0.82***							
St/PL	0.43***	0.26*	0.17						
St/GAD	0.16	-0.01	0.07	0.53***					
PA	-0.49***	0.35***	0.19	0.38**	0.15				
PPA	-0.70***	0.24*	0.15	0.29*	0.17	0.85***			
MPA	-0.19	0.38***	0.16	0.38**	0.05	0.88***	0.56***		
PR	0.11	0.03	0.03	0	-0.03	-0.02	-0.1	0.07	
MS	-0.37***	0.06	0.1	-0.28*	-0.35**	0.19	0.26*	0.12	0.09

TABLE 4. Correlation table showing the Pearson correlation coefficient for selected parameters (n=72). Stars indicate significance level, with * = p<0.05; ** = p<0.01, and *** = p<0.001.

Principal component analysis (PCA) was conducted on five selected variables (Fig. 8). PC1 (28% of variance) indicates a negative relationship between the manual supination angle and the stride length/GAD ratio (and thus, locomotion speed), which is statistically significant, as discussed above. PC2 (25% of variance) describes a negative relationship between the average pace angulation and the difference between the manual and pedal pace angulation, indicating that the wider the trackway, the greater the discrepancy between manual and pedal pace angulation values, complying with the result obtained from correlation

analysis (see above). Relationships proposed by PC3 (21% of variance) and PC4 (18% of variance) could not be confirmed by correlation analysis. Tafaytour trackways generally show very high loadings on PC1, and are best separated from other trackways based on this principal component. MANOVA performed on the same five variables reveals a significance difference between the Tafaytour trackways and the remaining sample (p=3.7E-06).

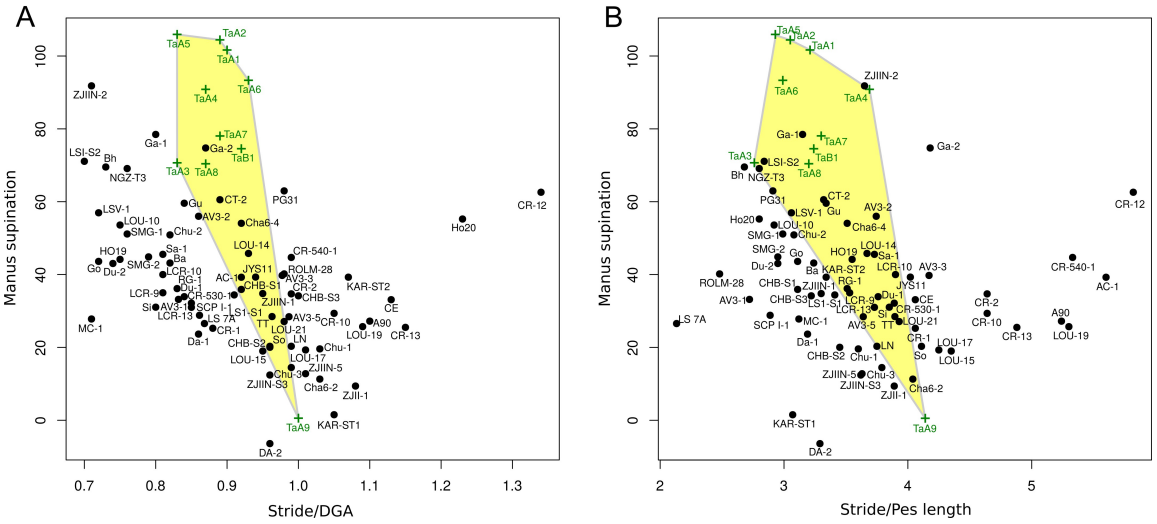

FIGURE 7. Statistical analysis of a larger sample (n = 79) of small-sized sauropod trackways from around the world. Plus signs represent the Tafaytour trackways described herein. See Supplementary Data 6 for references and information on the individual trackways; **A**, biplot, showing the relationship between the manual supination angle and the stride length/GAD ratio, which is a proxy for relative locomotion speed, revealing a clear negative correlation; **B**, the same negative correlation is evident when another speed proxy is used, the stride/pes length ratio.

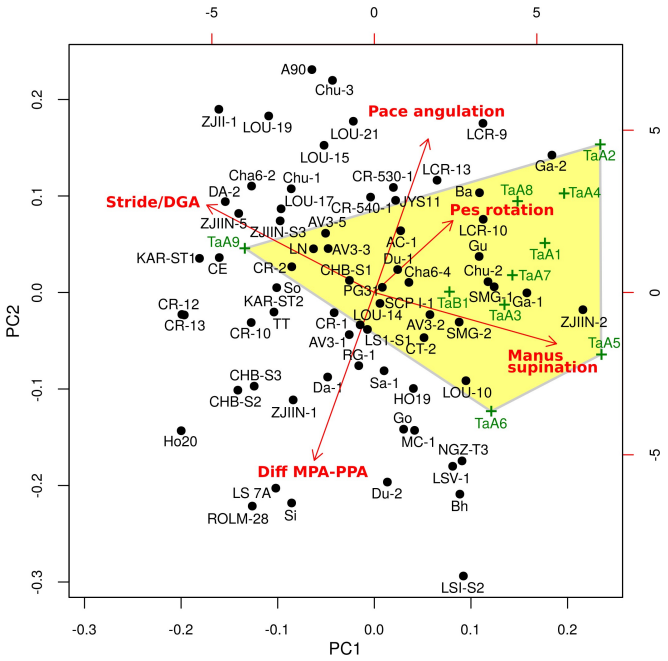

FIGURE 8. Biplot illustrating the results of PCA analysis carried out on five selected variables: the manual supination, the pedal rotation, the pace angulation, the difference between the manual and pedal pace angulation (Diff MPA-PPA), as well as the relative speed (stride length/GAD). Tafaytour trackways are indicated with plus signs. PC1 describes a negative relationship between relative speed and manual supination, and PC2 a negative correlation between the pace angulation and the difference between the manual and pedal pace angulation. pedal rotation is not strongly correlated with either of the two PCs, as indicated by the shorter arrow.

DISCUSSION

Variability and Comparisons

Tafaytour Tracksite A represents a highly trampled surface that preserves hundreds of partially superimposed sauropod footprints, complicating the recognition of individual trackways. High degrees of dinoturbation can be observed at many tracksites, especially when involving sauropod dinosaurs (e.g., Lockley and Conrad, 1989; Richter and Böhme, 2016). Preservational quality of individual footprints in highly bioturbated sauropod tracksites is often poor, as is, e.g., the case in the Moutier ‘dinosaur disco site’ in Switzerland, where individual trackways are barely identifiable (Meyer and Thüring, 2003). The preservation of distinct trackways and clear digit impressions at the present tracksites is therefore remarkable. Another noteworthy feature is the comparatively high percentage of manual prints, including at least three manus-only trackways, indicating a preservational bias against the pedal prints. Last but not least, the tracksite is characterized by an unusually high diversity of footprint morphologies and trackway patterns.

The marked variability of footprint shapes raises the question whether more than one trackmaker species was present, or whether it can be entirely attributed to variations in foot kinematics and substrate properties. Although generally well-preserved with digit impressions in many instances, the footprints of the tracksites are heavily affected by deformation, probably caused by changing substrate conditions in both time and space, and by other footprints subsequently left nearby. The pedal impressions are markedly longer than wide in some well-preserved examples (e.g., Fig. 5A–B), but can be as wide as long or, as in Trackway A9, even wider than long. At least in the latter trackway, this aberrant morphology can be ascribed to deformation given the marked variability within this trackway in both pes shape and size, and is possibly the result of suction effects acting during withdrawal of the foot from the sediment, drawing the footprint wall into the footprint and causing significant foreshortening of the impression. The most striking deformation is found in the manual prints, which incorporate many of the principal morphologies described for sauropod manual prints in the literature (e.g., Castanera et al., 2016), including narrow, slightly curved to crescent-shaped impressions; kidney- and dumbbell-shaped impressions; as well as tightly-bound horseshoe-shaped impressions. The kidney-shaped manual print morphology (e.g., Trackway B1, Fig. 5G–H) likely represents a preservational variant of the tightly-bond horseshoe-like morphology best shown by Trackway A7 (Fig. 5C–D), as both incorporate two characteristic oval impressions arranged in a "V"-like configuration, and as Trackway A7 also includes kidney-shaped impressions comparable to those in Trackway B1. The same oval impressions can be seen in Trackway A4, which predominantly shows the dumbbell-shaped morphology. Likewise, several trackways (Trackways A1, A3, A5, and A8) feature both very narrow, slit-like manual prints and much broader kidney-shaped or even horseshoe-shaped ones. The slit-like shape most probably results from suction effects closing the impression during foot uplift, or from subsequent deformation caused by the displacement rim of pedal prints left nearby. Variability of other features may be controlled by behavior, such as the orientations of the digital impressions in the pedal impressions, which can be directed anterolaterally (e.g., Trackway A4) or laterally to posterolaterally (e.g., Trackway A3). Anterolaterally directed claw marks indicate digital extension, possibly enhancing traction while walking on slippery substrates, whereas laterally to posterolaterally directed marks indicate plantar flexion (Bonnan, 2005; Hall et al., 2016). Furthermore, the degree of digital projection varies within trackways, with either the impressions of digits I or II being the most protruding (e.g., Trackway A4, RP2 and LP3). Therefore, the observed variability might be entirely due to interference with other footprints, trackmaker behavior, and varying substrate properties, probably in both time and space.

Likewise, the striking diversity in trackway patterns present at the tracksites might reflect trackmaker behavior rather than anatomical diversity. Both the manual supination angle and the trackway gauge have been shown to vary greatly even within single trackways, depending on trackmaker behavior (Marty, 2008; Castanera et al., 2012). Thus, the relatively longer strides, the markedly lower manual supination angles, and the reduced parallel manual-pedal print distance in the atypical Trackway A9 might be effects of the higher relative locomotion speed. As a conclusion, the notable variability present at the tracksites cannot be regarded as unequivocal evidence for separate trackmaker species.

The assignment of ichnotaxonomic labels to dinosaur tracks can rarely be done unequivocally, because ichnotaxa are rarely defined based on clear-cut autapomorphies. As most features generally used to distinguish sauropod ichnotaxa (e.g., Marty, 2008) are extremely variable in the described set of trackways, an objective ichnotaxonomic assignment is not possible at present. That being said, the subdivision of the

manual impressions into two separate oval pads arranged in a "V"-like configuration is unusual for sauropod tracks and was, to our knowledge, previously only known from the l'Assif-n-Sremt tracksite of Morocco, which is Pliensbachian in age (Jenny and Jossen, 1982; Ishigaki, 1988). The pedal prints are comparable with other reported sauropod tracks from the Middle Jurassic (Dutuit and Ouazzou, 1980; Romano et al., 1999; Day et al., 2004; Santos et al., 2009; Brusatte et al., 2016). Trackways from the Portuguese Galinha tracksite feature a claw impression associated with digital impression IV (Santos et al., 2009), which is not evident in any of the Tafaytour trackways, possibly due to loss or reduction of ungual IV in the trackmaker.

Trackway-Based Body Size Estimators

Estimators of body size are of crucial importance for the interpretation of fossil trackways. Body mass can be approximated based on footprint area or volume (e.g., Kubo, 2011; Schanz et al., 2013). Linear dimensions of the trackmaker, most importantly the hip height, are most frequently approximated using the pedal print length (Thulborn, 1990). Alexander (1976) suggested that hip height in sauropod, theropod and ornithopod dinosaurs can be estimated as four times pedal print length as a rule of thumb, providing the basis for estimations of absolute locomotion speeds based on trackways. In sauropods, however, footprint dimensions are often significantly affected by factors unrelated to the anatomy of the trackmaker (e.g., Lockley et al., 2002a; Romano et al., 2007), such as suction effects of the substrate, undertrack preservation, or orientation of the digits, which can be directed anteriorly or laterally, depending on behavior (González Riga, 2011; Hall et al., 2016). These factors can cause a systematic over- or underestimation of foot size, and thus cannot necessarily be overcome by simply taking the mean of multiple footprints of a trackway segment. An evaluation of the influence of these factors is difficult because most sauropod pedal prints are preserved as indistinct circular to oval impressions lacking anatomical detail.

An alternative size proxy, the GAD, is robust against the above-mentioned factors (Salisbury et al., 2017), but requires interpretations of the gait of the animal (Leonardi, 1987). Three different approaches have been proposed for sauropod trackways (Fig. 9). The first, developed by Baird (1952, 1954) for salamander and *Chirotherium* tracks, assumes a walking trot without a period of suspension, as it can be found in many modern amphibians and reptiles (Baird, 1952, 1954; Leonardi, 1987; Farlow et al., 1989). This gait is characterized by a contralateral (diagonal) limb pair moving forwards simultaneously while the other is in stance phase. The moment the support of the animal shifts from one limb pair to the other, all four limbs will be contacting the ground. In this moment, the position of the glenoid fossa roughly corresponds to the midpoint between the left and right manus position, and that of the acetabulum to the midpoint between the left and right pes position. In a trackway, the GAD can therefore be measured between the midpoints of a left (or right) pedal pace and the following right (or left) manual pace (Fig. 9B); this corresponds to the parallel manual-pedal distance plus half a stride (Baird, 1954; Leonardi, 1987). This is the most commonly employed approach to estimate the GAD in sauropod trackways (e.g., Marty, 2008), although the walking trot is rarely considered a feasible option in studies concerned with sauropod locomotion, as discussed below.

Aberrant formulae have to be used when the contralateral limb pair is not synchronized in its movement. In his approach to estimate body size of *Chirotherium* trackmakers, Soergel (1925) assumed a walk where

the contralateral limb pair moves one-half of the duration of one step cycle out of phase (corresponding to a limb phase of 0.75), which is equivalent to the lateral-sequence singlefoot walk of the Hildebrand gait classification scheme (Biknevicius and Reilly, 2006). At one moment during the step cycle, both hind limbs and the right (or left) forelimb would be in stance phase, while the left (or right) forelimb, being moved forwards, would be on level with the right (or left) forelimb. The GAD, consequently, can be measured between the midpoints of a left (or right) pes pace and the most advanced footprint of the following right (or left) manus pace (Soergel, 1925; Baird, 1954). This corresponds to 3/4 of the stride plus the parallel manual-pedal distance (Leonardi et al., 1987). It has to be noted that this formula was misquoted in both Vila et al. (2013) and Stevens et al. (2016), where it is given as SL/3 + MPDp instead of the correct 3/4SL + MPDp.

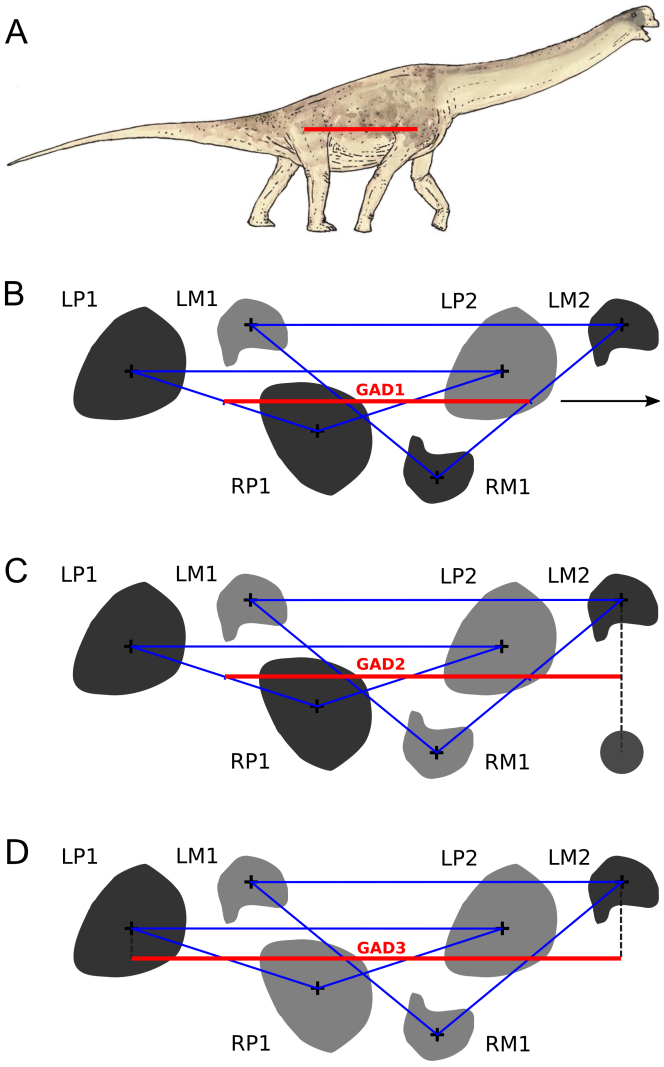

FIGURE 9. Diagram showing the three different approaches for calculating the apparent glenoacetabular distance (GAD) for sauropod trackways; **A**, life reconstruction of a generalized sauropod (artwork by

Joschua Knüppe). The bar represents the horizontal GAD, which can be measured in the trackways; **B**, approach assuming the walking trot. The moment the animal shifts its weight from one diagonal limb pair to another, four feet will contact the ground (dark grey); the GAD can be measured between the midpoints of the pedal- and manual prints; **C**, in a lateral-sequence singlefoot walk, only three feet will contact the ground at the same time. The right manual print is currently being dragged forwards (gray circle), reaching the height of the left manual print in a situation where both hind feet contact the ground; **D**, in a walking pace, a ipsilateral manual and a pedal print will contact the ground at the same time; the GAD can be measured between both.

A third formula has to be used when a walking pace gait can be assumed, where the ipsilateral fore- and hind limb are moving forwards while the contralateral fore- and hind limb are in stance phase, without periods of suspension. Assuming an exact walking pace, the GAD can be measured between coupled manual and pedal prints of the same step cycle. In sauropod trackways, the pedal impression of the next step cycle lies in between the coupled manual and pedal prints; the GAD therefore needs to be defined as the stride plus the apparent parallel manual-pedal print distance (Leonardi, 1987; Farlow et al., 1989).

Since the gait employed by sauropod dinosaurs is unknown, it is unclear which of the three approaches provides the most accurate body size estimations (Stevens et al., 2016). Farlow et al. (1989) discarded the first approach because sauropod pedal prints frequently overprint manual prints, which is not in accordance with an exact walking trot. Casanovas et al. (1997) and Vila et al. (2013) measured GAD/hip height-ratios in both selected trackways and skeletal reconstructions, in order to make inferences on the limb phase (and thus, gait) of the trackmakers. In skeletal reconstructions, this ratio was found to be close to one on average for both titanosaurs (Vila et al., 2013) and sauropods in general (Casanovas et al., 1997), and is similar in both small and large-sized individuals at least in some titanosaurs (Vila et al., 2013). Mazzetta and Blanco (2001) gave a slightly higher estimate of 1.09 (standard deviation = 0.11). Both Casanovas et al. (1997) and Vila et al. (2013) found that the analyzed trackways correspond most closely with the GAD/hip height-ratio predicted by the skeletal reconstructions when a walking pace (referred to as “amble gait” by these authors) is assumed for the calculation of the GAD. A walking pace was also proposed by Mezga et al. (2007). Mazzetta and Blanco (2001), however, noted that the walking pace is unstable at slow speeds, instead suggesting a lateral-sequence singlefoot walk. A lateral-sequence gait was also considered the most likely gait by both Alexander (1985) and Henderson (2006a).

In our sample, the average GAD/hip height ratio is 0.77, 0.99 and 1.21 when the walking trot, the lateral-sequence singlefoot walk, and the walking pace are assumed, respectively. Thus, the lateral-sequence singlefoot walk model is most closely matching the values predicted from skeletal reconstructions, which, as discussed above, are close to 1 (Casanovas et al., 1997; Mazzetta and Blanco, 2001; Vila et al., 2013). This gait can therefore be considered the most likely gait employed by the sauropods of our sample. In modern tetrapods, the lateral-sequence singlefoot walk is abundant at low speeds, and frequently employed when not energy economy but stability is to be maximized (Biknevicius and Reilly, 2006); it is also the most stable gait when at least three feet are kept on the ground at all times (McGhee and Frank, 1968), as it was argued to be the case in sauropods (Henderson, 2006a). Consequently, we employ the formula 3/4SL +

MPDp, which assumes the lateral-sequence singlefoot walk, for all our GAD estimations based on trackways.

Importantly, the discussed approaches make assumptions on the trackmaker's body length (Leonardi et al., 1987). In long-bodied trackmakers and/or when stride lengths are short due to low locomotion speeds, pedal and manual prints of the same cycle can be separated by two or more intermediate pedal and manual prints belonging to other step cycles; in such trackways, one or more additional stride lengths have to be added to the estimated GAD (Leonardi, 1987). Stevens et al. (2016) found that many sauropod trackways from the highway A16 in Switzerland show very short strides relative to the respective pedal print lengths, and suggested that in sauropods the manus could have been two or three, or even four steps ahead of the pes at any time during locomotion. For our sample of small-sized sauropod trackways from around the world (n = 79), we calculated GAD in various ways, employing the separate formulae in combination with different assumptions regarding the number of steps in between the respective step cycle. Assuming a lateral-sequence singlefoot walk, the mean GAD/hip height-ratio of the trackways of our sample is close to 1 (0.997), which closely conforms with the ratio derived from skeletal reconstructions, as discussed above. However, when one additional stride is added to the estimated GAD, the ratio would be nearly twice the hip height, which is not in accordance with published skeletal reconstructions. Consequently, it can be assumed that no additional strides have to be added for GAD calculations for most of the small-sized sauropod trackways sampled herein.

Each of the two discussed body size estimators comes with practical problems. A comprehensive analysis quantifying the possible effects of anatomy, gait and speed on the GAD measurements in trackways of modern animals is still lacking. In the Tafaytour trackways, the GAD, when measured at every possible location along the respective trackway, shows a significantly smaller coefficient of variation (CV) than the pedal print length ($p<0.01$). This indicates that the GAD is, at least, the more repeatable measurement.

A Method for Visual Comparisons of Mean Trackway Parameters

Unlike footprint morphologies, trackway configurations can be completely described by linear and angular measurements. Assuming a symmetrical gait, the average relative footprint positions of a quadrupedal trackway can be captured using only four values: the mean values of the stride and pace lengths of both the pedal and manual prints, and of the manual-pedal print distance. Two additional values, the mean manual supination and pedal rotation angles, describe the footprint orientations with respect to the direction of travel. The trackway configuration described by these six variables is henceforth called a mean configuration.

Mean configurations remove all variability within a trackway segment. They also remove trackway asymmetries, including discrepancies between left and right pace lengths, and lateral displacements of the manual relative to the pedal prints. The morphology of fossil footprints is controlled by three factors, namely the anatomy of the trackmaker, substrate properties, and behavior (Falkingham, 2014). This concept may be extended to trackway configurations. Intra-trackway variability can convey valuable information on trackmaker behavior. However, when the anatomy of the trackmaker is of interest, e.g., for trackmaker identification or for ichnotaxonomic purposes, this variability is unwanted noise (Thulborn, 1990:116–117).

Likewise, trackway asymmetries in sauropods usually represent peculiar behavior or pathologies of the individual (McCrea et al, 2015), and can complicate comparisons of separate trackways (although they may contain information on the anatomy of the trackmaker). In such cases, it can be beneficial to analyze the mean configuration, variability, and asymmetry of a trackway separately.

The relative position of the pedal and manual prints to each other is difficult to imagine from mean values alone. Here we visualize the mean configuration by plotting a set of xy-coordinates calculated directly from the six basic measurements, assembled with footprint length and width (Fig. 6A). These mean configuration plots were standardized for size (GAD), position, and orientation, allowing for direct visual comparisons of separate trackways. An OpenDocument spreadsheet calculating mean configuration coordinates from basic measurements is provided in Supplementary Data 4. Additionally, the data was scaled to the same stride length, allowing for plotting the position of the manual relative to the pedal prints (Fig. 6B). This plot indicates that the relative manual position is equally variable anterior to posterior and medial to lateral.

Trackway Asymmetries

Trackway asymmetries, as defined herein, encompass all discrepancies in the mean values of trackway parameters between the left and right sides. Asymmetries include both discrepancies in the anterior to posterior position of left relative to right footprints, and in the medial to lateral position of the manual relative to pedal prints.

Discrepancies in left and right pace lengths have been described in a number of cases for both bipedal and quadrupedal dinosaur trackways. Often referred to as 'limping dinosaurs', this gait pattern is commonly explained by assumed pathologies in the limb that leaves the longer pace (Dantas et al., 1994; Lockley et al., 1994b; Ishigaki and Lockley, 2010; McCrea et al., 2015; Razzolini et al., 2016). Farlow (written communication in Dantas et al., 1994:47) also suggested that some individuals could simply have been left- or right footed. Sauropod trackways exclusively consisting of or dominated by manual prints from the Jurassic Iouaridène Basin of the Morocco, which show extreme manual pace length discrepancies, have been interpreted as possible evidence for swimming behavior (Ishigaki, 1989; Ishigaki and Matsumoto, 2009a). Of the ten trackways described at Tafaytour, three examples show statistically significant left-right discrepancies in the pedal pace lengths, and a fourth example in the manual pace lengths (Supplementary Data 1). Given the high proportion of asymmetrical trackways at Tafaytour, possible pathologies appear unlikely to constitute the sole explanation (cf. Lockley et al., 1994b). Instead, these left-right discrepancies in sauropod trackways might in many cases merely represent individual behavior.

Discrepancies in the medial to lateral position of the manual relative to the pedal prints result in an offset of the pedal and manual trackway midlines. For sauropod trackways, this phenomenon has been first described by Ishigaki and Matsumoto (2009a) and is known as 'off-tracking'. Off-tracking can occur in straight trackway segments, but is most pronounced in turning trackways (Ishigaki and Matsumoto, 2009b; Castanera et al., 2012; Xing et al., 2015c). In order to quantify this phenomenon, we define a new parameter, the pedal-manual print angle, between the line connecting the pedal with the following manual print and the adjacent stride line (Fig. 4B). In the Tafaytour trackways, the left and right pedal-manual print an-

gles are significantly different in two examples (A4 and A5), suggesting that off-tracking might be a common phenomenon in sauropod trackways even when the trackway course is relatively straight.

Inferences on Sauropod Locomotion and Forelimb Orientation

The anatomy of the sauropod manus is unique among vertebrates, featuring parallel metacarpals arranged in an arched to U-shaped colonnade and strongly reduced or absent phalanges (e.g., Christiansen, 1997; Bonnan, 2003). The pes is remarkably different from the manus, showing a semi-plantigrade posture, a large plantar pad, robust digits, and pronounced asymmetry, and was obviously adapted for quite different functions (e.g., Christiansen, 1997; Bonnan, 2005). Unlike the hind limb, the forelimb probably had no major role in propulsion, but mainly served as a weight-bearing structure (e.g., Christiansen, 1997; Milàn et al., 2005).

The variability of manual supination angles in sauropod tracks remains poorly understood. Marty (2008) described a minute sauropod trackway (S12) from the Upper Jurassic Chevenez-Combe Ronde site of the Swiss Jura Mountains that showed very high supination angles in its middle section, but low angles within the distal sections. This indicates that the rotational range of motion in the sauropod forelimb is much greater than previously thought, and that variation in manual supination angles can be explained by trackmaker behavior (Marty, 2008). In the Swiss trackway, manual supination values are coupled with an unusually exterior position of the manual relative to the pedal prints. According to Marty (2008), the high supination angle and exterior position of the manual prints was probably not related to the minute body size of the individual (pedal print length: 19.6 cm) but can be explained by "an atypical gait due to an unusual behavior such as alternately turning the neck to the left and right side" (p. 126). Other trackways with high manual supination angles from the Jura Mountains were reported by Marty et al. (2013) and Mazin et al. (2016).

Kim and Lockley (2012) described two trackways from the Lower Cretaceous of South Korea showing manual supination angles of about 90°. The manual prints are well separated from the pedal prints and show five distinct digital impressions, whereas in other known sauropod tracks only impressions of digits I and V can be differentiated (but see Lockley et al, 2002; Santos et al., 2009). In an attempt to explain this prominent manual morphology and orientation, Kim and Lockley (2012) suggested that the described individuals could have placed more weight on the posterolateral portion of the manus, allowing for the registration of digit impressions.

The most extensive record of sauropod trackways with high manual supination angles has been reported from China. At least eight such trackways are known, showing average supination angles of between 51° and 86°, with maximum values of up to 131° (Xing et al., 2010, 2013, 2014a, 2015a, 2015b, 2016a; Zhang et al., 2012). Xing et al. (2015a) provided an extended discussion of the significance of sauropod manual supination angles in Chinese trackways, concluding that forelimb orientation in sauropods was not tightly constrained. The observed degree of variation of manual supination angles would have been possible due to large amounts of cartilage in the joints. Small rotational movements in the proximal forelimb, especially at the glenoid, would translate into substantial movements in the manus. Furthermore, Xing et al. (2015a)

suggested that the great rotational range of motion might have enabled the forelimb to passively adjust to the topography of the terrain.

Based on our literature review and statistical analysis, we are now able to draw the following conclusions: First, high manual supination angles (>60°) are restricted to small- and medium-sized trackmakers. Pedal print lengths of known examples generally do not exceed 60 cm. The absence of high manual supination angles in larger sauropod trackways may be explained by constrains imposed either by the increased body weight, or by the increased joint ossification in older, and therefore larger animals. An exception might be trackway QQ1 from the Qinquan Tracksite in China, which shows a mean pedal print length of 84 cm, while the left manual prints are supinated with 80° on average (Xing et al., 2016a). As stated by Xing et al. (2016a), the degree of supination in this trackway might be related to a slight turn of the trackmaker towards the left.

Second, manual supination angles are negatively correlated with both of the employed proxies for trackmaker locomotion speed, the stride length/GAD and the stride length/pes length ratio ($p<0.001$, respectively, Spearman). Intriguingly, the Tafaytour trackways plot somewhat outside of the monotonic relationship found for the remaining trackways, indicating that this population showed high manual supination angles at higher speeds than would be expected. This difference between the Tafaytour trackways and the remaining sample is statistically significant (MANOVA, $p = 7.4E-07$). Trackway S12 from the Chevenez-Combe Ronde site of Switzerland appears as a clear outlier, regardless if stride length/GAD or stride/pedal print length is used as speed proxy, which is possibly due to the very small body size of the trackmaker. Other outliers appear only in one of the two bivariate comparisons. Trackway Ho20 from the Hoewha locality of South Korea appears as a clear outlier when stride length/GAD is used as speed proxy, but not when stride/pes length is used, indicating an erroneous GAD estimate. The low pace angulation values (averaging at 82°) and the very low GAD/Hip height ratio (0.57) of this trackway indicate that the footprints of one step cycle are separated by intermediate footprints belonging to other step cycles; the used GAD formula thus would not be applicable, as discussed above. Conversely, the use of the stride/pedal print length ratio produced several outliers, none of which is apparent when the stride length/GAD ratio is employed; in these cases, the pedal print length estimates probably do not reflect the true dimensions of the trackmaker's foot.

Third, the manual supination angle is significantly correlated with the WAP/PL-ratio, a measure of trackway gauge width ($p<0.01$, Spearman). Thus, narrow-gauged trackways tend to show higher manual supination angles than wide-gauged trackways. As indicated by the multivariate linear model, the WAP/PL ratio represents an important additional factor explaining parts of the manual supination variability that cannot be explained by relative locomotion speed. Henderson (2006a) suggested that the trackway gauge in sauropods is a consequence of the relative positions of their centers of mass. Thus, the narrow-gauge would occur when the center of mass is located close to the hips, as in, e.g., *Diplodocus carnegii*, whereas the wide-gauge would be associated with more anterior centers of mass (as in, e.g., *Brachiosaurus altithorax*). This link between gauge and center of mass is further corroborated by skeletal modifications resulting in more outward angled limbs in those species with a more anterior center of mass, especially titanosaurs (Wilson and Carrano, 1999; Henderson, 2006a). Furthermore, Henderson (2006a) proposed the narrow-gauge to represent the plesiomorphic condition in sauropods, and predicted that all larger sauropods (>12

tons) were wide-gauged. While the earliest known sauropod trackways are indeed narrow-gauged (Wright, 2005; Lallensack et al., 2017), a correlation between gauge and body size has, to our knowledge, not been demonstrated in the track record (Wilson and Carrano, 1999).

We hypothesize that smaller sauropods tend to retain the plesiomorphic semi-supinated manus posture when there is no need for the forelimb to actively contribute to the propulsion of the animal. This would be the case when locomotion speed is low and the center of mass is located posteriorly: A center of mass located close to the hips, as it can be assumed for narrow-gauged sauropod trackways (Henderson, 2006a), would essentially resemble the condition seen in bipeds—the hind limbs would not only carry most of the weight but represent the main agents of locomotion, with the forelimbs playing only a supportive role. Forelimb usage can be expected to increase with locomotion speed and when the center of mass has a more anterior position, which is expected in wide-gauged trackways. As discussed above, both the relative locomotion speed and trackway gauge are clearly correlated with manual supination angles. Therefore, the rotation of the manus into a more anterior orientation would possibly have allowed for the active use of the forelimb in propulsion (Bonnan and Senter, 2007). In other words, the contribution of the forelimb to the propulsion of the animal might have increased with locomotion speed (depending on behavior) and wider trackway gauges (depending on anatomy), being enabled by a much more anteriorly directed manus.

CONCLUSIONS

Tafaytour Tracksite A, although being highly bioturbated by hundreds of imprints, features many well-preserved footprints showing impressions of both digits and claws, and at least nine recognizable trackways that include both pedal and manual prints, with one additional trackway located at Tracksite B. The sites feature both wide-gauged trackways and one of the narrowest sauropod trackways known. Manual impressions are especially variable and can be slit-like, kidney to dumbbell-shaped, or horseshoe-shaped. They are generally subdivided into two oval impressions arranged in a “V”-like configuration, a feature hitherto unknown from sauropod tracks outside of Morocco. The substantial variability of both the trackway configuration and the footprint morphology can probably be attributed to variations in substrate properties and trackmaker behavior rather than foot anatomy, and implies that the definition and application of ichnotaxonomic labels for sauropod tracks should be carried out with caution.

Most known sauropod trackways show an anterior or anterolateral manual print orientation. The Tafaytour trackways are unusual in showing laterally or even posterolaterally directed manual prints, with supination angles of up to 104°. Only Trackway A9 displays anteriorly directed manual prints. Laterally facing manual impressions can be explained by great degrees of freedom in the sauropod forelimb and are probably not restricted to specific taxa within Sauropoda. As indicated by our literature review, however, they are restricted to small to small medium-sized trackmakers (pes length < 60 cm), possibly due to constraints imposed by the increasing body size or due to continuing joint ossification with increasing age of the individuals. Statistical analysis on small-sized sauropod trackways from around the world reveals a negative correlation with both the relative locomotion speed and trackway gauge. High supination angles are preferred at low locomotion speeds and when the trackway gauge is narrow (and, thus, the center of mass is located close to the hips). In these situations, the forelimb is probably not actively involved in the propulsion of the animal. At higher speeds and wider trackway gauges, pronation would enable the fore-

limb to actively contribute to propulsion. Statistical analysis further indicates that variations in the sauropod forelimb posture and orientation are to some extent decoupled from those of the hind limb, probably reflecting the marked anatomical and functional differences of the manus and pes.

The apparent glenoacetabular distance (GAD) is a viable proxy for the body size of the trackmaker, although separate formulae have to be used for different gaits. The lateral-sequence singlefoot walk is argued to be the most likely gait employed by sauropods of our sample; the GAD should therefore be calculated using the formula GAD = 3/4SL + MP. Mean configuration plots visualize mean values of trackway parameters and, as intratrackway variability and asymmetry are removed, are especially beneficial for direct visual comparisons of separate trackways when the anatomy of the trackmaker is of interest. Trackway asymmetries are defined as discrepancies between the mean values of trackway parameters of the left and right footprints. Trackway asymmetries are a common feature in sauropod trackways, but in many cases might be better explained by unusual behaviors of the individuals rather than explicit causes such as pathologies.

ACKNOWLEDGMENTS

We are greatful to S. Läbe and P. M. Sander for fruitful discussions and comments on an early version of the manuscript. Joschua Knüppe is thanked for contributing artwork. We furthermore thank all participants of the field trip of the 2015 First International Congress on Continental Ichnology (ICCI) for their support. In particular, we thank D. Falk for his help during taking the photogrammetric photographs and F. Scholze, A. Uchman, H. Klein, M. Masrour, and F. Pérez-Lorente for contributing additional photographs. Last but not least, we thank editor S. Salisbury as well as D. Castanera and J. Nair for their constructive reviews which improved the manuscript. The work is performed according to the Russian Government Program of Competitive Growth of Kazan Federal University. VolkswagenStiftung grant no. 85 882 in the grant initiative 'Research in Museums' supported this research.

LITERATURE CITED

Alexander, R. M. 1976. Estimates of speeds of dinosaurs. Nature 261:129–130.

Alexander, R. M. 1985. Mechanics of posture and gait of some large dinosaurs. Zoological Journal of the Linnean Society 83:1–25.

Baird, D. 1952. Revision of the Pennsylvanian and Permian footprints *Limnopus*, *Allopus* and *Baropus*. Journal of Paleontology 26:832–840.

Baird, D. 1954. *Chirotherium lulli*, a pseudosuchian reptile from New Jersey. Bulletin of the Museum of Comparative Zoology 111:166–194.

Bennett, M. R., P. Falkingham, S. A. Morse, K. Bates, and R. H. Crompton. 2013. Preserving the impossible: Conservation of soft- sediment hominin footprint sites and strategies for three-dimensional digital data capture. PLOS ONE 8:e60755.

Biknevicius, A. R., and S. M. Reilly. 2006. Correlation of symmetrical gaits and whole body mechanics: debunking myths in locomotor biodynamics. Journal of Experimental Zoology Part A: Comparative Experimental Biology 305A:923–934.

Bonnan, M. F. 2003. The evolution of manus shape in sauropod dinosaurs: implications for functional morphology, forelimb orientation, and phylogeny. Journal of Vertebrate Paleontology 23:595–613.

Bonnan, M. F. 2005. Pes anatomy in sauropod dinosaurs: Implications for functional morphology, evolution, and phylogeny; pp. 346–380 in V. Tidwell and K. Carpenter (eds.), Thunder-Lizards: The Sauropodomorph Dinosaurs. Indiana University Press, Bloomington, Indiana.

Bonnan, M. F., and P. Senter. 2007. Were the basal sauropodomorph dinosaurs *Plateosaurus* and *Massospondylus* habitual quadrupeds? Special Papers in Palaeontology 77:139–155.

Borsuk-Bialynicka, M. 1977. A new camarasaurid sauropod *Opisthocoelicaudia skarzynskii* gen. n., sp. n. from the Upper Cretaceous of Mongolia. Palaeontologia Polonica 37:5–64.

Brusatte, S. L., T. J. Challands, D. A. Ross, and M. Wilkinson. 2016. Sauropod dinosaur trackways in a Middle Jurassic lagoon on the Isle of Skye, Scotland. Scottish Journal of Geology 52:1–9.

Casanovas, M., A. Fernández, F. Pérez-Lorente, and J. V. Santafé. 1997. Sauropod trackways from site El Sobaquillo (Munilla, La Rioja, Spain) indicate amble walking. Ichnos 5:101–107.

Castanera, D., C. Pascual, J. I. Canudo, N. Hernández, and J. L. Barco. 2012. Ethological variations in gauge in sauropod trackways from the Berriasian of Spain. Lethaia 45:476–489.

Castanera, D., J. L. Barco, I. Díaz-Martínez, J. H. Gascón, F. Pérez-Lorente, and J. I. Canudo. 2011. New evidence of a herd of titanosauriform sauropods from the lower Berriasian of the Iberian range (Spain). Palaeogeography, Palaeoclimatology, Palaeoecology 310:227–237.

Castanera, D., V. F. Santos, L. Piñuela, C. Pascual, B. Vila, J. I. Canudo, and J. J. Moratalla. 2016. Iberian sauropod tracks through time: variations in sauropod manus and pes track morphologies; pp. 120–137 in P. L. Falkingham, D. Marty, and A. Richter (eds.), Dinosaur Tracks: The Next Steps. Indiana University Press.

Christiansen, P. 1997. Locomotion in sauropod dinosaurs. Gaia 14:45–75.

Dalla Vecchia, F. M. 1994. Jurassic and Cretaceous sauropod evidence in the Mesozoic carbonate platforms of the Southern Alps and Dinarids. Gaia 10:65–73.

Dalla Vecchia, F. M., G. Tunis, S. Venturini, and A. Tarlao. 2001. Dinosaur track sites in the upper Cenomanian (Late Cretaceous) of Istrian Peninsula (Croatia). Bollettino Della Società Paleontologica Italiana 40:25–53.

Dantas, P., V. dos Santos, M. G. Lockley, and C. A. Meyer. 1994. Footprint evidence for limping dinosaurs from the Upper Jurassic of Portugal. Gaia 10:43–48.

Day, J. J., D. B. Norman, A. S. Gale, P. Upchurch, and H. P. Powell. 2004. A Middle Jurassic dinosaur trackway site from Oxfordshire, UK. Palaeontology 47:319–348.

Díaz-Martínez, I., L. Ladel, C. Z. Calvo, S. Haddad, I. Durán, M. Trachi, L. Porres, B. Boukil, S. Beníted, M. Masrour, F. Pérez-Lorente, and M. Boutakiout. 2010. Importancia y vulnerabilidad del patrimonio paleoicnológico del Alto Atlas marroquí. Cidaris 30:107–112.

Darcus, H. D., and N. Salter. 1953. The amplitude of pronation and supination with the elbow flexed to a right angle. Journal of Anatomy 87:169–184.

Dutuit, J.-M., and A. Ouazzou. 1980. Découverte d'une piste de dinosaure sauropode sur le site d'empreintes de Demnat (Haut-Atlas Marocain). Mémoires de La Société Géologique de France 139:95–102.

Enniouar, A., A. Lagnaoui, and A. Habib. 2014. A Middle Jurassic sauropod tracksite in the Argana Basin, Western High Atlas, Morocco: an example of paleoichnological heritage for sustainable geotourism. Proceedings of the Geologists' Association 125:114–119.

Falkingham, P. L. 2014. Interpreting ecology and behaviour from the vertebrate fossil track record. Journal of Zoology 292:222–228.

Farlow, J. O., J. G. Pittman, and J. M. Hawthorne. 1989. *Brontopodus birdi*, Lower Cretaceous sauropod footprints from the US Gulf coastal plain; pp. 371–394 in D. D. Gillette and M. G. Lockley (eds.), Dinosaur Tracks and Traces. Cambridge University Press.

Fernández-Baldor, F. T. 2015. Unusual sauropod tracks in the Jurassic-Cretaceous interval of the Cameros Basin (Burgos, Spain). Journal of Iberian Geology 41:141–154.

Fox, J., and S. Weisberg. 2011. An R Companion to Applied Regression, Second. Sage, Thousand Oaks CA, 472 pp.

Gierliński, G., and G. Sawicki. 1998. New sauropod tracks from the Lower Jurassic of Poland. Geological Quarterly 42:477–480.

González Riga, B. J. 2011. Speeds and stance of titanosaur sauropods: analysis of *Titanopodus* tracks from the Late Cretaceous of Mendoza, Argentina. Anais Da Academia Brasileira de Ciências 83:279–290.

González Riga, B. J., and J. O. Calvo. 2009. A new wide-gauge sauropod track site from the Late Cretaceous of Mendoza, Neuquén Basin, Argentina. Palaeontology 52:631–640.

Hall, L. E., A. E. Fragomeni, and D. W. Fowler. 2016. The flexion of sauropod pedal unguals and testing the substrate grip hypothesis using the trackway fossil record; pp. 138–151 in P. L. Falkingham, D. Marty, and A. Richter (eds.), Dinosaur Tracks: The Next Steps. Indiana University Press.

Hammer, Ø., and D. A. T. Harper. 2006. Paleontological Data Analysis. Blackwell Publishing, Malden, Oxfort, Carlton, 351 pp.

Hammer, Ø., D. A. T. Harper, and P. D. Ryan. 2001. Past: Paleontological Statistics Software Package for education and data analysis. Palaeontologia Electronica 4:1–9.

Harrell Jr., F. E. 2016. Hmisc: Harrell Miscellaneous. Available at https://CRAN.R-project.org/package=Hmisc. Accessed May 19, 2017.

Henderson, D. M. 2006a. Burly gaits: centers of mass, stability, and the trackways of sauropod dinosaurs. Journal of Vertebrate Paleontology 26:907–921.

Henderson, D. M. 2006b. Simulated weathering of dinosaur tracks and the implications for their characterization. Canadian Journal of Earth Sciences 43:691–704.

Hildebrand, M. 1965. Symmetrical gaits of horses. Science 150:701–708.

Hildebrand, M. 1980. The adaptive significance of tetrapod gait selection. Integrative and Comparative Biology 20:255–267.

Hildebrand, M. 1989. The quadrupedal gaits of vertebrates. BioScience 39:766.

Huh, M., K. G. Hwang, I. S. Paik, C. H. Chung, and B. S. Kim. 2003. Dinosaur tracks from the Cretaceous of South Korea: Distribution, occurrences and paleobiological significance. Island Arc 12:132–144.

Hutson, J. D. 2014. Quadrupedal dinosaurs did not evolve fully pronated forearms: new evidence from the ulna. Acta Palaeontologica Polonica 60:599–610.

Ishigaki, S. 1985. Dinosaur footprints of the Atlas Mountains. Nature Study, Osaka City Museum of Natural History 31:5–8.

Ishigaki, S. 1988. Les empreintes de dinosaures du Jurasique inférieur du Haut Atlas central marocain. Notes Du Service Géologique Du Maroc 44:79–86.

Ishigaki, S. 1989. Footprints of swimming sauropods from Morocco; pp. 83–86 in D. D. Gillette and G. M. Lockley (eds.), Dinosaur Tracks and Traces. Cambridge University Press.

Ishigaki, S. 2007. Footprint evidence of extreme outward rotation of the manus of sauropod dinosaur from Middle Jurassic of western Morocco. Journal of Vertebrate Paleontology 27 (Suppl. 3):94A.

Ishigaki, S. 2009. Trampled ground and extremely narrow gauge trackway of Jurassic sauropod dinosaur from Western High Atlas Mountains, Morocco. 1st International Congress on North African Vertebrate Paleontology, Marrakech, p. 25.

Ishigaki, S., and M. G. Lockley. 2010. Didactyl, tridactyl and tetradactyl theropod trackways from the Lower Jurassic of Morocco: evidence of limping, labouring and other irregular gaits. Historical Biology 22:100–108.

Ishigaki, S., and Y. Matsumoto. 2009a. Re-examination of manus-only and manus-dominated sauropod trackways from Morocco. Geological Quarterly 53:441–448.

Ishigaki, S., and Y. Matsumoto. 2009b. "Off-tracking"-like phenomenon observed in the turning sauropod trackway from the Upper Jurassic of Morocco. Memoir of the Fukui Prefectural Dinosaur Museum 8:1–10.

Jenny, J., and J. A. Jossen. 1982. Découverte d'empreintes de pas de Dinosauriens dans le Jurassique inferieur (Pliensbachien) du Haut Atlas central (Maroc). Comptes Rendues Hébdomanaires Séances Academie de Sciences 294:223–226.

Jenny, J., A. Le Marrec, and M. Monbaron. 1981. Les empreintes de pas de Dinosauriens dans le Jurassique moyen du Haut Atlas central (Maroc): Nouveaux gisements et précisions stratigraphiques. Geobios 14:427–431.

Kim, J. Y., and M. G. Lockley. 2012. New sauropod tracks (*Brontopodus pentadactylus* ichnosp. nov.) from the Early Cretaceous Haman Formation of Jinju Area, Korea: implications for sauropods manus morphology. Ichnos 19:84–92.

Kubo, T. 2011. Estimating body weight from footprints: application to pterosaurs. Palaeogeography, Palaeoclimatology, Palaeoecology 299:197–199.

Lallensack, J. N., H. Klein, J. Milàn, O. Wings, O. Mateus, and L. B. Clemmensen. 2017. Sauropodomorph dinosaur trackways from the Fleming Fjord Formation of East Greenland: evidence for Late Triassic sauropods. Acta Palaeontologica Polonica 62:833–843.

Lee, Y.-N., S.-Y. Yang, S.-J. Seo, K.-S. Baek, M.-S. Yi, D.-J. Lee, E.-J. Park, and S.-W. Han. 2000. Distribution and paleobiological significance of dinosaur tracks from the Jindong Formation (Albian) in Kosong County, Korey. Journal of the Paleontological Society of Korea Special Publication 4:1–12.

Leonardi, G. 1987. Discussion of the terms and methods; pp. 43–51 in G. Leonardi (ed.), Glossary and Manual of Tetrapod Footprint Palaeoichnology. Publicação do Departemento Nacional da Produção Mineral Brasil, Brasília.

Leonardi, G. (ed.). 1987.

Leonardi, G. (ed.). 1987. Glossary and Manual of Tetrapod Footprint Palaeoichnology. Publicação do Departemento Nacional da Produção Mineral Brasil, Brasília, 117 pp.

Leonardi, G., R. M. Casamiquela, G. R. Demathieu, H. Haubold, and W. A. S. Sarjeant. 1987. Glossary and Manual of Tetrapod Footprint Palaeoichnology (G. Leonardi, ed.). Publicação do Departemento Nacional da Produção Mineral Brasil, Brasília, 117 pp.

Lim, S.-K., S.-Y. Yang, and G. M. Lockley. 1989. Large dinosaur footprint assemblages from the Cretaceous Jindong Formation of southern Korea; pp. 333–336 in D. D. Gillette and M. G. Lockley (eds.), Dinosaur Tracks and Traces. Cambridge University Press.

Lockley, M. G., and K. Conrad. 1989. The paleoenvironmental context, preservation and paleoecological significance of dinosaur tracksites in the western USA; pp. 121–134 in D. D. Gillette and G. M. Lockley (eds.), Dinosaur Tracks and Traces. Cambridge University Press.

Lockley, M. G., and V. F. Santos. 1993. A preliminary report on sauropod trackways from the Avelino site, Sesimbra region, Upper Jurassic, Portugal. Gaia 6:38–42.

Lockley, M. G., J. O. Farlow, and C. A. Meyer. 1994a. *Brontopodus* and *Parabrontopodus* ichnogen. nov. and the significance of wide-and narrow-gauge sauropod trackways. GAIA 10:135–145.

Lockley, M. G., K. J. Houck, and N. K. Prince. 1986. North America's largest dinosaur trackway site: Implications for Morrison Formation paleoecology. Geological Society of America Bulletin 97:1163–1176.

Lockley, M. G., J. L. Wright, and D. Thies. 2004. Some observations on the dinosaur tracks at Münchehagen (Lower Cretaceous), Germany. Ichnos 11:261–274.

Lockley, M. G., A. P. Hunt, J. Moratalla, and M. Matsukawa. 1994b. Limping Dinosaurs? Trackway evidence for abnormal gaits. Ichnos 3:193–202.

Lockley, M. G., K. Houck, S.-Y. Yang, M. Matsukawa, and S.-K. Lim. 2006. Dinosaur-dominated footprint assemblages from the Cretaceous Jindong Formation, Hallyo Haesang National Park area, Goseong County, South Korea: evidence and implications. Cretaceous Research 27:70–101.

Lockley, M. G., A. S. Schulp, C. A. Meyer, G. Leonardi, and D. Kerumba Mamani. 2002a. Titanosaurid trackways from the Upper Cretaceous of Bolivia: evidence for large manus, wide-gauge locomotion and gregarious behaviour. Cretaceous Research 23:383–400.

Lockley, M. G., J. Wright, D. White, M. Matsukawa, L. Jianjun, F. Lu, and L. Hong. 2002b. The first sauropod trackways from China. Cretaceous Research 23:363–381.

Lockley, M. G., G. D. Gierlinski, K. Houck, J.-D. Lim, K. S. Kim, D. Y. Kim, T. K. Kim, S.-H. Kang, R. Hunt Foster, R. Li, C. Chesser, R. Gay, Z. Dubicka, K. Cart, and C. Wright. 2014. New excavations at the

Mill Canyon Dinosaur Track Site (Cedar Mountain Formation, Lower Cretaceous) of Eastern Utah. New Mexico Museum of Natural History and Science, Bulletin 62:287–300.
Maidment, S. C. R., and P. M. Barrett. 2012. Does morphological convergence imply functional similarity? A test using the evolution of quadrupedalism in ornithischian dinosaurs. Proceedings of the Royal Society of London B: Biological Sciences 279:3765–3771.
Mallison, H. 2010a. The digital *Plateosaurus* I: body mass, mass distribution, and posture assessed using CAD and CAE on a digitally mounted complete skeleton. Palaeontologia Electronica 13: 1–26.
Mallison, H. 2010b. The digital *Plateosaurus* II: an assessment of the range of motion of the limbs and vertebral column and of previous reconstructions using a digital skeletal mount. Acta Palaeontologica Polonica 55:433–458.
Mallison, H., and O. Wings. 2014. Photogrammetry in paleontology – A practical guide. Journal of Paleontological Techniques 12:1–31.
Marty, D. 2008. Sedimentology, taphonomy, and ichnology of Late Jurassic dinosaur tracks from the Jura carbonate platform (Chevenez-Combe Ronde Tracksite, NW Switzerland): insights into the tidal-flat palaeoenvironment and dinosaur diversity, locomotion, and palaeoecology. GeoFocus 21:1–278.
Marty, D., C. A. Meyer, M. Belvedere, J. Ayer, and K. L. Schäfer. 2013. Rochefort–Les Grattes: an Early Tithonian dinosaur tracksite from the Canton Neuchâtel, Switzerland. Revue de Paléobiologie 32:373–384.
Mazin, J.-M., P. Hantzpergue, and J. Pouech. 2016. The dinosaur tracksite of Loulle (early Kimmeridgian; Jura, France). Geobios 49:211–228.
Mazzetta, G. V., and R. E. Blanco. 2001. Speeds of dinosaurs from the Albian–Cenomanian of Patagonia and sauropod stance and gait. Acta Palaeontologica Polonica 46:235–246.
McCrea, R. T., D. H. Tanke, L. G. Buckley, M. G. Lockley, J. O. Farlow, L. Xing, N. A. Matthews, C. W. Helm, S. G. Pemberton, and B. H. Breithaupt. 2015. Vertebrate ichnopathology: pathologies inferred from dinosaur tracks and trackways from the Mesozoic. Ichnos 22:235–260.
McGhee, R. B., and A. A. Frank. 1968. On the stability properties of quadruped creeping gaits. Mathematical Biosciences 3:331–351.
Meyer, C. A., and B. Thüring. 2003. Dinosaurs of Switzerland. Comptes Rendus Palevol 2:103–117.
Meyer, C., G. M. Lockley, J. W. Robinson, and V. F. Dos Santos. 1994. A comparison of well-preserved sauropod tracks from the Late Jurassic of Portugal and the Western United States: evidence and implications. Gaia 10:57–64.
Mezga, A., B. C. Tešović, and Z. Bajraktarević. 2007. First record of dinosaurs in the Late Jurassic of the Adriatic-Dinaridic Carbonate Platform (Croatia). Palaios 22:188–199.
Milàn, J., P. Christiansen, and O. Mateus. 2005. A three-dimensionally preserved sauropod manus impression from the Upper Jurassic of Portugal: implications for sauropod manus shape and locomotor mechanics. Kaupia 14:47–52.
Milner, A. R. C., J. D. Harris, M. G. Lockley, J. I. Kirkland, and N. A. Matthews. 2009. Bird-like anatomy, posture, and behavior revealed by an Early Jurassic theropod dinosaur resting trace. PLOS ONE 4:e4591.
Nicosia, U., F. M. Petti, G. Perugini, S. D. Porchetti, E. Sacchi, M. A. Conti, N. Mariotti, and A. Zarattini. 2007. Dinosaur tracks as paleogeographic constraints: new scenarios for the Cretaceous geography of the Periadriatic region. Ichnos 14:69–90.
Pérez-Lorente, F. 2003. Icnitas de dinosaurios del Cretácico en España; pp. 49–108 in F. P. Lorente (ed.), Dinosaurios y otros Reptiles Mesozoicos en España. Universidad de La Rioja.
Pfau, T., E. Hinton, C. Whitehead, A. Wiktorowicz-Conroy, and J. R. Hutchinson. 2011. Temporal gait parameters in the alpaca and the evolution of pacing and trotting locomotion in the Camelidae. Journal of Zoology 283:193–202.

R Development Core Team. 2016. R: A Language and Environment for Statistical Computing. R Foundation for Statistical Computing, Vienna, Austria. Available at https://www.R-project.org/. Accessed May 19, 2017.

Razzolini, N. L., B. Vila, I. Díaz-Martínez, P. L. Manning, and A. Galobart. 2016. Pes shape variation in an ornithopod dinosaur trackway (Lower Cretaceous, NW Spain): New evidence of an antalgic gait in the fossil track record. Cretaceous Research 58:125–134.

Remes, K. 2008. Evolution of the pectoral girdle and forelimb in Sauropodomorpha (Dinosauria, Saurischia): osteology, myology and function. Munich: Fakultät für Geowissenschaften, Ludwig-Maximilians-Universität. 355 pp.

Richter, A., and A. Böhme. 2016. Too many tracks: preliminary description and interpretation of the diverse and heavily dinoturbated Early Cretaceous "Chicken Yard" ichnoassemblage (Obernkirchen Tracksite, northern Germany); pp. 334–357 in P. L. Falkingham, D. Marty, and A. Richter (eds.), Dinosaur Tracks: The Next Steps. Indiana University Press.

Romano, M., M. A. Whyte, and S. J. Jackson. 2007. Trackway ratio: a new look at trackway gauge in the analysis of quadrupedal dinosaur trackways and its implications for ichnotaxonomy. Ichnos 14:257–270.

Romano, M., M. A. Whyte, and P. L. Manning. 1999. New sauropod dinosaur prints from the Saltwick Formation (Middle Jurassic) of the Cleveland Basin, Yorkshire. Proceedings of the Yorkshire Geological Society 52:361–369.

Salisbury, S. W., A. Romilio, M. C. Herne, R. T. Tucker, and J. P. Nair. 2017. The dinosaurian ichnofauna of the Lower Cretaceous (Valanginian–Barremian) Broome Sandstone of the Walmadany area (James Price Point), Dampier Peninsula, Western Australia. Society of Vertebrate Paleontology Memoir 16. Journal of Vertebrate Paleontology 36 (6, Supplement). 152 pp.

Santos, V. F., J. J. Moratalla, and R. Royo-Torres. 2009. New sauropod trackways from the Middle Jurassic of Portugal. Acta Palaeontologica Polonica 54:409–422.

Schanz, T., Y. Lins, H. Viefhaus, T. Barciaga, S. Läbe, H. Preuschoft, U. Witzel, and P. M. Sander. 2013. Quantitative interpretation of tracks for determination of body mass. PLOS ONE 8:e77606.

Soergel, W. 1925. Die Fährten der Chirotheria: Eine paläobiologische Studie. Gustav Fischer Verlag, Jena, 92 pp.

Soulaimani, A., and H. Ouanaimi. 2011. Anti-Atlas et Haut Atlas, circuit occidental; pp. 9–72 in A. Michard, O. Saddiqi, A. Chalouan, E. Rjimati, and A. Mouttaqi (eds.), Nouveaux guides géologiques et miniers du Maroc. Notes et Mémoires du Service géologique du Maroc vol. 3.

Stevens, K. A., S. Ernst, and D. Marty. 2016. Uncertainty and ambiguity in the interpretation of sauropod trackways; pp. 226–243 in P. L. Falkingham, D. Marty, and A. Richter (eds.), Dinosaur Tracks: The Next Steps. Indiana University Press.

Thulborn, R. A. 1984. Preferred gaits of bipedal dinosaurs. Alcheringa 8:243–252.

Thulborn, R. A. 1990. Dinosaur Tracks. Chapman and Hall, London; New York, 410 pp.

Tixeront, M. 1974. Carte géologique et minéralogique du Couloir d'Argana, 1/ 100 000. Edition Du Service Géologique Du Maroc, Notes et Mémoires 205.

VanBuren, C. S., and M. Bonnan. 2013. Forearm posture and mobility in quadrupedal dinosaurs. PLOS ONE 8:e74842.

Vila, B., O. Oms, À. Galobart, K. T. Bates, V. M. Egerton, and P. L. Manning. 2013. Dynamic similarity in titanosaur sauropods: ichnological evidence from the Fumanya Dinosaur Tracksite (Southern Pyrenees). PLOS ONE 8:e57408.

Wilson, J. A., and M. T. Carrano. 1999. Titanosaurs and the origin of "wide-gauge" trackways: a biomechanical and systematic perspective on sauropod locomotion. Paleobiology 25:252–267.

Wright, J. L. 2005. Steps in understanding sauropod biology; pp. 252–285 in C. C. Rogers and J. Wilson (eds.), The sauropods: evolution and paleobiology. Oakland, California.

Xing, L. D., J. D. Harris, and P. J. Currie. 2011. First record of dinosaur trackway from Tibet, China. Geological Bulletin of China 30:173–178.

Xing, L. D., J. D. Harris, and C. K. Jia. 2010. Dinosaur tracks from the Lower Cretaceous Mengtuan Formation in Jiangsu, China and morphological diversity of local sauropod tracks. Acta Palaeontologica Sinica 49:448–460.

Xing, L. D., M. G. Lockley, J. Zhang, H. Klein, W. S. Persons IV., and H. Dai. 2014a. Diverse sauropod-, theropod-, and ornithopod-track assemblages and a new ichnotaxon Siamopodus xui ichnosp. nov. from the Feitianshan Formation, Lower Cretaceous of Sichuan Province, southwest China. Palaeogeography, Palaeoclimatology, Palaeoecology 414:79–97.

Xing, L. D., Y. Liu, D. Marty, H. Kuang, H. Klein, W. S. Persons IV, and Y. Lyu. 2016a. Sauropod trackway reflecting an unusual walking pattern from the Early Cretaceous of Shandong Province, China. Ichnos 24:1–10.

Xing, L. D., M. G. Lockley, J. Zhang, H. Klein, D. Li, T. Miyashita, Z. Li, and S. B. Kümmell. 2016b. A new sauropodomorph ichnogenus from the Lower Jurassic of Sichuan, China fills a gap in the track record. Historical Biology 28:881–895.

Xing, L. D., M. G. Lockley, T. Miyashita, H. Klein, T. Wang, W. S. Persons, S.-G. Pan, J.-P. Zhang, and Z.-M. Dong. 2014b. Large sauropod and theropod tracks from the Middle Jurassic Chuanjie Formation of Lufeng County, Yunnan Province and palaeobiogeography of the Middle Jurassic sauropod tracks from southwestern China. Palaeoworld 23:294–303.

Xing, L. D., M. G. Lockley, G. Yang, J. Cao, R. T. McCrea, H. Klein, J. Zhang, W. S. Persons, and H. Dai. 2016c. A diversified vertebrate ichnite fauna from the Feitianshan Formation (Lower Cretaceous) of southwestern Sichuan, China. Cretaceous Research 57:79–89.

Xing, L. D., G. Peng, Y. Ye, M. G. Lockley, H. Klein, W. S. Persons IV, J. Zhang, C. Shu, and B. Hao. 2014c. Sauropod and small theropod tracks from the Lower Jurassic Ziliujing Formation of Zigong City, Sichuan, China, with an overview of Triassic–Jurassic dinosaur fossils and footprints of the Sichuan Basin. Ichnos 21:119–130.

Xing, L. D., M. G. Lockley, M. F. Bonnan, D. Marty, H. Klein, Y. Liu, J. Zhang, H. Kuang, M. E. Burns, and N. Li. 2015a. Late Jurassic–Early Cretaceous trackways of small-sized sauropods from China: new discoveries, ichnotaxonomy and sauropod manus morphology. Cretaceous Research 56:470–481.

Xing, L. D., M. G. Lockley, D. Marty, H. Klein, L. G. Buckley, R. T. McCrea, J. Zhang, G. D. Gierliński, J. D. Divay, and Q. Wu. 2013. Diverse dinosaur ichnoassemblages from the Lower Cretaceous Dasheng Group in the Yishu fault zone, Shandong Province, China. Cretaceous Research 45:114–134.

Xing, L. D., J. Zhang, M. G. Lockley, R. T. McCrea, H. Klein, L. Alcalá, L. G. Buckley, M. E. Burns, S. B. Kümmell, and Q. He. 2015b. Hints of the early Jehol Biota: important dinosaur footprint assemblages from the Jurassic-Cretaceous boundary Tuchengzi Formation in Beijing, China. PLOS ONE 10:e0122715.

Xing, L. D., M. G. Lockley, D. Marty, H. Klein, G. Yang, J. Zhang, G. Peng, Y. Ye, W. S. Persons, X. Yin, T. Xu. 2016d. A diverse saurischian (theropod–sauropod) dominated footprint assemblage from the Lower Cretaceous Jiaguan Formation in the Sichuan Basin, southwestern China: a new ornithischian ichnotaxon, pterosaur tracks and an unusual sauropod walking pattern. Cretaceous Research 60:176–193.

Xing, L. D., M. G. Lockley, D. Marty, J. He, X. Hu, H. Dai, M. Matsukawa, G. Peng, Y. Ye, H. Klein, J. Zhang, B. Hao, W. S. Persons. 2016e. Wide-gauge sauropod trackways from the Early Jurassic of Sichuan, China: oldest sauropod trackways from Asia with special emphasis on a specimen showing a narrow turn. Swiss Journal of Geosciences 109:415–428.

Xing, L. D., D. Marty, K. Wang, M. G. Lockley, S. Chen, X. Xu, Y. Liu, H. Kuang, J. Zhang, H. Ran, and W. Scott Persons IV. 2015c. An unusual sauropod turning trackway from the Early Cretaceous of Shandong Province, China. Palaeogeography, Palaeoclimatology, Palaeoecology 437:74–84.

Zhang, J. P., L. D. Xing, G. D. Gierliński, F. D. Wu, M. Z. Tian, and P. J. Currie. 2012. First record of dinosaur trackways in Beijing, China. Chinese Science Bulletin 57:144–152.

Forelimb orientation and locomotion of sauropod dinosaurs: insights from the Middle Jurassic Tafaytour Tracksite (Argana Basin, Morocco)

JENS N. LALLENACK,[*, 1] SHINOBU ISHIGAKI,[2] ABDELOUAHED LAGNAOUI,[3, 4] MICHAEL BUCHWITZ,[5] and OLIVER WINGS[6]

[1]Division of Paleontology, Steinmann Institute, University of Bonn, Nussallee 8, 53115 Bonn, Germany;
[2]Department of Earth Science, Okayama University of Science, Okayama 700-8530, Japan;
[3]CONICET, Instituto de Ciencias de la Tierra y Ambientales de La Pampa – INCITAP, Facultad de Ciencias Exactas y Naturales – Universidad Nacional de La Pampa, Av. Uruguay 151, 6300 Santa Rosa, La Pampa, Argentina.
[4]Laboratory of Stratigraphy of Oil-and-Gas Bearing Reservoirs, Department of Paleontology and Stratigraphy, Institute of Geology and Petroleum Technologies, Kazan (Volga Region) Federal University, Kremlyovskaya str. 18, 420008, Kazan, Russia;
[5]Museum für Naturkunde Magdeburg, Otto-von-Guericke-Str. 68-73, 39104 Magdeburg;
[6]Zentralmagazin Naturwissenschaftlicher Sammlungen (ZNS), Martin-Luther-Universität Halle-Wittenberg, Domplatz 4, 06108 Halle (Saale), Germany

“Journal of Vertebrate Paleontology”

*Corresponding author.

INTRODUCTION

This supplementary information includes additional photographs and charts of the Tafaytour Tracksite; detailed descriptions of the trackways from the Tafaytour Tracksite; and a scatterplot matrix illustrating the results. The provided site charts include one chart showing tracksite 1 in its entirety (Fig. S1). Because of the large extent of the tracksite, the chart was subdivided into four sections, which are included as Figures S2–S5. Each chart comprises a photogrammetric orthophoto, a photogrammetric depth-color image, where blue parts represent low and red parts elevated regions, and an interpretive site map produced based on the photogrammetric data.

DESCRIPTIONS OF TRACKWAYS FROM THE TAFAYTOUR TRACKSITE

Trackway A1 (Figs 2S, 3S and 8S)

Identification—Trackway A1 was identified based on six pedal impressions (RP1–6). These impressions, although arranged in a slight arc, are very likely part of a single trackway given their equal spacing; similar length and width; similar morphology with a broad eastern and bluntly tapering western border (not visible in the deformed RP3); markings on the broad western margin that, at least in RP2, can be identified as digital impressions; their greater depth, better distinctiveness of the footprint margins and more pronounced displacement rims than seen in surrounding footprints; as well as their similar orientation that is consistent with a series of right pedal impressions. Three associated impressions (LP2, LP3 and LP4) are obvious candidates for left pedal prints within the same trackway, as they are similar in depth, expression of displacement rims, and in the clearness of footprint borders than the right pedal prints. These three pedal impressions form a zigzag pattern with the right pedal impressions of Trackway A1, as would be expected for a single trackway. Their mean stride length (171 cm) is only slightly smaller than the mean stride length of the five right pedal impressions (174 cm), a difference that might be explained by the slight left turn of the trackway, or simply by measurement error. While their position and distinctiveness strongly suggest a referral to Trackway A1, their morphology and orientation partly contradicts this hypothesis. If assumed to represent a single trackway, only LP2 shows a broad eastern margin, a bluntly tapering western margin, and a rotation away from the trackway midline to a similar degree as in the right pedal prints. LP1, however, is similar in size and appearance to LP2, but shows a broad western and tapering eastern margin as well as an orientation towards, and not away from, the trackway midline; these features would suggest an opposite direction of travel towards the west. A similar morphology and orientation can be seen in LP4, where the eastern end is markedly narrow.

Different hypotheses might explain the aberrant morphology of LP2 and LP4:

I) LP2 and LP4 are not part of Trackway A1 but represent the right pedal prints of either a single individual or two individuals traversing the surface in opposite directions. The actual left pedal imprints of Trackway A1, which would be expected in the same position, are either not readily impressed or overstepped. This hypothesis appears unlikely as, despite the depth and distinctiveness of these footprints, no indications of additional associated footprints of these possible trackway(s) can be seen.

II) LP2 and LP4 are part of Trackway A1, with the latter leading towards the west. This hypothesis is contradicted by the morphology and orientation of the majority of pedal imprints of the trackway (RP1–4; LP3) as well as the position of the associated manual impressions (see below) and therefore has to be discarded.

III) LP2 and LP4 are part of Trackway A1, but are distorted during the interaction of the foot with the sediment. Some degree of distortion within trackways A1 and A2 can be expected because of the greater depth of these footprints compared with other trackways at this tracksite, and is evident in RP3 of Trackway A1 and RP5 in Trackway A2, which appear to be narrowed, possibly due to suction effects acting during foot liftoff. Furthermore, LP4 differs in shape from LP2 in being narrow, strongly constricted at its eastern end and bluntly tapering at its western end, while LP2 is wider, shows a broad western end a moderately constricted eastern end. These shape differences are more conclusively explained as the result of distortion than the result of different foot morphologies. We therefore consider hypothesis III) to be the most likely.

A series of well-preserved manual impressions (RM1–2; RM 4–6) are consistently found in front of the right pedal impressions of Trackway A1. These footprints are similar in preservation, size, shape and orientation, tending to show a broader eastern and a somewhat tapering western margin, and with the convex site facing up the surface and the concave side facing down the surface, and therefore most probably belong to a single trackway. Other well-preserved associated manual impressions (LM3–4; LM 6) are equally distinctive and similar in size, and mirror the position and orientation of the other manual impressions, forming a zigzag pattern, and thus likely represent the manual impressions of the ipsilateral foot of the same trackway. Manual impression LM2 has been partly obliterated by RP3, but can be clearly identified on the orthophoto. A straight and very narrow slit medial to LP3 can be identified as RM3, because it is located exactly halfway between the RM2 and RM4, and shares the orientation and width seen in other manual impressions. LM1 and LM5 were originally well preserved but have been eroded since 1988; their position and orientation was reconstructed based on photographs taken in 1988. The mean manual stride length of trackway A1 (171 cm) is closely approaching the mean pedal stride length (173 cm), corroborating their referral to a single trackway. Additional pedal prints (LP1, LP6 and RP7) of the trackway, although less obvious and partly incomplete, were identified based on their morphology and position in accordance with the overall trackway configuration.

Trackway parameters—Trackway A1 is the longest recorded trackway. It is also the largest, both in terms of GAD (191–234 cm) and pedal track length (54 cm). The left manual pace length is larger (106 cm) than the right (89 cm), reaching statistical significance (p=0.0101). The trackway features a very narrow gauge, with a pedal pace angulation of 136° and a manual pace angulation of 125°. This difference in pace angulation in manual and pedal prints is statistically significant (p=0.0142). The average manual supination angle is very high (101°); the manus was therefore laterally to slightly posterolaterally oriented during track formation. Variability of the manual supination angle is low, with a standard deviation of 11°. Probable claw marks are present on RP2 of Trackway A1.

Footprint morphology—Pedal impressions are very variable in shape due to deformation during foot-sediment interaction. At least the right pedal impressions (RP1–6) are elongated and sub-triangular in shape, with a broad front and a somewhat tapering heel part. RP2 and RP6 are preserved with at least two digital impressions. Manual impressions are kidney-shaped (e.g., LM4) but can be reduced to narrow slits due to deformation during or after track formation. Some impressions (e.g., RM2 and RM4) appear to be broader on their radial margins, while the opposite seems to be true for others (e.g., LM6, LM4).

Trackway A2 (Figs 2S and 3S)

Identification—Trackway A2 can be clearly identified based on a series of pedal prints (RP2–LP5) arranged in a trackway pattern very similar to that of Trackway A1. These footprints share a similar depth, appearance, dimension, morphology, and orientation. Aberrant morphologies can be seen in the somewhat larger and circular LP3, which is probably enlarged due to overstepping and coalescing with another impression, as suggested by the slight offset of the posterior part of the displacement rim. RP5 has a more slender and irregular appearance due to a block of sediment intruding medially into the impression, which possibly already occurred during foot liftoff. The pedal trackway shows a pronounced asymmetry, with the right pace being shorter than the left pace. Claw impressions preserved in RP2, RP3 and LP5 as well as the rotation angle of the pedal impressions suggest a direction of travel towards the west. A continuous set of manual impressions (RM3 to LM5) is associated with the pedal trackway, and can be unambiguously referred to the same trackway. The western third of the trackway is less well preserved, although the complete impression RM1 can be confidently referred to the trackway based on position, morphology, size and orientation. Partially preserved impressions (RP1, LP1, LM1, RM2, LP2, LM2, RP5) likely also pertain to the trackway.

Trackway parameters—Trackway A2, running approximately parallel to trackway A1, is perhaps the most striking of the tracksite due to its high pace angulation and manual supination angles. It is similar to Trackway A1, especially in size (pedal track length: 52 cm; GAD: 176–216 cm) and speed (2.73 km/h). It shows a significant difference between the left (92 cm) and right (77 cm) pedal pace length ($p=0.009$). Pace angulation is as high as 140° in the pedal tracks and 141° in the manual tracks. Manual supination is 101°, varying with a standard deviation of 13°; similar to the values observed in trackways 1 and 5. Probable claw marks are present on RP2, RP3 and RP4.

Footprint morphology—Pedal impressions display a similar triangular shape than those of Trackway A1, with a broad front and a somewhat tapering rear. The medial margin of some of the impressions (RP2, RP3, RP4) is straight, while the lateral margin is convex. Three digital impressions are preserved in RP2. Manual impression shape is similar to that of manual track in Trackway A1, ranging from kidney-shaped to narrow slit-like morphologies. As in the latter trackway, the manual impressions tend to be broader at their medial (anterior-facing) end (e.g., RM1, RM3, LM4).

Trackway A3 (Figs 2S and 4S)

Identification—Trackway A3 was identified based on a series of five pedal impressions (LP2–RP3; LP1) showing pronounced digital (claw) impressions. All four impressions are similar in preservation, size, and shape, and show two to three digital impressions consistent with strongly laterally deflected unguals. RP2, however, is only partly preserved, with its rear part being coalesced with another impression. An incomplete impression corresponds to the expected position of footprint RP1. A complete series of five manual impressions (LM1 to LM3) shares the same direction with the pedal trackway. Although the mean stride of the manual tracks (131 cm) is slightly longer than the mean stride of the pedal tracks (120 cm), this difference is not statistically significant due to the shortness of the trackway, and probably represents variations in gait.

Trackway parameters—Trackway A3 is characterized by a very low relative stride length, translating into a locomotion speed of 1.94 km/h, the lowest recorded from the tracksite. Accordingly, the manual-pedal track distance is the highest of any trackway of the tracksite, with the manual prints placed on level with the opposite pedal print. Manual supination is moderate, accounting for 70° on average, and is more variable than in trackways 1 and 2, with a standard deviation of 20°. Pedal rotation is

pronounced, accounting for 29°. The trackway is narrow-gauged and lacks a significant difference between pedal- and manual pace angulations. Most pedal prints exhibit clear, laterally directed claw marks.

Footprint morphology—pedal print outlines are less distinctive than those in Trackways A1 and A2, but feature two to three well preserved, anterolaterally to posterolaterally directed claw impressions indicating fully flexed digits. Manual impressions are kidney-shaped.

Trackway A4 (Figs 2S and 4S)

Trackway identification—Trackway A4 is less deeply impressed and therefore less distinctive than other trackways. It was identified based on six subsequent pedal impressions (LP2–LP4), which all share a comparatively small size and a similar morphology and orientation. Although the footprints are less elongated than those of Trackways A1 and A2, their orientation can be unequivocally assessed based on well-preserved claw impressions, which are present in RP2, LP3, and LP4. Additional pedal impressions (RP4, LP5, and the partly preserved RP1) can probably be referred to the same trackway based on their position, size, and depth. Three consecutive, well-preserved manual impressions (LM3–LM4) can be referred to the same trackway based on their position, orientation, and stride length. The well-preserved LM1 and RM1 footprints at the beginning of the trackway very likely also pertain to this manual track succession based on size, morphology, orientation and position, as are three partly preserved prints (LM2, RM2, RM4).

Trackway parameters—Trackway A4 is the second smallest of the trackways in terms of pedal print size (PL=36 cm). The dumbbell-shaped manual impressions, on the other hand, are proportionally large; together with Trackway A7, this trackway shows the smallest heteropody index. Locomotion speed, averaging at 3.3 km/h, is amongst the highest of the analyzed trackways. Trackway gauge is medium to wide, with the mean WAP/PL ratio accounting for 1.23, which is only exceeded by the atypical Trackway A9 (1.5). Manual supination averages at 91° with a low standard deviation of 9°, while pedal rotation averages at 21°. There is a significant difference between the left and right pedal pace ($p=0.0498$), with the left pedal pace being 72 and the right pedal pace being 86 cm. Manual prints appear to be shifted to the left relative to the pedal prints: the mean pedal-manual track angles of left

and right prints are significantly different from each other (p=0.03). Pedal prints show straight and anteriorly directed digital or claw impressions.

Footprint morphology—Pedal impressions (e.g., RP2, RP3) are only slightly longer than wide and typically triangular in shape, with an outwards-directed anterior margin featuring the digital impressions, a straight medial margin and a convex lateral margin. The digits appear to have been extended; there is no evidence for strongly laterally deflecting claw impressions as seen in Trackway A3. Footprints LP2 and, to a lesser degree, LP5, appear to be distinctly elongated. This elongation might possibly be the result of the footprints being superimposed on other footprints not pertaining to the trackway. Alternatively, these footprints could represent slip marks, where the animal lost traction on slippery ground. Manual impressions are dumbbell-shaped, consisting of two circular impressions at the medial (anterior-facing) and lateral (posterior-facing) end, respectively. The medial impression is typically larger than the lateral impression (e.g., LM4, RM3). Manual impressions are large relative to the pedal impressions.

Trackway A5 (Figs 2S and 5S)

Trackway identification—Trackway A5 is located in close proximity to Trackway A6, which appears to have been made by a trackmaker headed in the opposite direction. The trackway was identified based on a series of pedal prints (RP1, RP2, LP3, RP3) with similar preservation, sub-circular morphology, strong outward-rotation, and well-preserved claw impressions indicating laterally deflected unguals. These footprints are also similar in size except for RP3, which is probably enlarged due to superposing, as indicated by a distinct step in its medial margin. Additional pedal prints (LP2, LP4, RP4, LP5, RP5) are likely also part of the trackway. However, the triangular LP3 is much more elongated than the other pedal impressions, maybe due to interference with other footprints or due to the presence of a slip mark. A continuous series of manual impressions (LM1 to RM4) very likely can be ascribed to the same trackway.

Trackway parameters—Trackway A5 is very similar to Trackway A3 in relative stride length and manual-pedal track distance; as in the latter, manual prints are placed approximately in line with the opposite pedal print. However, pedal rotation and manual supination angles are markedly higher, being for 38° and 106°, respectively. Manual supination variability is high (standard deviation: 28°). Pedal pace angulation is 121° and manual pace angulation 102°; this difference is significant (p=0.0016). As

in Trackway A4, manual prints are shifted towards the left relative to the pedal prints; the left and right mean manual-pedal track angles are significantly different (p=0.02). Pedal prints display well-preserved digital/claw impressions, which are oriented parallel or slightly laterally to the footprint axis and show laterally directed claw tips.

Footprint morphology—Pedal track morphology is indistinctly rounded, although RP1 and PR2 display a sub-triangular morphology comparable to that of Trackway A4. At least three claw impressions are present, which are directed anterolaterally (RP3, RP2), or laterally to slightly posterolaterally (LP3, RP1), indicating flexed digits during track formation. Manual track morphology is variable, ranging from the narrow slit-like and only slightly curved morphology of RM1 and RM3 to kidney-shaped (e.g., LM4) and even horseshoe-shaped appearances (LM3).

Trackway A6 (Figs 2S and 5S)

Trackway identification—Trackway A6 was identified based on four pedal impressions (RP3–RP4) leading down the surface. The three imprints feature a similar morphology, size and orientation. Well-preserved claw impressions can be seen at least in RP3 and LP3 and probably also in RP4. Associated manual impressions (RM1 to RM4) can be referred to the trackway. While the manual trackway can be followed up the surface (LM1, RM1), the respective pedal prints of this trackway section (RP1, LP1, RP2) could not be identified unequivocally.

Trackway parameters—Trackway A6 shows the highest pedal pace angulation of all trackways (141°). In contrast, manual pace angulation is considerably lower (101°); the difference is significant with a p-value of 0.005. The pedal-manual track angle is 15°, the highest of the described trackways. Pedal rotation is high, accounting for 37°; the manual supination is 93°, with a relatively high standard deviation of 26°. Two of the pedal prints show three well-preserved, laterally directed digital/claw marks.

Footprint morphology—Pedal prints are oval (RP3) to triangular (LP3) in shape. The anterior portion containing the digital impressions is separated from the heel impression by a bulge in RP3. Three claw marks are clearly impressed in RP3 and LP3, being orientated anterolaterally to laterally in LP3 and posterolaterally in RP3. An indentation in the anterior portion of the lateral margin in both footprints can be identified as the impression of digit IV, but a definitive claw trace is not preserved. Manual

impressions are kidney-shaped, but vary greatly in length, approaching the shape of a semicircle in LM3 and RM1. RM2 and LM1 show a subdivision into two distinct pads.

Trackway A7 (Figs 2S and 6S)

Trackway identification—Trackway A7 was identified based on a series of distinctive pedal and manual impressions (RP4–RM6). The manual trackway can be traced back to the upper margin of the surface, with RM3, RM2, LM1 and RM1 being relatively well defined (RM2 is best visible on the orthophoto). Based on the position of these manual tracks, the associated pedal tracks could be identified (RP1, LP1, RP2, RP3), except for LP2, which appears to be missing. LM3 is poorly preserved and its identification as part of the trackway is solely based on its position. An impression likely corresponding to LP3 is only incompletely preserved.

Trackway parameters—Trackway A7 is medium gauge on average. It shows the second lowest pedal pace angulation (112°), after the atypical Trackway A9. Manual pace angulation is 105°. Pedal rotation is high (36°), and manual supination moderate (78°) with high standard deviation (28°).

Footprint morphology—Pedal impressions are roundish to oval in shape. The medial margin of the clearly defined pedal impressions (RP4, LP4, LP5) feature a pronounced anterior protrusion, which probably represents the impression of digit I. Faint digital impressions are probably present in RP4 and LP4. Manual impression morphology ranges from indistinctly oval or kidney-shaped (e.g., LM1, RM3, RM6) to distinctly horseshoe-shaped (LM4) or "M"-shaped (RM4) impressions. In LM4, two slightly bowed, oval impressions are arranged in an angle to each other and coalesce axially; the impression is restricted by a distinct indent into the dorsal impression margin, as well as by a large sediment bar protruding from the posterior side. In RM4, the two impressions are offset to each other, and coalesce at their midlength, forming an 'M'-like shape. The sediment bar protruding from the posterior side is broad but less extensive than in LM4.

Trackway A8 (Figs 2S and 6S)

Trackway identification—Trackway A8 was identified based on a series of three pedal prints (LP3–LP4) associated with manual tracks (LM2–RM3). Footprint RP2 is less well preserved, but shows the straight medial footprint margin seen in the other pedal prints of the trackway, and therefore can confidently referred to Trackway A8. Footprint LP2, although shaped like a very large manual

impression, matches in width with the pedal prints of Trackway A8 and, based on its position, probably represents the anterior part of a pedal impression within this trackway. LM1 is, in contrast to most of the manual prints of Trackway A8 except for LM3, distinctly horseshoe-shaped, but can probably be referred to the same trackway based on its orientation and position, as it is located precisely one stride length away from LM2, and forms a straight line with LM2 and LM3. The last third of the trackway might be present as well, but candidates for further impressions of the trackway are poorly preserved and cannot be ascribed to the latter.

Trackway parameters—Trackway A8 is similar to Trackway A7. The trackway starts as a narrow-gauged trackway and then turns into a wide-gauged trackway; it is medium-gauged on average. The left pedal pace is 70 cm and the right pedal pace 81 cm, this difference is significant ($p=0.0343$). Pedal and manual pace angulation is very low (115° and 117°, respectively). Pedal rotation is high (29°), while manual supination is moderate (70°).

Footprint morphology—Pedal impressions RP2–LP4 are longer than wide and distinctly triangular in shape, with a straight medial margin, a broad, anterolaterally facing anterior margin, and a convex lateral margin. Faint digital impressions are present in LP4. Manual impressions are highly variable. On one extreme, LM2 is a very narrow, slightly bended impression which widens at both the medial (anterior) and lateral (posterior) ends. A posteriorly directed spur-like impression on the posteromedial edge corresponds to the assumed position of digit I. Impression RM3 approaches the shape of a semicircle with a concave posterior margin, again showing the posteromedially located spur-like impression, while the lateral end is broadly rounded. In impression LM3, two elongated impressions can be discerned, which meet in a V-like fashion, as can also be seen in LM4 of Trackway 7, as well as the spur-like impression. LM1 is distinctly horseshoe-shaped, with both elongated impressions well-separated from each other by sediment bars protruding from the posterior and anterior margins. Also in this footprint, the posterior margin of the medial oval impression is narrower and more spur-like than that of the lateral oval impression.

Trackway A9 (Figs 2S and 6S)

Trackway identification—Trackway A9 was identified based on three consecutive coupled manual and pedal tracks (RP2–RM3) whose appearance is clearly different than that of surrounding impressions. Additional footprints could be referred to the trackway based on position, appearance, shape and size,

including coupled manual and pedal tracks RP1/RM1 as well as LP1 and LM3. LM1 and LP3 as well as the coupled manual and pedal tracks RP4/RM4, although possibly present, could not be identified reliably.

Trackway parameters—Trackway A9 markedly differs from the other trackways of the site. It shows a very wide gauge (WAP/PL: 1.52), and belongs to the smallest recorded individual (GAD: 70 cm; pedal track length: 23 cm). Despite its smaller size, its large relative stride results in an estimated speed of 2.77 km/h, which is comparable with that of the larger trackways. Pedal and manual pace angulations are the lowest of the tracksite (106° and 92°, respectively), the difference is significant (p=0.0054). The pedal-manual track angle is 13°, and pedal rotation is high (33°). Strikingly, the manual supination angle is only 0.5°; the manual prints thus are oriented anteriorly.

Footprint morphology—Pedal impressions LP1, RP2 and LP2 display the triangular morphology seen in several of the other trackways. The rear of the track is narrowing into a blunt end. Manual impressions are crescent-shaped, where the lateral end is blunt and the medial end is acute and somewhat deflected posteriorly, and possibly corresponds to the impression of digit I (i.e., the pollex claw).

Trackway B1 (Figs 9S)

Trackway identification—Trackway B1 of Tracksite B could be unequivocally identified in the field by one of us (SI).

Trackway parameters—Trackway B1 of tracksite 2 is narrow-gauged. Pedal prints show a high pace angulation (133°), while manual prints form a somewhat wider trackway, with a pace angulation of 116°. Pedal rotation is 17° and manual rotation 74° with a low standard deviation (4.5°). Footprint depth ranges from 2 to 5 cm.

Footprint morphology—Pedal impressions are sub-triangular in shape, being broader anteriorly than posteriorly. Manual impressions, as in RM1 and LM1, are kidney-shaped and can be sub-divided into two halves, each containing an oval impression.

RESULTS OF STATISTICAL ANALYSIS

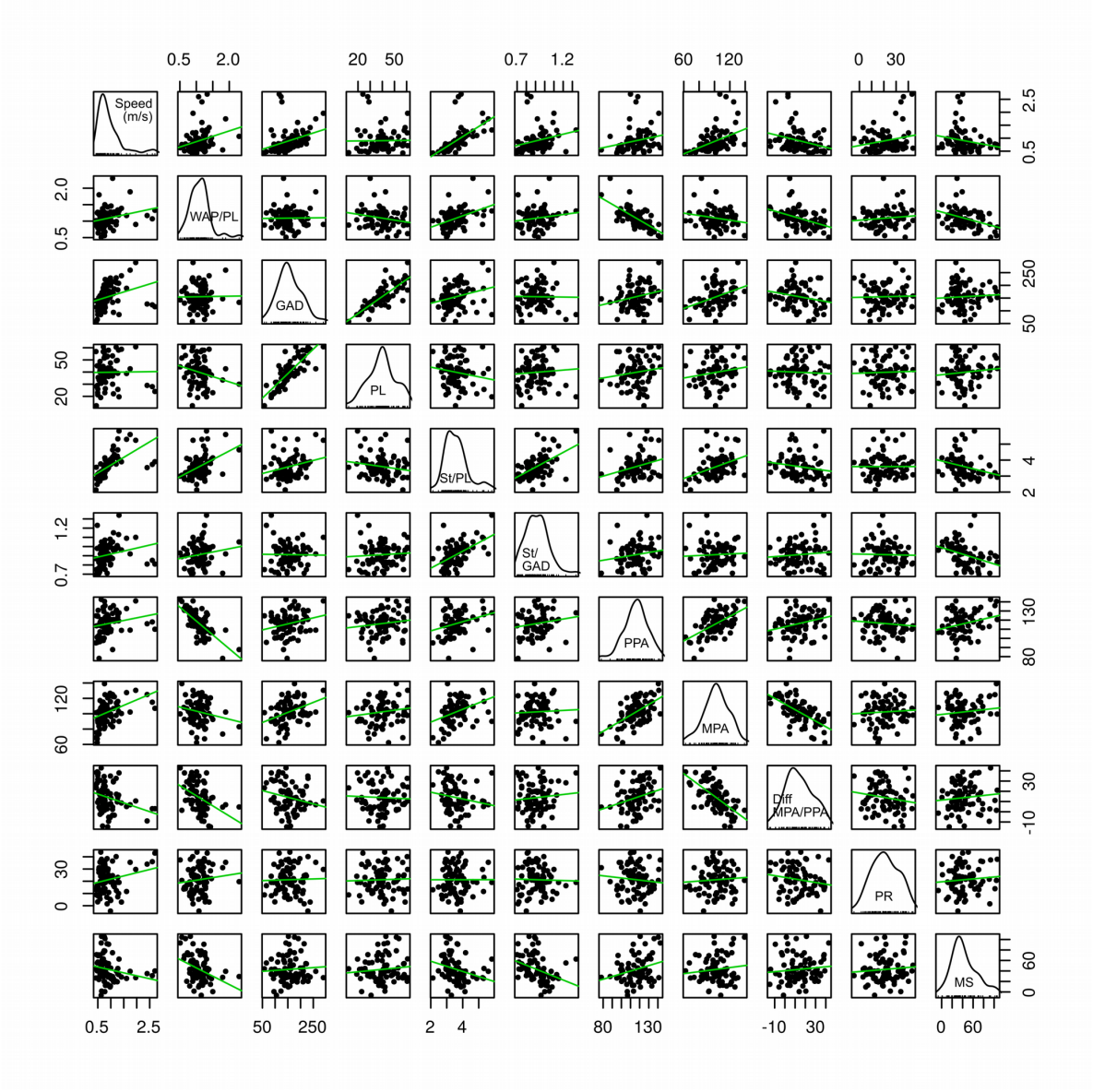

Figure 1S. Scatterplot matrix of selected variables, including frequency distributions for each variable.

DETAILED CHARTS OF THE TAFAYTOUR TRACKSITE

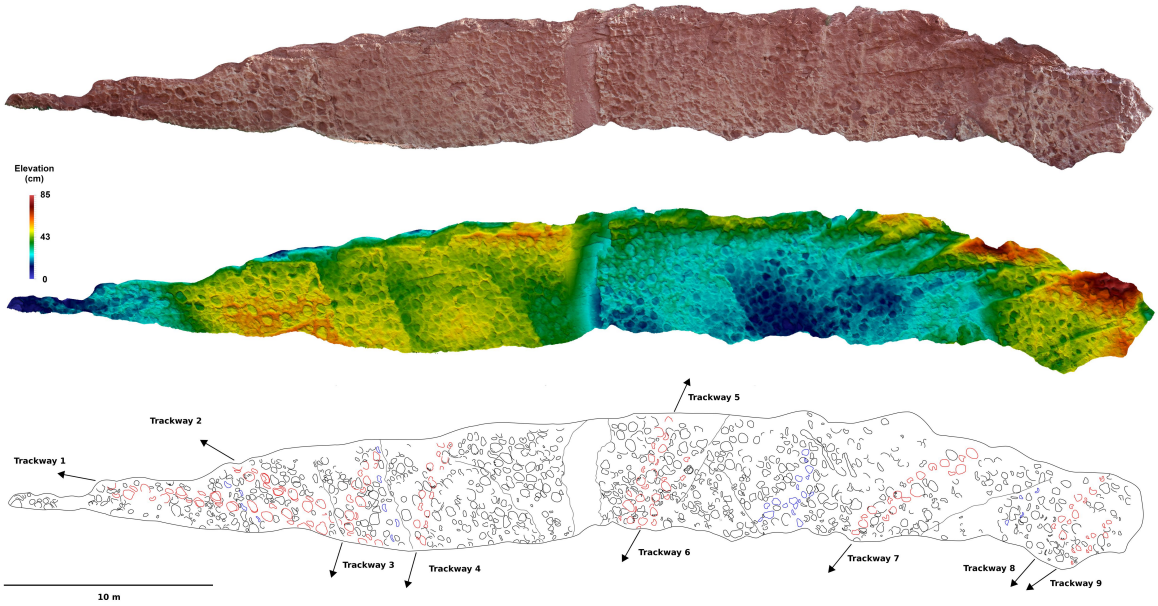

Figure 2S. Tracksite 1 as photogrammetric orthophoto (top); depth-color image (middle); and interpretive sitemap (bottom). Arrows show the direction of travel for each trackmaker.

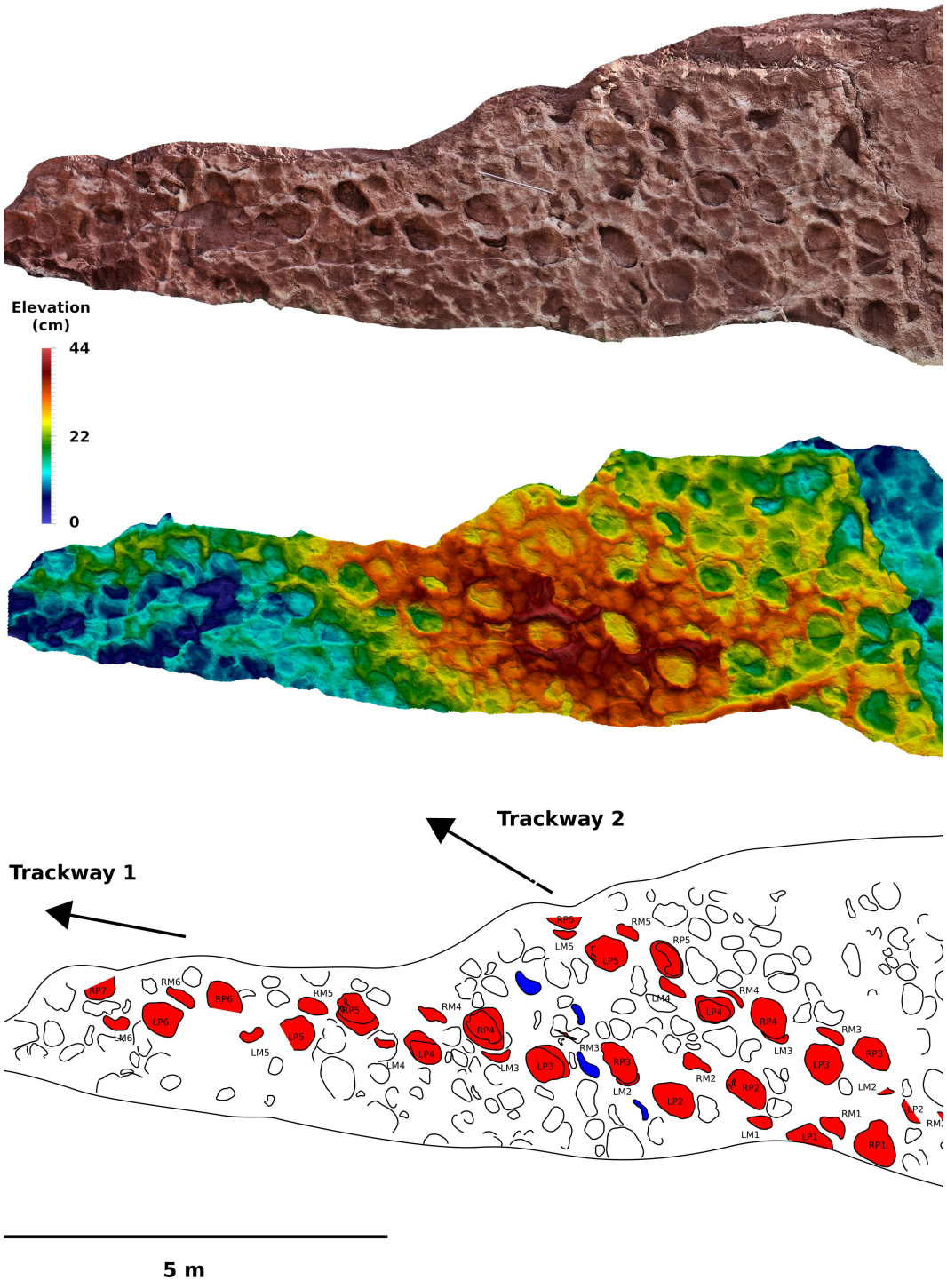

Figure 3S. Section 1 of Tracksite 1 as photogrammetric orthophoto (top); depth-color image (middle); and interpretive sitemap (bottom). Recognized trackways are shown in red, with possible additional trackways shown in blue. Arrows show the direction of travel for each trackmaker.

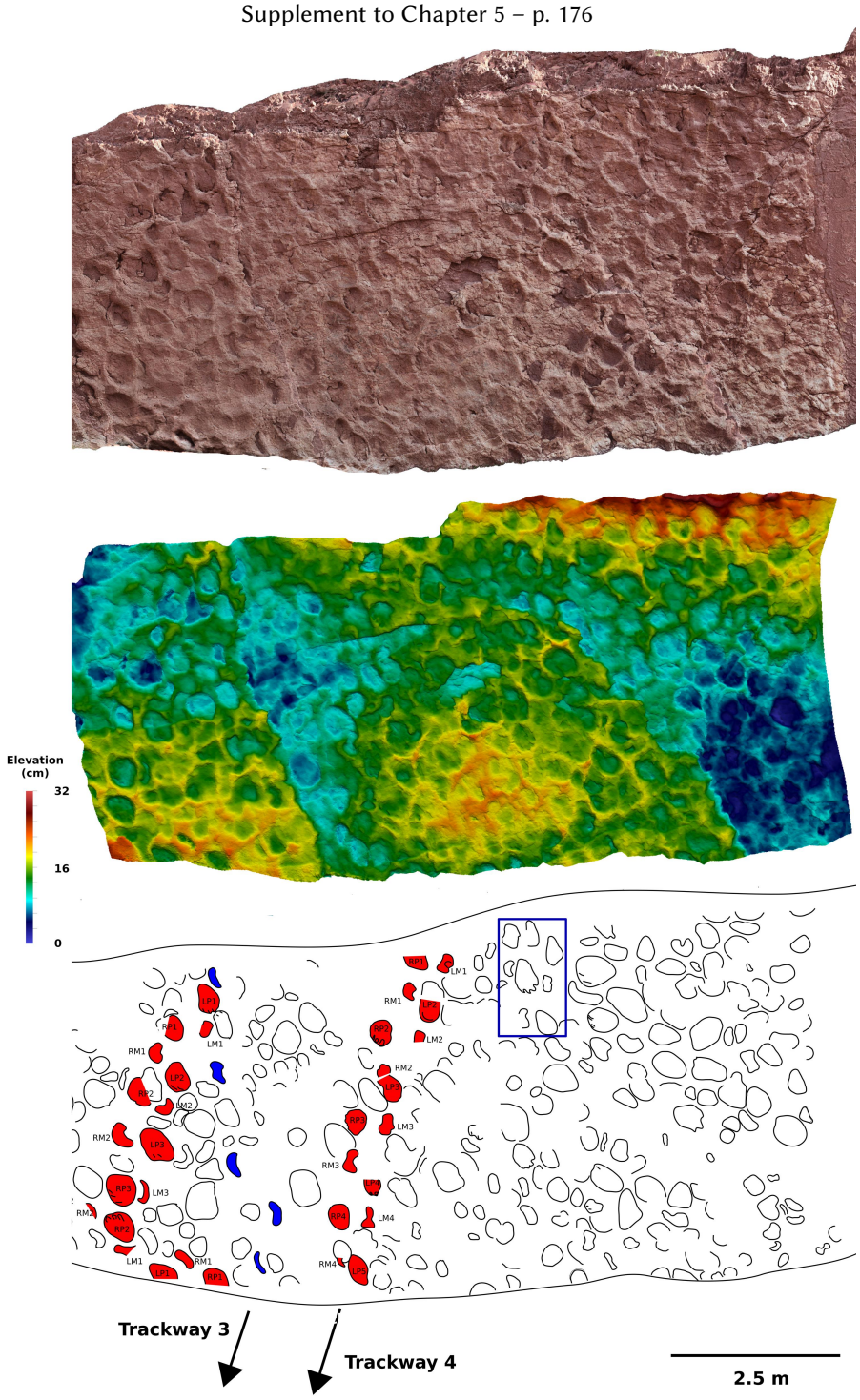

Figure 4S. Section 2 of Tracksite 1 as photogrammetric orthophoto (top); depth-color image (middle); and interpretive sitemap (bottom). Recognized trackways are shown in red, with possible additional trackways shown in blue. Arrows show the direction of travel for each trackmaker. The region within the blue rectangle is shown as close-up in Figure 7S.

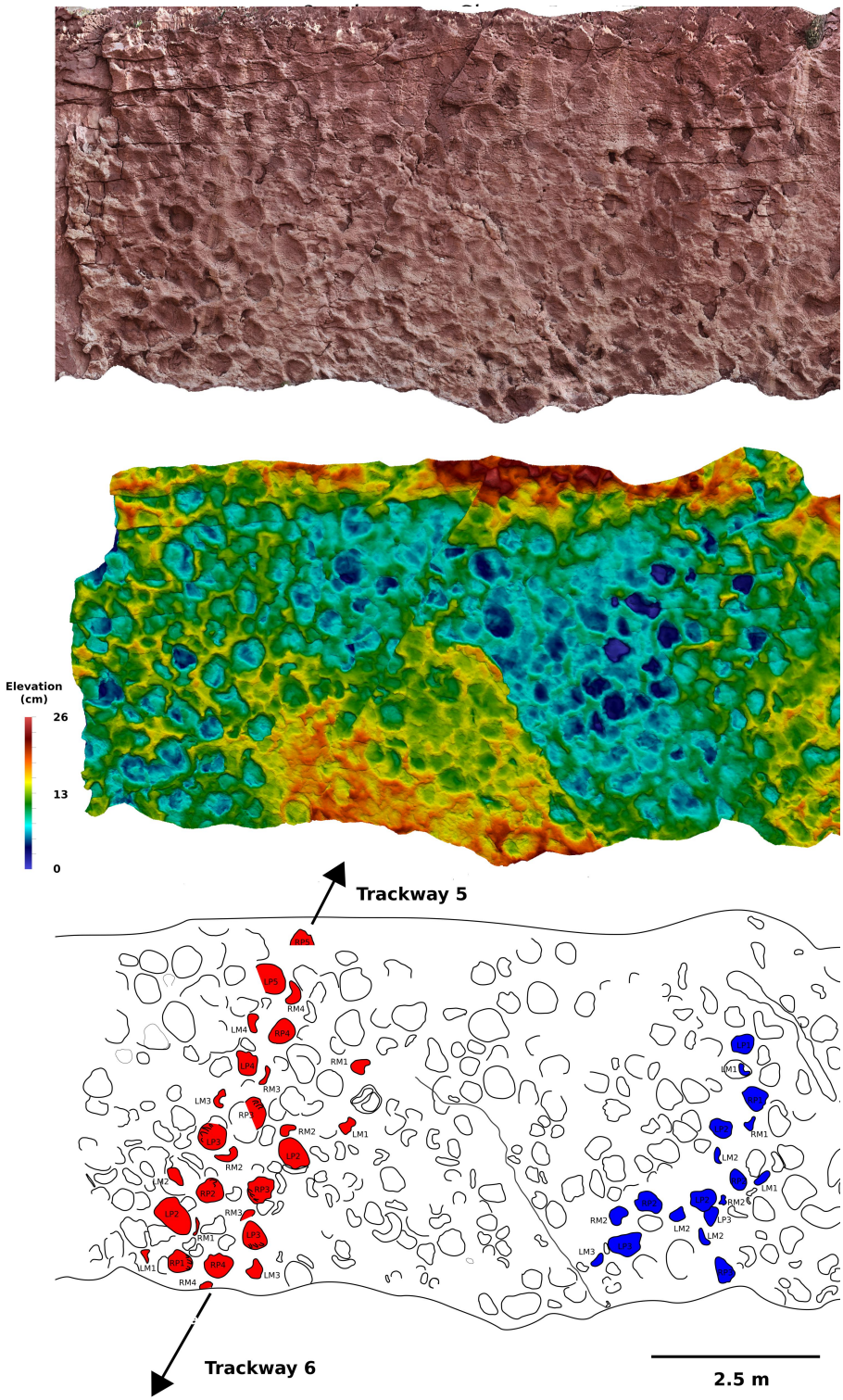

Figure 5S. Section 3 of Tracksite 1 as photogrammetric orthophoto (top); depth-color image (middle); and interpretive sitemap (bottom). Recognized trackways are shown in red, with possible additional trackways shown in blue. Arrows show the direction of travel for each trackmaker.

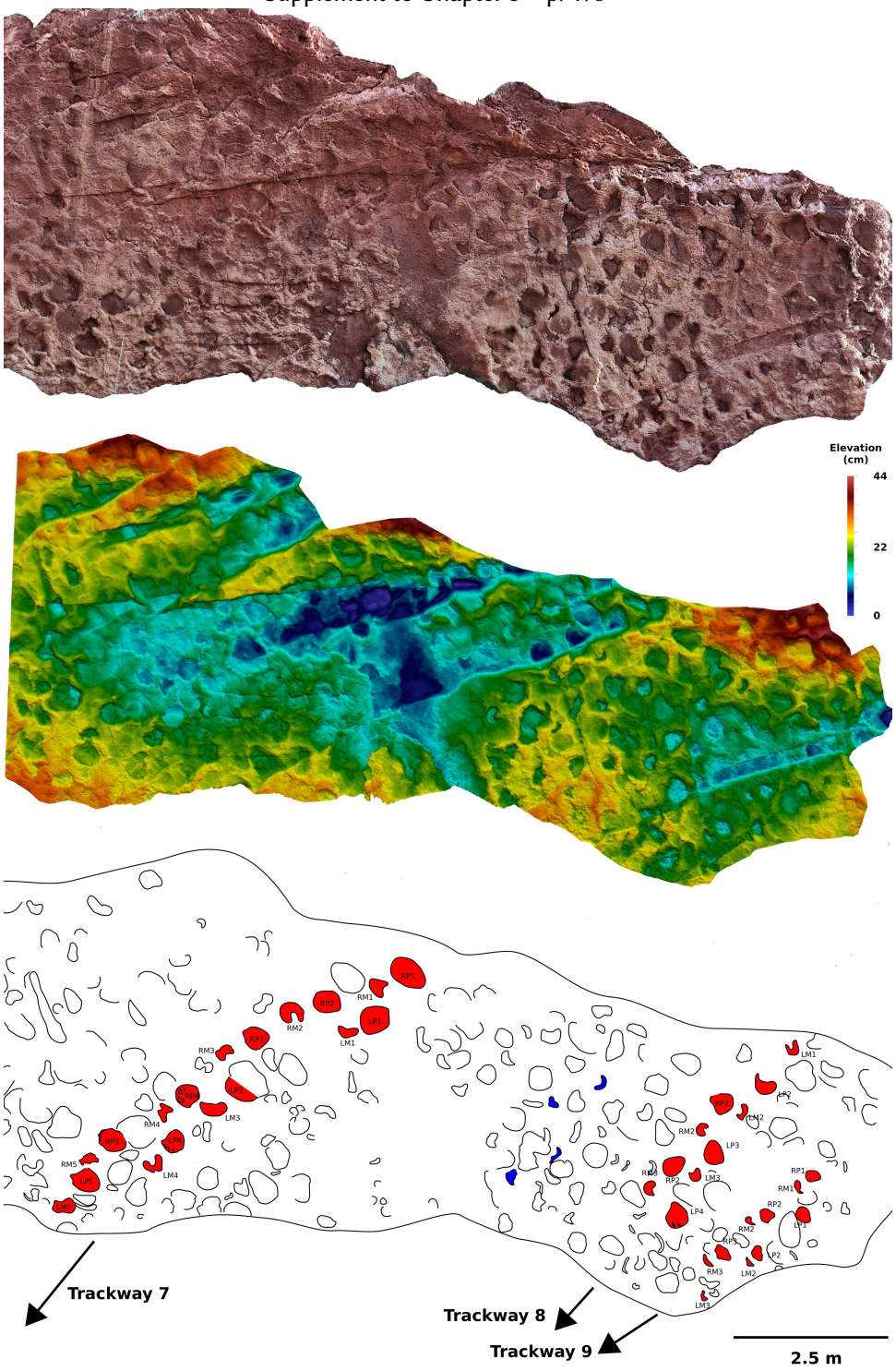

Figure 6S. Section 4 of Tracksite 1 as photogrammetric orthophoto (top); depth-color image (middle); and interpretive sitemap (bottom). Recognized trackways are shown in red, with possible additional trackways shown in blue. Arrows show the direction of travel for each trackmaker.

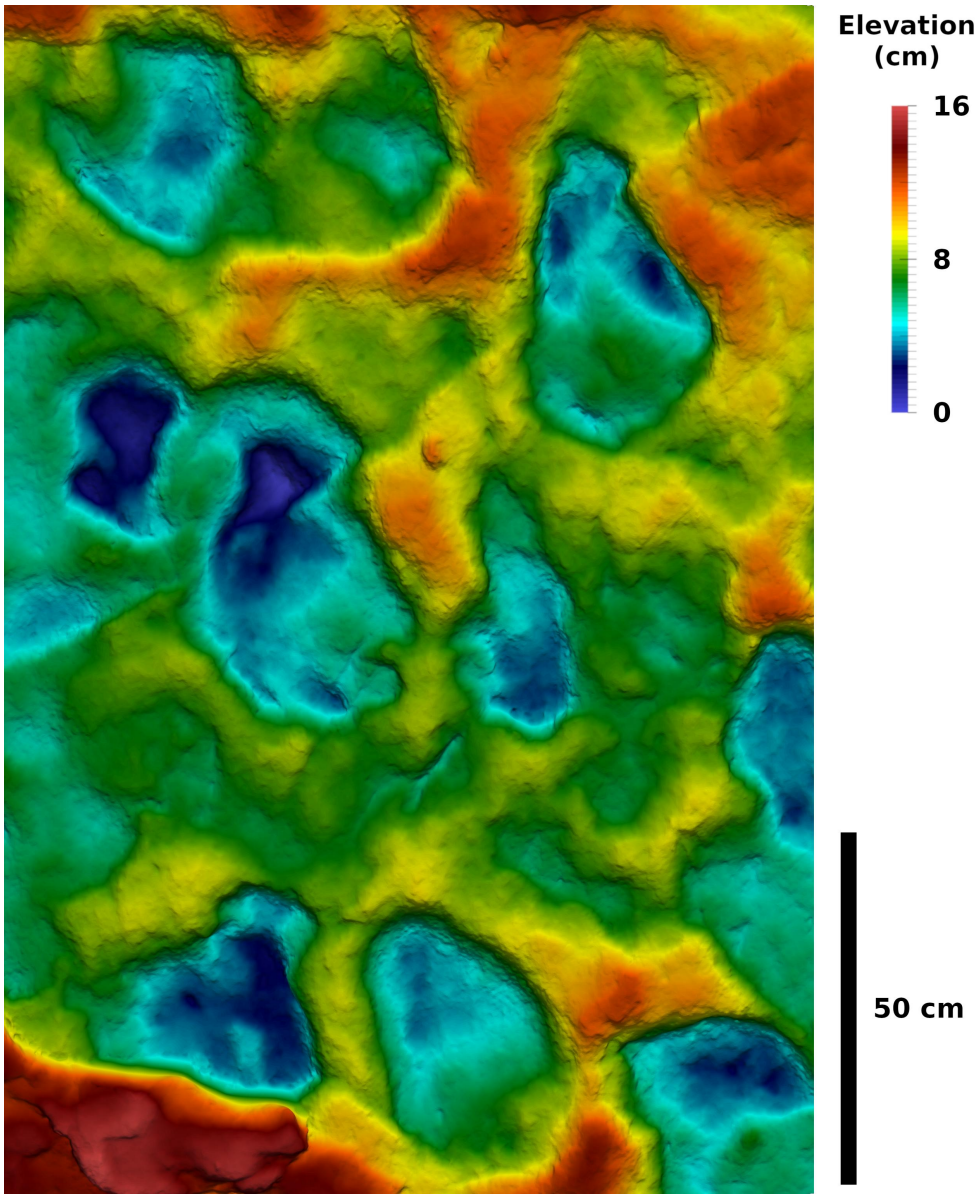

Figure 7S. Detail of section 2 (depth-color image). The exact location of the detail in the tracksite is shown in Figure 4S.

Figure 8S. Photograph made by one of us (SI) in 1984, showing the manual print LM5 of Trackway A1, which has since been lost to erosion.

Figure 9S. Photograph made by one of us (SI) in 1988, showing manual print LM1 of Trackway B1, displaying the characteristic separation into two distinct pads.

Supplemental Data 2: Data Sample

N	Trackway ID	Locality	Formation	Country	Age	Reference	PL [cm]	DGA [cm]	PA [°]	MS [°]	PR [°]
1	TaA1	Tafaytour site A	Ameskroud Formation	Morocco	Jurassic, Middle	this study	53.63	191.16	131.31	101.67	13.9
2	TaA2	Tafaytour site A	Ameskroud Formation	Morocco	Jurassic, Middle	this study	51.56	176.23	139.81	104.44	20.67
3	TaA3	Tafaytour site A	Ameskroud Formation	Morocco	Jurassic, Middle	this study	45.56	151.53	109.59	70.7	29.49
4	TaA4	Tafaytour site A	Ameskroud Formation	Morocco	Jurassic, Middle	this study	36.34	154.65	117.71	90.86	21.64
5	TaA5	Tafaytour site A	Ameskroud Formation	Morocco	Jurassic, Middle	this study	42.92	152.37	110.06	105.95	37.95
6	TaA6	Tafaytour site A	Ameskroud Formation	Morocco	Jurassic, Middle	this study	44.29	142.71	111.99	93.34	37.42
7	TaA7	Tafaytour site A	Ameskroud Formation	Morocco	Jurassic, Middle	this study	42.75	158.54	106.64	78.08	36.1
8	TaA8	Tafaytour site A	Ameskroud Formation	Morocco	Jurassic, Middle	this study	39.78	147.1	115.65	70.43	29.4
9	TaA9	Tafaytour site A	Ameskroud Formation	Morocco	Jurassic, Middle	this study	22.97	95.47	100.89	0.59	33.83
10	TaB1	Tafaytour site B	Ameskroud Formation	Morocco	Jurassic, Middle	this study	44.67	157.64	121.41	74.56	17.35
11	Ga-1	Gajin tracksite	Haman Formation	South Korea	Cretaceous, Early	Kim and Lockley, 2012 (Fig. 4b)	51.55	201.75	110.48	78.47	19.87
12	Ga-2	Gajin tracksite	Haman Formation	South Korea	Cretaceous, Early	Kim and Lockley, 2012 (Fig. 4b)	36.73	175.7	120.93	74.75	36.49
13	CR-1	Chevenez–Combe Ronde tracksite	Reuchenette Formation	Switzerland	Jurassic, Late	Marty, 2008 (p. 124)	37.5	172.5	102.95	25.25	22.15
14	CR-2	Chevenez–Combe Ronde tracksite	Reuchenette Formation	Switzerland	Jurassic, Late	Marty, 2008 (p. 124)	39	182.23	116.3	34.7	7.25
15	CR-10	Chevenez–Combe Ronde tracksite	Reuchenette Formation	Switzerland	Jurassic, Late	Marty, 2008 (p. 124)	30	133.09	85.35	29.35	19.65
16	CR-12	Chevenez–Combe Ronde tracksite	Reuchenette Formation	Switzerland	Jurassic, Late	Marty, 2008 (p. 124)	19.6	85.03	109	62.6	19.05
17	CR-13	Chevenez–Combe Ronde tracksite	Reuchenette Formation	Switzerland	Jurassic, Late	Marty, 2008 (p. 124)	22.1	93.75	105.65	25.5	19
18	CR-530-1	Chevenez–Combe Ronde tracksite	Reuchenette Formation	Switzerland	Jurassic, Late	Marty, 2008 (p. 127)	38.8	177.95	119.85	32.15	10.85
19	CR-540-1	Chevenez–Combe Ronde tracksite	Reuchenette Formation	Switzerland	Jurassic, Late	Marty, 2008 (p. 129)	25.7	139.05	121	44.7	23.15
20	RG-1	Rochefort-Les Grattes	Reuchenette Formation	Switzerland	Jurassic, Late	Marty et al., 2013 (Table 1)	32.3	137.38	115.95	36.15	10.55
21	CT-2	Courtedoux–Tchâfouè tracksite	Twannbach Formation	Switzerland	Jurassic, Late	Marty et al., 2013 (Table 1)	36	133.84	108.05	60.55	24.65
22	LOU-10	Loulle tracksite	Morillon Formation	France	Jurassic, Late	Mazin et al., 2016 (Table 1)	57.5	223.03	110.65	53.6	24.3
23	LOU-14	Loulle tracksite	Morillon Formation	France	Jurassic, Late	Mazin et al., 2016 (Table 1)	53	208.63	107.9	45.8	21.6
24	LOU-15	Loulle tracksite	Morillon Formation	France	Jurassic, Late	Mazin et al., 2016 (Table 1)	40.7	186.3	120.4	19	15.5
25	LOU-17	Loulle tracksite	Morillon Formation	France	Jurassic, Late	Mazin et al., 2016 (Table 1)	49.6	209.71	114.8	19.3	19.1
26	LOU-19	Loulle tracksite	Morillon Formation	France	Jurassic, Late	Mazin et al., 2016 (Table 1)	38.8	188.43	130.05	25.7	11.6
27	LOU-21	Loulle tracksite	Morillon Formation	France	Jurassic, Late	Mazin et al., 2016 (Table 1)	53.3	214.35	126.15	27.1	24.6
28	NGZ-T3	Nanguzhai tracksite	Tianjialou Formation	China	Cretaceous, Early	Xing et al., 2015a (Fig. 4 A)	35.51	130.04	113.44	69.11	15.08
29	LSV-1	Jishan tracksite	Tianjialou Formation	China	Cretaceous, Early	Xing et al., 2015a (Fig. 4EA)	25.95	109.94	108.98	56.96	17.27
30	KAR-ST1	Karigador tracksite	–	Croatia	Cretaceous, Late	Dalla Vecchia, 2001 (Text-fig. 8)	42.14	122.99	106.49	1.52	25.3
31	KAR-ST2	Karigador tracksite	–	Croatia	Cretaceous, Late	Dalla Vecchia, 2001 (Text-fig. 8)	39.01	121.66	110.26	39.28	23.59
32	AC-1	Agua del Choique tracksite	Loncoche Formation	Argantina	Cretaceous, Late	Gonzáles Riga and Calvo, 2009 (Text-Fig. 4)	42.67	259.76	107.3	39.26	35.46
33	ROLM-28	Lavini di Marco	Grey Limestones Formation	Italy	Jurassic, Early	Dalla Vecchia, 1994 (Fig. 2)	45.13	114.83	88.36	40.18	15.24
34	A90	Ardley trackway site	White Limestone Formation	England	Jurassic, Middle	Day et al., 2004 (Text-fig. 7E)	60.8	289.6	135.73	27.21	29.66
35	PG31	Purgatoire River tracksite	Morrison Formation	US	Jurassic, Late	Lockley et al., 1986 (Fig. 7A)	60.77	181.36	124.34	62.97	13.6
36	CE	Cabo Espichel	–	Portugal	Jurassic, Late	Meyer, 1994 (Fig. 4)	58.03	208.26	111.1	33.1	10.02
37	Cha6-2	Du Situ River (Chabu 6) tracksite	Jin Chuan Formation	China	Cretaceous, Early	Lockley et al., 2002b (Fig. 6)	40.45	158.17	124.53	11.3	19.44
38	Cha6-4	Du Situ River (Chabu 6) tracksite	Jin Chuan Formation	China	Cretaceous, Early	Lockley et al., 2002b (Fig. 6)	57.95	220.77	104.3	54.07	25.14
39	Chu-1	Chuxiongpus tracksite	Jiang Di He Formation	China	Cretaceous, Late	Lockley et al., 2002b (Fig. 10)	37.45	131.68	108.52	19.59	28.53
40	Chu-2	Chuxiongpus tracksite	Jiang Di He Formation	China	Cretaceous, Late	Lockley et al., 2002b (Fig. 10)	41.92	157.91	108.51	50.89	43.8
41	Chu-3	Chuxiongpus tracksite	Jiang Di He Formation	China	Cretaceous, Late	Lockley et al., 2002b (Fig. 10)	38.03	145.44	113.3	14.47	28.49
42	Bh	Barkhausen tracksite	Süntel Formation	Germany	Jurassic, Late	Lockley et al., 2004 (Fig. 5A)	40.23	147.02	90.81	69.53	8.6
43	ZJII-1	Zhaojue tracksite II	Feitianshan Formation	China	Cretaceous, Early	Xing et al., 2014b (Fig. 12)	42.2	151.86	122.03	9.39	5.21
44	ZJIIN-1	Zhaojue tracksite IIN	Feitianshan Formation	China	Cretaceous, Early	Xing et al., 2014b (Fig. 12)	40.95	142.02	103.38	34.78	21.65
45	ZJIIN-2	Zhaojue tracksite IIN	Feitianshan Formation	China	Cretaceous, Early	Xing et al., 2014b (Fig. 12)	41.42	214.08	124.53	91.81	1.51
46	ZJIIN-3	Zhaojue tracksite IIN	Feitianshan Formation	China	Cretaceous, Early	Xing et al., 2014b (Fig. 12)	37.12	139.29	109.31	12.42	18.97
47	ZJIIN-5	Zhaojue tracksite IIN	Feitianshan Formation	China	Cretaceous, Early	Xing et al., 2014b (Fig. 12)	38.22	137.32	112.3	12.78	6.89
48	Ho20	Hoewha District, locality 20	Jindong Formation	South Korea	Cretaceous, Early	Lee et al. 2000 (Fig. 8B)	28.95	65.74	81.42	55.25	16.35
51	Ho19	Hoewha District, locality 19	Jindong Formation	South Korea	Cretaceous, Early	Lockley 2006 (Fig. 11l)	12.28	57.95	114.12	44.17	8.85
49	Du-1	Dukmyeongri	Jindong Formation	South Korea	Cretaceous, Early	Lim et al. 1989 (Fig. 35.4A)	18.98	84.71	113.08	33.93	24.09
50	Du-2	Dukmyeongri	Jindong Formation	South Korea	Cretaceous, Early	Lim et al. 1994 (Fig. 6, middle)	21.28	85.46	103.52	43.04	8.15
52	Sa-1	Sangjock	Jindong Formation	South Korea	Cretaceous, Early	Lockley 2006 (Fig. 11D)	43	199.27	102.16	45.55	4.26
53	Si	Silbawi	Jindong Formation	South Korea	Cretaceous, Early	Lockley 2006 (Fig. 11E)	47.47	228.79	103.27	31.04	-4.39
54	So	Soltykow (=Odrowaz site)	Zagaje Formation	Poland	Jurassic, Early	Gierliński and Sawicki, 1998 (Plate II)	39.19	167.32	121.25	20.3	16.67
55	MC-1	Mill Canyon	Cedar Mountain Formation	US	Cretaceous, Early	Lockley et al. 2014 (Fig. 10A)	33.43	147.14	75.33	27.8	31.09
56	LCR-9	Las Cerradicas	Villar del Arzobispo Formation	Spain	Cretaceous, Early	Castanera et al. 2011 (Table 1)	29	126.62	120.5	35	34
57	LCR-10	Las Cerradicas	Villar del Arzobispo Formation	Spain	Cretaceous, Early	Castanera et al. 2011 (Table 1)	24	116.11	108.5	40	43
58	LCR-13	Las Cerradicas	Villar del Arzobispo Formation	Spain	Cretaceous, Early	Castanera et al. 2011 (Table 1)	28	123.36	116.5	31	36
59	Go	Goseong	Jindong Formation	South Korea	Cretaceous, Early	Huh et al. 2003 (Fig. 6A)	23.03	98.84	96.07	43.61	3.13
60	LN	Las Navillas	Middle Enciso Group	Spain	Cretaceous, Early	Lorente 2003 (Figura 48)	60.47	229.35	119.58	20.31	40.14
61	SMG-1	Shimiaogou	Jiaguan Formation	China	Cretaceous, Early	Xing et al. 2016d (Fig. 2)	43.76	171.44	100.65	51.14	31.42
62	SMG-2	Shimiaogou	Jiaguan Formation	China	Cretaceous, Early	Xing et al. 2016d (Fig. 8)	41.74	156.18	101.19	44.85	35.64
63	CHB-1	Changhebian	Zhenzhuchong Formation	China	Jurassic, Early	Xing et al. 2016c (Fig. 4)	31.55	106.55	99.92	35.92	19.92
64	CHB-2	Changhebian	Zhenzhuchong Formation	China	Jurassic, Early	Xing et al. 2016c (Fig. 4)	34.72	124.19	91.79	20.03	14.03
65	CHB-3	Changhebian	Zhenzhuchong Formation	China	Jurassic, Early	Xing et al. 2016c (Fig. 4)	31.49	101.62	105.94	34.16	10.01
66	JYS11	Jiaoyuan	Ziliujing Formation	China	Jurassic, Early	Xing et al. 2016a (Fig. 10B)	26.32	112.95	115.84	39.3	31.77
67	Da-1	Dazu tracksite	Zhenzhuchong Formation	China	Jurassic, Early	Xing et al. 2014c (Fig. 6A)	35.18	129.7	93.59	23.65	27.28
68	Da-2	Dazu tracksite	Zhenzhuchong Formation	China	Jurassic, Early	Xing et al. 2011 (Fig. 4, second from left)	30.74	105.16	107.46	-6.41	12.42
69	Ba	Bajiu	Feitianshan Formation	China	Cretaceous, Early	Xing et al. 2016b (Fig. 3B)	40.75	160.64	101.04	43.17	35.28
70	Gu	Gulin	Ziliujing Formation	China	Jurassic, Early	Xing et al. 2014a (Fig 6B)	39.89	159.34	115.45	59.58	25.94
71	LS1-1	Jishan	Dasheng Group	China	Cretaceous, Early	Xing et al. 2013a (Fig. 6)	52.57	197.49	98.07	34.41	38.48
72	LSI-2	Jishan	Dasheng Group	China	Cretaceous, Early	Xing et al. 2013a (Fig. 6)	28.11	114.31	94.55	71.09	13.17
73	AV3-1	Avelino	Azoia Unit	Portugal	Jurassic, Late	Lockley and Santos, 1993 (Fig. 1)	48.71	159.33	109.16	33.18	5.56
74	AV3-2	Avelino	Azoia Unit	Portugal	Jurassic, Late	Lockley and Santos, 1993 (Fig. 1)	31.55	137.35	115.73	56	20.95
75	AV3-3	Avelino	Azoia Unit	Portugal	Jurassic, Late	Lockley and Santos, 1993 (Fig. 1)	49.36	210.67	122.41	39.76	12.36
76	AV3-5	Avelino	Azoia Unit	Portugal	Jurassic, Late	Lockley and Santos, 1993 (Fig. 1)	43.37	159.98	114.89	28.42	30.04
77	LS7A	Las Sereas	Rupelo Formation	Spain	Jurassic–Cretaceous	Fernández-Baldor, 2015 (Fig. 2b)	56.88	139.7	84.51	26.55	13.03
78	TT	Toro Toro	Toro Toro Formation	Bolivia	Cretaceous, Late	Lockley et al., 2002 (Fig. 12)	58.76	237.68	104.47	28.47	2.99
79	SCP I-1	Sezze Cava Petrianni	Laziale-Abruzzese-Campano domain	Italy	Cretaceous, Late	Nicosia et al., 2007 (Fig. 8)	56.76	190.3	94.03	28.82	35.35

Supplemental Data 3: Trackway measurements

	WAP/PL	Speed m/s	DGA 1	DGA 2	DGA 3	Pes length	Stride/PL	Stride/DGA1	Stride/DGA2	Stride/DGA3	Pace ang.	pes pace ang.	manus pace ang.	diff pes manus ang.	PR	MS
TaA1	0.67	0.78	148.17	191.16	234.15	53.63	3.21	0.9	0.9	0.73	131.31	135.88	124.79	11.09	13.9	101.67
TaA2	0.56	0.76	136.89	176.23	215.56	51.56	3.05	0.89	0.89	0.73	139.81	140.52	139.1	1.43	20.67	104.44
TaA3	0.76	0.54	120.06	151.53	182.99	45.56	2.76	0.83	0.83	0.69	109.59	114.53	103	11.53	29.49	70.7
TaA4	1.23	0.92	121.14	154.65	188.17	36.34	3.69	0.87	0.87	0.71	117.71	113.04	122.38	-9.34	21.64	90.86
TaA5	0.82	0.64	120.88	152.37	183.85	42.92	2.93	0.83	0.83	0.69	110.06	120.6	99.52	21.08	37.95	105.95
TaA6	0.51	0.63	109.56	142.71	175.85	44.29	2.99	0.93	0.93	0.75	111.99	142.62	99.74	42.88	37.42	93.34
TaA7	1.15	0.77	123.23	158.54	193.86	42.75	3.3	0.89	0.89	0.73	106.64	111.59	103.67	7.91	36.1	78.08
TaA8	1.12	0.59	115.29	147.1	178.92	39.78	3.2	0.87	0.87	0.71	115.65	114.66	117.13	-2.48	29.4	70.43
TaA9	1.5	0.77	71.72	95.47	119.23	22.97	4.14	1	1	0.8	100.89	106.48	92.5	13.98	33.83	0.59
TaB1	0.73	0.7	121.43	157.64	193.84	44.67	3.24	0.92	0.92	0.75	121.41	134.04	115.09	18.95	17.35	74.56
Ga-1	1.05	0.74	161.15	201.75	242.34	51.55	3.15	0.8	0.8	0.67	110.48	111.72	109.49	2.24	19.87	78.47
Ga-2	1.26	1.07	137.34	175.7	214.07	36.73	4.18	0.87	0.87	0.72	120.93	119.27	122.59	-3.33	36.49	74.75
CR-1	1.46	1.01	134.4	172.5	210.6	37.5	4.06	0.88	0.88	0.72	102.95	109.6	96.3	13.3	22.15	25.25
CR-2	1.28	1.27	137	182.23	227.45	39	4.64	0.99	0.99	0.8	116.3	123.3	109.3	14	7.25	34.7
CR-10	2.3	1.07	98.3	133.09	167.88	30	4.64	1.05	1.05	0.83	85.35	87.7	83	4.7	19.65	29.35
CR-12	1.31	1.32	56.5	85.03	113.55	19.6	5.82	1.34	1.34	1	109	128	90	38	19.05	62.6
CR-13	1.22	1.1	66.8	93.75	120.7	22.1	4.88	1.15	1.15	0.89	105.65	120.7	90.6	30.1	19	25.5
CR-530-1	1.13	0.92	140.2	177.95	215.7	38.8	3.89	0.85	0.85	0.7	119.85	117.2	122.5	-5.3	10.85	32.15
CR-540-1	1.34	1.27	104.8	139.05	173.3	25.7	5.33	0.99	0.99	0.79	121	126	116	10	23.15	44.7
RG-1	0.8	0.73	109	137.38	165.75	32.3	3.51	0.83	0.83	0.68	115.95	129.4	102.5	26.9	10.55	36.15
CT-2	0.9	0.66	104	133.84	163.68	36	3.32	0.89	0.89	0.73	108.05	118	98.1	19.9	24.65	60.55
LOU-10	0.87	0.78	181	223.03	265.05	57.5	2.92	0.75	0.75	0.63	110.65	123.1	98.2	24.9	24.3	53.6
LOU-14	0.99	0.87	160	208.63	257.25	53	3.67	0.93	0.93	0.76	107.9	117.9	97.9	20	21.6	45.8
LOU-15	1.28	1.14	142	186.3	230.6	40.7	4.35	0.95	0.95	0.77	120.4	118.7	122.1	-3.4	15.5	19
LOU-17	1.26	1.25	157	209.71	262.43	49.6	4.25	1.01	1.01	0.8	114.8	119.6	110	9.6	19.1	19.3
LOU-19	1.17	1.61	137	188.43	239.85	38.8	5.3	1.09	1.09	0.86	130.05	132.6	127.5	5.1	11.6	25.7
LOU-21	0.98	1.07	162	214.35	266.7	53.3	3.93	0.98	0.98	0.79	126.15	127.3	125	2.3	24.6	27.1
NGZ-T3	0.64	0.51	105.22	130.04	154.86	35.51	2.8	0.76	0.76	0.64	113.44	130.71	92.73	37.98	15.08	69.11
LSV-1	0.83	0.5	90.12	109.94	129.76	25.95	3.06	0.72	0.72	0.61	108.98	124.1	88.81	35.29	17.27	56.96
KAR-ST1	0.93	0.65	90.69	122.99	155.29	42.14	3.07	1.05	1.05	0.83	106.49	113.32	92.84	20.48	25.3	1.52
KAR-ST2	1.06	0.77	89.08	121.66	154.23	39.01	3.34	1.07	1.07	0.84	110.26	112.54	82.88	29.66	23.59	39.28
AC-1	1.89	1.75	200.01	259.76	319.51	42.67	5.6	0.92	0.92	0.75	107.3	109.02	102.16	6.86	35.46	39.26
ROLM-28	1.01	0.48	86.81	114.83	142.85	45.13	2.48	0.98	0.98	0.78	88.36	101.37	62.35	39.02	15.24	40.18
A90	0.9	1.96	209.94	289.6	369.27	60.8	5.24	1.1	1.1	0.86	135.73	141.02	130.44	10.57	29.66	27.21
PG31	0.62	0.71	137.14	181.36	225.58	60.77	2.91	0.98	0.98	0.78	124.34	132.39	108.25	24.15	13.6	62.97
CE	1.18	1.3	149.38	208.26	267.15	58.03	4.06	1.13	1.13	0.88	111.1	119.25	102.96	16.28	10.02	33.1
Cha6-2	0.8	0.99	117.37	158.17	198.97	40.45	4.04	1.03	1.03	0.82	124.53	133.33	115.73	17.59	19.44	11.3
Cha6-4	1.23	0.91	169.87	220.77	271.66	57.95	3.51	0.92	0.92	0.75	104.3	107.86	100.73	7.12	25.14	54.07
Chu-1	1.16	0.76	97.92	131.68	165.43	37.45	3.6	1.03	1.03	0.82	108.52	110.07	105.41	4.66	28.53	19.59
Chu-2	1.02	0.61	125.66	157.91	190.16	41.92	3.08	0.82	0.82	0.68	108.51	113.69	98.17	15.52	43.8	50.89
Chu-3	1.43	0.88	109.41	145.44	181.47	38.03	3.79	0.99	0.99	0.79	113.3	105.93	120.67	-14.75	28.49	14.47
Bh	1.26	0.58	120.05	147.02	173.98	40.23	2.68	0.73	0.73	0.62	90.81	96.36	79.71	16.65	8.6	69.53
ZJII-1	1.07	0.97	110.79	151.86	192.93	42.2	3.89	1.08	1.08	0.85	122.03	120.89	126.61	-5.72	5.21	9.39
ZJIIN-1	0.94	0.74	108.22	142.02	175.82	40.95	3.3	0.95	0.95	0.77	103.38	120.64	86.12	34.51	21.65	34.78
ZJIIN-2	0.9	0.86	176.32	214.08	251.83	41.42	3.65	0.71	0.71	0.6	124.53	126.11	123.34	2.77	1.51	91.81
ZJIIN-S3	1.09	0.79	105.74	139.29	172.84	37.12	3.62	0.96	0.96	0.78	109.31	112.15	107.04	5.11	18.97	12.42
ZJIIN-5	1.19	0.85	102.65	137.32	171.98	38.22	3.63	1.01	1.01	0.81	112.3	113.68	110.91	2.76	6.89	12.78
Ho20	1.25	0.48	45.5	65.74	85.98	28.95	2.8	1.23	1.23	0.94	81.42	95.58	67.27	28.32	16.35	55.25
Du-1	1.04	0.61	66.88	84.71	102.54	18.98	3.76	0.84	0.84	0.7	113.08	118.83	107.33	11.5	24.09	33.93
Du-2	0.8	0.5	69.75	85.46	101.18	21.28	2.95	0.74	0.74	0.62	103.52	124.53	93.01	31.52	8.15	43.04
HO19	0.88	0.44	47.06	57.95	68.84	12.28	3.55	0.75	0.75	0.63	114.12	124.73	101.38	23.34	8.85	44.17
Sa-1	1.28	1	159.13	199.27	239.4	43	3.73	0.81	0.81	0.67	102.16	107.43	99.53	7.9	4.26	45.55
Si	1.08	0.99	183.08	228.79	274.51	47.47	3.85	0.8	0.8	0.67	103.27	120.72	85.81	34.91	-4.39	31.04
So	0.71	1.1	127.01	167.32	207.63	39.19	4.11	0.96	0.96	0.78	121.25	135.86	106.65	29.21	16.67	20.3
MC-1	1.8	0.55	121.11	147.14	173.17	33.43	3.12	0.71	0.71	0.6	75.33	78.06	73.5	4.56	31.09	27.8
LCR-9	1.17	2.4	101	126.62	152.25	29	3.53	0.81	0.81	0.67	120.5	116	125	-9	34	35
LCR-10	1.33	2.7	92.74	116.11	139.49	24	3.9	0.81	0.81	0.67	108.5	110	107	3	43	40
LCR-13	1.07	2.6	97.24	123.36	149.49	28	3.73	0.85	0.85	0.7	116.5	118	115	3	36	31
Go	1.27	0.49	80.94	98.84	116.74	23.03	3.11	0.72	0.72	0.61	96.07	100.33	91.11	9.22	3.13	43.61
LN	0.89	1.21	172.6	229.35	286.09	60.47	3.75	0.99	0.99	0.79	119.58	130.46	97.8	32.66	40.14	20.31
SMG-1	1.22	0.66	138.67	171.44	204.2	43.76	2.99	0.76	0.76	0.64	100.65	100.17	101.01	-0.83	31.42	51.14
SMG-2	1.07	0.58	125.35	156.18	187	41.74	2.95	0.79	0.79	0.66	101.19	107.15	95.22	11.94	35.64	44.85
CHB-S1	1.25	0.6	82	106.55	131.09	31.55	3.11	0.92	0.92	0.75	99.92	100.55	98.05	2.5	19.92	35.92
CHB-S2	1.28	0.74	94.25	124.19	154.14	34.72	3.45	0.96	0.96	0.78	91.79	100.25	80.51	19.75	14.03	20.03
CHB-S3	0.92	0.59	76.3	101.62	126.95	31.49	3.22	1	1	0.8	105.94	117.46	86.74	30.72	10.01	34.16
JYS11	1.05	0.79	86.52	112.95	139.38	26.32	4.02	0.94	0.94	0.76	115.84	119.87	111.81	8.06	31.77	39.3
Da-1	1.21	0.54	101.68	129.7	157.72	35.18	3.19	0.86	0.86	0.71	93.59	103.26	83.92	19.35	27.28	23.65
DA-2	1.15	0.63	79.85	105.16	130.47	30.74	3.29	0.96	0.96	0.78	107.46	106.77	108.14	-1.37	12.42	-6.41
Ba	1.38	0.68	127.59	160.64	193.69	40.75	3.24	0.82	0.82	0.68	101.04	99.3	113.28	-13.98	35.28	43.17
Gu	0.85	0.69	126.02	159.34	192.66	39.89	3.34	0.84	0.84	0.69	115.45	119.24	111.65	7.6	25.94	59.58
LS1-S1	1.24	0.86	152.62	197.49	242.35	52.57	3.41	0.91	0.91	0.74	98.07	110.24	89.96	20.28	38.48	34.41
LSI-S2	0.86	0.45	94.34	114.31	134.28	28.11	2.84	0.7	0.7	0.59	94.55	113.74	75.37	38.37	13.17	71.09
AV3-1	0.87	0.59	126.19	159.33	192.46	48.71	2.72	1.05	0.83	0.69	109.16	114.52	103.14	11.37	5.56	33.18
AV3-2	1	0.8	107.82	137.35	166.88	31.55	3.74	1.1	0.86	0.71	115.73	123.1	103.45	19.65	20.95	56
AV3-3	0.99	1.22	159.2	210.67	262.14	49.36	4.17	1.29	0.98	0.79	122.41	130.98	113.84	17.14	12.36	39.76
AV3-5	0.92	0.9	120.51	159.98	199.45	43.37	3.64	1.31	0.99	0.79	114.89	123.81	105.96	17.85	30.04	28.42
LS 7A	1.01	0.43	109.37	139.7	170.02	56.88	2.13	1.11	0.87	0.71	84.51	95.03	68.75	26.28	13.03	26.55
TT	1.39	1.41	180.46	237.68	294.91	58.76	3.9	1.27	0.96	0.78	104.47	108.75	100.19	8.56	2.99	28.47
SCP I-1	1.13	0.71	149.32	190.3	231.27	56.76	2.89	1.1	0.86	0.71	94.03	97.65	90.41	7.24	35.35	28.82

Chapter 6

Published as:

Lallensack, J.N., Klein, H., Milàn, J., Wings, O., Mateus, O., Clemmensen, L.B., 2017. Sauropodomorph dinosaur trackways from the Fleming Fjord Formation of East Greenland: evidence for Late Triassic sauropods. Acta Palaeontologica Polonica 62, 833–843. **p. 185–196.**

Author contributions:

- Jens N. Lallensack collected data, analyzed the data, wrote the paper, prepared figures, reviewed drafts of the paper.
- Jesper Milàn collected data, wrote the paper, prepared figures, reviewed drafts of the paper.
- Lars B. Clemmensen collected data, wrote the paper, reviewed drafts of the paper.
- Hendrik Klein wrote the paper, reviewed drafts of the paper.
- Oliver Wings and Octávio Mateus collected data, reviewed drafts of the paper.

Supplementary Material:

- SOM 1: Selected high-resolution photographs showing the described trackways in the field. **p. 197–203.**
- SOM 2–4: Photogrammetric 3D-data (available from DVD or online).

Sauropodomorph dinosaur trackways from the Fleming Fjord Formation of East Greenland: Evidence for Late Triassic sauropods

JENS N. LALLENSACK, HENDRIK KLEIN, JESPER MILÀN, OLIVER WINGS, OCTÁVIO MATEUS, and LARS B. CLEMMENSEN

Lallensack, J.N., Klein, H., Milán, J., Wings, O., Mateus, O., and Clemmensen, L.B. 2017. Sauropodomorph dinosaur trackways from the Fleming Fjord Formation of East Greenland: Evidence for Late Triassic sauropods. *Acta Palaeontologica Polonica* 62 (4): 833–843.

The Late Triassic (Norian–early Rhaetian) Fleming Fjord Formation of central East Greenland preserves a diverse fossil fauna, including both body and trace fossils. Trackways of large quadrupedal archosaurs, although already reported in 1994 and mentioned in subsequent publications, are here described and figured in detail for the first time, based on photogrammetric data collected during fieldwork in 2012. Two trackways can be referred to *Eosauropus*, while a third, bipedal trackway may be referred to *Evazoum*, both of which have been considered to represent sauropodomorph dinosaur tracks. Both the *Evazoum* and the *Eosauropus* trackways are distinctly larger than other trackways referred to the respective ichnogenera. The trackmaker of the best preserved *Eosauropus* trackway is constrained using a synapomorphy-based approach. The quadrupedal posture, the entaxonic pes structure, and five weight-bearing digits indicate a derived sauropodiform trackmaker. Other features exhibited by the tracks, including the semi-digitigrade pes and the laterally deflected unguals, are commonly considered synapomorphies of more exclusive clades within Sauropoda. The present trackway documents an early acquisition of a eusauropod-like pes anatomy while retaining a well-developed claw on pedal digit IV, which is reduced in eusauropods. Although unequivocal evidence for sauropod dinosaurs is no older than the Early Jurassic, the present trackway provides evidence for a possible Triassic origin of the group.

Key words: Dinosauria, Sauropodomorpha, trackway, Triassic, Greenland.

Jens N. Lallensack [jens.lallensack@uni-bonn.de], Steinmann-Institut für Geologie, Mineralogie und Paläontologie, Rheinische Friedrichs-Wilhelm Universität Bonn, Nußallee 8, 53115 Bonn, Germany.
Hendrik Klein [Hendrik.Klein@combyphone.eu], Saurierwelt Paläontologisches Museum, Alte Richt 7, D-92318 Neumarkt, Germany.
Jesper Milàn [jesperm@oesm.dk], Geomuseum Faxe/Østsjællands Museum. Østervej 2, DK-4640 Faxe, Denmark, and Natural History Museum of Denmark, Øster Voldgade 5-7, DK-1350 Copenhagen, Denmark.
Oliver Wings [dr.wings@gmail.com], Zentralmagazin Naturwissenschaftlicher Sammlungen (ZNS), Martin-Luther-Universität Halle-Wittenberg, Domplatz 4, 06108 Halle (Saale), Germany.
Octávio Mateus [omateus@fct.unl.pt], GEOBIOTEC, Faculdade de Ciências e Tecnologia, FCT, Universidade Nova de Lisboa, 2829-526 Caparica, Portuga, and Museu da Lourinhã, Rua João Luís de Moura, 2530-157 Lourinhã, Portugal.
Lars B. Clemmensen [larsc@ign.ku.dk], Department of Geosciences and Natural Resource Management, University of Copenhagen, Øster Voldgade 10, DK-1350 Copenhagen, Denmark.

Received 21 April 2017, accepted 28 June 2017, available online 4 September 2017.

Introduction

The Triassic body fossil record of sauropods is extremely poor. Although *Isanosaurus* from the Nam Phong Formation of Thailand had been described as the oldest known sauropod (Buffetaut et al. 2000), its proposed late Norian or Rhaetian age was recently questioned, possibly placing the fossil within the Jurassic (Racey and Goodall 2009; McPhee et al. 2015). The sauropod status of Late Triassic forms such as *Antetonitrus* is unclear, given current disagreements on the taxonomic definition of Sauropoda (McPhee et al. 2014). Thus, undisputed evidence for Sauropoda sensu stricto from the Triassic is currently lacking, with some authors arguing that sauropods diverged from other

sauropodomorphs as late as close to the Triassic–Jurassic boundary (McPhee et al. 2015).

Jenkins et al. (1994) briefly mentioned the occurrence of three large, quadrupedal trackways referable to large archosaurs from the Late Triassic (Norian–Rhaetian) Fleming Fjord Formation of East Greenland. The best preserved of these trackways (herein, trackway S1) was noted to show "four clawed digits, oriented anterolaterally" and "small, crescentic impressions of the manus" (Jenkins et al. 1994: 19), and included in a sitemap showing its position amongst multiple smaller, bipedal trackways referred to the ichnogenus *Grallator*. These large trackways were frequently mentioned in subsequent literature, but have never been described or illustrated in detail. Lockley and Meyer (2000) suggested that these tracks are attributable to basal sauropodomorph ("prosauropod") dinosaurs, and possibly to the ichnogenus *Tetrasauropus*. Lockley et al. (2001, 2006a) mention that the trackways might be those of sauropod trackmakers, with Lockley et al. (2006a) stating that the tracks are similar to those referred to the ichnogenus *Eosauropus*. Fieldwork carried out in 2012 was able to relocate two of the three trackways (Sulej et al. 2014; Clemmensen et al. 2016). The better-preserved trackway was identified as that of a biped with "rounded pes and weak indications of outwards-rotated claws", and "a weak impression that could indicate the presence of a thin semilunate-shaped manus" (Clemmensen et al. 2016: 43). A second trackway, "quadrupedal, with an extreme degree of heteropody" and elongated pes imprints (Clemmensen et al. 2016: 43), was ascribed to a different type. A newly discovered third trackway showing tetradactyl pes prints was referred to cf. *Evazoum*, suggesting a basal sauropodomorph trackmaker (Sulej et al. 2014; Clemmensen et al. 2016). Klein et al. (2016) noted that, given the lack of a complete description and detailed figures, it cannot be excluded that these tracks might not belong to dinosaurs but to large chirotheriids. The purpose of the present paper is to describe these trackways in detail for the first time. In light of a possible sauropod affinity of the quadrupedal trackways, footprint features are compared with skeletal features of sauropodomorphs, allowing for trackmaker identification based on synapomorphies, and possibly providing additional data on the poorly known early evolutionary history of sauropods.

Other abbreviations.—LM, left manus; LP, left pes; PL, pes length; RM, right manus; RP, right pes; WAP, width of the angulation pattern.

Geological setting

Lake deposits of the Late Triassic Fleming Fjord Formation of central East Greenland have yielded diverse vertebrate remains, including both body and trace fossils. Body fossils include selachians, bony fishes, temnospondyl amphibians, mammaliaforms, possible sphenodonts and lepidosaurs, testudinatans, phytosaurs, aetosaurs, a possible rauisuchian, pterosaurs, and dinosaurs (theropods and basal sauropodomorphs), while the ichnofauna includes a large number of theropod-like (*Grallator*), sauropodomorph-like, and stem-crocodylian archosaur trackways (Sulej et al. 2014; Clemmensen et al. 2016; Klein et al. 2016). The three sauropodomorph-like trackways described herein come from the Track Mountain locality at Wood Bjerg-Macknight Bjerg (Fig. 1) along Carlsberg Fjord near the eastern margin of the basin (Clemmensen et al. 2016). Trackway S1 (71°24.853' N, 22°33.322' W; 534 m above sea level) and trackway S2 (71°24.955' N, 22°32.952' W) represent quadrupedal trackways, while trackway S3 (71°24.857' N, 22°33.334' W) is bipedal. The tracks are preserved as concave epireliefs on a thin, laterally extensive siltstone bed that is under- and overlain by red mudstone. The siltstone bed has a thickness between 1 and 5 cm, is multistorey and contains wave-formed structures including even lamination and tiny wave ripples. The upper surface is cut by polygonal mudcracks and reveals micro-ridges of uncertain origin. Tridactyl *Grallator* tracks are seen locally in close association with the sauropodomorph-like tracks. Selected high-resolution photographs showing the described trackways in the field are provided as SOM 1 (Supplementary Online Material available at http://app.pan.pl/SOM/app62-Lallensack_etal_SOM.pdf). During Late Triassic times, the study area was located at the northern rim of the Pangaean supercontinent at about 40°N (Clemmensen et al. 2016). The track-bearing siltstone bed is situated in the lowermost part of the Tait Bjerg Beds of the Ørsted Dal Member within the Fleming Fjord Formation (Clemmensen et al. 1998, 2016). The Ørsted Dal Member has been dated to the late Norian–early Rhaetian, based on invertebrate fossils, land-derived palynomorphs, and paleomagnetic data; the track-bearing bed probably formed around 208 mya (Clemmensen 1980; Kent and Clemmensen 1996; Clemmensen et al. 1998, 2016). The track-bearing part of the succession was deposited in an ephemeral to semi-perennial lake with annual and longer-term fluctuations in lake water. The siltstone bed records flooding events of mudflats by lake water (Clemmensen et al. 1998).

Material and methods

The three trackways described herein (S1, S2, S3) were found in close proximity to each other (Fig. 1C). Descriptions and measurements are based on high-resolution photogrammetric 3D-models generated from photographs taken during fieldwork following the procedures described by Mallison and Wings (2014). Photographs of trackway S1 were taken by OW using a Canon EOS 30D digital SLR camera (8.19 Mpx), while those of trackways S2 and S3 were taken by JM using a Canon EOS 400D digital SLR camera (10 Mpx). Photogrammetric models were generated using Agisoft PhotoScan Professional 1.2.4 (www.agisoft.com). The hori-

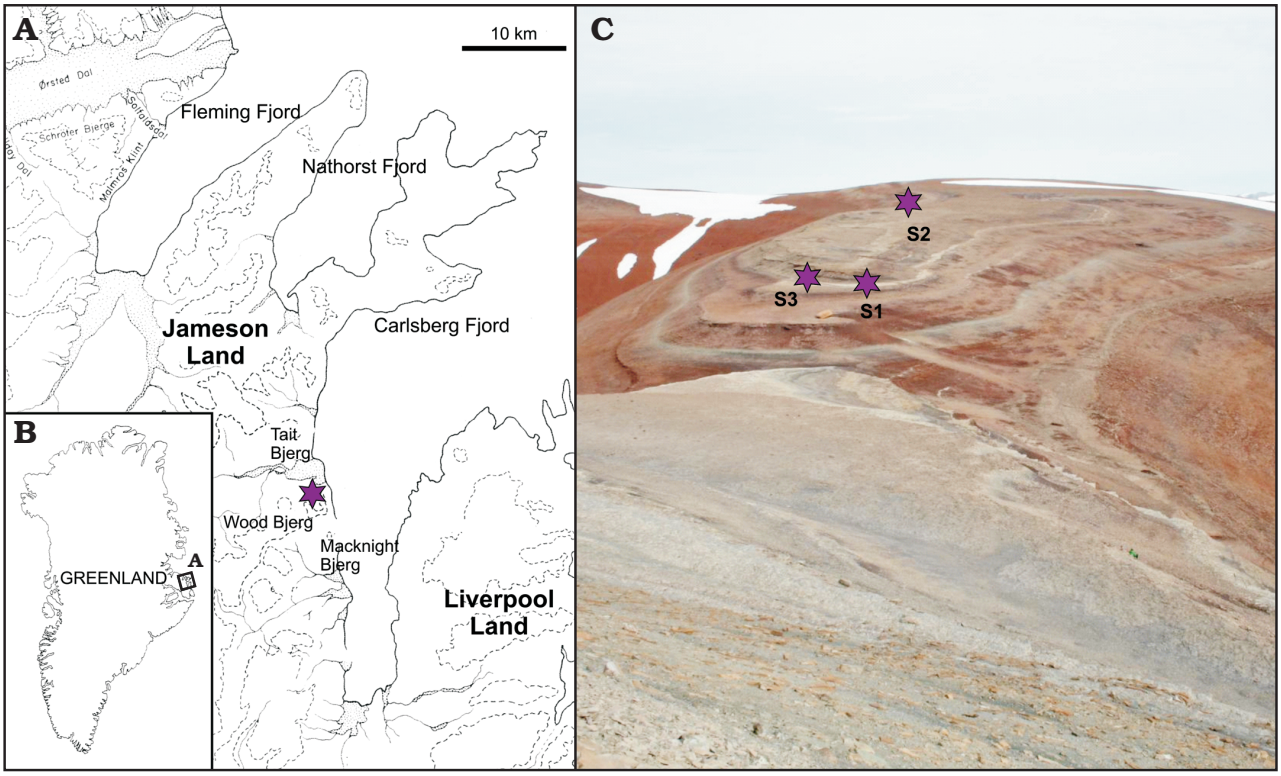

Fig. 1. **A**. Location of the "Track Mountain" locality (star) on a ridge on the northeastern slope of Wood Bjerg in the Late Triassic sediments at the west side of Carsberg Fjord. **B**. Location of Jameson Land (A) in central East Greenland. **C**. Photograph of the "Track Mountain" locality showing the approximate location of trackways S1, S2, and S3 (view towards the east).

zontal plane of the model was automatically determined using the free software CloudCompare 2.6 (www.cloudcompare.org). Orthographic depth-color maps were generated using the free software Paraview 5.0 (www.paraview.org). Trackway parameters and footprint dimensions were calculated using standard trigonometric functions, based on xy-coordinates taken from the depth-color maps using the free software Inkscape 0.48 (www.inkscape.org). Measurements were taken according to Marty (2008). Terminology follows, until otherwise noted, that of Leonardi (1987). Photogrammetric models, including textured high-resolution .ply files and PDFs detailing the process of model generation, are provided as SOM 2–4.

Description

Trackway S1.—It consists of five consecutive pes and four manus impressions (Fig. 2, SOM 1, 2) leading towards the south-west. The layer preserving the first pes-manus set is destroyed by erosion in the remaining section of the trackway, revealing a second, slightly lower layer. It is unclear on which of these layers the animal walked on. Well preserved claw impressions might indicate that the footprints of the lower layer represent true tracks, with the more indistinct pes-manus set of the upper layer preserved as an overtrack. Alternatively, the lower layer could represent a subsurface layer preserving undertracks or deep tracks that recorded the foot anatomy more precisely than the, in this case incompetent, surface layer (Gatesy 2003; Milàn and Bromley 2006). The pes-manus sets RP1/RM1 and RP2/RM2 are the best preserved, while LP3 appears markedly more elongated than the remaining pes footprints, probably due to sediment drawn into the footprint during track formation. The trackway shows a narrow gauge (sensu Marty 2008), with a WAP/PL-ratio of 0.85. The pes pace angulation (128°) is slightly larger than the manus pace angulation (115°). The manus impressions RM1 and RM2 are broader than long and gently arched with a concave posterior margin, although this could be the result of overstepping by the pes. Clear manus digit impressions are not identifiable, possibly due to imperfect preservation. The right manus impressions are directed anteriorly, while the left ones are slightly rotated outwards. Heteropody, i.e., the ratio between the pes and manus footprint area, is about 1:3. The pes footprints, measuring 42 cm in length on average, are oval in shape and consistently rotated outwards by about 30°. Five digit impressions can be observed in the pes. The trace of digit I can be clearly identified only in RP2, where it appears broader and more protruding than the remaining digit impressions, leaving a pronounced displacement rim. In RP1, the trace of digit I

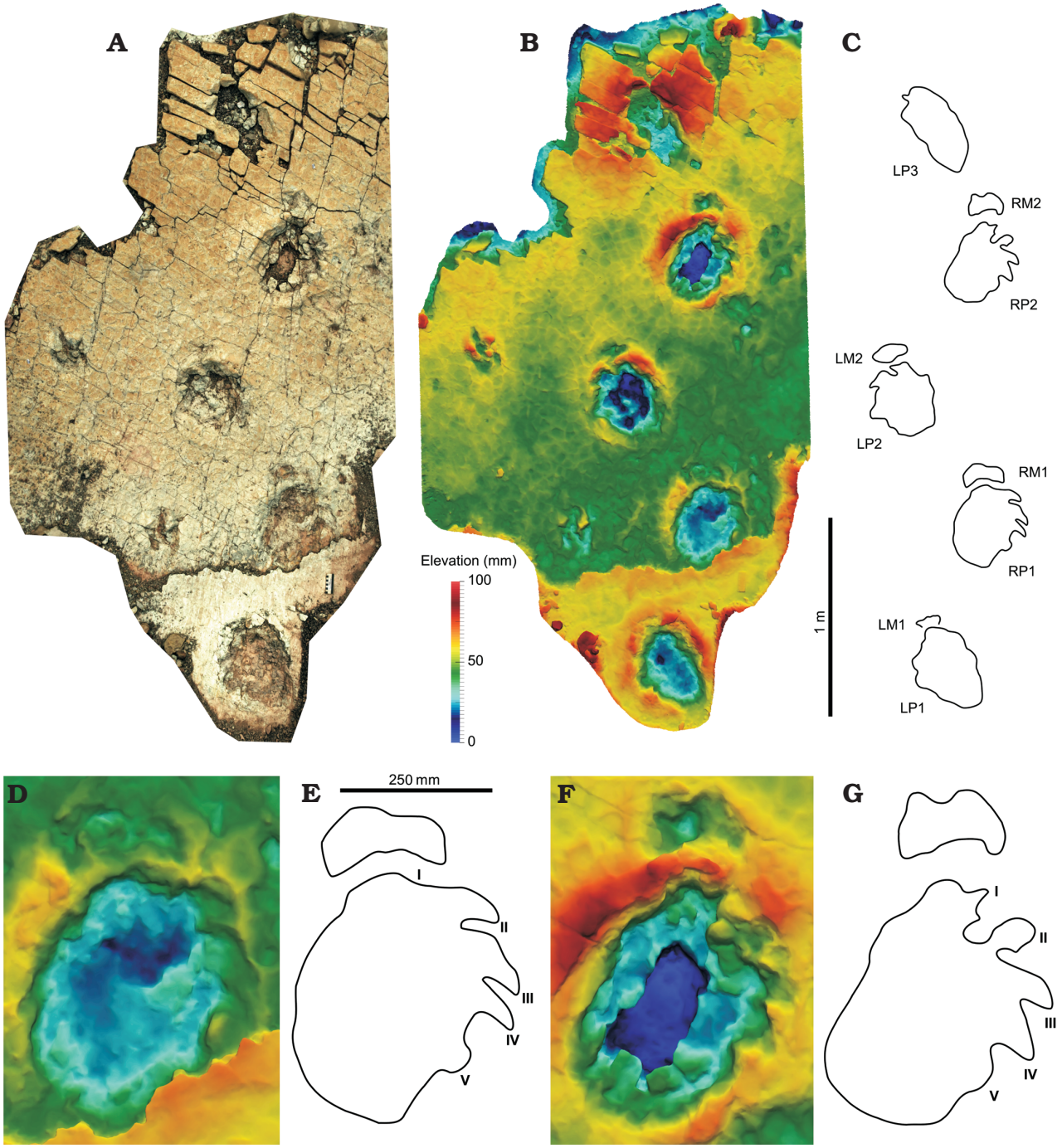

Fig. 2. **A**–**C**. Trackway S1 (*Eosauropus* sp.), here attributed to a sauropod trackmaker based on pedal synapomorphies; trackmaker is moving towards the south-west. Two consequtive pes impressions of a tridactyl *Grallator* trackway can be seen left to the S1 trackway. **D**, **E**. Detail of representative pes-manus set RP1/RM1. **F**, **G**. Detail of representative pes-manus set RP2/RM2. Photogrammetric orthophoto (A), depth-color images (B, D, F), interpretative drawings (C, E, G). Abbreviations: LM, left manus; LP, left pes; RM, right manus; RP, right pes.

is indistinct and shorter than the trace of digit II, either because of incomplete preservation, or because the ungual of digit I was deflected laterally or postero-laterally due to strong flexion, and therefore left no trace. Claw marks of digits II–IV are well preserved in RP1 and RP2, extending from the anterior half of the lateral margin of the footprint, directed laterally with respect to the long axis of the footprint and posterolaterally with respect to the direction of travel. The claw marks probably represent the impressions of the medial sides of the claws, as indicated by their broad

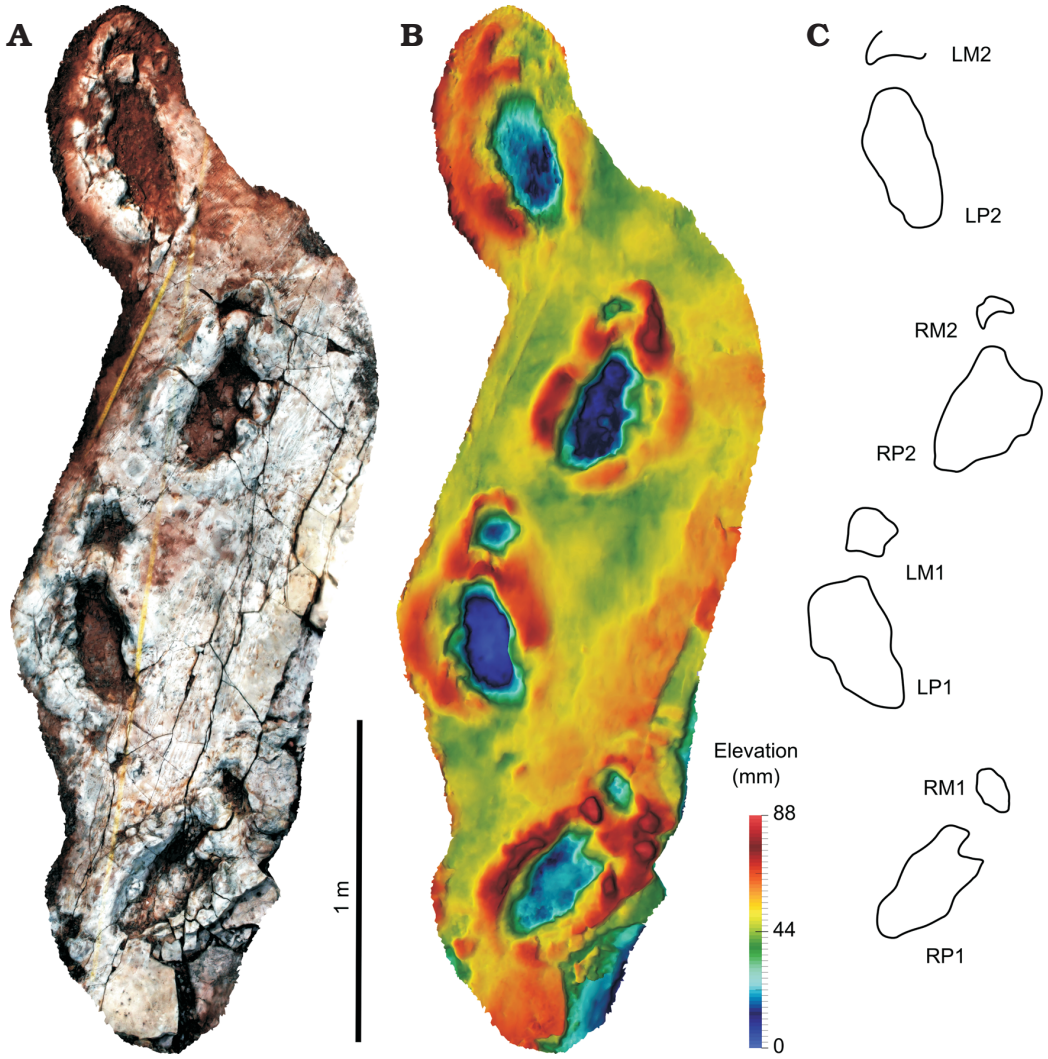

Fig. 3. Trackway S2 (*Eosauropus* sp.), which probably represents the same trackmaker species, or even the same individual, as trackway S1; trackmaker is moving towards the southwest. **A**. Photogrammetric orthophoto. **B**. Depth-color image. **C**. Interpretative drawing. Abbreviations: LM, left manus; LP, left pes; RM, right manus; RP, right pes.

bases and curved tips, and not the ventral sides as would be expected in anteriorly directed claws. A small semi-circular bulge, which is well separated from claw impression IV by a sediment bar, can be consistently found slightly below the midlength of the footprint, and is here interpreted as the clawless digit impression V.

Trackway S2.—It consists of four consecutive pes-manus pairs (Fig. 3, SOM 1, 3) leading towards the south-west, located ca. 290 m away from trackway S1. With a pes length of 41 cm, it is very similar in size to trackway S1. When compared with the latter, the pes impressions are much more elongated, and surrounded by broad displacement rims. The pes impressions are also more indistinct. While the medial margin of the pes prints is only slightly irregular, the lateral side shows irregular extensions which suggest the presence of digits, although the identification of specific digit impressions is not possible. All manus impressions are clearly visible, surrounded by displacement rims, and are either oval in shape or show a concave posterior margin. The trackway is somewhat narrower than trackway S1, with a WAP/PL ratio of 0.7. As in trackway S1, the pes pace angulation (137°) is higher than the manus pace angulation (128°). Pes prints are rotated outwards relative to the trackway midline by about 24° on average, only slightly less than in trackway S1, while the rotation angles of the manus prints are variable, being strongly rotated outwards in LM1 and slightly inwards in LM2.

Trackway S3.—It is the trackway of a biped consisting of four consecutive pes imprints (Fig. 4, SOM 1, 4), located ca. 10 m away from trackway S1. Only RP1 shows sufficient detail for inferences on the foot anatomy (Fig. 4B, C). This footprint is slightly longer (36 cm) than wide (33 cm)

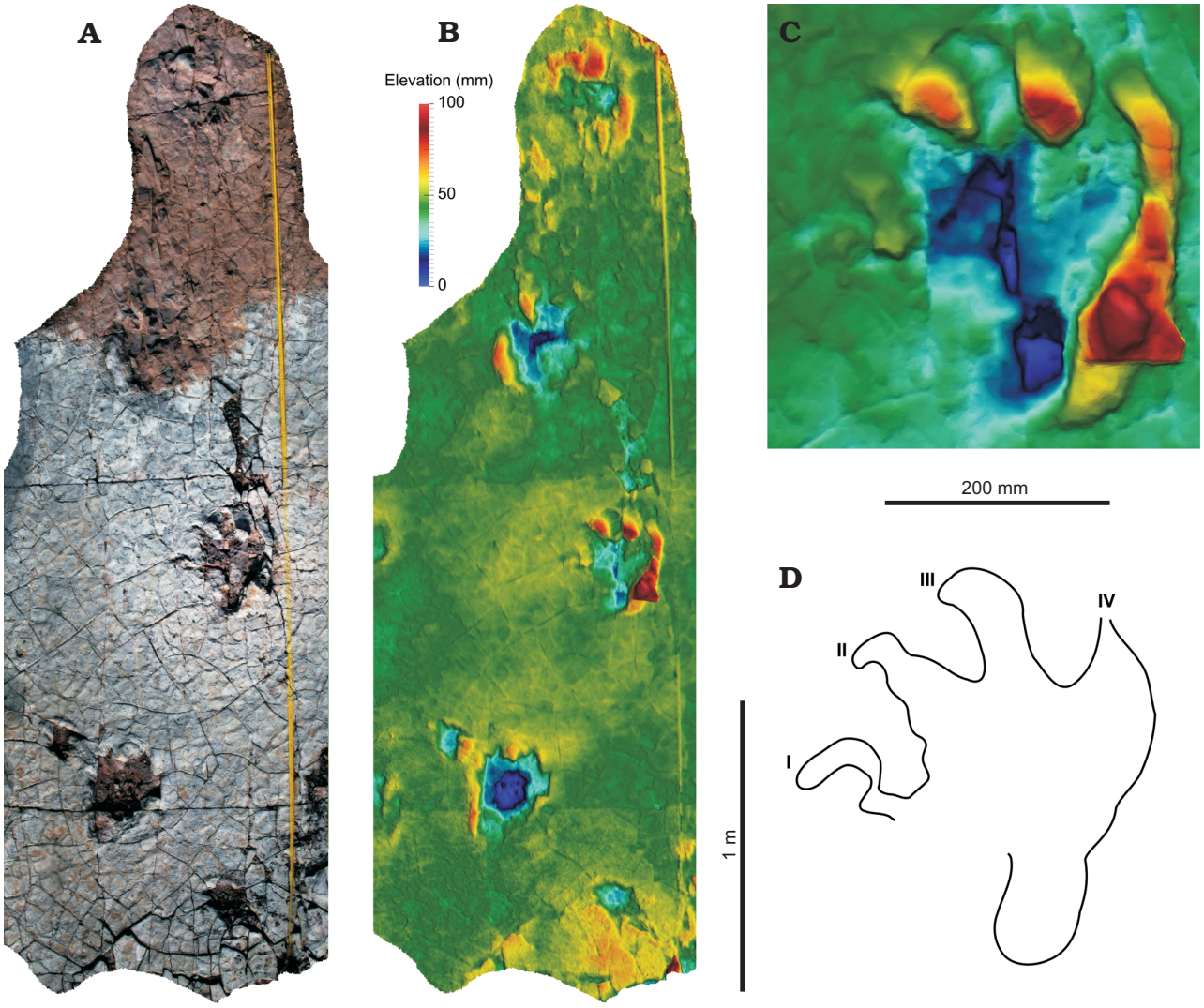

Fig. 4. **A**, **B**. Trackway S3 (*Evazoum* sp.). This bipedal trackway can possibly be attributed to a non-sauropod sauropodomorph trackmaker. Two smaller tridactyl trackways can be identified in close association with trackway S3. **C**, **D**. Detail of the best preserved pes impression RP1 (total depth represented by the color scale is 58 mm). Photogrammetric orthophoto (A), depth-color images (B, C), interpretative drawing (D).

and shows impressions of digits I–IV, with digit impression III being the longest, followed by II and IV. Digit IV is incompletely preserved distally. Digit I is thin and strongly deformed, possibly due to mud collapse. Digit impressions I–III preserve claw traces that are curved medially. Digit impression I is somewhat separated from, and much more posterior to, digit impressions II–IV. The elongated heel impression is deep and narrow, and well defined laterally, being separated from digit IV by an embayment of the lateral track wall. The medial border of the heel impression is less well defined and separated from digit impression I by an extensive embayment. The posterior margin of the heel is distinctly rounded. The trackway shows a relatively wide gauge, with a pace angulation of 144°. Footprints are slightly rotated inwards by about 6° with respect to the direction of travel.

Discussion

Number of trackmaker taxa and ichnotaxonomy.—Clemmensen et al. (2016) assigned trackways S1 and S2 to separate types, suggesting different sauropodomorph trackmakers, due to the much more elongated pes shape seen in trackway S2. However, trackway S2 also differs from S1 in the more indistinct shape and the broad displacement rims, indicating different substrate conditions at the time of track formation. Indeed, LP3 of trackway S1 appears to be elongated to a similar degree seen in trackway S2, indicating that the elongated morphotype results from suction effects narrowing the footprint during track formation. Furthermore, as both trackways lead to the south-west, closely match in pes length, and are preserved on the same bedding plane ca. 290 m apart from each other, it is well

possible that trackway S1 represents the continuation of trackway S2. Consequently, trackways S1 and S2 are here regarded a single track type, possibly left by the same species or even the same individual.

Trackway S3 is clearly distinct, differing from trackways S1 and S2 in a number of features, including the lack of manus prints, the anteriorly to slightly inward rotated pes prints, the constricted heel-region, the relative lengths of the digit impressions, where digit impression III is the most protruding, the claw impressions, which are directed medially rather than laterally, and the lack of an impression of digit V.

Many tetrapod trackways from the Upper Triassic have been assigned to sauropodomorph, mainly "prosauropod", trackmakers. Widely discussed examples include the ichnotaxa *Tetrasauropus* and *Pseudotetrasauropus* from the Lower Elliot Formation of southern Africa (Ellenberger 1972; Porchetti and Nicosia 2007). Subsequently identified trackways from Europe and North America have been attributed to the ichnotaxa *Evazoum*, *Otozoum*, and *Eosauropus* (Gand et al. 2000; Lockley and Meyer 2000, Nicosia and Loi 2003; Lockley et al. 2006a, b; Lucas et al. 2010; Lockley and Lucas 2013; Meyer et al. 2013). Of these track types, *Tetrasauropus* and *Eosauropus* reflect a quadrupedal locomotion. In *Tetrasauropus*, the pes is oriented parallel to the trackway midline, and claw traces are strongly curved inwards, whereas in trackways S1 and S2 from Greenland both the pes and the claw traces are directed outwards.

Trackways S1 and S2 comply best with the description of *Eosauropus* (Lockley et al. 2006a), and can be referred to this ichnogenus. However, the pes footprints of the present trackways are about twice the size of those of the *Eosauropus* type trackway and distinctly larger than any other trackways referred to this ichnogenus. The outwardly rotated digit impressions of the manus seen in *Eosauropus* (Lockley et al. 2006a) are not discernible in the present trackways, which could be due to preservation. Trackway S3 may be referred to the ichnogenus *Evazoum* (Nicosia and Loi 2003; Lockley et al. 2006b), and differs from the similar ichnogenera *Kalosauropus* and *Otozoum* in the more splayed pes and the greater trackway width (cf. Nicosia and Loi 2003). Strikingly, with a pes length of 36 cm, the present trackway is distinctly larger than other tracks referred to this ichnogenus, including the type trackway (10.5 cm) as well as the larger ichnospecies *Evazoum gatewayensis*, which was described to be up to 23 cm in pes length, "much larger than any other *Evazoum* morphotypes" (Lockley and Lucas 2013: 347). Porchetti et al. (2008) suggested that *Evazoum* is restricted to paleolatitudes between 0° and 30° N. The present trackway suggests the occurrence of this ichnogenus at 40° N, expanding the known range of this footprint type. *Evazoum* tracks are commonly referred to basal sauropodomorph trackmakers (Nicosia and Loi 2003; Lockley et al. 2006b), although a bipedal crurotarsan cannot be excluded (Porchetti et al. 2008). Bipedal poposauroids similar to *Effigia* (cf. Nesbitt 2007) and *Poposaurus* (Farlow et al. 2014) show developments in the locomotor apparatus that are partly convergent to those in Dinosauromorpha. In particular, *Poposaurus gracilis* had a mesaxonic pes that could have left tri-tetradactyl dinosauroid footprints (Farlow et al. 2014). However, these were probably of gallatorid morphology with a relatively long impression of middle digit III, whereas in *Evazoum* digit impression III is only slightly longer than digit impressions II and IV. The Fleming Fjord Formation has also produced body fossils of a basal sauropodomorph, which was previously referred to *Plateosaurus* by Jenkins et al. (1994) and might qualify as a possible trackmaker of the described trackway. Preliminary analysis suggests this form to be distinct from *Plateosaurus*, recommending a suprageneric classification within Plateosauria (Marco Marzola, personal communication 2017). Given the incomplete preservation of trackway S3, a synapomorphy-based identification of the trackmaker is not attempted here.

Evolution of the manus and pes skeleton in early sauropods, and the Triassic sauropod fossil record.—The anatomy of the sauropod manus and pes is highly distinctive. The manus consists of vertically oriented metacarpals arranged in a tight semicircle, while digits are strongly shortened or, as is the case in some titanosaurs, completely absent, resulting in horseshoe-shaped manus footprints. The much larger pes is rotated outwards. The metatarsals are spreading with a semi-plantigrade posture and a fleshy heel pad as support. Five proportionally short digits contact the ground, the first three of which showing long, deep and narrow unguals decreasing in length from digit I to III, resulting in an asymmetric, entaxonic pes footprint. Unguals are reduced or absent on digit IV and absent on digit V. When flexed, the claws are laterally or posterolaterally oriented (e.g., Wilson and Sereno 1998; Bonnan 2005).

The evolution of this peculiar autopodial anatomy in early sauropods remains poorly understood given the extremely sparse body fossil record of preserved pes and manus skeletons. Although the seminal works of Wilson and Sereno (1998) and Wilson (2002, 2005) established a number of autopodial synapomorphies of Sauropoda, Eusauropoda, and Neosauropoda, newly described taxa show that some of these features are not as straightforward as previously thought.

To date, no unambiguous sauropod tracks are known from the Triassic, although a possible sauropod origin was repeatedly proposed for trackways from the Chinle Group of western North America, which are Norian–Rhaetian in age (ca. 210 Mya; Lockley et al. 2001) and ascribed to the ichnogenus *Eosauropus* (previously *Tetrasauropus*) (Lockley et al. 2001, 2006a; Wilson 2005). *Eosauropus* tracks feature proportionally large pes and small manus footprints, suggesting a quadrupedal locomotion. Manus footprints typically show four to five short, clawless digits arranged in a gentle crescent. Pes footprints show four claw-bearing and a fifth non-claw bearing digit, and an extensive heel-region. Claw impressions are consistently anterolaterally directed (Wright 2005; Lockley et al. 2006a). In an attempt to identify

the trackmaker based on synapomorphies, Wilson (2005) proposed a sauropod origin, based on the quadrupedal gait and digitigrade manus, and even linked several track features with synapomorphies of Eusauropoda. Thus, the short digits and the extensive heel region suggest a semi-digitigrade pes (sensu Wilson 2005), which is absent in non-eusauropod sauropods such as *Vulcanodon* (Cooper 1984). Furthermore, Wilson (2005) proposed that the tracks show laterally directed claw impressions, which he considered a synapomorphy of eusauropods more derived than *Shunosaurus*. The early appearance of these features might indicate an eusauropod origin in the Triassic, implying ghost linages. However, based on a stratocladistic approach, Wilson (2005) favored the idea that these eusauropod-like characters might had evolved independently in the *Eosauropus* trackmakers.

More recent studies questioned a sauropod origin of the *Eosauropus* tracks. Bonnan and Yates (2007) suggested that quadrupedal non-sauropod sauropodomorphs closely related to sauropods may also qualify as possible trackmakers, based on the morphological similarity between *Eosauropus* manus footprints and the manus skeleton of *Melanorosaurus*. Lockley et al. (2011) noted that in *Eosauropus* digit impression I is relatively short in comparison with a typical sauropod pes, and suggested that this feature might indicate a "prosauropod" trackmaker. Nesbitt et al. (2007) considered the *Eosauropus* tracks discussed by Wilson (2005) to be indeterminate, and claimed that the synapomorphies cited by the latter author are also found in the non-dinosaurian ichnogenus *Brachychirotherium* (see also Lucas et al. 2010). However, the footprint morphology in the present trackway is clearly distinct from *Brachychirotherium*, given the asymmetric, entaxonic pes, and the extremely laterally directed claw impressions, leaving sauropodomorph dinosaurs as the most probable trackmakers.

Synapomorphy-based trackmaker identification.—In the following, we discuss and evaluate previously proposed synapomorphies which might be identifiable in the present footprints.

(i) Obligate quadrupedal posture, as indicated by the consistent appearance of manus footprints. The obligatory quadrupedal posture was considered a sauropod synapomorphy (Wilson and Sereno 1998; Wilson 2005), but it probably evolved independently in taxa close to, but not commonly regarded as sauropods, such as *Melanorosaurus*. Facultative quadrupedality probably appeared early in sauropodomorph evolution, as evidenced by the track record (McPhee et al. 2015).

(ii) Semi-digitigrade pes (sensu Wilson 2005) with a spreading metatarsus, in which the shortened metatarsals are held nearly horizontally, as indicated by the extensive and broad heel pad impression (Wilson 2005). This feature is considered an eusauropod synapomorphy (Upchurch 1995; Wilson 2002, 2005; Allain and Aquesbi 2008), and is absent in basal sauropods such as *Vulcanodon* and *Tazoudasaurus*, which show the plesiomorphic elongated metatarsus. As suggested by Wilson (2005), this synapomorphy can be identified in trackways referred to *Tetrasauropus* (= *Eosauropus*) from the Late Triassic of North America, suggesting either an early appearance of eusauropods or convergent evolution in sauropods and the *Eosauropus* trackmaker.

(iii) Laterally deflected unguals, as a result of the asymmetric position of the flexor tubercle of the unguals (Bonnan 2005). This feature was considered a synapomorphy of a clade containing *Barapasaurus* and more derived taxa (Wilson and Sereno 1998; Wilson 2002, 2005), or *Omeisaurus* and more derived taxa (Upchurch et al. 2007; Yates et al. 2010). An incipient lateral deflection of pedal ungual I, where the convex dorsal surface of the latter faces slightly medially, can be already observed in *Antetonitrus* (McPhee et al. 2014). Wilson (2005) identified this feature in *Tetrasauropus* (*=Eosauropus)* trackways, which, however, typically show anterolaterally oriented claw impressions not reaching the degree of deflection seen in many sauropod trackways. It has to be cautioned that the orientation of the claw marks might be to some extent influenced by the foot kinematics during footprint formation, and therefore do not necessarily mirror the exact anatomical ungual orientations of the foot. Furthermore, claw orientation is controlled by the degree of plantar flexion of the pes, and thus trackmaker behavior—while laterally deflected unguals in a flexed pes are indicative of the peculiar eusauropod pes anatomy, more anteriorly directed claw marks only indicate digit extension and do not preclude an eusauropod trackmaker (cf. Bonnan 2005; Hall et al. 2016). Nevertheless, the present trackway provides evidence of claw impressions arranged in a right angle to the pes long axis, indicating a larger degree of ungual deflection than observed in other *Eosauropus* trackways, closely corresponding to the condition seen in a flexed sauropod pes. Claw impressions appear to show the medial side of the claws, not the ventral side as would be expected in anteriorly directed claws.

(iv) Pes entaxony, listed as a sauropod synapomorphy by Wright (2005), and outward rotation of pes. Wilson and Sereno (1998) considered the increased robustness of metatarsal I a sauropod synapomorphy, indicating a medial shift of the weight-bearing axis. In the present trackway, the relative length of digit impression I cannot be determined with certainty, but the digit appears robust at least in RP3. Digit II is more protruding than digit III, although it cannot be determined whether this reflects the relative lengths of the individual digits. Yates et al. (2010) noted the sauropod-like metatarsal in the bipedal non-sauropod sauropodomorph *Aardonyx*, and suggested that a robust digit I predated the acquisition of an obligate quadrupedal gait.

Another conspicuous feature of sauropod trackways, the outward rotation of the pes, was suggested to be associated with the increased entaxony, where the more robust inner digits carry the majority of the weight. Due to this outward rotation, digit I is the leading digit despite being shorter than digits II and III. Bonnan (2005: 360) suggested that "perhaps the lateral, outward turn of the pes occurred in the

neosauropod forms, with more primitive eusauropods retaining a pes orientation closer to those of other saurischian dinosaurs". The marked pes outward rotation in the present trackway (30°), which is arguably not produced by a neosauropod trackmaker given the broadly arched manus imprints, argues against this interpretation. Outwards rotated pes impressions are also commonly observed in other trackways that possibly pertain to basal sauropods (e.g., cf. Lockley et al. 2001, 2006a; Xing et al. 2016). This feature, therefore, might be characteristic for sauropods in general or for an even more inclusive grouping.

(v) Increased length of metatarsal V, with all five digits contacting the ground and playing an active role in bearing the animal's weight; suggested as a sauropod synapomorphy (Wilson and Sereno 1998), or as the synapomorphy of a slightly more inclusive grouping (*Gongxianosaurus* plus more derived taxa; Yates 2007; Yates et al. 2010). The proportionally much longer metatarsal V suggests that in footprints digit impression V would be much more protruding than in basal sauropodomorphs, where it usually would not have made contact with the ground. The position of digit impression V in the present trackway matches the sauropod pes configuration.

Other synapomorphies which can be potentially identified in tracks cannot be evaluated for the present trackway. The reduction of manual phalanges is a eusauropod synapomorphy according to Wilson and Sereno (1998), although Wilson (2005) points out that digit reduction must have begun prior to the Lower Jurassic, as indicated by trackway evidence. Both trackways S1 and S2 lack indications for free manual digits, possibly due to poor preservation. Synapomorphies related to pedal ungual I cannot be evaluated in the present trackway since claw impression I is not readily preserved. The deep and narrow morphology of pedal ungual I is considered a sauropod synapomorphy, while the increased size of this ungual is considered a synapomorphy of both Sauropoda (pedal ungual I being 25% longer than pedal ungual II) and Eusauropoda (pedal ungual I longer than metatarsal I) (Wilson and Sereno 1998). A pedal ungual II which is 90% or less the size of the ungual of pedal digit I was resolved as a synapomorphy of a clade consisting of *Gongxianosaurus* plus more derived taxa (Yates 2007; Yates et al. 2010). A proposed eusauropod synapomorphy, the pedal digits II to III show sickle-shaped, laterally compressed unguals similar to that of digit I (Wilson and Sereno 1998; Wilson 2002; Upchurch et al. 2007). Although appearing sickle-shaped, a comparison of claw impressions II and III with that of digit I is not possible as the latter is not preserved in the present trackway; the trackmakers however for sure lacked the distinctly dorsoventrally flattened unguals seen in *Vulcanodon*.

Other features exhibited by the present trackway represent plesiomorphies which are lost in derived sauropods. Although poorly preserved, the elongated manus impressions indicate metacarpals arranged in a broad arc, as exemplified by the complete articulated manus of *Tazoudasaurus* (Allain and Aquesbi 2008). The tightly bound, horseshoe-like manus configuration seen in later sauropods probably occurred relatively late in sauropod evolution, and was suggested to be a synapomorphy of Neosauropoda (Wilson and Sereno 1998; Wilson 2005; Allain and Aquesbi 2008). Furthermore, claw impression IV is well developed in the present trackway, but the reduction or loss of pedal ungual IV is considered a synapomorphy of Eusauropoda (Wilson and Sereno 1998; Wilson 2002; Allain and Aquesbi 2008).

The present trackway therefore exhibits a mixture of primitive and derived features. The similarities with trackways attributed to derived sauropods are intriguing, in fact, trackway S1 can be differentiated from the latter only based on the absence of the horseshoe-like manus configuration characteristic for neosauropods and the presence of a fully developed ungual on pedal digit IV, which is reduced or absent in eusauropods. The quadrupedal posture, the pentadactyly of the pes and the extent of digit V relative to digit IV, as well as the entaxony of the pes suggest a derived sauropodiform trackmaker. Other synapomorphies, including the semi-digitigrady of the pes and the laterally deflected unguals, are even suggestive to a more exclusive grouping containing sauropods more derived than *Tazoudasaurus* and *Vulcanodon*.

Conclusions

The Norian–early Rhaetian Fleming Fjord Formation of central East Greenland adds significant information to the diversity and distribution of Late Triassic vertebrate tracks. The described bipedal trackway is referred to the ichnogenus *Evazoum*, and might represent a non-sauropod sauropodomorph trackmaker. The two quadrupedal trackways, possibly of sauropod origin, are here referred to *Eosauropus*. The described tracks represent the first evidence for the presence of these ichnotaxa in Greenland, expanding their known paleogeographical range. Both track types are distinctly larger than other known tracks ascribed to these ichnogenera.

The early evolution of sauropods is poorly known, and undisputed evidence for an appearance of this clade prior to the Jurassic is currently lacking. The quadrupedal trackways described herein suggest the adoption of a sauropod-like foot posture, where the pes is semi-digitigrade, oriented antero-laterally, and shows laterally deflected unguals, as early as the late Norian–early Rhaetian. Pedal synapomorphies (quadrupedal posture, entaxonic pes, five weight-bearing digits) suggest a derived sauropodiform trackmaker, with two synapomorphies (semi-digitigrade pes, laterally deflected unguals) suggesting a sauropod trackmaker more derived than *Tazoudasaurus* and *Vulcanodo*n. These trackways, therefore, might provide further evidence for the appearance of sauropods as early as the Late Triassic, and represent the first evidence of this group from Greenland. It cannot be excluded, however, that the trackmaker taxon

was a non-sauropod sauropodiform which convergently acquired a eusauropod-like pes that is both semi-digitigrade and shows laterally deflected unguals (cf. Wilson 2005).

Two of the aforementioned features of the present trackways (semi-digitigrade pes and laterally directed unguals) have been considered eusauropod synapomorphies, while the retention of a large ungual on digit IV represents a plesiomorphic feature thought to be absent in eusauropods. This previously unknown combination of characters might therefore indicate mosaic evolution in the pes skeleton of early sauropods.

Acknowledgements

We thank P. Martin Sander (Steinmann Institute, University of Bonn, Bonn, Germany) for constructive comments on an early version of the manuscript. Nadia Rosendal Nielsen (Geocenter Møns Klint, Borre, Denmark) is thanked for logistic support and contact to the media; Jan Schulz Adolfssen (Ministry of Mineral Resources, Nuuk, Greenland) and Nicole Klein (Steinmann Institute, University of Bonn, Bonn, Germany) are thanked for help in the field. Jakob Søndergaard, POLOG, was in charge of safety during the expedition, and a great help during the excavations. Finally, we thank Nils Natorp, Director of the Geocenter Møns Klint, for organizing the expedition. Blair McPhee (University of the Witwatersrand, Johannesburg, South Africa) and an anonymous reviewer provided constructive comments that helped to improve the manuscript substantially. Furthermore, we are grateful for the generous support to the 2012 expedition from the following foundations: Dronning Margrethes og Prins Henriks Fond, Arbejdsmarkedets Feriefond, Oticon Fonden, Knud Højgaards Fond, Louis Petersens Legat, Det Obelske Familiefond, and Ernst og Vibeke Husmans Fond. POLOG provided professional expedition logistics and camp solutions.

References

Allain, R. and Aquesbi, N. 2008. Anatomy and phylogenetic relationships of *Tazoudasaurus naimi* (Dinosauria, Sauropoda) from the late Early Jurassic of Morocco. *Geodiversitas* 30: 345–424.

Bonnan, M.F. 2005. Pes Aanatomy in sauropod dinosaurs: implications for functional morphology, evolution, and phylogeny. *In*: V. Tidwell and K. Carpenter (eds.), *Thunder-Lizards: The Sauropodomorph Dinosaurs*, 346–380. Indiana University Press, Bloomington.

Bonnan, M.F. and Yates, A.M. 2007. A new description of the forelimb of the basal sauropdomorph *Melanoosaurus*: implications for the evolution of pronation, manus shape and quadrupedalism in sauropod dinosaurs. *Special Papers in Palaeontology* 77: 157–168.

Buffetaut, E., Suteethorn, V., Cuny, G., Tong, H., Le Loeuff, J., Khansubha, S., and Jongautchariyakul, S. 2000. The earliest known sauropod dinosaur. *Nature* 407: 72–74.

Clemmensen, L.B. 1980. Triassic lithostratigraphy of East Greenland between Scoresby Sund and Kejser Franz Josephs Fjord. *Bulletin Grønlands Geologiske Undersøgelse* 139: 1–56.

Clemmensen, L.B., Kent, D.V., and Jenkins Jr., F.A. 1998. A Late Triassic lake system in East Greenland: facies, depositional cycles and palaeoclimate. *Palaeogeography, Palaeoclimatology, Palaeoecology* 140: 135–159.

Clemmensen, L.B., Milàn, J., Adolfssen, J.S., Estrup, E.J., Frobøse, N., Klein, N., Mateus, O., and Wings, O. 2016. The vertebrate-bearing Late Triassic Fleming Fjord Formation of central East Greenland revisited: stratigraphy, palaeoclimate and new palaeontological data. In: B.P. Kear, J. Lindgren, J.H. Hurum, J. Milàn, and V. Vajda (eds.), Mesozoic Biotas of Scandinavia and its Arctic Territories. *Geological Society, London, Special Publications* 434: 31–47.

Cooper, M.R. 1984. A reassessment of *Vulcanodon karibaensis* Raath (Dinosauria: Saurischia) and the origin of the Sauropoda. *Palaeontologia Africana* 25: 203–231.

Ellenberger, P. 1972. Contribution à la classification des Pistes de Vertébrés du Trias: les types du Stormberg d'Afrique du Sud (I). *Palaeovertebrata, Memoire Extraordinaire*: 1–104.

Farlow, J.O., Schachner, E.R., Sarrazin, J.C., Klein, H., and Currie, P.J. 2014. Pedal proportions of *Poposaurus gracilis*: convergence and divergence in the feet of archosaurs. *Anatomical Record* 297: 1022–1046.

Gand, G., Vianey-Liaud, M., Demathieu, G., and Garric, J. 2000. Deux nouvelles traces de pas de dinosaures du Trias supérieur de la bordure Cévenole (La Grand-Combe, Sud-Est de la France). *Geobios* 33: 599–624.

Gatesy, S.M. 2003. Direct and indirect track features: what sediment did a dinosaur touch? *Ichnos* 10: 91–98.

Hall, L.E., Fragomeni, A.E., and Fowler, D.W. 2016. The flexion of sauropod pedal unguals and testing the substrate grip hypothesis using the trackway fossil record. *In*: P.L. Falkingham, D. Marty, and A. Richter (eds.), *Dinosaur Tracks: The Next Steps*, 138–151. Indiana University Press, Bloomington.

Jenkins, F.J., Shubin, N.H., Amarel, W.W., Gatesy S.M., Schaff, C.R., Clemmensen, L.B., Downs, W.R., Davidson, A.R., Bonde, N.C., and Osbaeck, F. 1994. Late Triassic continental vertebrates and depositional environments of the Fleming Fjord Formation, Jameson Land, east Greenland. *Meddelelser Om Grønland, Geoscience* 32: 1–25.

Kent, D.V. and Clemmensen, L.B. 1996. Paleomagnetism and cycle stratigraphy of the Triassic Fleming Fjord and Gipsdalen formations of East Greenland. *Bulletin of the Geological Society of Denmark* 42: 121–136.

Klein, H., Milàn, J., Clemmensen, L.B., Frobøse, N., Mateus, O., Klein, N., Adolfssen, J.S., Estrup, E.J., and Wings, O. 2016. Archosaur footprints (cf. *Brachychirotherium*) with unusual morphology from the Upper Triassic Fleming Fjord Formation (Norian–Rhaetian) of East Greenland. *In*: B.P. Kear, J. Lindgren, J.H. Hurum, J. Milàn, and V. Vajda (eds.), Mesozoic Biotas of Scandinavia and its Arctic Territories. *Geological Society, London, Special Publications* 434: 71–85.

Leonardi, G. 1987. Discussion of the terms and methods. *In*: G. Leonardi (ed.), *Glossary and Manual of Tetrapod Footprint Palaeoichnology*, 43–51. Publicação do Departemento Nacional da Produção Mineral Brasil, Brasília.

Lockley, M.G. and Lucas, S.G. 2013. *Evazoum gatewayensis*, a new Late Triassic archosaurian ichnospecies from Colorado: implications for footprints in the ichnofamily Otozoidae. *In*: L.H Tanner, J.A. Spielmann, and S.G. Lucas (eds.), The Triassic System. *New Mexico Museum of Natural History and Science Bulletin* 61: 345–353.

Lockley, M.G. and Meyer, C. 2000. *Dinosaur Tracks and Other Fossil Footprints of Europe*. 323 pp. Columbia University Press, New York.

Lockley, M.G., Lucas, S.G., and Hunt, A. P. 2006a. *Eosauropus*, a new name for a Late Triassic track: Further observations on the Late Triassic ichnogenus *Tetrasauropus* and related forms, with notes on the limits of interpretation. *In*: J.D. Harris, S.G. Lucas, J.A. Spielmann, M.G. Lockley, A.R.C. Milner, and J.I. Kirkland (eds.), The Triassic–Jurassic Terrestrial Transition. *New Mexico Museum of Natural History and Science Bulletin* 37: 192–198.

Lockley, M.G., Lucas, S.G. and Hunt, A.P. 2006b. *Evazoum* and the renaming of northern hemisphere "*Pseudotetrasauropus*": implications for tetrapod ichnotaxonomy at the Triassic–Jurassic boundary. *In*: J.D. Harris, S.G. Lucas, J.A. Spielmann, M.G. Lockley, A.R.C. Milner, and J.I. Kirkland (eds.), The Triassic–Jurassic Terrestrial Transition. *New Mexico Museum of Natural History and Science Bulletin* 37: 199–206.

Lockley, M.G., Wright, J.L., Hunt, A.P., and Lucas, S.G. 2001. The Late Triassic sauropod track record comes into focus: old legacies and new paradigms. *New Mexico Geological Society Guidebook* 52: 181–190.

Lockley, M.G., Hups, K., Cart, K., and Gerwe, S. 2011. A zone of sauropodomorph footprints in the basal Wingate Sandstone (latest Trias-

sic) of western Colorado and eastern Utah: Is *Eosauropus* a common ichnogenus in this region? *New Mexico Museum of Natural History and Science Bulletin* 53: 337–343.

Lucas, S.G., Spielmann, J.A., Klein, H., and Lerner, A.J. 2010. Ichnology of the Upper Triassic Redonda Formation (Apachean) in east-central New Mexico. *New Mexico Museum of Natural History and Science Bulletin* 47: 1–75.

Mallison, H. and Wings, O. 2014. Photogrammetry in paleontology—a practical guide. *Journal of Paleontological Techniques* 12: 1–31.

Marty, D. 2008. Sedimentology, taphonomy, and ichnology of Late Jurassic dinosaur tracks from the Jura carbonate platform (Chevenez-Combe Ronde tracksite, NW Switzerland): Insights into the tidal-flat palaeoenvironment and dinosaur diversity, locomotion, and palaeoecology. *GeoFocus* 21: 1–278.

McPhee, B.W., Bonnan, M.F., Yates, A.M., Neveling, J., and Choiniere, J.N. 2015. A new basal sauropod from the pre-Toarcian Jurassic of South Africa: Evidence of niche-partitioning at the sauropodomorph–sauropod boundary? *Scientific Reports* 5: 13224.

McPhee, B.W., Yates, A.M., Choiniere, J.N., and Abdala, F. 2014. The complete anatomy and phylogenetic relationships of *Antetonitrus ingenipes* (Sauropodiformes, Dinosauria): implications for the origins of Sauropoda. *Zoological Journal of the Linnean Society* 171: 151–205.

Meyer, C.A., Marty, D., Thüring, B., Stecher, R., and Thüring, S. 2013. Dinosaurierspuren aus der Trias der Bergüner Stöcke (Parc Ela, Kanton Graubünden, SE Schweiz). *Mitteilungen der Naturforschenden Gesellschaften beider Basel* 14: 135–144.

Milàn, J. and Bromley, R.G. 2006. True tracks, undertracks and eroded tracks, experimental work with tetrapod tracks in laboratory and field. *Palaeogeography, Palaeoclimatology, Palaeoecology* 231: 253–264.

Nesbitt, S.J. 2007. The anatomy of *Effigia okeeffeae* (Archosauria, Suchia), theropod-like convergence, and the distribution of related taxa. *Bulletin of the American Museum of Natural History* 302: 1–84.

Nesbitt, S.J., Irmis, R.B., and Parker, W.G. 2007. A critical re-evaluation of the Late Triassic dinosaur taxa of North America. *Journal of Systematic Palaeontology* 5: 209–243.

Nicosia, U. and Loi, M. 2003. Triassic footprints from Lerici (La Spezia, northern Italy). *Ichnos* 10: 127–140.

Porchetti, S.D. and Nicosia, U. 2007. Re-examination of some large early Mesozoic tetrapod footprints from the African collection of Paul Ellenberger. *Ichnos* 14: 219–245.

Porchetti, S.D., Nicosia, U., Mietto, P., Petti, F.M., and Avanzini, M. 2008. *Atreipus*-like footprints and their co-occurrence with *Evazoum* from the upper Carnian (Tuvalian) of Trentino-Alto Adige. *Studi Trentini Di Scienze Naturali: Acta Geologica* 83: 277–287.

Racey, A. and Goodall, J.G. 2009. Palynology and stratigraphy of the Mesozoic Khorat Group red bed sequences from Thailand. *Geological Society, London, Special Publications* 315: 69–83.

Sulej, T., Wolniewicz, A., Bonde, N., Błażejowski, B., Niedźwiedzki, G., and Tałanda, M. 2014. New perspectives on the Late Triassic vertebrates of East Greenland: preliminary results of a Polish-Danish palaeontological expedition. *Polish Polar Research* 35: 541–552.

Upchurch, P. 1995. The evolutionary history of sauropod dinosaurs. *Philosophical Transactions of the Royal Society of London B: Biological Sciences* 349: 365–390.

Upchurch, P., Barrett, P.M., and Galton, P.M. 2007. A phylogenetic analysis of basal sauropodomorph relationships: implications for the origin of sauropod dinosaurs. *Special Papers in Palaeontology* 77: 57.

Wilson, J.A. 2002. Sauropod dinosaur phylogeny: critique and cladistic analysis. *Zoological Journal of the Linnean Society* 136: 215–275.

Wilson, J.A. 2005. Integrating ichnofossil and body fossil records to estimate locomotor posture and spatiotemporal distribution of early sauropod dinosaurs: a stratocladistic approach. *Paleobiology* 31: 400–423.

Wilson, J.A. and Sereno, P.C. 1998. Early evolution and higher-level phylogeny of sauropod dinosaurs. *Journal of Vertebrate Paleontology* 18 (Supplement to Number 2): 1–79.

Wright, J.L. 2005. Steps in understanding sauropod biology. *In*: K.C. Rogers and J.A. Wilson (eds.), *The Sauropods: Evolution and Paleobiology*, 252–285. University of California Press, Berkeley.

Xing, L.D., Lockley, M.G., Zhang, J., Klein, H., Li, D., Miyashita, T., Li, Z., and Kümmell, S.B. 2016. A new sauropodomorph ichnogenus from the Lower Jurassic of Sichuan, China fills a gap in the track record. *Historical Biology* 28: 881–895.

Yates, A.M. 2007. The first complete skull of the Triassic dinosaur *Melanorosaurus* Haughton (Sauropodomorpha: Anchisauria). *Special Papers in Palaeontology* 77: 9–55.

Yates, A.M., Bonnan, M.F., Neveling, J., Chinsamy, A., and Blackbeard. M.G. 2010. A new transitional sauropodomorph dinosaur from the Early Jurassic of South Africa and the evolution of sauropod feeding and quadrupedalism. *Proceedings of the Royal Society of London B: Biological Sciences* 277: 787–794.

http://app.pan.pl/SOM/app62-Lallensack_etal_SOM.pdf

SUPPLEMENTARY ONLINE MATERIAL FOR

Sauropodomorph dinosaur trackways from the Fleming Fjord Formation of East Greenland: Evidence for Late Triassic sauropods

Jens N. Lallensack, Hendrik Klein, Jesper Milàn, Oliver Wings, Octávio Mateus, and Lars B. Clemmensen

Published in *Acta Palaeontologica Polonica* 2017 62 (4): 833–843.
https://doi.org/10.4202/app.00374.2017

Supplementary Online Material

SOM 1. Selected high-resolution photographs showing the described trackways in the field.

SOM 2–4. Photogrammetric models, including textured high-resolution

available at

http://app.pan.pl/SOM/app62-Lallensack_etal_SOM/SOM_2/trackway_S1.pdf
http://app.pan.pl/SOM/app62-Lallensack_etal_SOM/SOM_2/trackway_S1.jpg
http://app.pan.pl/SOM/app62-Lallensack_etal_SOM/SOM_2/trackway_S1.ply

http://app.pan.pl/SOM/app62-Lallensack_etal_SOM/SOM_3/trackway_S2.pdf
http://app.pan.pl/SOM/app62-Lallensack_etal_SOM/SOM_3/trackway_S2.jpg
http://app.pan.pl/SOM/app62-Lallensack_etal_SOM/SOM_3/trackway_S2.ply

http://app.pan.pl/SOM/app62-Lallensack_etal_SOM/SOM_4/trackway_S3.pdf
http://app.pan.pl/SOM/app62-Lallensack_etal_SOM/SOM_4/trackway_S3.jpg
http://app.pan.pl/SOM/app62-Lallensack_etal_SOM/SOM_4/trackway_S3.ply

SOM 1. Fig. 1. Trackway S1

SOM 1. Fig. 2. Trackway S1

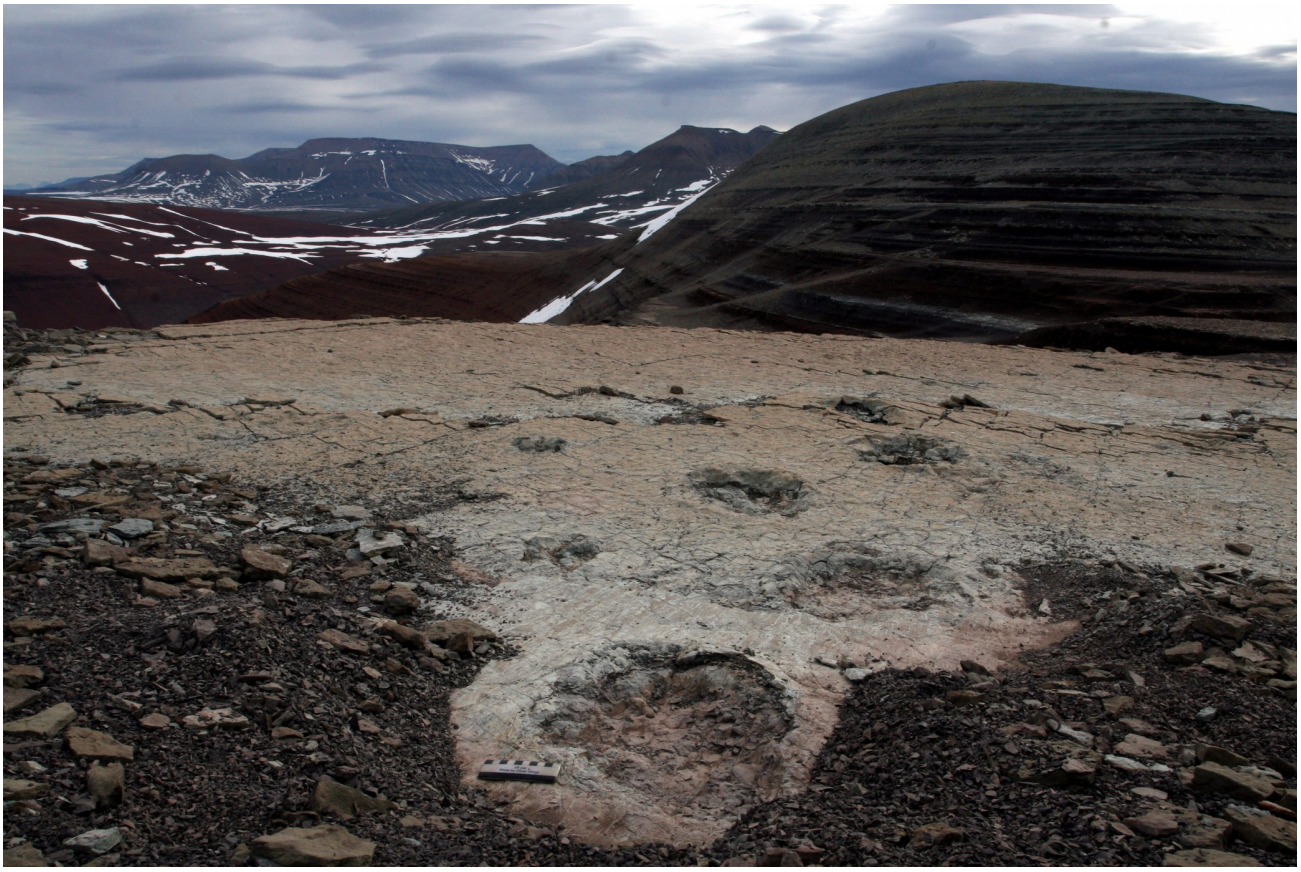

SOM 1. Fig. 3. Trackway S1. Pes-Manus set P3-M3

SOM 1. Fig. 4. Trackway S2

SOM 1. Fig. 5. Trackway S2

SOM 1. Fig. 6. Trackway S2. Pes-Manus set P3-M3

SOM 1. Fig. 7. Trackway S3

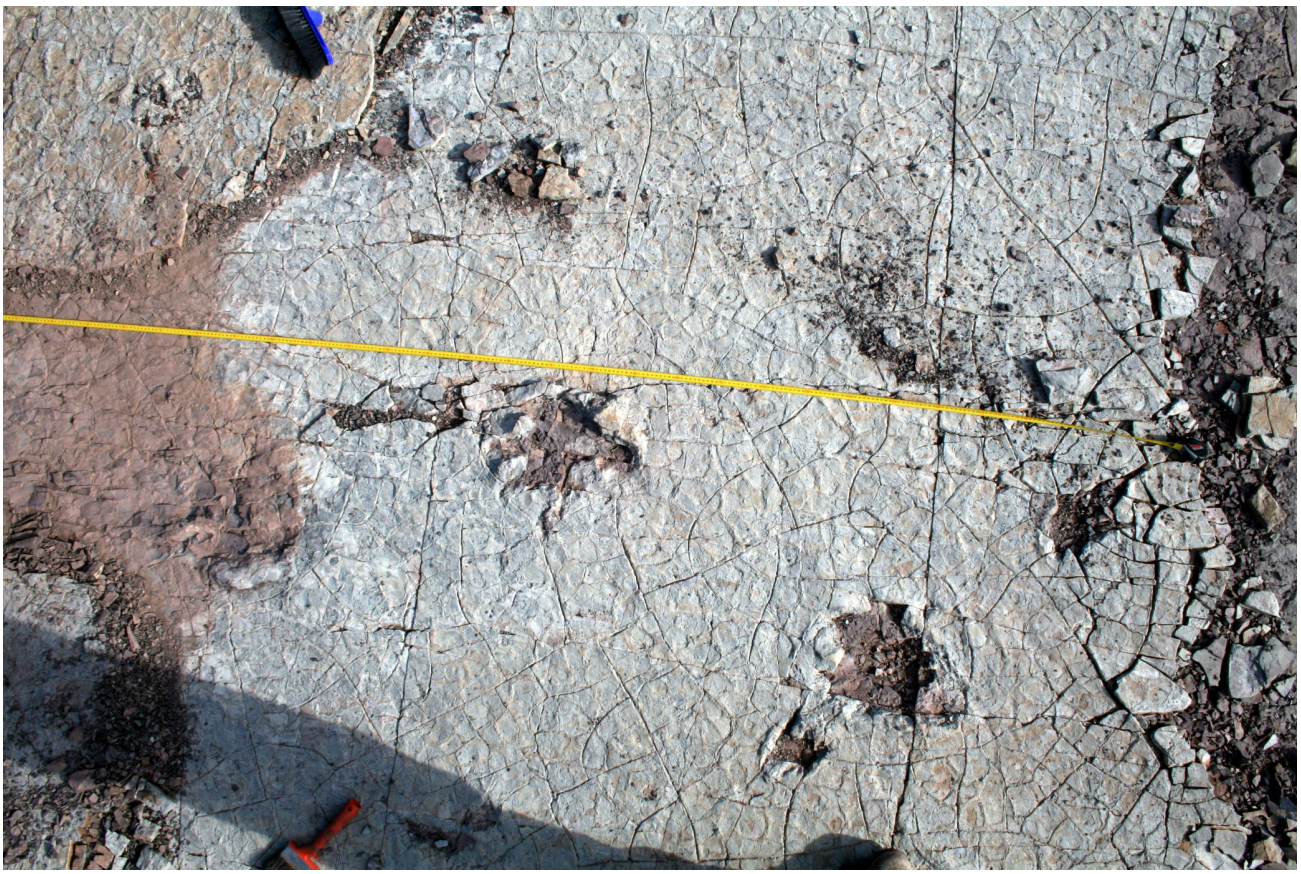

SOM 1. Fig. 8. Trackway S3

Chapter 7

submitted to "Current Biology".

Sander, P.M., Lallensack, J.N., submitted. Dinosaurs: Four legs good, two legs bad. Current Biology. **p. 204–210.**

Author contributions:

- P. Martin Sander wrote the paper, prepared figures, reviewed drafts of the paper.
- Jens N. Lallensack wrote the paper, prepared figures, reviewed drafts of the paper.

Dinosaurs: Four legs good, two legs bad

P. Martin Sander[1,2] & Jens N. Lallensack[1]

[1] Steinmann Institute of Geology, Mineralogy and Paleontology, University of Bonn, Nussallee 8, 53115 Bonn, Germany

[2] The Dinosaur Institute, Natural History Museum of Los Angeles County, Los Angeles, CA, United States of America

Two new quadrupedal prosauropod dinosaur from South Africa and Argentina and a new method for differentiating quadrupeds from bipeds indicates that very large flexed-limbed sauropodomorphs coexisted with early columnar-limbed sauropods for 20 million years.

Just like in the famous Orwell quote, the number of legs one walks on has been of central importance in dinosaur research. "One" being, of course, the dinosaurs. However, dinosaurs several times underwent the reverse transition than in "Animal Farm", from two legs to four (1,2). And every time, this transition was soon after accompanied by a marked increase in body size, a credible measure of "good". The ultimate "good" animals on the dinosaur farm were, by a long shot, the giant long-necked sauropods of the Jurassic and Cretaceous. In fact, sauropod dinosaurs were the largest animals to ever walk the earth and were an order of magnitude heavier than any other land animal, past or present. Weighing in at 80 or more metric tons (3), it has long been understood sauropods required four pillar-like limbs to distribute this weight (4,5). Two new papers (6,7) now shed light on the early evolution of these giants, describing remarkably similar dinosaurs from very different places (South Africa and Argentina) and times (before and after the major extinction event 201 million years ago). Both teams of paleontologist reached very similar conclusions, culminating in the naming of a new group of dinosaurs. In a remarkably case of independent scientific discovery, both teams proposed the same name for this group, the Lessemsauridae.

Sauropods arose from some sort of prosauropods (more properly "basal Sauropodomorpha") in the Late Triassic. Prosauropods, like all basal dinosaurs, originally walked on their hind legs only (bipedal), and sauropod origins thus entailed the transition from a bipedal gait to a quadrupedal gait (walking on all four legs). This transition also occurred in several other plant-eating dinosaur groups (1,2). Only the meat-eating dinosaurs (theropods), a subgroup of which are the living birds, never evolved quadrupedality.

Quadrupedality being such a prevalent pattern and its apparent link to large to giant body size justifies the attention any new dinosaur skeleton will garner that informs on these issues. One such find is the one described by McPhee et al. (6) from the Early Jurassic Upper Elliot Formation of South Africa and is about 200 to 195 million years old. The other is markedly older at about 209 million years old and comes from the Late Triassic of Argentina. The Argentinian animal, christened *Ingentia pirma* ("first giant") by

Apaldetti et al. (7), was about 70% of the linear size of *Ledumahadi*. New material of the oldest lessemsaurid, *Lessemsaurus,* also indicates animals of 7 to 10 t (7). The paper on the South African dinosaur, *Ledumahadi mafube* ("dawn giant thunderclap"), is accomponied by a simple yet stringent method for distinguishing bipeds from quadrupeds. *Ledumahadi* reached the enormous (by non-sauropod standards) body mass of 12 t and walked on four legs, as did *Ingentia* and *Lessemsaurus*. However, lessemsaurids resemble more those other dinosaurian quadrupeds like *Stegosaurus* and *Triceratops* in lacking the columnar forelimbs of sauropods. This is apparent from the different shape of their ulna, wrist and thigh bone (femur) that are more reminiscent of prosauropods like the familiar *Plateosaurus*. *Ledumahadi*, *Ingentia* and other Lessemsauridae probably planted their forefeet rather far apart and with a distinctly flexed elbow when walking.

True sauropods, which at the latest split from the Lessemsauridae at the end of the the Norian stage of the Late Triassic (209 million years ago, Figure 1), have columnar limbs as a key adaptation (5). While *Ledumahadi* and *Lessemsaurus* might have been close to the upper body size limit possible for animals with a flexed limb posture (6), the columnar limbs paved the way for reaching gigantic sizes far surpassing those of all other dinosaurs, and for a major radiation starting in the Early Jurassic, while other sauropodomorph lineages died out. Yet, early sauropods were smaller or equal in size to *Ledumahadi* and *Lessemsaurus*, suggesting that size increase might not have been the only driving factor leading to the evolution of columnar limbs. In fact, as so often in nature, the story is much more complex, and sauropod gigantism was made possible by a unique combination of primitive features and evolutionary innovations (4,5).

The most important advance made by South African study (6), however, probably is not describing a new "giant" dinosaur but developing a method for determining whether a given animal was bipedal or quadrupedal. The new method relies on the observation that in bipeds the forelimb bones are much more slender than the hind limb bones. Thus, a dataset of the shaft circumferences of the upper arm bone (humerus) and the femur of species of known stance can be used to statistically predict stance by linear discriminant analysis. But can data derived from a fundamentally different group such as mammals be used to predict stance in dinosaurs? Sauropod dinosaurs, in contrast to mammals and ornithischian dinosaurs, had large parts of their neck and trunk space filled with air sacs, shifting the center of mass backwards (8), with effects on relative limb bone circumferences. Despite this and other potential drawbacks, the new method predicts stance in mammals based on dinosaurian data surprisingly well, with only 10% misclassification (identifying the beaver as bipedal, for example).

Walking, on two legs or on four, leaves tracks behind, and such tracks have the potential of fossilizing, spawning the discipline of dinosaur ichnology. While tracks will provide an unequivocal answer to what an animal really did, their disadvantage is the difficulty of identifying the track maker. No dinosaur ever was found dead in its tracks (unlike some Jurassic horseshoe crabs from Germany), requiring some detective work. The evidence in the case of dinosaur tracks consists of evolutionary innovations (synapomorphies), e.g., in the foot anatomy, that are reflected in the track. The uncertainties associated with track maker identification have sometime led to an unwarranted neglect of the track evidence.

Fossil tracks are essential for the understanding of early quadrupedal sauropodomorphs, especially in light of the scarce body fossil record and the many evolutionary novelties in both the foot and hand that

are potentially registered in tracks. Although McPhee et al. mention that tracks of quadrupedal prosauropods are present in the Late Triassic, especially of southern Africa, most of these tracks probably were not made by dinosaurs (9). The only trackway widely agreed to originate from a quadrupedal prosauropod comes from the Late Triassic (late Norian to Rhaetian) Lower Elliot Formation of Lesotho (9,10,11). This trackway, *Tetrasauropus,* was left by a large animal (hip height ~2 m) that appears to have resembled *Ledumahadi*. *Tetrasauropus* shows a number of primitive features lost in sauropods, including the widely spaced forefoot impressions, consistent with the flexed limb posture inferred for *Ledumahadi*.

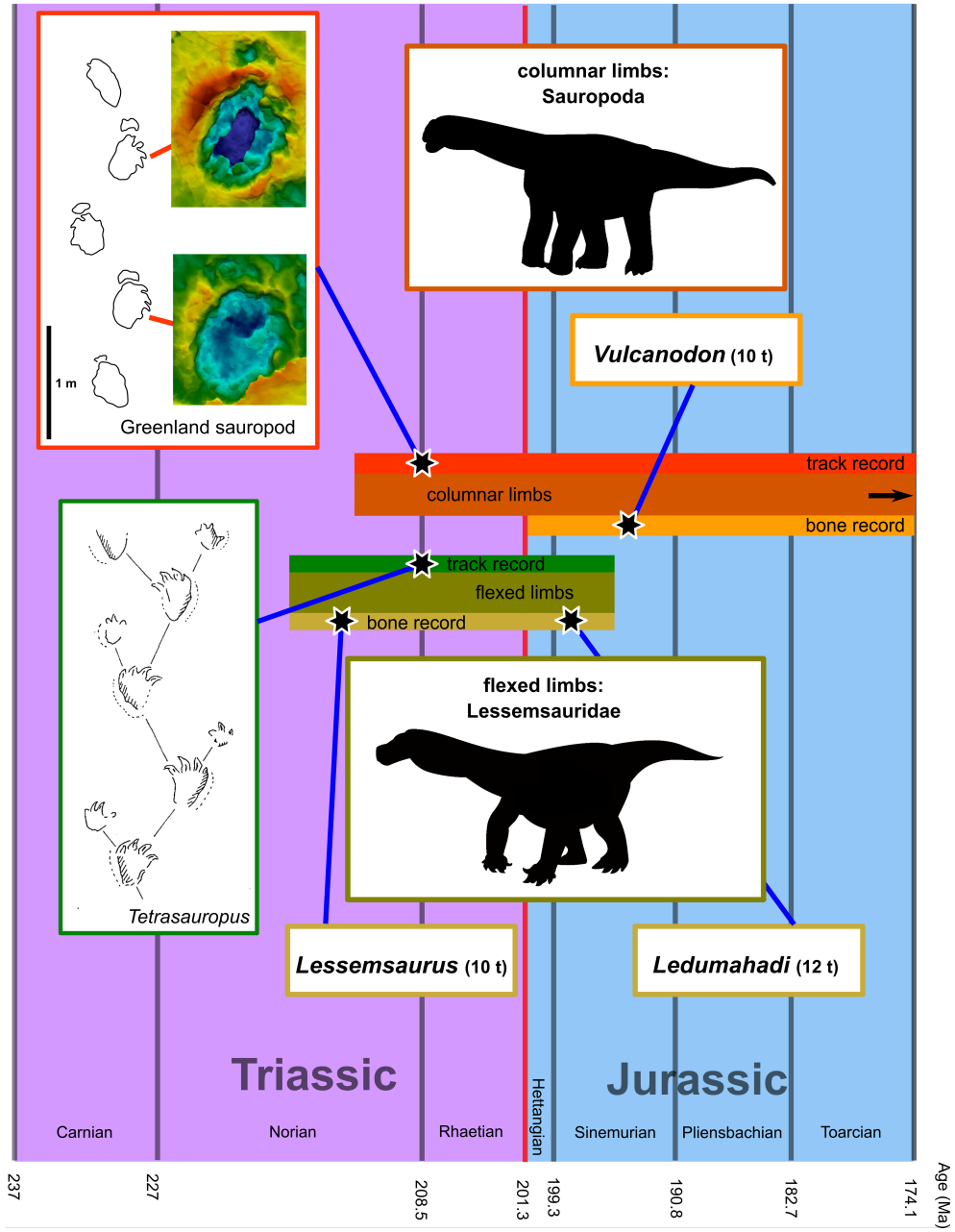

Figure 1. Tracks are a crucial part of the fossil record of four-legged sauropodomorphs. *Tetrasauropus*, a large trackway from the Upper Triassic of Lesotho, shows flexed and splayed forelimbs, corresponding to the condition inferred for the sauropod sister group Lessemsauridae, here represented by the Late Triassic *Lessemsaurus* and the Early Jurassic *Ledumahadi* (trackway drawing taken from (9)). Sauropods, which are characterized by columnar, unflexed limbs, appear in the bone record not before the Early Jurassic, but a trackway from Greenland attests to their presence in the Late Triassic (trackway drawing after (12)). Both columnar-limbed and flexed-limbed sauropodomorphs thus coexisted for 20 million years. Geologic time is from reference (20).

However, the track record also provides the earliest convincing evidence for the columnar sauropod-type stance and mode of locomotion, and it considerably predates both *Ledumahadi* and the earliest sauropod body fossils. The trackway is about 209 million years old and comes from the late Norian–early Rhaetian of Greenland (12). The prints of both the forefoot and hind foot are located close to the midline of the trackway, indicating a parasagittal gait and an upright posture (12,13). These features do not appear in the body fossil record before the Early Jurassic, where they are found in early sauropods such as *Vulcanodon*, also from South Africa. The Greenland trackway shows evolutionary innovations of sauropods, such as the laterally deflected foot claws, and is practically indistinguishable from sauropod trackways from the later Mesozoic, except for the presence of a claw mark on the impression of the fourth toe. The Greenland trackway thus suggests that sauropods were around in the Late Triassic, which is consistent with the phylogenetic evidence (6,7) and shows that sauropods must have coexisted with bipedal as well as quadrupedal prosauropods such as the lessemsaurids. The new Argentinian giants now corroborates this view because it is of the same age of the tracks, Late Triassic, and could have left those *Tetrasauropus* tracks. This also is plausible scenario because South Africa and Argentina were geographically close at the time

These considerations question some claims made in the new South African paper. As for body size, McPhee et al. are likely correct in stating that *Ledumahadi* was the largest animal of its time (Early Jurassic), and bone histological analysis of the holotype femur indicates that it was fully grown. Bone histological evidence (6,7) also supports the systematic position of Lessemsauridae outside of Sauropoda because of the presence of regularly spaced growth marks in the long bones. Lessemsaurids combine the primitive growth stops with the fast-growing tissue of later sauropods (7,14,15), indicting that these animals also were intermediate in growth rate between, e.g., *Plateosaurus*, and true sauropods which grew too fast to lay down growth marks (7,14,15).

However, at the estimated 12 t, *Ledumahadi* was only marginally larger than the contemporary or slightly younger (16) *Vulcanodon* and the much older *Lessemsaurus,* estimated at 7-10 t (7). In addition, there are unpublished fossil bones (17) from a bipedal prosauropod giant (10-15 t), also from the Lower Elliot Formation (Late Triassic). Finally, the track record also indicates that sizes similar to that of *Vulcanodon* were reached already in the Late Triassic, as evidenced by both the sauropod tracks from Greenland (hind foot length 43 cm) and the *Tetrasauropus* tracks. Columnar-limbed sauropods and flexed-limb prosauropods coexisted for the considerable time of at least 20 million years (Figure 1), and body size in sauropodomorphs did not increase after the end-Triassic extinctions but well before it. The extinction event thus does not seem to have affected this dinosaur lineage.

After the extinction of flexed-limbed prosauropods about 190 million years ago, “four legs” were good for another 125 million years until the end of the Cretaceous, and sauropods were to remain the dominant plant eaters (18). But, as in Orwell’s story, the claim that “four legs are good, two legs are better” may be justified by the surviving dinosaurs, the birds. Bipedality, retained by all meat-eating dinosaurs, means that there is a pair of limbs that can be put to other good uses, such as catching dinner, waving at the girls, and flying (19).

References

1. Maidment, S.C., and Barrett, P.M. (2012). Osteological correlates for quadrupedality in ornithischian dinosaurs. Acta Palaeontologica Polonica *59*, 53-70.

2. Barrett, P.M., and Maidment, S.C.R. (2017). The evolution of ornithischian quadrupedality. Journal of Iberian Geology *43*, 363-377. 1. Sander, P.M., Christian, A., Clauss, M., Fechner, R., Gee, C.T., Griebeler, E.-M., Gunga, H.-C., Hummel, J., Mallison, H., and Perry, S.F. (2011). Biology of the sauropod dinosaurs: the evolution of gigantism. Biological Reviews *86*, 117–155.

3. Benson, R.J.B., Gene Hunt, G., Carrano, M.T., Campione, N. (2018). Cope's rule and the adaptive landscape of dinosaur body size evolution. Palaeontology 61, 13-48.

4. Sander, P.M., Christian, A., Clauss, M., Fechner, R., Gee, C., Griebeler, E.M., Gunga, H.-C., Hummel, J., Mallison, H., Perry, S., et al. (2011). Biology of the sauropod dinosaurs: the evolution of gigantism. Biological Reviews of the Cambridge Philosophical Society *86*, 117–155.

5. Sander, P.M. (2013). An evolutionary cascade model for sauropod dinosaur gigantism-overview, update and tests. PLoS One *8*, e78573.

6. McPhee, B.W., Benson, R.B.J., Botha-Brink, J., Bord, E.M., and Choiniere, J.N. (2018). A giant dinosaur from the earliest Jurassic of South Africa and the transition to quadrupedality in early sauropodomorphs. Current Biology.

7. Apaldetti, C., Martínez, R.N., Cerda, I.A., Pol, D., and Alcober, O. (2018). An early trend towards gigantism in Triassic sauropodomorph dinosaurs. Nature Ecology & Evolution *2*, 1227–1232.

8. Henderson, D.M. (2006). Burly gaits: centers of mass, stability, and the trackways of sauropod dinosaurs. Journal of Vertebrate Paleontology *26*, 907–921.

9. Porchetti, S.D., and Nicosia, U. (2007). Re-examination of some large early Mesozoic tetrapod footprints from the African collection of Paul Ellenberger. Ichnos *14*, 219–245.

10. Ellenberger, F., Ellenberger, P., and Ginsburg, L. (1970). Les dinosaures du Trias et du Lias en France et en Afrique du sud, d'après les pistes qu'ils ont laissées. Bulletin de la Société géologique de France *7*, 151–159.

11. Ellenberger, P. (1972). Contribution à la classification des pistes de vertébrés du Trias: Les types du Stormberg d´Afrique du Sud (I). Palaeovertebrata, Memoire Extraordinaire, 1–152.

12. Lallensack, J.N., Klein, H., Milàn, J., Wings, O., Mateus, O., and Clemmensen, L.B. (2017). Sauropodomorph dinosaur trackways from the Fleming Fjord Formation of East Greenland: evidence for Late Triassic sauropods. Acta Palaeontologica Polonica 62, 833–843.

13. Remes, K. (2008). Evolution of the pectoral girdle and forelimb in Sauropodomorpha (Dinosauria, Saurischia): osteology, myology and function. PhD thesis, University of Munich.

14. Sander, P.M., Klein, N., Stein, K., and Wings, O. (2011). Sauropod bone histology and implications for sauropod biology. In Biology of the Sauropod Dinosaurs. Understanding the Life of Giants, N. Klein, K. Remes, C.T. Gee and P.M. Sander, eds. (Bloomington: Indiana University Press), pp. 276-302.

15. Cerda, I.A., Chinsamy, A., Pol, D., Apaldetti, C., Otero, A., Powell, J.E., and Martínez, R.N. (2017). Novel insight into the origin of the growth dynamics of sauropod dinosaurs. PLoS ONE *12*, e0179707.

16. Viglietti, P.A., Barrett, P.M., Broderick, T.J., Munyikwa, D., MacNiven, R., Broderick, L., Chapelle, K., Glynn, D., Edwards, S., Zondo, M., *et al.* (2018). Stratigraphy of the *Vulcanodon* type locality and its implications for regional correlations within the Karoo Supergroup. Journal of African Earth Sciences *137*, 149–156.

17. Wedel, M.J., and Yates, A.M. 2011. A *Diplodocus*-sized bipedal basal sauropodomorph from the Late Triassic of South Africa. Symposium of Vertebrate Palaeontology and Comparative Anatomy, 59th Annual Meeting Proceedings, p. 22.

18. Klein, N., Remes, K., Gee, C.T., and Sander, P.M. eds. (2011). Biology of the Sauropod Dinosaurs. Under8standing the Life of Giants (Bloomington: Indiana University Press).

19. Koschowitz, M.-C., Fischer, C., and Sander, P.M. (2014). Beyond the rainbow. Science *346*, 416–418.

20. Cohen, K.M., Finney, S.C., Gibbard, P.L., and Fan, J.-X. (2013; updated) The ICS International Chronostratigraphic Chart. Episodes *36*, 199-204.

Chapter 8

unpublished.

Lallensack, J.N., unpubl. Dinosaur tracks: state of research, challenges, and prospectus. Doctoral thesis 2018 (chapter 8). Bonn, Germany. **p. 212–228.**

Dinosaur tracks: state of research, challenges, and prospectus

Jens N. Lallensack

Division of Paleontology, Steinmann Institute, University of Bonn, Bonn, Germany

ABSTRACT

Although often neglected, fossil footprints played an important role in shaping our modern understanding of dinosaurs, informing on aspects as diverse as distribution, ecology, and abundance; size, anatomy, and pathologies; posture and range of motion; foot kinematics, gaits, and speeds; as well as functional morphology and behavior. Yet, the study of dinosaur tracks faces a number of problems adding significant ambiguity to their interpretation, and are thus seriously limiting their utility. The five most vexing categories of problems might include the collection and dissemination of data; the definition of footprint margins; the understanding and distinction of separate sources of footprint shape variation; the identification of the trackmaker; and time-averaging of footprint assemblages. All of these problems are much more relevant for the track record than equivalent problems are for the skeletal record, mainly due to the nature of tracks as life traces and sedimentary structures. It is argued that objective and quantitative methods, which remain widely underused in ichnology, bear the potential to effectively account for these problems, and thus open the way for more fully exploiting tracks to augment our understanding of dinosaurs. While the taxonomic resolution of tracks might have been overestimated by ichnotaxonomy, other determinants of track variation, especially functional adaptations, bear great potential for future studies.

INTRODUCTION

Tracks constitute a valuable data source for inferences on the anatomy, biology, ecology, and evolution of dinosaurs. Essentially being sedimentary structures, tracks pass through different taphonomical filters than do body fossils, and thus are often preserved where bones are not. They can, therefore, be used to complement and test the completeness of the body fossil record. Furthermore, tracks are life traces, and as such do not represent the trackmaker itself but record its activities at a certain time and place (e.g., Lockley 1997). They thus record information, especially on behavior, that cannot be recorded by body fossils. This very different nature of tracks, however, also makes it challenging to incorporate tracks in studies concerned with body fossils. In fact, tracks are often neglected in studies developing the general understanding of dinosaurs despite their obvious potential, and studies focused on tracks did not yet contribute as much to this understanding as they potentially can.

In the following, I will first review the significant contributions studies of tracks made—and continue to make—to our modern understanding of dinosaurs. Then, I describe what I consider the five main challenges that complicate the interpretation of tracks, with emphasis on possible solutions and advances made in the present dissertation. I end the discussion with a note on the current practice of ichnotaxonomy, and conclude that especially functional interpretations of tracks bear high potential for future study. As an un-

dertone throughout this chapter, the application of objective and quantitative methods is strongly advocated, and it is considered paramount for the future advance of the study of tracks.

WHAT TRACKS CONTRIBUTE TO THE UNDERSTANDING OF DINOSAURS

Distribution, ecology, and abundance

Fossil footprints are often more abundant than body fossils and can be found in rock formations that do not preserve bones (Lockley 1998*a*), providing valuable data on the temporal and spatial distribution of taxa. This is especially true for the Triassic, which has an especially scarce body fossil record (e.g., Molnar 2012) despite being a critical interval in tetrapod evolution (Sues and Fraser 2010). Quadrupedal dinosauromorph tracks from the Polish Holy Cross Mountains date to the early Olenekian (ca 249–251 Ma), indicating that the dinosaur stem lineage emerged soon after the Permian/Triassic mass extinction (252.3 Ma), while the earliest dinosauromorph body fossils only date to the latest Anisian (ca 242–244 Ma) (Brusatte et al. 2011). While the oldest undisputed dinosaur body fossils come from near the Carnian—Norian boundary (Brusatte et al. 2010; Langer et al. 2010), the oldest probable dinosaur tracks date to the Ladinian (Gand and Demathieu 2005; Melchor and De Valais 2006; Brusatte et al. 2011). Sauropods first emerge in the body fossil record in the Lower Jurassic (Viglietti et al. 2018), as *Isanosaurus*, originally described as a Late Triassic sauropod, has probably been dated incorrectly (Racey and Goodall 2009; McPhee et al. 2015). Again, footprint evidence suggests a substantially earlier origin (Wilson 2005; Lockley et al. 2006); the currently most convincing example, a trackway from close to the Norian—Rhaetian boundary (ca 208 Ma), shows a number of synapomorphies otherwise only known from eusauropods (Lallensack et al. 2017; chapter 6).

Tracks furthermore yield important implications on the spatial distribution of dinosaurs. For example, ornithopod footprints described in 1960 from Spitzbergen had provided the first evidence of non-avian dinosaurs at polar latitudes (Lapparent 1962; Rich et al. 2002). Tracks from Brazil provide the only uncontentious evidence for Jurassic thyreophorans in South America (Francischini et al. 2018). Tracks revealed an unexpected abundance of sauropod and theropod dinosaurs on carbonate platforms, sometimes far from the continents (e.g., Dalla Vecchia 2005; Petti et al. 2011). Large theropod tracks found in marine strata of the Upper Jurassic of Germany have been suggested to record a sea level fall that allowed for dispersal onto previously isolated islands that had developed a dwarfed island fauna (Lallensack et al. 2015).

Tracks allow inferences on the species composition of dinosaur communities, habitat preferences, and population structures (Lockley 1998*a*). For example, tracks have been used to reconstruct the composition and evolution of dinosaur faunas of the Middle Jurassic, where terrestrial body fossils are rare globally (e.g., Lockley and Meyer 2000; Whyte et al. 2007). A hadrosaurid tracksite from the Late Cretaceous of Alaska provided insights into herd structures at polar latitudes, with relative abundances of separate size classes being in accordance with growth curves deduced from bone histology (Fiorillo et al. 2014). Both tracks and body fossils have been cited as evidence of age segregation in sauropods, contradicting notions of parental care in this group (Myers and Fiorillo 2009).

In contrast to bones, tracks are not biased by any spatial averaging, and periods of time averaging are generally shorter (Cohen et al. 1993). They thus can record which animals, and at which abundance, frequented a specific habitat at a higher spatial and temporal resolution. Bones, on the other hand, provide a more general picture, where the effects of habitat specificity and seasonality are less severe. Paleoecological inferences are therefore optimally based on both lines of evidence (Cohen et al. 1993).

Size, anatomy, and pathologies

Tracks may provide important data on body size evolution in dinosaurs. Body size is most frequently estimated from pedal footprint length, which correlates with hip height (e.g., Thulborn 1990). In quadrupedal trackways, an alternative measure, the gleno-acetabular distance, can be employed (Lallensack et al. accepted; chapter 5). In principle, weight can be directly estimated from tracks (Schanz et al. 2013; Läbe 2017), with exiting prospects for future studies. In chapter 3 (Lallensack et al. unpubl.), footprint centroid size was employed as size proxy, showing that bipedal ornithischians underwent a gradual size increase from the Late Triassic/Early Jurassic to the Late Cretaceous, surpassing theropods from the Early Cretaceous onwards. Maximum body size in tridactyl trackmakers was found to be highest in the Late Cretaceous, followed by the Late Jurassic (Lallensack et al. unpubl.; chapter 3). It has been noted that the sauropod track record generally suggests a much smaller body size than the skeletal record (Lockley 1997). Indeed, a larger sample of 124 sauropod trackways from around the world, all including both manual and pedal imprints, shows an average pedal footprint length of only 52 cm, indicating a hip height of little more than two meters (Lallensack, unpublished data). While it remains unclear which taphonomic filters led to this discrepancy, the track record is consistent with the high number of offspring and high mortality rates before sexual maturity that have been inferred for sauropods (Sander et al. 2008).

Obviously, tracks provide information on the trackmaker's foot anatomy, which is of relevance given the scarcity of articulated manual and pedal skeletons. Sometimes, anatomy inferred from tracks is without an obvious analogue in the body fossil record; this is the case for the bilobed sauropod manual impressions described in chapter 5 (Lallensack et al. accepted), which indicate a subdivision of the distal metacarpal colonnade into two functional units. Much of the current knowledge on the soft part anatomy of dinosaur autopodia was derived from tracks, including the presence of heel pads in the pedes of graviportal taxa such as sauropods (Bonnan 2005) and ornithopods (Moreno et al. 2007), but also of deinonychosaurians (Li et al. 2008); the amount of soft tissue enclosing the digits (Lockley et al. 1998); the number and shape of phalangeal pads as well as their generally mesarthral condition (Thulborn 1990); the bilobed heel pad typical for many hadrosaurid tracks (e.g., Díaz-Martínez et al. 2015); the shape and size of claws and hoofs (e.g., Lallensak et al. 2017 unpublished; chapters 3 and 6); as well as the nature of the integument of the foot sole, which can be deduced from skin impressions (e.g., Currie et al. 1991; Paik et al. 2017).

Dinosaur tracks yield also a number of examples of inferred pathologies (McCrea et al. 2015). These can be inferred either directly from the footprint morphology, including, e.g., aberrant or missing digital impressions. They can also be deduced from the trackway pattern—a right step consistently shorter than the left, or vice versa, can be due to a pathology in the left (or right) leg resulting in a limp. In some cases, pathologies are expressed in both the footprint morphology and the trackway pattern (McCrea et al. 2015; Razzolini et al. 2016), allowing for studying both the pathologies themselves and their influence on locomotion. In chapter 5 (Lallensack et al. accepted), statistically significant discrepancies of step lengths were demonstrated to be a common phenomenon, suggesting that such patterns can simply be behavioral without resulting from an explicit pathology.

Posture and range of motion

A quadrupedal trackway provides unequivocal evidence for at least facultative quadrupedality of the trackmaker, although the reverse—the bipedal condition—cannot always be inferred with certainty given the possibility that manual impressions are simply not preserved (Falkingham et al. 2011*a*, *b*). Tracks show

that many early dinosauromorphs were quadrupedal, including the earliest evidence for this clade (Brusatte et al. 2011). Tracks demonstrate quadrupedality in many larger ornithopods, being in unison with osteological inferences, and so far provide the only evidence that several small-sized ornithopods were quadrupedal (Lockley and Wright 2001; Castanera et al. 2013). Furthermore, there is evidence that basal ornithischians were able to switch between bipedal and quadrupedal gaits as a response to changing terrain and substrate properties (Wilson et al. 2009). Tracks likewise show quadrupedality in basal sauropodomorphs with flexed limb postures (Lallensack et al. 2017; Sander and Lallensack submitted; chapters 6 and 7), and confirm quadrupedality in hatchlings of *Massospondylus*, suggesting a shift from quadrupedality to bipedality during ontogeny in basal sauropodomorphs (Reisz et al. 2012). Tracks, therefore, play a crucial role in the understanding of secondary quadrupedalism, which is a rare transition in tetrapod locomotion (Maidment and Barrett 2012; VanBuren and Bonnan 2013).

Secondarily quadrupedal dinosaurs face the problem of rotating their manus into a pronated, forward-facing position to allow it to contribute to propulsion during locomotion. Both osteological (Bonnan 2003) and track evidence (Milner et al. 2009) show that the plesiomorphic condition in dinosaurs was semi-supination, where the palms of the hands are facing each other, and that active pronation of the forearm was not possible. In sauropods, manus orientation is difficult to infer based on the osteology given the large amount of cartilage within the joints. Indeed, osteological edivence appeared to support the plesiomorphic lateral manus orientation, while trackways demonstrated that an almost fully anterior manus position is possible (Borsuk-Bialynicka 1977; Bonnan 2003). Trackway evidence further revealed a considerable rotational range of movement in the sauropod forelimb, much of which was apparently achieved by rotation in the shoulder (Marty 2008; Xing et al. 2015). Orientations of manual impressions in sauropod trackways were analyzed in chapter 5 (Lallensack et al. accepted), showing that manus orientations were correlated with trackmaker size, locomotion speed, and trackway gauge, suggesting that more anterior orientations are employed when the manus is contributing to propulsion.

Tracks inform on the degree of sprawling seen in the forelimb. Somewhat sprawling or semi-sprawling limbs were inferred for some basal sauropodomorphs (Lallensack et al. 2017; Sander and Lallensack submitted; chapters 6 and 7). Trackways provided crucial evidence for a long-standing debate on forelimb posture in ceratopsians, demonstrating that, while not fully erect, the forelimb was less sprawling than it has been assumed prior to the discovery of such tracks (Lockley and Hunt 1995; Paul and Christiansen 2000; Thompson and Holmes 2007). Sauropod trackways feature an astonishing variability of gauges, ranging from very narrow gauge to wide gauge (Lallensack et al. accepted; chapter 5). Osteological correlates for somewhat abducted limbs were identified in titanosaurians, demonstrating that this group was producing wide gauge trackways (Wilson and Carrano 1999). However, the track record also shows that part of this variability was behavioral (Wright 2005; Castanera et al. 2012). A biomechanical analysis suggested that narrow gauge trackways are correlated with a posterior position of the center of mass, while wide gauge trackways indicate a more anterior position, providing insights into the relationship between build and locomotion in sauropods (Henderson 2006*a*).

Tracks furthermore inform on pes orientation, suggesting that an outward rotation of the pes might be a defining feature of sauropods (Lallensack et al. 2017; chapter 6). In ornithopods, footprints are typically rotated inwards, indicating that the weight-bearing parts of the foot are moved closer to the sagittal plane. This might have reduced the need for medial to lateral swinging of the body during locomotion, which is necessary in trackmakers showing a wide gauge to keep the center of mass above the weight-bearing foot (Casanovas et al. 1995; Pérez-Lorente 2015).

Tracks also record which parts of the foot made contact with the ground. In the digitigrade pedal impressions of theropods and basal ornithischians, the metatarsophalangeal joint of digits II and III did not make contact with the ground, while digit IV was impressed over its whole length (Farlow et al. 2000). Deinonychosaurian tracks confirm that only the base of digit II was weight-bearing, with the characteristic sickle-shaped claw held clear off the ground (Li et al. 2008). Sauropods tracks indicate a semi-digitigrade pes, where the metatarsals are supported by a heel pad (Wilson 2005). Tracks furthermore show that posture may change due to individual behavior. Thus, theropods may in some cases lift the posterior part of the foot above the ground during running (Sarjeant 1975; Thulborn 1990; Viera and Torres 1995), but, in rare cases, have also been suggested to walk with their metatarsus fully impressed (Kuban 1989).

Foot kinematics, gaits, and speeds

Tracks provide information on foot kinematics during locomotion. Especially in deeply penetrating footprints, entry and exit traces of digits as well as striation marks from individual scales may be differentiated, allowing for a precise reconstruction of how the foot moved within the substrate (Avanzini et al. 2012). For bipedal dinosaurs, these marks indicate that the foot swung outwards during the stride, describing an arc (Thulborn 1990). Within theropods, foot kinematics were found to be conservative (Avanzini et al. 2012). As discussed in chapter 3 (Lallensack et al. unpubl.), modern ratites draw their digits together while swinging the foot forwards but splayed them before contacting the ground, providing a larger base of support. In many theropod footprints, however, the interdigital angles are very narrow; the reduced base of support might have been compensated by the of the presence of a long tail acting as a stabilizer (Lallensack et al. unpubl.; chapter 3). Sauropod manual impressions from the Late Jurassic of Portugal showed that the deeply penetrating manus was leaving the substrate vertically, suggesting that it did not play a major role in propulsion of the animal (Milàn et al. 2005).

Absolute speeds can be estimated based on the stride length of the trackway and the hip height estimated from footprint length (Alexander 1976). The vast majority of known trackways were left by walking animals (e.g., Thulborn 1984). Evidence for running dinosaurs (e.g., Farlow 1981; Thulborn and Wade 1984; Irby 1996; Weems 2006; Kim and Huh 2010; Xing et al. 2016) remains rare, and is restricted to small and medium-sized bipedal trackmakers, with maximum recorded speeds of up to 40 km/h (Farlow et al. 2012*a*). As running can be considered a rare activity in dinosaurs, as it is for modern animals, tracks may seldom record the maximum locomotory ability of their makers (Farlow et al. 2012*a*). However, it has become clear that theropods moved generally faster than did herbivorous dinosaurs (Currie 1983).

Gaits in theropods were similar to those of modern ratites in showing a continuous transition from walking to running, in contrast to the discontinuous transition in humans, which involves distinct gaits (Bishop et al. 2017). The exact gait used to produce a quadrupedal trackway can often be determined only when size and body proportions of the trackmaker are given, as separate gaits may produce identical trackway patterns (Stevens et al. 2016). The walking pace (referred to as an "ambling gait"), where the fore- and hindlimb of one side are in ground contact while the limbs of the opposite side of the body are swinging forwards, was suggested as the most likely gait employed by some wide gauge sauropod trackmakers (Casanovas et al. 1997; Vila et al. 2013). However, such a gait requires the trackmaker to constantly shift its center of mass towards that side of the body where the feet are in ground contact, which appears unlikely in a wide gauge sauropod trackmaker. In chapter 5 (Lallensack et al. accepted), the lateral-sequence single-foot walk was found to be the most likely employed gait in sauropods, at least for smaller trackmakers.

Functional morphology and behavior

Tracks provide valuable evidence for functional morphology. Wide gauge sauropod tracks were used to make sense of peculiar features of the appendicular skeleton of titanosaurs, including the strongly elliptical femora (Wilson and Carrano 1999). Functional interpretations for tridactyl tracks remain rare, but bear great potential for studies on dinosaur locomotion. As demonstrated in chapter 3 (Lallensack et al. unpubl.), a proportionally long digital impression III can be regarded as an adaptation for cursoriality, while thin and widely splayed digits improve stability. Short footprints with broad digits reflect graviportal features. While graviportality is common in large ornithopods, it is absent in equally-sized theropods, possibly because retaining a greater degree of cursoriality and maneuverability is essential for predators (Farlow et al. 2013).

Tracks provide both direct and indirect evidence for behavior. Theropod tracks are often more abundant than tracks of herbivorous dinosaurs, which is in sharp contrast to the faunal composition suggested by the skeletal record. Tracks record the activity of animals rather than the animals itself; therefore, this theropod domination might reflect the greater activity of these predators (Farlow et al. 2012*a*). Alternatively, their larger home ranges and lower habitat specificity could have caused them to cross environmental barriers more frequently, increasing the probability of track registration (c.f., Farlow 1987; Cohen et al. 1993). Trackways record how individuals adjust their mode of locomotion to environmental conditions. Sauropods tended to extend their pedal digits forwards when walking on soft substrates, improving traction (Hall et al. 2016). A theropod trackmaker responded to a sloping and slippery substrate by gripping with its claws, while ornithischian trackmakers responded to the same slope by shifting to a quadrupedal gait, increasing gauge width, and adopting a more plantigrade foot posture (Wilson et al. 2009). Swim tracks demonstrate that at least some theropod dinosaurs did swim, and furthermore record how individuals reacted to current changes (Milner and Lockley 2016).

Multiple tracksites of sauropods (see Myers and Fiorillo 2009 and references therein), theropods (e.g., Ostrom 1972; Lockley and Matsukawa 1999; Li et al. 2008), and ornithischians (e.g., Matsukawa et al. 2001; Lockley et al. 2012; Piñuela et al. 2016) have been cited as evidence for gregarious behavior. Criteria for inferring gregariousness from tracks include the presence of multiple trackways on the same surface, which are of the same type, parallel to each other, equally spaced, corresponding in locomotion speed values, and influencing each other (e.g., Lockley and Matsukawa 1999; Piñuela et al. 2016). Although it is difficult to assess if a set of trackways was left simultaneously the body of evidence for gregariousness increases when body fossil and trackway data are combined (Myers and Fiorillo 2009). Such an combined approach provided evidence for age segregation in sauropods (Myers and Fiorillo 2009).

CHALLENGES

As shown by the above review, tracks form an important part of the evidence leading to the modern conception of dinosaur anatomy, biology, and ecology. Next, I turn to the many difficulties, or challenges, in interpreting trackway data, which result from the very nature of fossil tracks, which are both sedimentary structures and life traces. These difficulties currently add significant ambiguity to interpretations derived from tracks and are mostly not sufficiently accounted for. The most important of these challenges are reviewed below, and possible solutions are discussed.

Data collection and dissemination

Most of the information recorded in a footprint is not preserved in the footprint itself but in its context. Any excavation will separate footprints from their context, and is therefore often considered undesirable (Bennett et al. 2013). Therefore, and in contrast to body fossils, tracks typically remain in the field in often remote locations, which does not only hinder access to scientists but also exposes the tracks to the elements, leading to degradation over time. This difficult, and in some cases impossible, access often prohibits re-evaluation of results made by previous studies. Often, researchers have to solely rely on published literature of the track assemblage of interest, where footprint morphologies are typically depicted using interpretative outline drawings that may introduce significant interpretational bias.

Fortunately, a solution to these long-lasting problems is in sight. Photogrammetry, which allows for the generation of high-resolution digital three-dimensional models of footprints and whole tracksites with minimal time and monetary expenses (Falkingham 2012; Mallison and Wings 2014; Matthews et al. 2016), has gained wide usage and support in recent years and now is considered standard practice by many researchers in the field (Falkingham et al. 2018). When supplemented with sedimentological data and samples as well as GPS data, such three-dimensional models allow for capturing most of the information contained in a tracksite. Models can be both shared directly and used to derive informative two-dimensional figures, including depth-color images and contour plots, allowing for independent re-evaluation of results.

Definition of footprint margins

Footprints often do not show distinct margins, but may fade out gradually into the surrounding sediment, making it difficult to define the extent of a footprint. As a result, linear and angular measurements as well as outline drawings made by the researcher will introduce a significant degree of subjectivity. Falkingham (2016) quantified the range of subjectivity for an exemplary footprint and showed that footprint length varies as much as 27% depending on the height level chosen for measurement. Similarly, interpretations of footprint shape can greatly differ between observers (Thulborn 1990). This degree of subjectivity does not allow for obtaining objective quantitative and repeatable results (Falkingham 2016). A solution to this problem is presented in chapter 4 (Lallensack unpubl.). Based on three-dimensional models, a computer script determines the trackway margin automatically, allowing for completely objective quantitative shape analysis.

Sources of footprint shape variation

Traditionally, footprint shape features are interpreted regarding their possible phylogenetic and ichnotaxonomic meaning, while other possible sources of variation are often ignored. These various determinants of footprint shape variation are summarized below.

Mode of preservation—A surface containing tracks is not necessarily the tracking surface (i.e., the surface the animal walked on). Tracks may be transmitted onto sediment layers below the tracking surface, in which case they are both larger and more indistinct (e.g., Allen 1997; Farlow et al. 2006; Milàn and Bromley 2006; Jackson et al. 2010). Such undertracks, however, may only form under special circumstances, and are not as common as often assumed (Marty et al. 2009). Therefore, shallow and indistinct footprint shapes are often the result of a firmer substrate rather than undertrack preservation (Nadon 2001). Shallow and indistinct shapes may also result from thin layers deposited above the tracking surface, either by multiple sedimentation events or by the growth of microbial mats, forming an overtrack (Marty et al. 2009). Footprints

preserved as natural casts do not appear to be significantly different in shape than their respective molds (Wings et al. 2016).

Post-formation alteration—Footprint shape is often markedly deformed and/or degraded after footprint formation, both before burial and after modern-day exposure. Degradation may occur as continuous and gradual weathering slowly reducing the topography of tracks (Henderson 2006*b*), and/or of localized erosion of larger pieces (Lallensack et al. accepted; chapter 5). Footprint shape may also be altered during burial, where strain acting on the track surface can cause significant deformation (Schulp 2002).

Substrate and behavior—The combination of substrate properties and trackmaker behavior at the time of track formation has, besides the anatomy of the trackmaker, the greatest impact on the final footprint shape (Falkingham 2014). Important substrate factors influencing footprint shape include the topography of the tracking surface and the structure, composition, and water content of the sediment. Behavioral sources of variation include different activities such as resting and swimming, changes in speed and direction of travel, and more subtle variations in the foot kinematics. Effects of variation in substrate and behavior can be studied by comparing separate footprints of a single trackway (Lallensack et al. 2016; chapter 2). Furthermore, such effects can be studied experimentally using living animals (e.g., Farlow 1989; Milàn 2006), mechanical substrate impactors (e.g., Jackson et al. 2010), and computer simulations (e.g., Falkingham and Gatesy 2014).

Interspecific variation—Phylogeny is a major determinant of footprint shape especially when more inclusive taxa are considered. However, widespread convergence and conservatism in pedal morphologies indicate that functional demands play an equally important role. As shown in chapter 3 (Lallensack et al. unpubl.), shape trajectories are recurrent in separate groups of tridactyl dinosaurs, and important shape features are clearly correlated with size, reflecting changing functional requirements. Therefore, dinosaur footprints might not be as phylogenetically informative as often assumed. It has also been suggested that parts of the interspecific variation can be due to intrinsic developmental factors such as heterochrony without explicit functional meanings (Lockley 2007*a*, 2009). However, given the importance of a functionally well-adapted pes for survival especially in larger bipedal trackmakers, studying footprints from a functional point of view may provide valuable insights into dinosaur biology (Lallensack et al. unpubl.; chapter 3).

Intraspecific variation—Last but not least, foot shape varies from individual to individual of the same species. Such variation may be due to genetic diversity, environmental influences, pathologies, and, most importantly, ontogeny. Olsen (1980) demonstrated that toe extension (the projection of digital impression III beyond digital impressions II and IV) decreases continuously with increasing footprint size in a sample of theropod footprints from the Newark Supergroup of New Jersey, US. As toe extension is the primary feature distinguishing the three ichnotaxa contained in the sample (*Grallator*, *Anchisauripus*, and *Eubrontes*), Olsen proposed that all three might simply represent different ontogenetic stages of one and the same trackmaker species that form an allometric trajectory (Olsen 1980). Until now, the degree to which dinosaur feet may grow allometrically remains poorly constrained (Farlow et al. 2012*b*), and Olsen's original claim was neither convincingly refuted nor corroborated.

Trackmaker identification

The utility of tracks to supplement the body fossil record depends on the resolution to which the trackmakers can be identified (Carrano and Wilson 2001). As tracks are seldom be found in association with

body fossils, the trackmaker taxon often remains unclear even at the level of more inclusive taxa. For example, the different groups of large theropod dinosaurs cannot currently be reliably differentiated based on their tracks despite their wide phylogenetic separation (Farlow et al. 2013). At the genus or species level, trackmaker assignment is not possible except in rare cases, and only by considering additional geographic and temporal constraints (e.g., Lockley and Hunt 1994).

The synapomorphy-based approach (Olsen 1995; Carrano and Wilson 2001) is commonly regarded as the most rigorous method for trackmaker identification (e.g., Brusatte et al. 2011). Its applicability is restricted by the rarity of articulated pedal skeletons as well as conservatism and convergence in pedal morphologies shown by some lineages such as theropods and sauropods, often necessitating the use of alternative methods (e.g., Smith and Farlow 2003; Buckley et al. 2015). Nevertheless, the potential for identifying dinosaurian trackmakers based on synapomorphies is not yet fully exploited (Lallensack et al. 2017; Sander and Lallensack submitted; chapters 6 and 7), and new fossil discoveries continue to allow for new assignments to be made (e.g. Brusatte et al. 2011).

Time-averaging

Interpretations of trackmaker interactions such as gregariousness often rely on the assumption that the tracks in question have been made simultaneously. Time averaging can be inferred based on differences in track preservation and depth, the number of individuals crossing the surface in different directions, or overprinting of tracks by other tracks (e.g., Myers and Fiorillo 2009). The absence of such indicators, however, is by no means evidence that the trackways were left simultaneously. Although periods of time averaging tend to be shorter for track assemblages than for bone assemblages and typically range from days to weeks (Cohen et al. 1993), even a very short temporal separation of trackmaker actions can fundamentally change their interpretation (Myers and Fiorillo 2009).

ICHNOTAXONOMY: PROBLEMS AND POSSIBLE SOLUTIONS

The need for rigorous objective approaches to the analysis of dinosaur tracks is particularly evident in ichnotaxonomy. Ichnotaxonomy aims to categorize the variation present in the track record, and thus is potentially a powerful tool for placing individual tracks in a broader context and in recognizing yet unreported characteristics. Ichnotaxa are only based on features that are thought to reflect the phylogeny of the trackmaker—ideally, an ichnotaxon encompasses the footprints of a biological taxon at some level (Farlow et al. 2012*a*). In this regard, vertebrate ichnotaxonomy is fundamentally different from that applied to invertebrate traces, which is not based on trackmaker anatomy but on trackmaker activity (Lockley 2007*b*; Farlow et al. 2012*a*). The ideally close correspondence between ichnotaxa and biological taxa allows for additional inferences to be made from ichnotaxonomical data, including estimates of the diversity and composition of dinosaur faunas and their evolution (Lockley 2007*b*).

This ichnotaxonomic approach, however, relies heavily on the assumption that enough track characteristics can be found that inform on phylogenetic relationships of the producing biological taxa. As discussed above ("Sources of footprint shape variation"), many features can instead be attributed to a multitude of other factors determining the final shape of the footprint. Importantly, the widespread convergence and conservativeness in foot morphologies results in very similar footprints even in distantly related taxa (Farlow et al. 2012*a*; Lallensack et al. unpubl.; chapter 3). Many features traditionally employed in ichnotaxonomy may reflect substrate properties and behavior rather than foot anatomy (chapter 2). Other features

might be related to intraspecific variation, including ontogenetic variation. For example, the common practice of defining ichnotaxa based on size (e.g., Olsen et al. 1998; McCrea et al. 2014) can lead to an overestimation of the number of trackmaker species, especially given the large size difference between hatchlings and adults in dinosaurs (Lallensack et al. 2016; chapter 2).

A different problem is associated with the non-discrete nature of many features used in ichnotaxonomy. Such features, e.g., the toe extension and the length-to-width ratio, can be near-continuous between proposed ichnotaxa (e.g., Olsen 1980). The validity of ichnotaxa based on such features can consequently only be demonstrated using quantitative approaches. In the absence of such methods, the use of near-continuous features rather than clear-cut distinguishing characters leads to ambiguity in ichnotaxonomical diagnoses, so that unambiguous referrals to specific ichnotaxa are often not possible. In fact, individual tracks do commonly match diagnoses of multiple separate ichnotaxa. Instead of relying on diagnoses, referrals to specific ichnotaxa are often based on comparisons with published outline drawings (e.g., Falkingham et al. 2018), which can be highly subjective (Lallensack et al. 2016; Lallensack unpubl.; chapters 2 and 4). This ambiguity creates the risk that tracks are preferentially ascribed to ichnotaxa already known from the same time and region rather than to equally similar tracks from different times and regions. In the worst case, usage of such data for broader inferences may result in circular arguments.

The problems outlined above raise the suspicion that the number of dinosaur taxa distinguishable based on footprint data has been overestimated (see also Farlow et al. 2012*a*). For example, the larger sample of tridactyl tracks analyzed in chapter 3 (Lallensack et al. unpubl.) includes 193 theropod footprints, over half of which have been ascribed to a total of 40 ichnogenera that mostly are currently considered valid, or at least have not been formally synonymized. The actual number of valid tridactyl theropod ichnotaxa is expected to be even higher. This apparent diversity is in sharp contrast with the fact that tridactyl theropod feet are generally conservative, and thus offer few distinguishing characters (contra Lockley 1998*b*).

For these reasons, the application of rigorous objective methods is paramount for much needed ichnotaxonomical revisions. Although such methods potentially reveal additional means to differentiate ichnotaxa, it is expected that their strict application would drastically reduce the number of valid dinosaur ichnotaxa (Farlow et al. 2012*a*). But even if results derived from ichnotaxonomy would eventually stay behind expectations, other approaches to the interpretation of tracks, particularly those seeking to infer function, may prove more fruitful than previously recognized.

CONCLUSIONS AND PROSPECTUS

Despite their highly significant contributions to the modern understanding of dinosaurs, which have been summarized above (section "What tracks contributed to the modern understanding of dinosaurs"), tracks continue to be neglected in many studies dealing with body fossils despite potentially yielding crucial evidence. Part of the reason for this reluctance are the many unresolved problems in interpreting track data, which add significant ambiguity to many interpretations, as was also summarized above (section "Challenges"). Another reason, however, likely lies in the difficulties in applying rigorous objective and quantitative methods to tracks. For this reason, inferences made from track data, especially when related to footprint shape, do often not fulfill standards of objective and repeatable data analysis already established in other fields of dinosaur paleontology.

The present thesis was aimed at demonstrating the value of objective and quantitative methods for the study of dinosaur footprints. On the one hand, objective and quantitative methods were developed and em-

ployed to address some of the most urgent challenges faced by the field: Chapters 2 and 5 (Lallensack et al. 2016, unpubl.) are considering intratrackway variability to demonstrate how footprint shape (Lallensack et al. 2016; chapter 2) and trackway patterns (Lallensack et al. accepted; chapter 5) may vary with changing behavior and substrate properties. Chapter 3 (Lallensack et al. unpubl.) demonstrates that important shape features of tridactyl tracks convey less phylogenetic information as previously thought. Chapter 4 (Lallensack unpubl.) provides a novel method for the automatic and fully objective generation of footprint outlines. Chapters 6 and 7 (Lallensack et al. 2017; Sander and Lallensack submitted) reveal unused potential for the synapomorphy-based approach for trackmaker identification. At the same time, the developed methods were used to improve on the understanding of dinosaur biology and evolution, with a focus on interpreting function, both based on footprint shape (Lallensack et al. unpubl.; chapter 3) and trackway parameters (Lallensack et al. accepted; chapter 5).

As a quintessence, this work suggests that phylogenetic information conserved in tracks is limited, but that tracks may instead carry a stronger functional signal than previously recognized. Functional signals are preserved in both the trackway pattern and footprint shapes, especially those of large, bipedal dinosaurs, where foot morphology is tightly constrained by functional requirements. Studies attempting functional interpretation of footprint and trackway features might still have much to add to our understanding of dinosaurs.

ACKNOWLEDGEMENTS

Ideas and insights provided in this work evolved over time, and are greatly influenced by the input of many. I especially thank Sashima Läbe, Michael Buchwitz, Oliver Wings, Anthony Romilio, and James O. Farlow for enlightening discussions. I furthermore wish to thank P. Marin Sander for helpful comments on an early version of this chapter.

REFERENCES

Alexander, R.M. 1976. Estimates of speeds of dinosaurs. *Nature* 261 (5556): 129–130.

Allen, J.R. 1997. Subfossil mammalian tracks (Flandrian) in the Severn Estuary, SW Britain: mechanics of formation, preservation and distribution. *Philosophical Transactions of the Royal Society of London B: Biological Sciences* 352 (1352): 481–518.

Avanzini, M., Piñuela, L. and García-Ramos, J.C. 2012. Late Jurassic footprints reveal walking kinematics of theropod dinosaurs. *Lethaia* 45 (2): 238–252.

Bennett, M.R., Falkingham, P., Morse, S.A., Bates, K. and Crompton, R.H. 2013. Preserving the impossible: Conservation of soft- sediment hominin footprint sites and strategies for three-dimensional digital data capture. *PLoS One* 8 (4): e60755.

Bishop, P.J., Clemente, C.J., Weems, R.E., Graham, D.F., Lamas, L.P., Hutchinson, J.R., Rubenson, J., Wilson, R.S., Hocknull, S.A., Barrett, R.S. and Lloyd, D.G. 2017. Using step width to compare locomotor biomechanics between extinct, non-avian theropod dinosaurs and modern obligate bipeds. *Journal of The Royal Society Interface* 14 (132): 20170276.

Bonnan, M.F. 2003. The evolution of manus shape in sauropod dinosaurs: implications for functional morphology, forelimb orientation, and phylogeny. *Journal of Vertebrate Paleontology* 23 (3): 595–613.

Bonnan, M.F. 2005. Pes Anatomy in Sauropod Dinosaurs: Implications for Functional Morphology, Evolution, and Phylogeny. *In*: Tidwell, V. and Carpenter, K. (eds.), *Thunder-Lizards: The Sauropodomorph Dinosaurs*, 346–380. Indiana University Press, Bloomington, Indiana.

Borsuk-Bialynicka, M. 1977. A new camarasaurid sauropod *Opisthocoelicaudia skarzynskii* gen. n., sp. n. from the Upper Cretaceous of Mongolia. *Palaeontologia Polonica* 37 (5): 5–64.

Brusatte, S.L., Niedźwiedzki, G. and Butler, R.J. 2011. Footprints pull origin and diversification of dinosaur stem lineage deep into Early Triassic. *Proceedings of the Royal Society of London B: Biological Sciences* 278 (1708): 1107–1113.

Brusatte, S.L., Nesbitt, S.J., Irmis, R.B., Butler, R.J., Benton, M.J. and Norell, M.A. 2010. The origin and early radiation of dinosaurs. *Earth-Science Reviews* 101 (1–2): 68–100.

Buckley, L.G., McCrea, R.T. and Lockley, M.G. 2015. Birding by foot: a critical look at the synapomorphy- and phenetic-based approaches to trackmaker identification of enigmatic tridactyl Mesozoic traces. *Ichnos* 22 (3–4): 192–207.

Carrano, M.T. and Wilson, J.A. 2001. Taxon distributions and the tetrapod track record. *Paleobiology* 27 (3): 564–582.

Casanovas, L., Ezquerra, R., Fernández, A., Montero, D., Pérez-Lorente, F., Santafé, J.V., Torcida, F. and Viera, L.I. 1995. El yacimiento de La Canal (Munilla, La Rioja, España): La variación de velocidad en función del tamaño del pie de los ornitópodos. *Zubía* (13): 55–81.

Casanovas, M., Fernández, A., Pérez-Lorente, F. and Santafé, J.V. 1997. Sauropod trackways from site El Sobaquillo (Munilla, La Rioja, Spain) indicate amble walking. *Ichnos* 5 (2): 101–107.

Castanera, D., Pascual, C., Canudo, J.I., Hernández, N. and Barco, J.L. 2012. Ethological variations in gauge in sauropod trackways from the Berriasian of Spain. *Lethaia* 45 (4): 476–489.

Castanera, D., Vila, B., Razzolini, N.L., Falkingham, P.L., Canudo, J.I., Manning, P.L. and Galobart, À. 2013. Manus track preservation bias as a key factor for assessing trackmaker identity and quadrupedalism in basal ornithopods. *PLoS One* 8 (1): e54177.

Cohen, A.S., Halfpenny, J., Lockley, M. and Michel, E. 1993. Modern vertebrate tracks from Lake Manyara, Tanzania and their paleobiological implications. *Paleobiology* 19 (4): 433–458.

Currie, P.J. 1983. Hadrosaur trackways from the Lower Cretaceous of Canada. *Acta Palaeontologica Polonica* 28 (1–2).

Currie, P.J., Nadon, G.C. and Lockley, M.G. 1991. Dinosaur footprints with skin impressions from the Cretaceous of Alberta and Colorado. *Canadian Journal of Earth Sciences* 28 (1): 102–115.

Dalla Vecchia, F. 2005. Between Gondwana and Laurasia: Cretaceous Sauropods in an Intraoceanic Carbonate Platform. *In*: Tidwell, V. and Carpenter, K. (eds.), *Thunder-Lizards: The Sauropodomorph Dinosaurs*, 395–429. Indiana University Press, Bloomington.

Díaz-Martínez, I., Pereda-Suberbiola, X., Pérez-Lorente, F. and Canudo, J.I. 2015. Ichnotaxonomic review of large ornithopod dinosaur tracks: temporal and geographic implications. *PLoS One* 10 (2): e0115477.

Falkingham, P.L. 2012. Acquisition of high resolution three-dimensional models using free, open-source, photogrammetric software. *Palaeontologia Electronica* 15 (1).

Falkingham, P.L. 2014. Interpreting ecology and behaviour from the vertebrate fossil track record. *Journal of Zoology* 292 (4): 222–228.

Falkingham, P.L. 2016. Applying Objective Methods to Subjective Track Outlines. *In*: Falkingham, P.L., Marty, D. and Richter, A. (eds.), *Dinosaur Tracks: The Next Steps*, 72–81. Indiana University Press, Bloomington.

Falkingham, P.L. and Gatesy, S.M. 2014. The birth of a dinosaur footprint: Subsurface 3D motion reconstruction and discrete element simulation reveal track ontogeny. *Proceedings of the National Academy of Sciences* 111 (51): 18279–18284.

Falkingham, P.L., Bates, K.T., Margetts, L. and Manning, P.L. 2011a. Simulating sauropod manus-only trackway formation using finite-element analysis. *Biology Letters* 7 (1): 142–145.

Falkingham, P.L., Bates, K.T., Margetts, L. and Manning, P.L. 2011b. The 'Goldilocks' effect: preservation bias in vertebrate track assemblages. *Journal of the Royal Society Interface* 8 (61): 1142–1154.

Falkingham, P.L., Bates, K.T., Avanzini, M., Bennett, M., Bordy, E.M., Breithaupt, B.H., Castanera, D., Citton, P., Díaz-Martínez, I., Farlow, J.O., Fiorillo, A.R., Gatesy, S.M., Getty, P., Hatala, K.G., Hornung, J.J., Hyatt, J.A., Klein, H., Lallensack, J.N., Martin, A.J., Marty, D., Matthews, N.A., Meyer, C.A., Milàn, J., Minter, N.J., Razzolini, N.L., Romilio, A., Salisbury, S.W., Sciscio, L., Tanaka, I., Wiseman, A.L.A., Xing, L.D. and Belvedere, M. 2018. A standard protocol for documenting modern and fossil ichnological data. *Palaeontology* 61 (4): 469–480.

Farlow, J.O. 1981. Estimates of dinosaur speeds from a new trackway site in Texas. *Nature* 294 (5843): 747.

Farlow, J.O. 1987. A guide to Lower Cretaceous dinosaur footprints and tracksites of the Paluxy River Valley, Somervell County, Texas. *Field Trip Guidebook, South-Central Section, Geological Society of America, Baylor University, Waco, Texas*: 50.

Farlow, J.O. 1989. Ostrich footprints and trackways: implications for dinosaur ichnology. *In*: Gillette, D.D. and Lockley, M.G. (eds.), *Dinosaur Tracks and Traces*, 243–248. Cambridge University Press.

Farlow, J.O., Chapman, R.E., Breithaupt, B.H. and Matthews, N.A. 2012a. The Scientific Study of Dinosaur Footprints. *In*: Brett-Surman, M.K., Holtz, T.R. and Farlow, J.O. (eds.), *The Complete Dinosaur*, 712–759. Indiana University Press.

Farlow, J.O., Holtz Jr, T.R., Worthy, T.H. and Chapman, R.E. 2013. Feet of the fierce (and not-so-fierce): pedal proportions in large theropods, other non-avian dinosaurs and large ground birds. *In*: Parrish, J.M., Molnar, R.E., Currie, P.J. and Koppelhus, E.B. (eds.), *Tyrannosaurid Paleobiology*, 89–132. Indiana University Press, Bloomington.

Farlow, J.O., Gatesy, S.M., Holtz, T.R., Hutchinson, J.R. and Robinson, J.M. 2000. Theropod locomotion. *American Zoologist* 40 (4): 640–663.

Farlow, J.O., Bonnan, M.E., Rainforth, E.C., Benson, J. and Shearer, K. 2012b. Emus, alligators, and *Eubrontes*: assessing intraspecific and interspecific variability in foot and footprint shape. *Dinosaur Tracks 2011, An International Symposium, Obernkirchen, April 14–17, 2011. Abstracts Volume and Field Guide to Excursions*: 21.

Farlow, J.O., Langston Jr, W., Deschner, E.E., Solis, R., Ward, W., Kirkland, B.L., Hovorka, S., Reece, T.L. and Whitcraft, J. 2006. *Texas giants: dinosaurs of the Heritage Museum of the Texas Hill Country*. The Heritage Museum of the Texas Hill Country, Canyon Lake, Texas.

Fiorillo, A.R., Hasiotis, S.T. and Kobayashi, Y. 2014. Herd structure in Late Cretaceous polar dinosaurs: A remarkable new dinosaur tracksite, Denali National Park, Alaska, USA. *Geology* 42 (8): 719–722.

Francischini, H., Sales, M.A., Dentzien–Dias, P. and Schultz, C.L. 2018. The presence of ankylosaur tracks in the Guará Formation (Brazil) and remarks on the spatial and temporal distribution of Late Jurassic dinosaurs. *Ichnos* 25 (2–3): 177–191.

Gand, G. and Demathieu, G. 2005. Les pistes dinosauroides du Trias moyen francais: interprétation et réévaluation de la nomenclature. *Geobios* 38 (6): 725–749.

Hall, L.E., Fragomeni, A.E. and Fowler, D.W. 2016. The flexion of sauropod pedal unguals and testing the substrate grip hypothesis using the trackway fossil record. *In*: Falkingham, P.L., Marty, D. and Richter, A. (eds.), *Dinosaur Tracks: The Next Steps*, 138–151. Indiana University Press.

Henderson, D.M. 2006a. Burly gaits: centers of mass, stability, and the trackways of sauropod dinosaurs. *Journal of Vertebrate Paleontology* 26 (4): 907–921.

Henderson, D.M. 2006b. Simulated weathering of dinosaur tracks and the implications for their characterization. *Canadian Journal of Earth Sciences* 43 (6): 691–704.

Irby, G.V. 1996. Paleoichnological evidence for running dinosaurs worldwide. *The Continental Jurassic* Museum of Northern Arizona Bulletin 60: 109–112.

Jackson, S.J., Whyte, M.A. and Romano, M. 2010. Range of experimental dinosaur (*Hypsilophodon foxii*) footprints due to variation in sand consistency: How wet was the track? *Ichnos* 17 (3): 197–214.

Kim, B.S. and Huh, M. 2010. Analysis of the acceleration phase of a theropod dinosaur based on a Cretaceous trackway from Korea. *Palaeogeography, Palaeoclimatology, Palaeoecology* 293 (1–2): 1–8.

Kuban, G.J. 1989. Elongate dinosaur tracks. *In*: Gillette, D.D. and Lockley, G.M. (eds.), *Dinosaur Tracks and Traces*, 57–72. Cambridge University Press.

Läbe, S. 2017. Estimating sauropod body mass and gait-by the analysis of recent and fossil tetrapod tracks with photogrammetry and soil mechanics. Doctoral thesis 2017, Bonn, Germany.

Lallensack, J.N. unpubl.. Automatic generation of objective footprint outlines. Doctoral thesis 2018 (chapter 4), Bonn, Germany.

Lallensack, J.N., Engler, T. and Barthel, H.J. unpubl.. Shape variability in tridactyl dinosaur footprints: The significance of size and function. Doctoral thesis 2018 (chapter 3), Bonn, Germany.

Lallensack, J.N., van Heteren, A.H. and Wings, O. 2016. Geometric morphometric analysis of intratrackway variability: a case study on theropod and ornithopod dinosaur trackways from Münchehagen (Lower Cretaceous, Germany). *PeerJ* 4: e2059.

Lallensack, J.N., Sander, P.M., Knötschke, N. and Wings, O. 2015. Dinosaur tracks from the Langenberg Quarry (Late Jurassic, Germany) reconstructed with historical photogrammetry: Evidence for large theropods soon after insular dwarfism. *Palaeontologia Electronica* 18.2.24A: 1–34.

Lallensack, J.N., Ishigaki, S., Lagnaoui, A., Buchwitz, M. and Wings, O. accepted. Forelimb orientation and locomotion of sauropod dinosaurs: insights from the Middle Jurassic Tafaytour Tracksite (Argana Basin, Morocco). *Journal of Vertebrate Paleontology*.

Lallensack, J.N., Klein, H., Milàn, J., Wings, O., Mateus, O. and Clemmensen, L.B. 2017. Sauropodomorph dinosaur trackways from the Fleming Fjord Formation of East Greenland: evidence for Late Triassic sauropods. *Acta Palaeontologica Polonica* 62 (4): 833–843.

Langer, M.C., Ezcurra, M.D., Bittencourt, J.S. and Novas, F.E. 2010. The origin and early evolution of dinosaurs. *Biological Reviews* 85 (1): 55–110.

Lapparent, A. de. 1962. Footprints of dinosaur in the Lower Cretaceous of Vestspitsbergen-Svalbard. *Norsk Polarinstitutt, Årbok* 1960: 14–21.

Li, R., Lockley, M.G., Makovicky, P.J., Matsukawa, M., Norell, M.A., Harris, J.D. and Liu, M. 2008. Behavioral and faunal implications of Early Cretaceous deinonychosaur trackways from China. *Naturwissenschaften* 95 (3): 185–191.

Lockley, M.G. 1997. The paleoecological and paleoenvironmental utility of dinosaur tracks. *In*: Farlow, J.O. and Brett-Surman, M.K. (eds.), *The Complete Dinosaur*, 554–578. Indiana University Press, Bloomington.

Lockley, M.G. 1998a. The vertebrate track record. *Nature* 396 (6710): 429–432.

Lockley, M.G. 1998b. Philosophical perspectives on theropod track morphology: blending qualities and quantities in the science of ichnology. *GAIA* 15: 279–300.

Lockley, M.G. 2007a. The morphodynamics of dinosaurs, other archosaurs, and their trackways: holistic insights into relationships between feet, limbs, and the whole body. *Sediment-organism interactions: a multifaceted ichnology. SEPM Special Publication No. 88*: 27–51.

Lockley, M.G. 2007b. A tale of two ichnologies: the different goals and potentials of invertebrate and vertebrate (tetrapod) ichnotaxonomy and how they relate to ichnofacies analysis. *Ichnos* 14 (1–2): 39–57.

Lockley, M.G. 2009. New perspectives on morphological variation in tridactyl footprints: clues to widespread convergence in developmental dynamics. *Geological Quarterly* 53 (4): 415–432.

Lockley, M.G. and Hunt, A.P. 1994. A track of the giant theropod dinosaur *Tyrannosaurus* from close to the Cretaceous/Tertiary boundary, northern New Mexico. *Ichnos* 3 (3): 213–218.

Lockley, M.G. and Hunt, A.P. 1995. Ceratopsid tracks and associated ichnofauna from the Laramie Formation (Upper Cretaceous: Maastrichtian) of Colorado. *Journal of Vertebrate Paleontology* 15 (3): 592–614.

Lockley, M.G. and Matsukawa, M. 1999. Some observations on trackway evidence for gregarious behavior among small bipedal dinosaurs. *Palaeogeography, Palaeoclimatology, Palaeoecology* 150 (1–2): 25–31.

Lockley, M.G. and Meyer, C. 2000. *Dinosaur tracks and other fossil footprints of Europe*. Columbia University Press, New York.

Lockley, M.G. and Wright, J.L. 2001. Trackways of large quadrupedal ornithopods from the Cretaceous: a review. *In*: Tanke, D. and Carpenter, K. (eds.), *Mesozoic Vertebrate Life*, 428–442. Indiana University Press.

Lockley, M.G., Meyer, C.A. and Moratalla, J.J. 1998. *Therangospodus*: trackway evidence for the widespread distribution of a Late Jurassic theropod with well-padded feet. *GAIA* 15: 339–353.

Lockley, M.G., Lucas, S.G. and Hunt, A.P. 2006. *Eosauropus*, a new name for a Late Triassic track: Further observations on the Late Triassic ichnogenus *Tetrasauropus* and related forms, with notes on the limits of interpretation. *The Triassic-Jurassic Terrestrial Transition. New Mexico Museum of Natural History and Science Bulletin* 37: 192–198.

Lockley, M.G., Huh, M., Gwak, S.-G., Hwang, K.G. and Paik, I.S. 2012. Multiple tracksites with parallel trackways from the Cretaceous of the Yeosu City area Korea: Implications for gregarious behavior in ornithopod and sauropod dinosaurs. *Ichnos* 19 (1–2): 105–114.

Maidment, S.C.R. and Barrett, P.M. 2012. Does morphological convergence imply functional similarity? A test using the evolution of quadrupedalism in ornithischian dinosaurs. *Proceedings of the Royal Society of London B: Biological Sciences* 279 (1743): 3765–3771.

Mallison, H. and Wings, O. 2014. Photogrammetry in paleontology – A practical guide. *Journal of Paleontological Techniques* 12: 1–31.

Marty, D. 2008. Sedimentology, taphonomy, and ichnology of Late Jurassic dinosaur tracks from the Jura carbonate platform (Chevenez-Combe Ronde tracksite, NW Switzerland): insights into the tidal-flat palaeoenvironment and dinosaur diversity, locomotion, and palaeoecology. *GeoFocus* 21: 1–278.

Marty, D., Strasser, A. and Meyer, C.A. 2009. Formation and taphonomy of human footprints in microbial mats of present-day tidal-flat environments: implications for the study of fossil footprints. *Ichnos* 16 (1–2): 127–142.

Matsukawa, M., Matsui, T. and Lockley, M.G. 2001. Trackway evidence of herd structure among ornithopod dinosaurs from the Cretaceous Dakota Group of northeastern New Mexico, USA. *Ichnos: An International Journal of Plant & Animal* 8 (3–4): 197–206.

Matthews, N.A., Noble, T. and Breithaupt, B.H. 2016. Close-Range Photogrammetry for 3-D Ichnology: The Basics of Photogrammetric Ichnology. *In*: Falkingham, P.L., Marty, D. and Richter, A. (eds.), *Dinosaur Tracks: The Next Steps*, 28–55. Indiana University Press.

McCrea, R.T., Buckley, L.G., Farlow, J.O., Lockley, M.G., Currie, P.J., Matthews, N.A. and Pemberton, S.G. 2014. A 'terror of tyrannosaurs': The first trackways of tyrannosaurids and evidence of gregariousness and pathology in Tyrannosauridae. *PLoS One* 9 (7): e103613.

McCrea, R.T., Tanke, D.H., Buckley, L.G., Lockley, M.G., Farlow, J.O., Xing, L., Matthews, N.A., Helm, C.W., Pemberton, S.G. and Breithaupt, B.H. 2015. Vertebrate ichnopathology: pathologies inferred from dinosaur tracks and trackways from the Mesozoic. *Ichnos* 22 (3–4): 235–260.

McPhee, B.W., Bonnan, M.F., Yates, A.M., Neveling, J. and Choiniere, J.N. 2015. A new basal sauropod from the pre-Toarcian Jurassic of South Africa: evidence of niche-partitioning at the sauropodomorph–sauropod boundary? *Scientific reports* 5.

Melchor, R.N. and De Valais, S. 2006. A review of Triassic tetrapod track assemblages from Argentina. *Palaeontology* 49 (2): 355–379.

Milàn, J. 2006. Variations in the morphology of emu (Dromaius novaehollandiae) tracks reflecting differences in walking pattern and substrate consistency: ichnotaxonomic implications. *Palaeontology* 49 (2): 405–420.

Milàn, J. and Bromley, R.G. 2006. True tracks, undertracks and eroded tracks, experimental work with tetrapod tracks in laboratory and field. *Palaeogeography, Palaeoclimatology, Palaeoecology* 231 (3–4): 253–264.

Milàn, J., Christiansen, P. and Mateus, O. 2005. A three-dimensionally preserved sauropod manus impression from the Upper Jurassic of Portugal: implications for sauropod manus shape and locomotor mechanics. *Kaupia* 14.

Milner, A.R.C. and Lockley, G.M. 2016. Dinosaur Swim Track Assemblages: Characteristics, Contexts, and Ichnofacies Implications. *In*: Falkingham, P.L., Marty, D. and Richter, A. (eds.), *Dinosaur Tracks: The Next Steps*, 152–180. Indiana University Press.

Milner, A.R.C., Harris, J.D., Lockley, M.G., Kirkland, J.I. and Matthews, N.A. 2009. Bird-like anatomy, posture, and behavior revealed by an Early Jurassic theropod dinosaur resting trace. *PLoS One* 4 (3): e4591.

Molnar, R.E. 2012. Principles of Paleobiogeography in the Mesozoic. *In*: Brett-Surman, M.K., Holtz, T.R., Farlow, J.O. and Walters, B. (eds.), *The Complete Dinosaur*, 925–958. Indiana University Press.

Moreno, K., Carrano, M.T. and Snyder, R. 2007. Morphological changes in pedal phalanges through ornithopod dinosaur evolution: a biomechanical approach. *Journal of Morphology* 268 (1): 50–63.

Myers, T.S. and Fiorillo, A.R. 2009. Evidence for gregarious behavior and age segregation in sauropod dinosaurs. *Palaeogeography, Palaeoclimatology, Palaeoecology* 274 (1–2): 96–104.

Nadon, G.C. 2001. The impact of sedimentology on vertebrate track studies. *In*: Tanke, D.H. and Carpenter, K. (eds.), *Mesozoic Vertebrate Life*, 395–407. Indiana University Press, Bloomington.

Olsen, P.E. 1980. Fossil great lakes of the Newark Supergroup in New Jersey. *In*: Manspeizer, W. (ed.), *Field Studies of New Jersey Geology and Guide to Field Trips: New York State Geological Association, 52nd Annual Meeting, Newark, New Jersey*, 352–398. Rutgers University, Newark College of Arts and Sciences, Geology Department.

Olsen, P.E. 1995. A new approach for recognizing track makers. *Geological Society of America Abstracts with Programs* 27: 72.

Olsen, P.E., Smith, J.B. and McDonald, N.G. 1998. Type material of the type species of the classic theropod footprint genera *Eubrontes*, *Anchisauripus*, and *Grallator* (Early Jurassic, Hartford and Deerfield basins, Connecticut and Massachusetts, USA). *Journal of Vertebrate Paleontology* 18 (3): 586–601.

Ostrom, J.H. 1972. Were some dinosaurs gregarious? *Palaeogeography, Palaeoclimatology, Palaeoecology* 11 (4): 287–301.

Paik, I.S., Kim, H.J., Lee, H. and Kim, S. 2017. A large and distinct skin impression on the cast of a sauropod dinosaur footprint from Early Cretaceous floodplain deposits, Korea. *Scientific Reports* 7 (1): 16339.

Paul, G.S. and Christiansen, P. 2000. Forelimb posture in neoceratopsian dinosaurs: implications for gait and locomotion. *Paleobiology* 26 (3): 450–465.

Pérez-Lorente, F. 2015. *Dinosaur Footprints and Trackways of La Rioja*. Indiana University Press, .

Petti, F.M., Bernardi, M., Todesco, R. and Avanzini, M. 2011. Dinosaur footprints as ultimate evidence for a terrestrial environment in the late sinemurian trento carbonate platformearly jurassic dinosaur tracks from the trento platform. *PALAIOS* 26 (10): 601–606.

Piñuela, L., García-Ramos, J.C., Romano, M. and Ruiz-Omeñaca, J.I. 2016. First Record of Gregarious Behavior in Robust Medium-Sized Jurassic Ornithopods: Evidence from the Kimmeridgian Trackways of Asturias (N. Spain) and Some General Considerations on Other Medium-Large Ornithopod Tracks in the Mesozoic Record. *Ichnos* 23 (3–4): 298–311.

Racey, A. and Goodall, J.G. 2009. Palynology and stratigraphy of the Mesozoic Khorat Group red bed sequences from Thailand. *Geological Society, London, Special Publications* 315 (1): 69–83.

Razzolini, N.L., Vila, B., Díaz-Martínez, I., Manning, P.L. and Galobart, À. 2016. Pes shape variation in an ornithopod dinosaur trackway (Lower Cretaceous, NW Spain): new evidence of an antalgic gait in the fossil track record. *Cretaceous Research* 58: 125–134.

Reisz, R.R., Evans, D.C., Roberts, E.M., Sues, H.-D. and Yates, A.M. 2012. Oldest known dinosaurian nesting site and reproductive biology of the Early Jurassic sauropodomorph *Massospondylus*. *Proceedings of the National Academy of Sciences of the United States of America* 109 (7): 2428–2433.

Rich, T.H., Vickers-Rich, P. and Gangloff, R.A. 2002. Polar dinosaurs. *Science* 295 (5557): 979–980.

Sander, P.M. and Lallensack, J.N. submitted. Dinosaurs: Four legs good, two legs bad. Current Biology.

Sander, P.M., Peitz, C., Jackson, F.D. and Chiappe, L.M. 2008. Upper Cretaceous titanosaur nesting sites and their implications for sauropod dinosaur reproductive biology. *Palaeontographica Abteilung A*: 69–107.

Sarjeant, W.A.S. 1975. Fossil Tracks and Impressions of Vertebrates. *In*: Frey, R.W. (ed.), *The Study of Trace Fossils*, 283–324. Springer Berlin Heidelberg.

Schanz, T., Lins, Y., Viefhaus, H., Barciaga, T., Läbe, S., Preuschoft, H., Witzel, U. and Sander, P.M. 2013. Quantitative Interpretation of Tracks for Determination of Body Mass. *PLoS One* 8 (10): e77606.

Schulp, A.S. 2002. The effects of tectonic deformation on dinosaur trackway morphology. *Sargetia. Acta Musei Devensis, Series Scientia Naturae, Deva* 19 (27): e32.

Smith, J.B. and Farlow, J.O. 2003. Osteometric Approaches to Trackmaker Assignment for the Neward Supergroup Ichogenera *Grallator*, *Anchisauripus*, and *Eubrontes*. *In*: LeTourneau, P.M. and Olsen, P.E. (eds.), *The Great Rift Valleys of Pangea in Eastern North America. Volume 2. Sedimentology, Stratigraphy and Paleontology*, 273–292. Columbia University Press, New York.

Stevens, K.A., Ernst, S. and Marty, D. 2016. Uncertainty and ambiguity in the interpretation of sauropod trackways. *In*: Falkingham, P.L., Marty, D. and Richter, A. (eds.), *Dinosaur Tracks: The Next Steps*, 226–243. Indiana University Press.

Sues, H.-D. and Fraser, N.C. 2010. *Triassic life on land: the great transition*. Columbia University Press, .

Thompson, S. and Holmes, R. 2007. Forelimb stance and step cycle in *Chasmosaurus irvinensis* (Dinosauria: Neoceratopsia). *Palaeontologia Electronica* 10 (1): 1–17.

Thulborn, R.A. 1984. Preferred gaits of bipedal dinosaurs. *Alcheringa* 8 (3): 243–252.

Thulborn, R.A. 1990. *Dinosaur tracks*. Chapman and Hall, London, New York.

Thulborn, R.A. and Wade, M. 1984. Dinosaur trackways in the Winton Formation (mid-Cretaceous) of Queensland. *Memoirs of the Queensland Museum* 21 (2): 413–517.

VanBuren, C.S. and Bonnan, M. 2013. Forearm posture and mobility in quadrupedal dinosaurs. *PLoS One* 8 (9): e74842.

Viera, L.I. and Torres, J.A. 1995. Análisis comparativo sobre dos rastros de dinosaurios theropodos. Forma de marcha y velocidad. *Munibe Ciencias Naturales* 47: 53–56.

Viglietti, P.A., Barrett, P.M., Broderick, T.J., Munyikwa, D., MacNiven, R., Broderick, L., Chapelle, K., Glynn, D., Edwards, S., Zondo, M., Broderick, P. and Choiniere, J.N. 2018. Stratigraphy of the *Vulcanodon* type locality and its implications for regional correlations within the Karoo Supergroup. *Journal of African Earth Sciences* 137: 149–156.

Vila, B., Oms, O., Galobart, À., Bates, K.T., Egerton, V.M. and Manning, P.L. 2013. Dynamic similarity in titanosaur sauropods: Ichnological evidence from the Fumanya Dinosaur Tracksite (Southern Pyrenees). *PLoS One* 8 (2): e57408.

Weems, R.E. 2006. Locomotor speeds and patterns of running behavior in non-maniraptoriform theropod dinosaurs. *The Triassic-Jurassic Terrestrial Transition. New Mexico Museum of Natural History and Science Bulletin* 37: 379–389.

Whyte, M.A., Romano, M. and Elvidge, D.J. 2007. Reconstruction of Middle Jurassic dinosaur-dominated communities from the vertebrate ichnofauna of the Cleveland Basin of Yorkshire, UK. *Ichnos* 14 (1–2): 117–129.

Wilson, J.A. 2005. Integrating ichnofossil and body fossil records to estimate locomotor posture and spatiotemporal distribution of early sauropod dinosaurs: a stratocladistic approach. *Paleobiology* 31 (03): 400–423.

Wilson, J.A. and Carrano, M.T. 1999. Titanosaurs and the origin of "wide-gauge" trackways: a biomechanical and systematic perspective on sauropod locomotion. *Paleobiology* 25 (2): 252–267.

Wilson, J.A., Marsicano, C.A. and Smith, R.M. 2009. Dynamic locomotor capabilities revealed by early dinosaur trackmakers from Southern Africa. *PLoS One* 4 (10): e7331.

Wings, O., Lallensack, J.N. and Mallison, H. 2016. The Early Cretaceous Dinosaur Trackways in Münchehagen (Lower Saxony, Germany) – 3D photogrammetry as basis for geometric morphometric analysis of shape variation and evaluation of material loss during excavation. *In*: Falkingham, P.L., Marty, D. and Richter, A. (eds.), *Dinosaur Tracks: The Next Steps*, 56–71. Indiana University Press, Bloomington.

Wright, J.L. 2005. Steps in understanding sauropod biology. *In*: Rogers, C.C. and Wilson, J. (eds.), *The Sauropods: Evolution and Paleobiology*, 252–285. Oakland, California.

Xing, L.D., Lockley, M.G., Bonnan, M.F., Marty, D., Klein, H., Liu, Y., Zhang, J., Kuang, H., Burns, M.E. and Li, N. 2015. Late Jurassic–Early Cretaceous trackways of small-sized sauropods from China: New discoveries, ichnotaxonomy and sauropod manus morphology. *Cretaceous Research* 56: 470–481.

Xing, L.D., G. Martin Lockley, Yang, G., Cao, J., Benton, M., Xu, X., Zhang, J., Klein, H., Persons, W.S., Kim, J.Y., Peng, G., Ye, Y. and Ran, H. 2016. A new *Minisauripus* site from the Lower Cretaceous of China: Tracks of small adults or juveniles? *Palaeogeography, Palaeoclimatology, Palaeoecology* 452 (Supplement C): 28–39.